CAVE AIR CO_2 AND DRIP-WATER GEOCHEMICAL VARIABILITY AT DESOTO CAVERNS: IMPLICATIONS FOR SPELEOTHEM-BASED PALEOCLIMATE STUDIES

by

RAJESH DHUNGANA

PAUL AHARON, COMMITTEE CHAIR
FRED ANDRUS
GEOFFREY R. TICK
JOE LAMBERT
DAVID C. KOPASKA-MERKEL

A DISSERTATION

Submitted in partial fulfillment of the requirements for
the degree of Doctor of Philosophy in the
Department of Geological Sciences
in the Graduate School of
The University of Alabama

TUSCALOOSA, ALABAMA

2017

ABSTRACT

This study has addresses the question whether speleothems from DeSoto Caverns (Childersburg, AL) can be used as paleoclimate archives for the Southeast USA. The monitoring program encompassed determination of cave air CO_2, cave ambient conditions (i.e., air temperature, humidity), drip-water geochemistry and local rainfall amount, and stable isotopes of oxygen and hydrogen (Tuscaloosa, AL).

The substantial attenuation of drip water isotope ranges (-3.1 to – 5.3 ‰ V-SMOW) relative to rainwater (-1.2 to -6.4 ‰ V- SMOW) is likely caused by mixing of freshwater with residual evaporated water in the epikarst zone. The cave drip water $\delta^{18}O$ shows an interannual negative trend from the warm/dry year (2012) to the relatively cool/wet year (2013) suggesting that evapotranspiration above the cave plays an important role in drip water $\delta^{18}O$ variability. Drip water Ca, Mg and Sr and Mg/Ca and Sr/Ca ratios exhibit lower values and higher ratios, respectively, during the warm/dry relative to the cool/wet year. The interannual rainfall amount variability likely exerts a dominant control on the elemental concentrations and elemental ratios of the drips. Cave air pCO_2 varies seasonally with high values (up to 5.0 atm $\times 10^3$) during summer when cave air flow is in stagnation mode and low values (down to 0.48 atm $\times 10^3$) during winter when cave air flow is in ventilation mode. The data suggest that seasonal variations in the concentration of cave air CO_2 affect the $\delta^{13}C$ of drip water and by extension that of speleothem $\delta^{13}C$ values. The documented abrupt hydroclimate changes at ~5 ka in a DeSoto stalagmite is synchronous with the reduction of the North Atlantic Deep Water (NADW) production suggesting the latter being the likely controlling factor. The periodic (68 ± 4 yrs

periodicity) switches of seasonal rainfall amount dominance from winter to summer and back are a prominent feature of the mid-to-late Holocene $\delta^{18}O$ time series of the speleothem. The observed 68 ± 4 yrs periodicity in stalagmite ^{18}O agrees well with the ~ 70 yrs periodicity of the Atlantic Multidecadal Oscillation (AMO) suggesting the latter played a dominant role in the hydroclimate changes in the southeastern US during the late Holocene.

DEDICATION

I dedicate this dissertation to my wife Anju and our two beautiful daughters Asara and Jahnavi. I also dedicate this dissertation to my parents, sisters as well as my parents-in-law, brothers-in- law, nephews, niece, uncles, aunts, and cousin brothers and sisters.

LIST OF ABBREVIATIONS AND SYMBOLS

A.D.	Anno Domini
AMO	Atlantic Multidecadal Oscillation
Atm	Standard atmosphere
BH	Bermuda High
BP	Before present relative to 1950 A.D.
C	Carbon
Ca	Calcium
Cal.	Calendar
cm	Centimeter
CO_2	Carbon dioxide
Corr.	Corrected
DBT	Depth below top
d-excess	Deuterium excess
DIC	Dissolved inorganic carbon
DSSG	DeSoto stalagmite
e.g.	For example (Latin: *exempli gratia*)
ENSO	El Niño Southern Oscillation
et al.	And others (Latin: *et alii*)
GCMWL	Gulf Coast Meteoric Water Line
GOM	Gulf of Mexico

i.e.	That is to say (Latin: *id est*)
ka	Kilo-annum
km	Kilometer
l	Liter
ln	Natural log
M	meter
Mg	Magnesium
mm	Millimeter
mM	Millimoles/liter
n	Number of observations
NBS	National Bureau of Standards
O	Oxygen
op. cit.	In the work cited (Latin: *opera citato*)
pH	Potential of hydrogen
r^2	Coefficient of determination
SI_{AR}	Saturation index of aragonite
SNAO	Southern North Atlantic Oscillation
Sr	Strontium
SST	Sea Surface Temperature
U/Th	Uranium to Thorium ratio
VPDB	Vienna Pee Dee Belemnite
VSMOW	Vienna standard mean ocean water
^{18}O	Oxygen atom with atomic mass of 18

^{13}C	Carbon atom with atomic mass of 13
$\delta^{18}O$	Oxygen isotopic composition
$\delta^{13}C$	Carbon isotopic composition
δD	Hydrogen isotopic composition
$\delta^{13}C_{DIC}$	Carbon isotopic composition of the dissolved inorganic carbon
$\delta^{13}C_{CO_2}$	Carbon isotopic composition of carbon dioxide
pCO_2	Partial pressure of carbon dioxide
µm	Micrometer
µl	Microliter
µg	Microgram
°C	Degrees Celcius
%	Percent
‰	Per mil
σ	Standard deviation

ACKNOWLEDGMENTS

I thank many people who made the completion of this dissertation possible. First, I offer my sincere gratitude to my supervisor, Dr Paul Aharon. Throughout my dissertation-writing period, he provided encouragement, sound advice, good company and lots of good ideas. I would not have finished my dissertation research without his support. I also thank my committee members, Dr Fred Andrus, Dr Geoffrey Tick, Dr David C. Kopaska-Merkel and Dr. William J. Lambert for their invaluable suggestions and support during the dissertation research and my academic progress. Dr. William J. Lambert and Eric Mucinskas offered excellent assistance during the coring expedition. I am very much thankful to both graduate and undergraduate students who have assisted me in the field and laboratory. I am pleased to thank the Department of Geological Sciences at the University of Alabama, the Geological Sciences Advisory Board (GSAB) and the Gulf Coast Association of Geological Societies (GCAGS faculty and student grants) for providing funding to complete my dissertation research. Furthermore, funding for stalagmite coring at DeSoto Caverns in August 2008 and subsequent U/Th dating of the cored stalagmites was provided by a grant to Dr. Paul Aharon from the Alabama State Climatologist's Office (State Climatologist: Professor John Christy).

My dissertation research project would not have been possible without support of the DeSoto cave owner Al Mathis and DeSoto Caverns' president Tim Lacy. I am very much thankful to them. Finally, I would like to thank my family for their support in my pursuit of the Ph.D.

CONTENTS

LIST OF TABLES

LIST OF FIGURES

CHAPTER 1

INTRODUCTION

The rainfall variability in the southeastern US is important for regional hydrology, agriculture and ecological diversity. The major source of moisture for the region is the Gulf of Mexico (GOM) and reduction in normal moisture flux from the GOM even for short periods of a year to a few years places serious stresses on local economies and water supplies (Seager et al., 2009). For example, the Southeast drought of 1986 caused severe crop damage (Karl and Young, 1987). Similarly, the recent 2007 drought ranked as the worst in 100 years, causing more than a billion dollars of crop losses and placing a massive strain on the region's water supply system (Maxwell and Soulé, 2009; Wang et al., 2010). The recurrence of severe droughts in the southeastern US, which is one of the fastest growing regions in the nation, underscores the need to better understand the southeastern rainfall variability.

In the present climate state, rainfall in the Southeast is consistently distributed throughout the year with two distinct modes. In the summer, the rainfall is typically derived by convection style thunderstorms whose frequency is influenced by the east-west position of the Bermuda High (BH) pressure cell (Schroeder et al., 1964). The western flank of the BH in summer moves eastward of its mean position during reduced surface temperatures in the Atlantic Ocean. Consequently, owing to enhanced horizontal surface temperature gradient between the Atlantic and the surrounding continents, the anticyclonic airflow around the BH becomes strong, which increases summer moisture delivery from GOM to the Southeast. By contrast, enhanced surface temperatures in the Atlantic Ocean weaken anticyclonic airflow around the BH resulting in less

summer moisture delivery to the Southeast (Ortegren et al., 2011). In the winter, the rainfall variability is modulated by the north-south position of the polar jet stream (Asmerom et al., 2010). The southerly position of the jet stream, owing to lower than normal polar temperatures causes the collision of opposing cold and GOM derived warm air masses and increases the winter rainfall across the Southeast. However, drier conditions persist in the Southeast when the jet stream is positioned farther to the north owing to higher than normal polar temperatures.

Sadly, the past rainfall records are poorly documented in the Southeast. The majority of studies have used pollen, tree rings and lake sediments. For example, Stahle et al. (2007) analyzed tree rings and concluded that the Southeast was wetter in A.D. 1864 while most other parts of USA witnessed severe droughts. Donders et al. (2005) showed evidence of stepwise increase in wetland vegetation in the Southeast during the past 5000 years based on pollen analysis of peat deposits from southwest Florida. However, published tree ring data comprise only the last millennium (e.g., Stahle and Cleaveland, 1994) whereas documented pollen records are of low resolution (e.g., Goshen Springs sediments, Delcourt, 1980). Moreover, the marine-based record of hydroclimate variability from the Gulf of Mexico (Poore et al, 2003) and the Caribbean (Hodell et al, 1991) do not necessarily reflect continental climatic oscillations. Clearly new detailed studies are required to understand the past rainfall variability in the Southeast.

This dissertation uses speleothems (i.e., secondary carbonates precipitated in caves, such as stalagmites) from DeSoto Caverns, AL (Fig. 1.1) to produce a high-resolution record of past rainfall variability for the Southeast. Speleothem-based studies are playing an increasingly important role in obtaining highly detailed climate records from continental settings (Fairchild and Treble, 2009). These terrestrial archives are effective in paleoclimate research because they: (i) capture the changes in the external environment preserving paleoclimate proxies such as

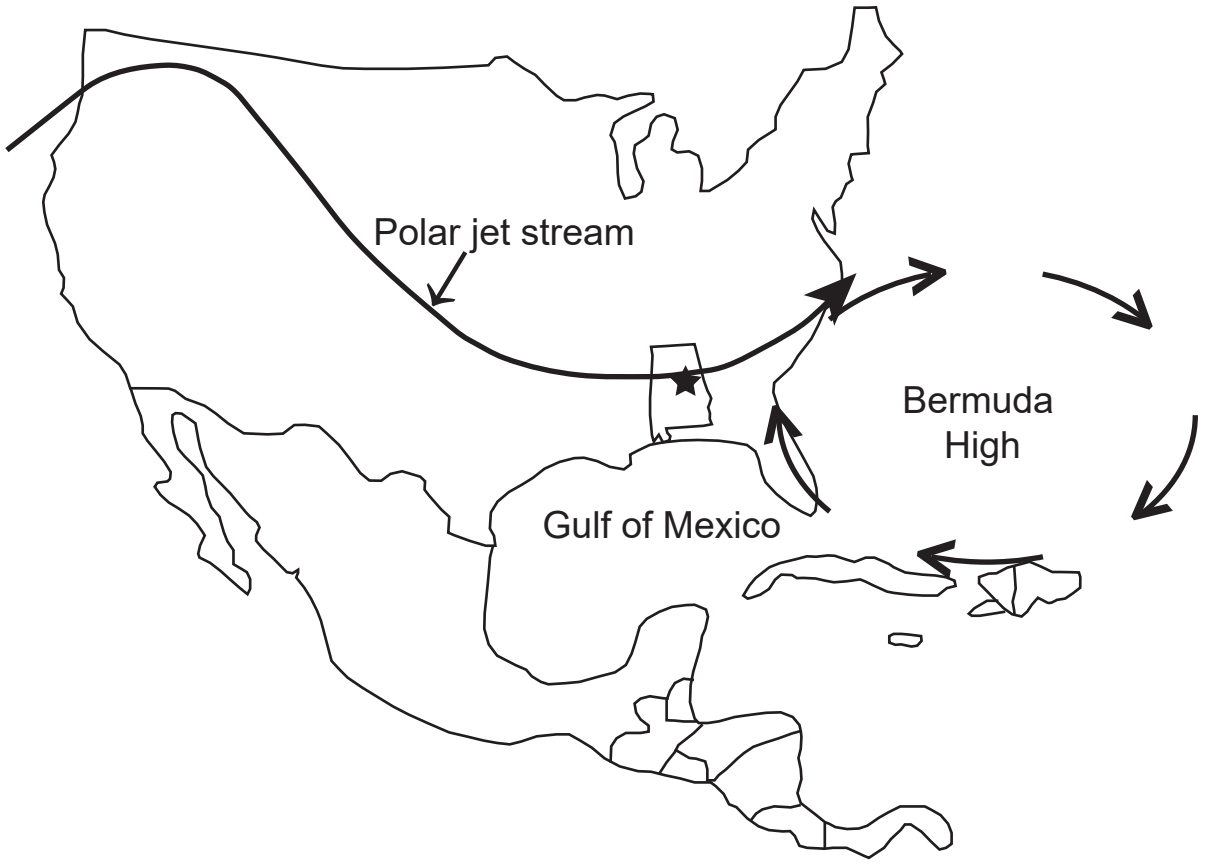

Fig. 1.1. Map of study area in relation to present-day position of jet stream in winter and position of Bermuda High in summer. The study site is marked with a star. Map modified after Willard et al. (2005) and Hardt et al. (2010).

growth rates, oxygen and carbon isotope composition, annual band thickness, and trace elements, (ii) deposit continuously for thousands of years and have the potential to provide high-resolution (seasonal to decadal scale) records, and (iii) can be precisely dated by U-series methods (McDermott, 2004; Lachniet, 2009).

DeSoto Caverns is located on the outskirts of Childersburg and is separated from its major moisture source, the Gulf of Mexico, by 365 km of low elevation coastal plains. The cave encompasses a karst system developed in the Ordovician dolomite and is richly decorated with numerous active and fossils speleothems composed predominantly of aragonite. The cave provides a unique opportunity to investigate rainfall variability in the southeastern US because: (i) the cave's aquifer is recharged by the north-tracking moisture that originates over the Gulf of Mexico (Lambert and Aharon, 2010), (ii) it is located at the southern boundary of the winter polar front, and (iii) humidity and air temperature inside the cave are almost constant throughout the seasons. I use stalagmite oxygen and carbon isotope and drip-water trace-element (e.g., Mg/Ca and Sr/Ca) data to examine past rainfall records. The carbon isotope compositions of speleothems, although complex, have the potential to yield valuable information on paleoenvironmental changes (Hodge et al., 2008; Cosford et al., 2009). The oxygen-isotope compositions of speleothems are generally interpreted in terms of variation in amount of rainfall at a constant mean annual temperature and high (>95%) relative humidity (Neff et al., 2001; Burns et al., 2002; Cruz et al., 2005; Baker et al., 2007). Unlike inferences made using carbon and oxygen isotopes, the paleoclimatic interpretation of speleothem-based Mg/Ca and Sr/Ca ratios is still a subject of debate. For example, Wong et al., (2011) argued that trace-elemental ratios are controlled by cave ventilation shifts, whereas Tremaine and Froelich (2013) suggested that trace-elemental ratios vary with the amount of rainfall.

The main objective of this dissertation was to unravel past hydroclimate variability in the southeastern US by means of high-resolution climate proxy records and to compare these findings with global climate events. To help the paleohydroclimatic interpretation of proxy records of DeSoto Caverns, stable isotopes ($\delta^{18}O$, δD and $\delta^{13}C$) and trace elements (Ca, Mg, Sr) of cave drip waters were monitored.

The body of the dissertation is divided into three chapters. The coming chapter discusses the relationship between Tuscaloosa rainfall, collected at the University of Alabama (located ~ 140 km west of the study site) and cave drip waters in terms of oxygen and hydrogen isotopic compositions. Cave drip waters were collected at monthly intervals for 2 years (Jan 2012-Dec 2013) to examine variations in drip water oxygen and hydrogen isotopes as well as trace-element concentrations (Ca, Mg and Sr) and their ratios to the major Ca cation (Mg/Ca and Sr/ Ca). The chapter describes the interpretation of variation in geochemical proxies in drip waters and its bearing on the paleohydroclimate archived in the stalagmites.

The next chapter discusses how carbon enters the cave atmosphere and affects speleothem growth rates, as well as carbon isotopic compositions of drip waters and hence of speleothems. Variations in $\delta^{13}C$ of speleothems are much more complicated than previously thought owing to multiple factors that can alter the final $^{13}C/^{12}C$ of the stalagmite (McDermott, 2004; Xinggong et al., 2005). This chapter describes the effects of seasonal cave ventilation on cave air pCO_2, $\delta^{13}C$cave air pCO_2 and drip water carbonate chemistry (such as, pH, alkalinity, dissolved inorganic carbon and $\delta^{13}C$ of dissolved inorganic carbon) variability based on monthly sampling of cave air CO_2 and drip waters over 2 years (Jan 2012-Dec 2013). The aim of this study is to examine mechanisms leading to variations in $\delta^{13}C$ of stalagmites prior to interpretation in terms of past hydroclimate change. Finally, the last chapter deals with the past

hydroclimate changes documented in $\delta^{18}O$ and $\delta^{13}C$ records from a stalagmite DSSG 5, spanning the time interval from 6.0 to 1.1 cal ka BP and the interpretations are largely based on the findings of the previous two chapters. Petrographic studies indicate that the stalagmite is mostly aragonite with secondary calcite in some places. Limited areas of aragonite neomorphism to calcite were avoided as much as possible during samples collection for U/Th dating and isotope analysis because replacement calcite might fail to preserve original chemistry. The stalagmite, whose chronology is constrained by 35 precise $^{230}Th/^{234}U$ absolute dates, provides a better than decadal-resolution record of climatic and environmental changes in the GOM and adjacent land areas during the past 6.0 ka. This chapter discusses the link/s between climate variability and human history as well as atmospheric processes controlling rainfall variability in the southeastern US, based on $\delta^{18}O$ and $\delta^{13}C$ variations observed in the stalagmite.

The results and interpretations of this dissertation help to provide high-resolution climate proxy records and assess the major drivers of climate variability in the mid-to-late Holocene in the southeastern US, where paleoclimate reconstruction has been hampered by a lack of high-resolution continental paleo-climate records, such as those from speleothems.

CHAPTER 2

OXYGEN AND HYDROGEN ISOTOPES AND TRACE ELEMENTS IN DRIP-WATERS AT DESOTO CAVERNS RECORD INTERANNUAL RAINFALL VARIATION

ABSTRACT

A monitoring study at DeSoto Caverns during two years (2012-2013) of contrasting rainfall variation and air temperature presents the opportunity to test the response of the hydroclimate proxies in drips and active speleothems to seasonal and interannual forcing factors.

The weighted monthly mean rainwater $\delta^{18}O$ and δD values during the monitoring years range from -1.2 to -6.4 (‰ V-SMOW) and -4 to -41.6 (‰ V-SMOW), respectively, and show modest interannual variation. In contrast, d-excess values show seasonality with high values during winter (14.2 ± 1.6‰, n =12) and low values during summer (9.6 ± 1.1‰, n =12) suggesting primary control by subcloud evaporation processes. Coeval drip-water $\delta^{18}O$ and δD values vary from -3.1 to - 5.3 (‰ V-SMOW) and -9.9 to -30.5 (‰ V-SMOW), respectively, and exhibit interannual negative trends from the 2012 warm/dry year to the 2013 relatively cool/wet year. The substantial attenuation of drip-water isotope amplitudes relative to rainwater is likely due to mixing of fresh with residual evaporated water in the epikarst zone.

Drip-water Ca, Mg and Sr concentrations and Mg/Ca and Sr/Ca ratios exhibit an inverse relation with respect to the contrasting hydroclimate years. Lower values and higher ratios occur during the warm/dry year and higher values and lower ratios occur during the cool/wet year. Interannual variation in the amount of rainfall exerts a dominant control on the elemental concentrations and ratios of the drips through changes of biomass productivity in the soils

overlying the cave, and prior aragonite precipitation in the epikarst. The distribution coefficients of Mg (DMg = 0.00349 ± 0.00106) and Sr (DSr = 1.12 ± 0.041) between drips and speleothems estimated in this study are in broad agreement with experimental values. Coeval changes of trace elements and $\delta^{18}O$ in response to interannual rainfall variability confirm the usefulness of coupling stable isotopes and elemental chemistry in order to better constrain their controlling factors.

1. INTRODUCTION

Speleothem-based climate proxies, $\delta^{18}O$ and trace element ratios (e.g., Mg/Ca and Sr/ Ca) specifically, have been used to understand past climate changes on account of their potential to provide continuous records of past rainfall, temperature variability and atmospheric circulation patterns on various timescales (Burns et al., 2001; Cruz et al., 2007; Wang et al., 2008; Fairchild and Treble, 2009; Mattey et al., 2008, 2010; Wong et al; 2011). However, coeval occurrence of multiple climate factors impacting the geochemical proxies could make their interpretation tenuous. For example, observed $\delta^{18}O$ variability in speleothems can be caused by changes in rainfall amount, temperature, moisture sources and kinetic isotope effects (Hendy, 1971; Lachniet, 2009; McDermott et al., 2011; Feng et al., 2013). Similarly, variations of trace element ratios in speleothems can be caused by soil and bedrock trace element compositional variability, changes in water-rock interaction and groundwater residence time, prior carbonate precipitation in the epikarst and drip-water flow-routing shifts (Fairchild et al., 2000; McDonald et al., 2007; Karmann et al., 2007).

Whereas $\delta^{18}O$ compositions of drip-waters and speleothems in tropical and subtropical caves are generally interpreted in terms of rainfall amount variability at a constant mean annual temperature and >95% relative humidity (Burns et al., 2002; Fleitmann et al., 2003a; Tremaine et

al., 201l), the paleoclimate interpretation of cave drip-water Mg/Ca and Sr/ Ca ratios variability is still a subject of debate. For example, Mattey et al. (2010) and Wong et al. (2011) have argued that seasonal variability is caused by cave ventilation shifts whereas Johnson et al. (2006) and Oster et al. (2012) suggested that seasonal rainfall shift is the dominant factor controlling the observed drip-water trace-element ratio variability. Here I report the results of a two-year monitoring study carried out monthly from the thinly capped (~ 10 m) large front chamber at DeSoto Caverns (Fig. 2.1) in order to improve our understanding of the complexities associated with seasonal and inter-annual variability of drip-water geochemical proxies. Drip-water stable-isotope measurements were previously collected over a three-year period (June-2005 to May 2008) from the thickly (~ 40 m) capped small back- chamber of the cave (Lambert and Aharon, 2010). This study aims to investigate the: (i) relationship between monthly rainfall, drip rates and estimated water budget; (ii) spatial and temporal drip-water isotope variability, and (iii) spatial and temporal variations in drip-water trace elements (Mg and Sr) and their ratios to the major Ca cation (Mg/Ca and Sr/ Ca). Finally, I will discuss implications for the utility of the paleoclimate archive in the stalagmites of variation in geochemical proxies in drip-waters.

2. STUDY SITE AND REGIONAL CLIMATE

Cave drip-waters were collected from DeSoto Caverns (86°16’36’’ W, 33°18’26’’ N) located on the outskirts of Childersburg, AL in the foothills of the Appalachian Mountains. The cave, situated at an elevation of 170 m, lies within the Upper Ordovician dolomite karst system. It is approximately 150 m long and consists of two contiguous segments: (i) a large, 70 m long and 50 m wide, front chamber with ~10 m thick overlying bedrock, and (ii) small chambers in the back of the cave with relatively thicker (~30-40 m) overlying bedrock (Fig. 2.1). Both inactive and active speleothems found within the cave are deposited as aragonite (Lambert and

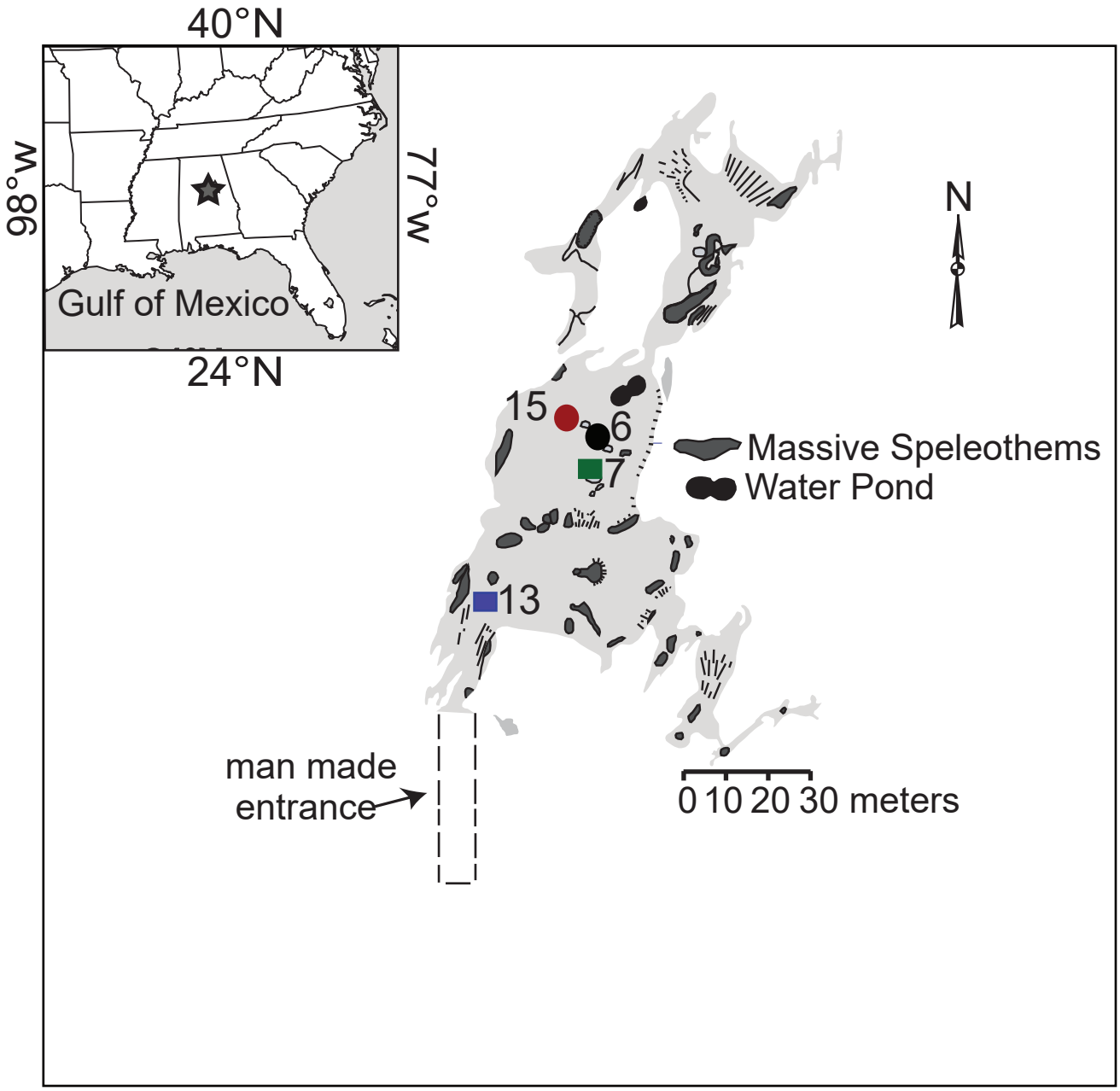

Fig. 2.1. Plan view map of DeSoto Caverns (modified from Lambert and Aharon, 2010) showing the four drip water sampling locations: site 6 (solid black circle), site 7 (solid green square), site 13 (solid blue square) and site 15 (solid red circle). The inset shows the map of southeastern US with the location of DeSoto Caverns (solid green star).

Aharon, 2010; Aharon and Dhungana, 2017).

The climate of the study area is humid subtropical and rainfall occurs throughout the year (Baigorria et al., 2007). The average monthly air temperatures range from ~7°C in January to ~27°C in July while average monthly rainfall ranges from ~80 mm in October to ~150 mm in March. The area experiences a mean annual air temperature of 17.2 °C and an average annual rainfall total of 1417 mm, based on 1958-2004 data (Lambert and Aharon, 2010). Rainfall is consistently distributed throughout the year with two distinct modes. In the winter the collision of opposing cold and warm air masses often results in rain-producing storm systems that are carried west to east by the polar jet stream (Baigorria et al., 2007). In contrast, summer rainfall is typically derived by convection-style thunderstorms whose frequency is influenced by the east-west position of the Bermuda High pressure cell (Schroeder et al., 1964).

3. METHODS

The cave system was monitored monthly for a two-year period (Jan. 2012 – Dec. 2013) including sampling of drip-waters for geochemical analysis with the goal of unraveling the dominant factors controlling the geochemistry of drip-waters and thereby of the speleothems.

3.1. FIELD METHODS

Weekly- integrated rainwater samples were collected during the study period from the rain- gauge station established at the University of Alabama following the method described by Lambert and Aharon (2010). Cave drip-waters were collected from four locations in the front chamber of the cave (Fig. 2.1) where the cap rock is relatively thin and the drip falling distance is ~25 m. Among the four sampling drips, drips 6, 7 and 15 are stalagmite-precipitating drips and lie at the center of the chamber whereas drip 13 lies close to the entrance of the cave and is not associated with a stalagmite. Drip-water was collected in clean plastic bags that were

subsequently placed in 1000 ml nalgene bottles. Funnels, 15-cm in diameter, were used to direct the falling drips into the plastic bags. With the exception below, aliquots of drip-water for $\delta^{18}O$ and δD measurements were stored in 15 ml septum-capped glass serum bottles. The exception occurred during the period December 2012-September 2013 when 8 ml Low Density Polyethylene (LDPE) nalgene bottles were used. In both cases bottles were completely filled to avoid headspace. Aliquots of drip-water for trace-element measurements were stored in acid-washed 60 ml High Density Polyethylene (HDPE) nalgene bottles. Cave-air temperature time-series was monitored between January and March 2012 and November 2012 to Dec 2013 using an HTAB-176 Certified Hygro/Temp Indicator and between April and October 2012 using an HOBO Pro v2 Temp/RH Data Logger (Table 2.1). Drip flow rates were estimated by measuring the fluid volume collected during a given time span.

3.2. LABORATORY METHODS

The rainwater and cave drip-water samples were analyzed on a Gasbench online with a CF- IRMS (modified Delta-plus). The $\delta^{18}O$ and δD values of rainwater and drip-water were determined by headspace equilibration methods using CO_2 (Epstein and Mayeda, 1953) and H_2 (Horita, 1988) pure gases of known isotope compositions, respectively, and final values were normalized to VSMOW/SLAP standards according to Nelson (2000). Isotope values are reported relative to the Vienna Standard Mean Ocean Water (V-SMOW). Analytical precisions for the oxygen and hydrogen measurements are ±0.1‰ and ±1.0‰ respectively, based on sample repeats as well as internal and international standards. For major (Ca) and trace element (Mg and Sr) measurements the drip-water samples were filtered through 0.2-µm pore-size filters and acidified with nitric acid. Analyses for the major and trace elements were performed using a Perkin Elmer Optima 3000 DV ICP-OES (Inductively Coupled Plasma – Optical Emission

Spectrometer). Machines were calibrated using multiple element standards from CPI International Inc. and quality-control standards from High Purity Inc. Major and trace-element concentrations are expressed as millimoles/liter (mM/l). Standard error of the mean for major and trace element measurements is better than 2% based on standard analysis.

4. RESULTS

4.1. OXYGEN AND HYDROGEN ISOTOPE COMPOSITIONS OF RAINWATER DURING THE PERIOD 2012-2013

The stable-isotope composition of rainwater from the rain gauge station at the University of Alabama, located ~ 140 km west of the study site, was determined in order to understand the factors that control oxygen- and hydrogen- isotope composition of cave drip-waters. Table 2.1 summarizes the monthly averages of rainfall and drip-water monitoring data. Over the 2-year monitoring program the rainfall record indicates that 2012 was relatively dry (1405 mm) compared to 2013 (1606 mm) (Fig. 2.2 A, see Appendix 2.1 for data). During the first monitoring year, monthly rainfall amounts varied from 231.6 to 15.8 mm with the highest rainfall in December and the lowest in April whereas during the second year of study rainfall amounts varied from 255.9 to 37 mm with the highest rainfall in December and the lowest in May. Weekly $\delta^{18}O$ and δD isotopic compositions (n = 87) varied from 0.8 to -9.5 (‰ V-SMOW) and 8.1 to -66 (‰ V-SMOW) respectively, whereas weighted monthly mean $\delta^{18}O$ (n = 24) and δD (n = 24) values varied from -1.2 to -6.4 (‰ V-SMOW) and -4 to -41.6 (‰ V-SMOW), respectively. Slight interannual ^{18}O and ^{2}H depletion trends correspond with the observed increase in rainfall amount (Fig. 2.2). With one significant exception below, no obvious seasonal trend in rainfall $\delta^{18}O$ and δD time-series is noticed over the study period. The exception is the weighted monthly mean deuterium excess values (d-excess = $\delta D - 8\delta^{18}O$; Craig, 1961) that exhibit significant seasonality trends with high values during winter (up to 18.5 ‰) and low

Table 2.1. Averages of rainfall and drip water monitoring data. Uncertainties are standard error of the mean (1σ). Drip water data are from drip site #6 (Fig. 1), which has a continuous flow record and is representative of the other front chamber drips. Data other than Drip 6 are listed in Appendix 2.

Period	Rain fall (mm)	Drip rate (ml/h)	Outside cave T (°C)	cave T (°C)	$\delta^{18}O_{rain}$ (‰ V-SMOW)	$\delta^{2}H_{rain}$ (‰ V-SMOW)	$\delta^{18}O_{drips}$ (‰ V-SMOW)	$\delta^{2}H_{drips}$ (‰ V-SMOW)
2-Year (2012-2013)	1505 ±29	301 ±57.4 (n=21)	17.8 ±1.4 (n=24)	18.2 ±0.1 (n=23)	-4.4 ±0.3 (n=24)	-23.6 ±2.0 (n=24)	-4.7 ±0.1 (n=23)	-24.3 ±0.6 (n=22)
Year 2012	1405	97 ±26 (n=9)	18.8 ±1.9 (n=12)	17.9 ±0.1 (n=11)	-4.4 ±0.4 (n=12)	-23.0 ±2.8 (n=12)	-4.5 ±0.1 (n=11)	-22.4 ±0.7 (n=10)
Year 2013	1606	471 ±69.3 (n=12)	16.8 ±2.0 (n=12)	18.5 ±0.2 (n=12)	-4.5 ±0.3 (n=12)	-24.2 ±2.9 (n=12)	-4.8 ±0.1 (n=12)	-25.8 ±0.6 (n=12)

values during summer (down to 6.2 ‰) (Fig. 2.2 E). Neither rainfall amount ($r^2 = 0.012$ for $\delta^{18}O$ and $r^2 = 0.004$ for δD) nor air temperature ($r = 0.03$ for $\delta^{18}O$ and $r^2 = 0.004$ for δD) seem to control rainwater $\delta^{18}O$ and δD variability. In contrast, summer low and winter high d-excess values observed in monthly d-excess time series exhibit a negative correlation with monthly mean air temperatures ($r^2 = 0.4$) (Figs. 2.2 B and E). Lower summer/ higher winter d-excess rainfall values are likely caused by either one, or a combination, of the following two factors: (i) maximum (minimum) subcloud evaporation changes related to higher (lower) air temperature (Gat, et al., 1996; Guan et al, 2013), and (ii) regional climate system variability in the study area. During summer months, low pressure or trough systems build on the western edge of the Bermuda High, causing convective-style rainfall, while winter rainfall is often associated with cold frontal systems that are driven eastward by jet streams (Lambert and Aharon, 2010). The latter factor is supported by a recent study of Guan et al. (2013) demonstrating that rainfall d-excess values caused by low pressure or trough systems are significantly lower than those caused by cold frontal systems. Hence, there is likely a effect of regional climate setting on rainfall d-

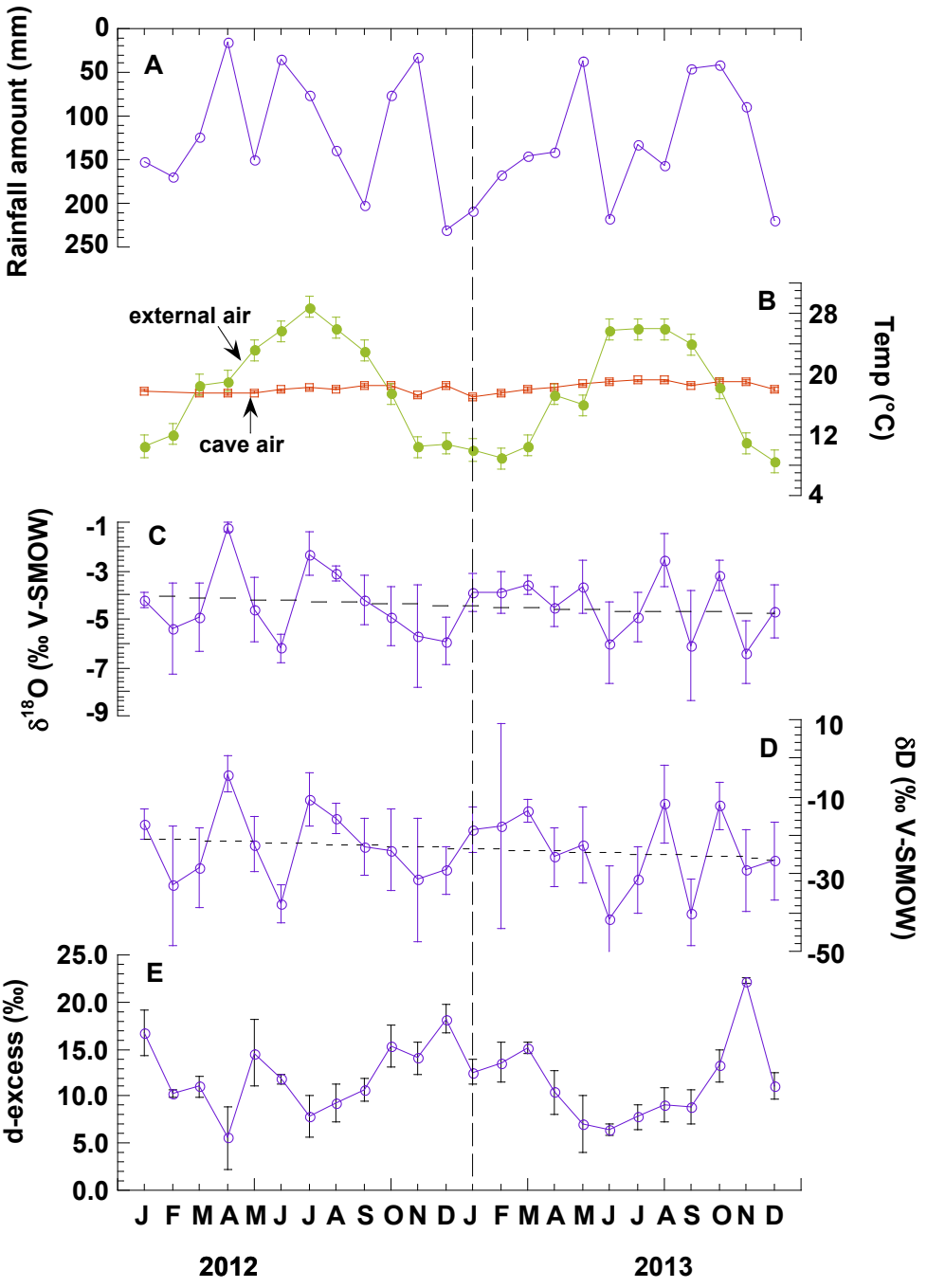

Fig. 2.2. Time series of monitoring data during 2012-2013 years.Uncertainty bars are standard error of the mean. Monthly precipitation from the rain-gauge at the University of Alabama in Tuscaloosa. (B) Monthly mean air temperature recorded at Childersburg water plant station (www.ncdc.noaa.gov) and superimposed cave air temperature. (C) Weighted monthly $\delta^{18}O$ mean of rainwater. (D) Weighted monthly δD mean of rainwater. (E) Weighted monthly d-excess mean of rainwater. Modest interannual ^{18}O and D depletion trends, marked by an interrupted line, are observed in $\delta^{18}O$ and δD time series.

excess seasonal variations in the study area.

4.2. DRIP FLOW RATE TIME SERIES AND DRIP-WATER OXYGEN AND HYDROGEN ISOTOPE COMPOSITIONS

The rainfall record from the Childersburg water plant station, which is ~7 km from the DeSoto Caverns, indicates that 2012 was drier than 2013 in terms of total annual precipitation (www.ncdc.noaa.gov) (Fig. 2.3 A). The monthly water budget calculated using potential evapotranspiration estimates (Samani, 2000) shows that 2012 had 6 months of moisture-deficit compared to only 2 months in 2013 (Fig 2.3 B). At the annual scale, the cave drip-water flow rates were substantially higher in 2013 compared to 2012 (Fig. 2.3 C) and qualitatively correlate with the water-budget variability. Among four sampled drip sites, only drip site 6 had continuous drip-water discharge throughout the study period with substantially higher drip flow rate in 2013 than in 2012. The average drip flow rate was about 4.8 times higher in 2013 than in 2012 (97.3 ml/h in 2012 and 471.3 ml/h in 2013). The lowest drip flow rate (3.0 ml/h) was observed at drip site 13 in June 2012 whereas the highest drip flow rate (3330 ml/h) was recorded at drip site 7 in April 2013. The higher drip flow rates in 2013 are likely due to the combined effect of increased rainfall and decreased potential evapotranspiration.

Drip-water $\delta^{18}O$, δD, and d-excess time series are plotted in Figures 2.4 A, B, and C respectively (see Appendix 2.2 for data). Cave drip-water $\delta^{18}O$ varies between -5.3 and -3.1 ‰, and δD varies between -30.5 and -9.9 (‰ V-SMOW). The drip-water $\delta^{18}O$ and δD records from drip site 6 (the only drip site that had continuous drip-water discharge throughout the study period) show small but significant interannual trends, with heavier ^{18}O and ^{2}H in the warm/dry year 2012 and lighter in the cool/wet year 2013. The relatively heavy isotope values during the warm/dry year 2012 are likely caused by enhanced evaporation processes in the epikarst zone (Bar Matthews et al., 1996). The interannual trends of depletion of heavy isotopes recorded by

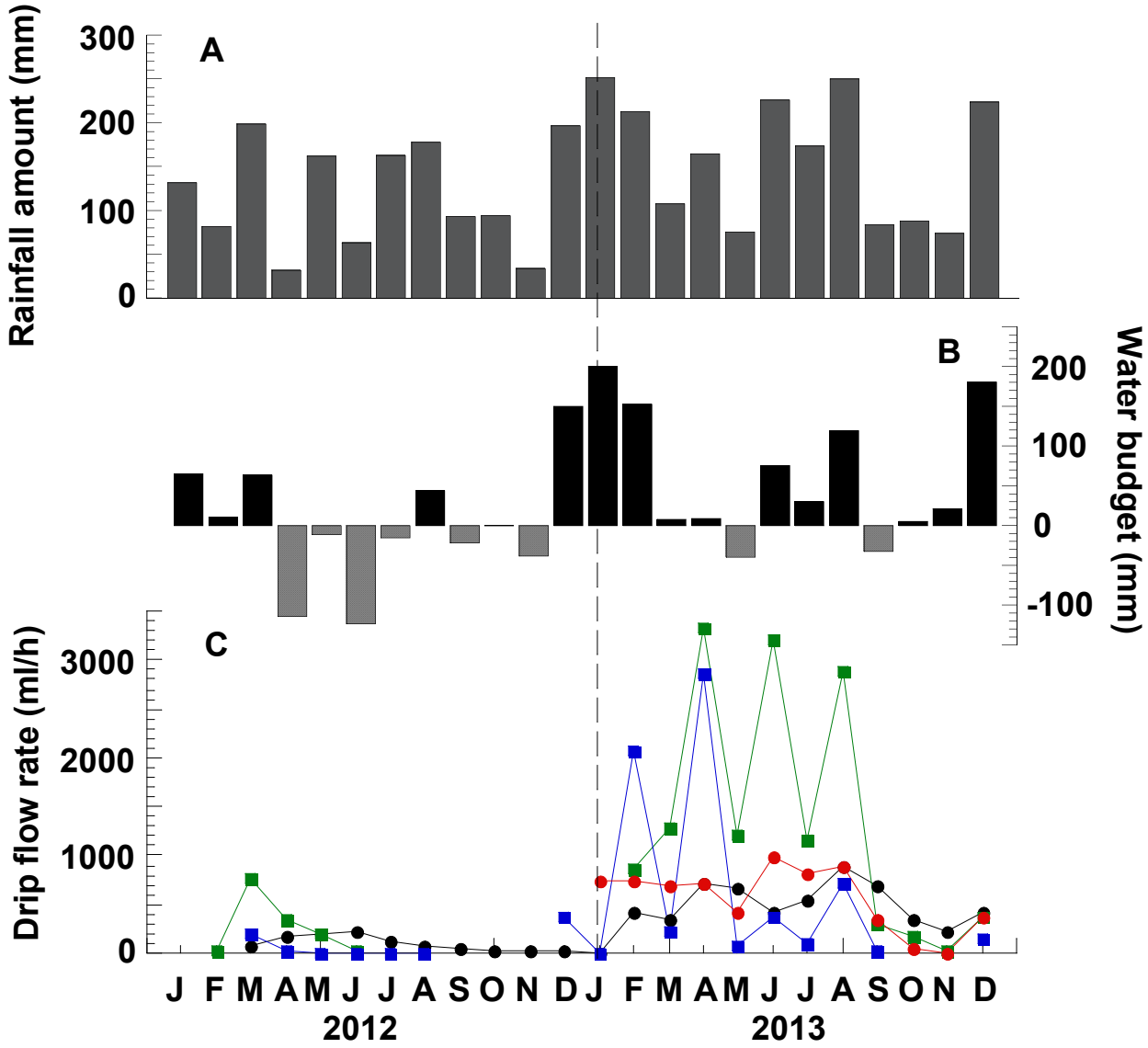

Fig. 2.3. Drip-flow rates are compared to coeval rainfall descriptive rainfall parameters. (A) Rainfall amount record at Childersburg water plant station from January 2012 to December 2013 (www.ncdc.noaa.gov). (B) Net water budget after accounting for evapotranspiration (ET) using an equation from Samani (2000). (C) Drip-flow rates (ml/h) for all four monitored drips; refer to Fig. 2.1 for drip site locations and symbols.

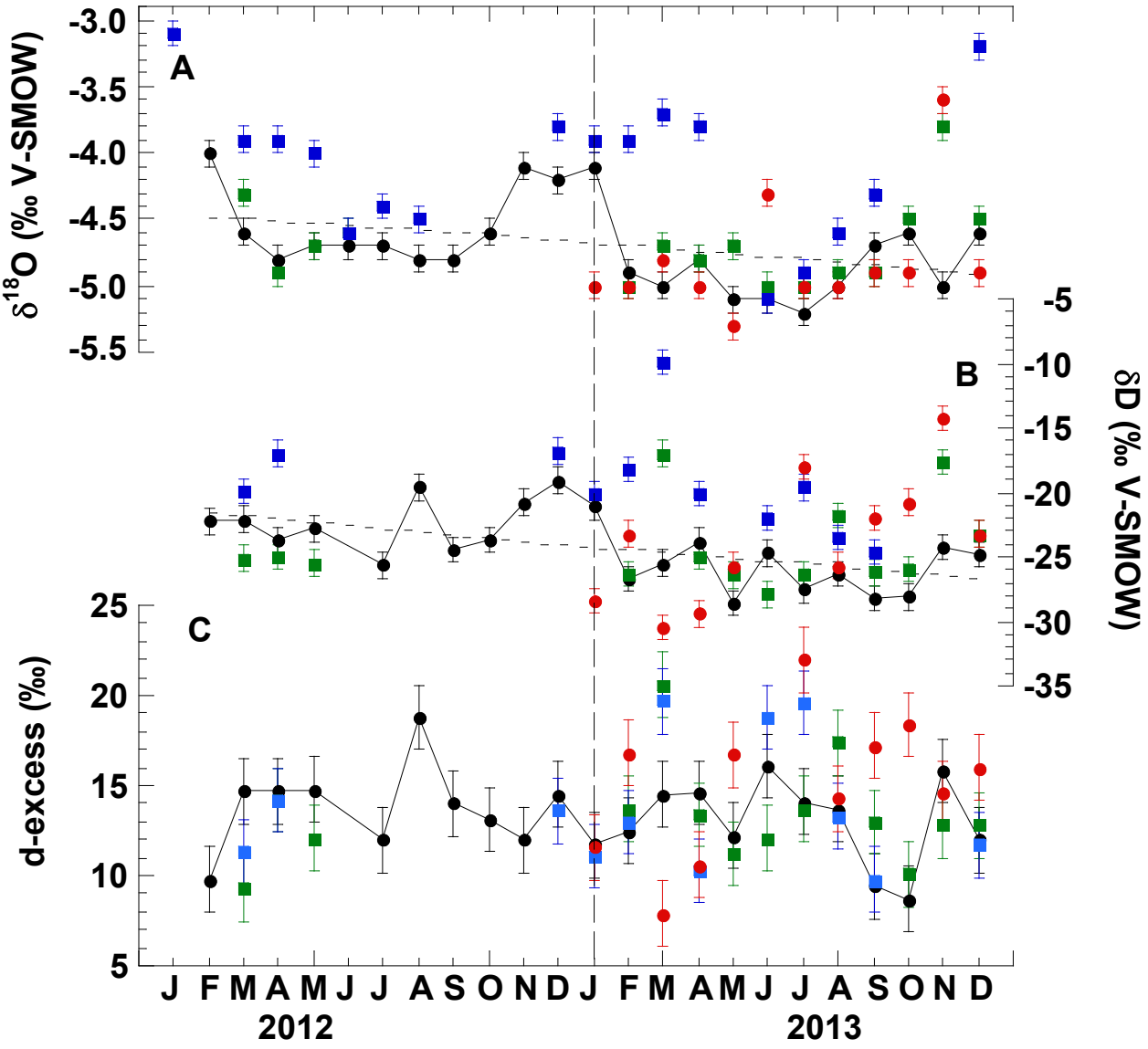

Fig. 2.4. Time series of isotope composition of drip-water at DeSoto Caverns. Refer to Fig. 2.1 for drip site locations and symbols. Interrupted lines in (A) and (B) mark interannual negative $\delta^{18}O$ and δD trends for drip site 6. (A) $\delta^{18}O$ time series; (B) δD time series and (C) d-excess time series.

the drips at the front chamber of the cave are in good agreement with the results of a 3-yr (2005-2008) monitoring study of drip-waters at the back of the cave by Lambert and Aharon (2010). These authors (op. cit.) reported interannual trends of ^{18}O and D enrichments from a wet year (2005) to a dry year (2008) and attributed the trends to the onset of regional drought conditions. The drip-water d-excess values lie between 7.9 and 22 ‰ and do not exhibit an interannual trend (Fig. 2.4 C). Unlike the rainfall d-excess values (Fig. 2.2 C), those of the drip-waters do not vary seasonally; their mean value of 13.9 ± 0.5 ‰ (n=47) is statistically indistinguishable from the winter rainfall mean value of 14.2 ± 1.6‰ (n=12) suggesting that the cave drip-water may be controlled chiefly by winter precipitation. The Gulf Coast Meteoric Water Line (GCMWL), stablished on the basis of monthly weighted mean $\delta^{18}O$ and δD data (unpublished) from Tuscaloosa precipitation over a decade ((2005-2015), is shown in Figure 2.5. The intercept of the GCMWL equation (8.9 ±1.01) trends towards the global average of 10 (Craig, 1961). However, the slope (7.02 ±0.2) is lower than the global average of 8 (Craig, 1961), likely reflecting modifications by secondary processes of re- evaporation and mixing (Rozanski, et al., 1993). $\delta^{18}O$ and δD values of rainwater and drip-waters sampled during the study period fall along the GCMWL line, suggesting a common source.

4.3. TRACE-ELEMENT CONCENTRATIONS IN DRIP-WATERS

Trace-element concentrations in drips at DeSoto Caverns vary as follows: 0.30 to 1.59 mM/l in Ca (mean = 1.19 ± 0.04 mM/l; n = 61), 1.4×10^{-4} to 5.5×10^{-4} mM/l in Sr (mean = $4.3 \times 10^{-4} \pm 1.1 \times 10^{-5}$ mM/l; n = 61) and 0.68 to 1.57 mM/l in Mg (mean = 1.32 ± 0.03 mM/l; n = 61) (see Appendix 2.3 for complete data). Table 2.2 lists the mean trace-elements data from drip site 6 (which has a continuous record).

Trace-element compositions of both fresh and weathered dolomite bedrock samples were

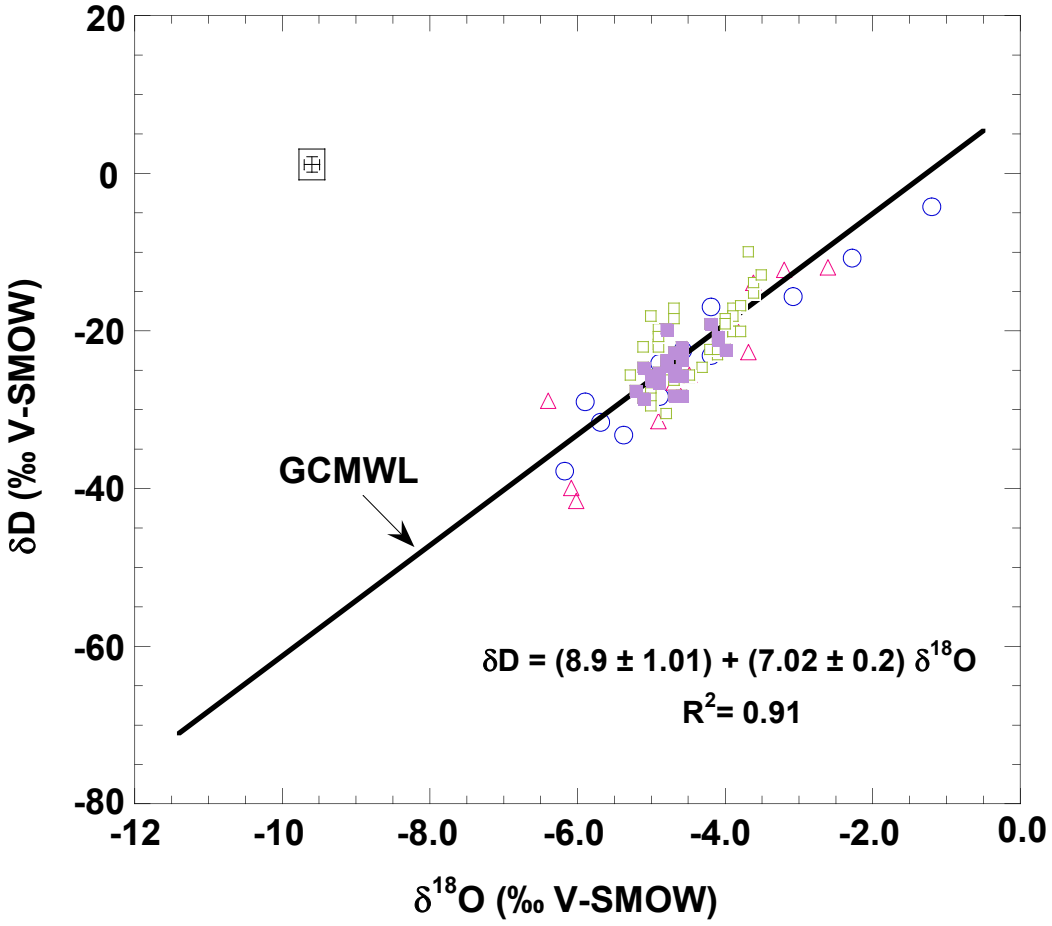

Fig. 2.5. Cross plot of oxygen and hydrogen isotope compositions of rainfall and drips measured in this study. Open circles and triangles are the isotope compositions of rainwater during 2012 and 2013, respectively. Open squares are the isotope compositions of cave drip- water except site 6 represented by filled purple squares. Both rain and drip samples line-up along the the Gulf Coast Meteoric Water Line (GCMWL) that is established on the basis on monthly weighted mean $\delta^{18}O$ and δD decadal data (2005-2015, unpublished) at the University of Alabama gauge station. The GCMWL regression equation is:
$\delta D = (8.9 \pm 1.01) + (7.02 \pm 0.2)\ \delta^{18}O$ ($r^2 = 0.91$).

Table 2.2. Drip water trace elements monitoring data from site #6. Uncertainties are standard error of the mean (1σ).

Period	Ca^{2+} (mM/l)	Mg^{2+} (mM/l)	Sr^{2+} (mM/l $\times 10^4$)	Mg^{2+}/Ca^{2+}	Sr^{2+}/Ca^{2+} ($\times 10^3$)
2-Year (2012-2013)	1.2 ±0.1 (n=22)	1.3 ±0.04 (n=22)	4.2 ±0.2 (n=22)	1.1 ±0.04 (n=22)	0.35 ±0.01 (n=22)
Year 2012	1.0 ±0.1 (n=11)	1.1 ±0.03 (n=11)	3.5 ±0.2 (n=11)	1.2 ±0.1 (n=11)	0.37 ±0.01 (n=11)
Year 2013	1.4 ±0.03 (n=11)	1.5 ±0.03 (n=11)	4.8 ±0.1 (n=11)	1.0 ±0.03 (n=11)	0.33 ±0.01 (n=11)

Table 2.3. Trace element data from pristine and weathered bedrock dolomite. Uncertainties are standard error of the mean (1σ).

Dolomite	Ca^{2+} (mM/l)	Mg^{2+} (mM/l)	Sr^{2+} (mM/l)	Mg^{2+}/Ca^{2+}	Sr^{2+}/Ca^{2+} ($\times 10^3$)
Pristine	4416.8 ±25.6 (n=3)	4334.1 ±14.9 (n=3)	1.7 ±0.004 (n=3)	0.98 ±0.003 (n=3)	0.38 ±0.001 (n=3)
Weathered	5084.7 ±97.1 (n=3)	4895.9 ±46.9 (n=3)	1.1 ±0.02 (n=3)	0.96 ±0.01 (n=3)	0.21 ±0.004 (n=3)

analyzed in order to determine whether trace elements in cave drip-waters are derived from dissolution of pristine dolomite or weathered dolomite. Table 2.3 lists means of trace-element data from fresh and weathered bedrock dolomite and Figure 2.6 shows a comparison of drip-waters from weathered and pristine dolomite in terms of Sr/Ca vs Mg/Ca ratios. Here I suggest that the trace elements of cave drip-waters are extracted from dissolution of pristine dolomite based on the proximity of their ratios and significant departure from the ratios of weathered dolomite.In general, the time-series of Ca, Sr and Mg concentrations in drip-waters at all four drip- sampling stations (Fig. 2.1) exhibit an interannual variability coherent with the drip-water $\delta^{18}O$ record (Fig. 2.7). Specifically, the continuous time series at drip site 6 indicate that delivery of Ca, Mg and Sr to cave drip-water is higher during a “wet” year (2013) than a “dry” year (2012) by a factor of 1.5, 1.3 and 1.4 respectively. Trace elemental concentrations are

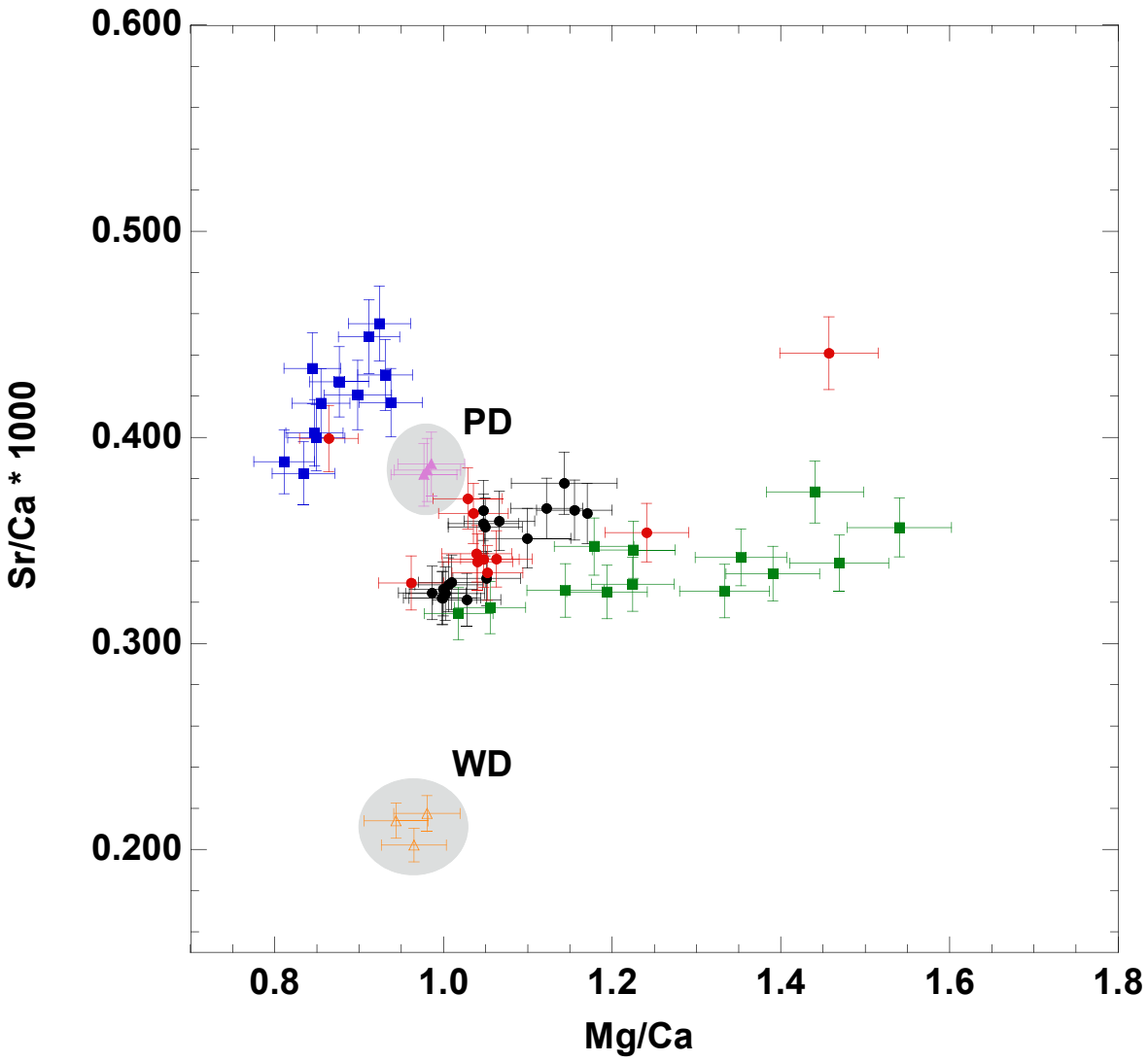

Fig. 2.6. Cross plot of Sr/Ca and Mg/Ca ratios of drips and weathered (WD) and pristine dolomites (PD) at DeSoto Caverns. The proximity of the trace-element ratios of drip-water to that of pristine dolomite field suggests that dissolution of the latter forms the source of trace-elements in the drips.

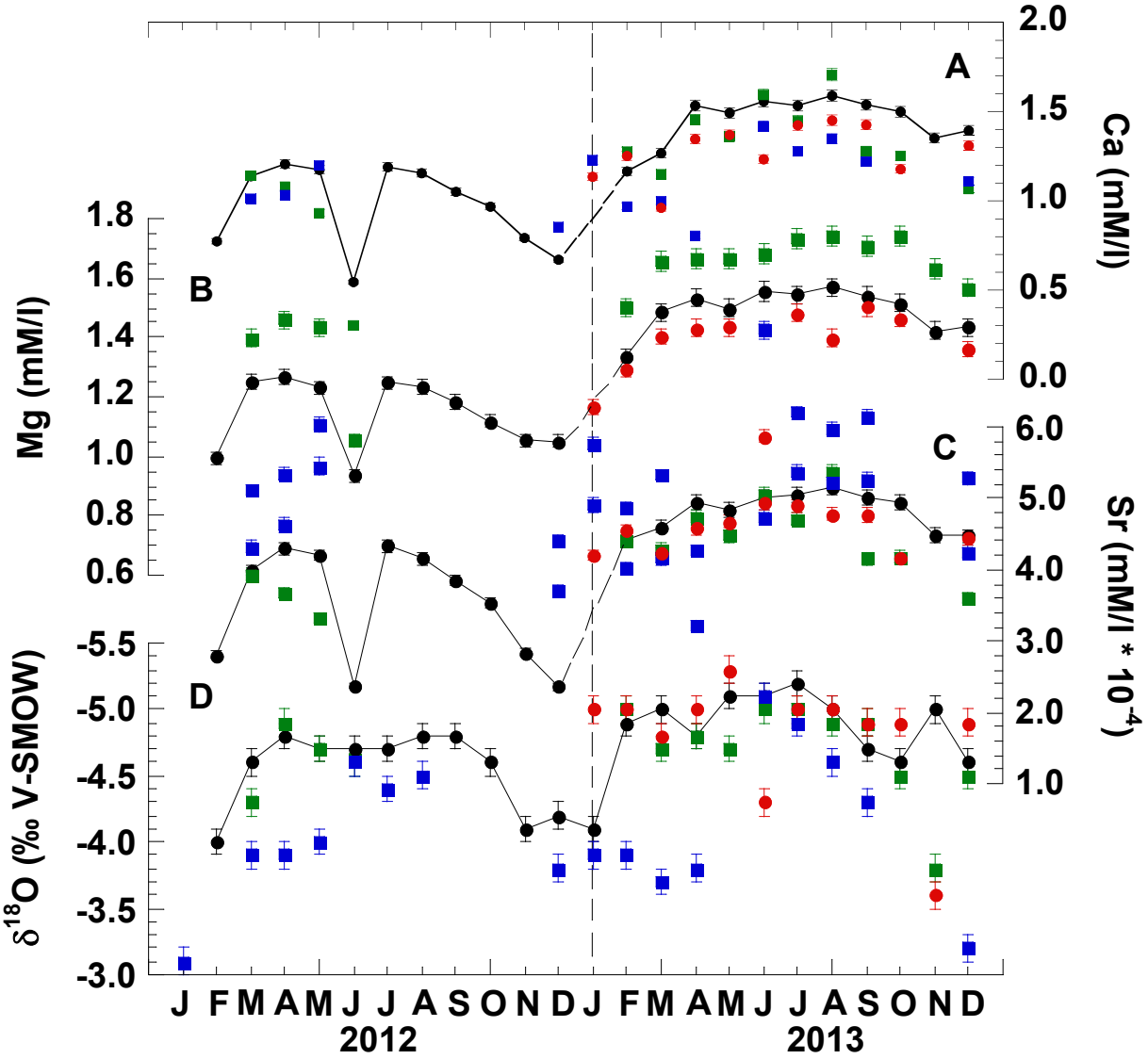

Fig. 2.7. In-phase variations of trace-elements and $\delta^{18}O$ time series in drip-water at DeSoto Caverns. (A) Ca time series; (B) Sr time series; (C) Mg time series, and (D) $\delta^{18}O$ time series. Symbols representing drip-water sites as in Figure 2.1. Time series data for drip-water at site 6 are connected by lines.

exceptionally low in June and December 2012 and correspond with the observed increase in $\delta^{18}O$ value (Fig. 2.7). The time series of Mg/Ca and Sr/Ca ratios in drip-water at site 6 show interannual trends with slightly higher values during the dry year and lower values during the wet year (Fig. 2.8 A and B), and the exceptionally high Mg/Ca ratio in December of 2012. The observed trends of elemental ratios in drip-waters at DeSoto Caverns corroborate the findings of similar studies in other caves (Fairchild et al., 2000; Tooth and Fairchild, 2003; Cruz et al., 2007; Karmann et al., 2007; Tremaine and Froelich, 2013).

5. DISCUSSION

5.1. RELATION BETWEEN RAINWATER AND DRIP-WATER ISOTOPES

Alignment of cave drip-water isotope values with the GCMWL (Fig. 2.5) offers evidence of drip-water sourcing in modern-day rainfall. Over the 2-year study period the rainwater exhibits weighted monthly mean $\delta^{18}O$ and δD values ranging from -1.2 to -6.4 ‰ and -4 to -41.6 ‰ respectively, that are relatively large compared with the ranges of drip-water $\delta^{18}O$ values of -3.1 to – 5.3 ‰ and δD of -9.9 to – 30.5 ‰ (Figs. 2.2 & 2.4). The substantial reduction of drip-water isotopic variation relative to rainwater in the thinly capped, large, front chamber of the cave (this study) agrees with the results of a previous 3-year monitoring study from the thickly capped, small, back chamber of the cave (Lambert and Aharon, 2010). The differences in isotope compositions between rainwater and cave drip-water are likely due to mixing of fresh with residual evaporated water in the epikarst zone (Bar Matthews et al., 1996; Williams and Fowler, 2002; Cruz et al., 2005; Lambert and Aharon, 2010) and bias towards winter precipitation (Aharon and Dhungana, 2017). The following observations support the contention of epikarstic water storage and concomitant seasonal mixing processes: (i) drip-water ^{18}O and ^{2}H depletion trends (Figs. 2.4 A and B) are 5% and 11% higher than the values exhibited by the coeval

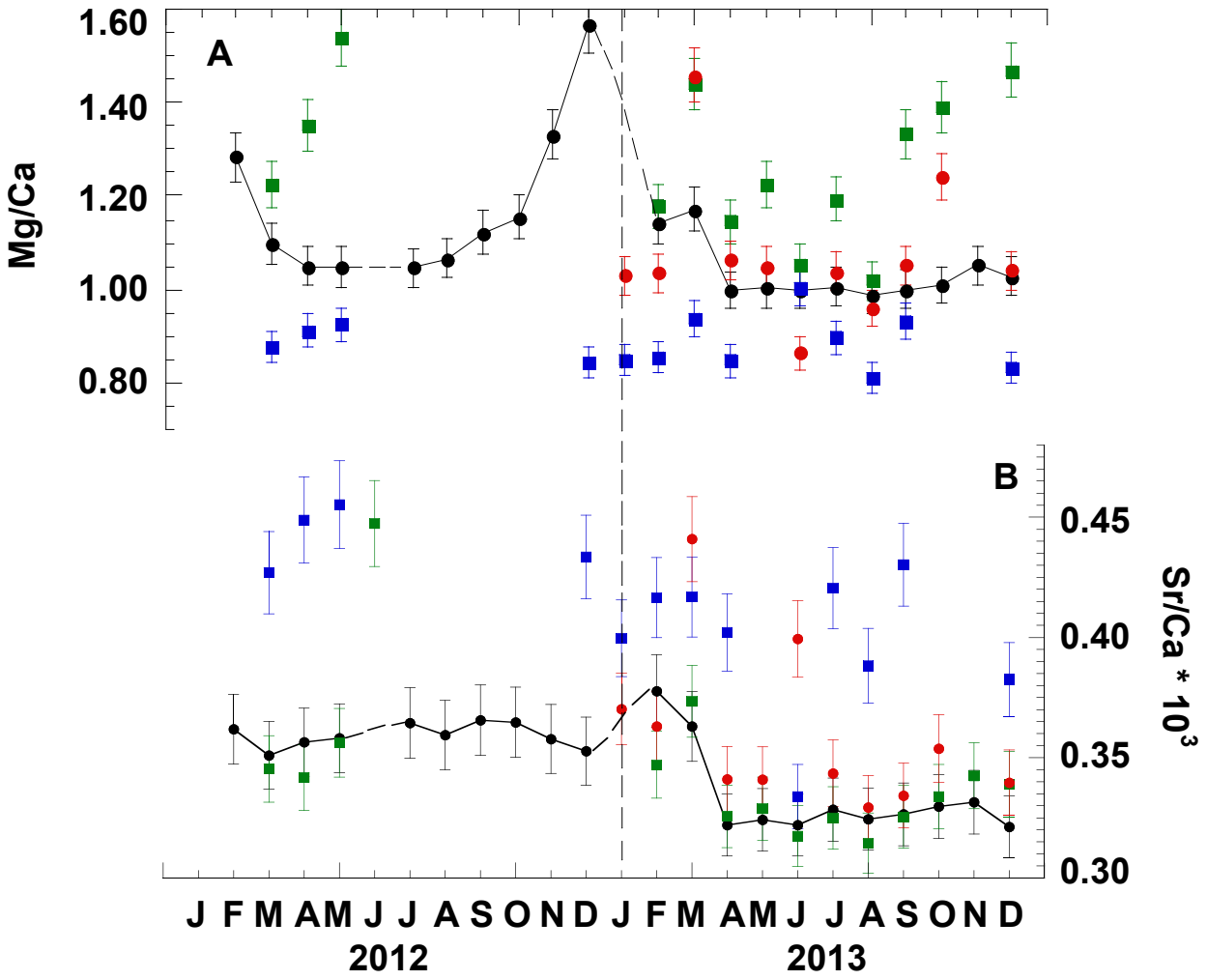

Fig. 2.8. Time series of drip-water trace-element ratios at DeSoto Caverns. Symbols representing drip-water sites as in Figure 2.1. Time series data for drip-water at site 6 are connected by lines. (A) Mg/Ca ratios; (B) Sr/Ca ratios. Time series of Mg/Ca and Sr/Ca exhibit similar interannual phase changes, with higher ratios during the 2012 dry year and lower ratios during the 2013 wet year.

rainwater (Figs. 2.2 B and C); (ii) drip-water mean values of $\delta^{18}O$ (- 4.6 ± 0.1‰, n =67) and δD (- 23.0 ± 0.5‰, n =59) are statistically indistinguishable from the weighted means of $\delta^{18}O$ (- 4.5 ± 0.4‰, n = 12) and δD (- 22.8 ± 2.5‰, n =12) of local winter rainfall suggesting a greater proportion of winter precipitation is being stored in the epikarst; (iii) greater groundwater recharge during winter relative to summer months is likely caused by the lesser extent of evapotranspiration in winter relative to summer (Figs. 2.3 A and B), and (iv) absence of seasonality in drip-water d-excess values stands in stark contrast to the d-excess values of rainwater, which exhibit a seasonality with higher values during winter relative to summer months.. The inconsistencies observed between rainwater and drip-water d-excess values are explained by the occurrence of post rainfall evaporation in the vadose zone prior to storage in the epikarst (Luo et al., 2012).

5.2. DRIP-WATER TRACE-ELEMENT VARIABILITY

Two principal factors have been proposed to control the variability of trace-element concentrations in drips, and subsequently in speleothems: (i) seasonal change in cave ventilation (Mattey et al., 2010; Wong et al; 2011), and (ii) seasonal variation in amount of rainfall. The latter governs change in biomass productivity in the soils overlying caves (Fairchild and Treble, 2009; Uchida et al., 2013; Treble et al., 2015), and prior carbonate precipitation (PCP) in the epikarst zone (Fairchild et al., 2000; Sinclair, 2011). The factors controlling the trace-elements variability reported in this study are evaluated below.

Although cave pCO_2 data at DeSoto Caverns exhibit pronounced seasonal changes, which have been interpreted to result from seasonal changes in ventilation (Dhungana and Aharon, manuscript in prep.), absence of clear evidence of seasonal variability in the Ca, Sr and Mg time- series (Fig. 2.7) refutes a seasonal change in cave ventilation as a principal controlling

factor. Instead, I argue that seasonal variation in the amount of rainfall exerts a dominant control on the elemental concentrations and elemental ratios of the drips through the coupling of biomass productivity overlying the cave and PCP variability in the epikarst. The following lines of evidence corroborate my contention.

First, the relatively high elemental concentrations in the "wet" year (2013) compared to the "dry" year (2012) is likely linked to higher biomass productivity (Fig. 2.7). The enhanced plant- root respiration during vigorous growth of vegetation increases soil-CO_2 concentrations and its uptake in the fluid moving through the epikarst, finally causing enhanced dissolution of carbonates (Li et al., 2010). Second, PCP up-stream from the drips likely affects the trace-elemental concentrations and consequently the Mg/Ca and Sr/Ca ratios in drip-water and thus speleothems. This is because distribution coefficients of trace-element ratios (i.e., *DE = (TE/Ca)carbonate/(TE/Ca)solution*) during dissolution show strong preference for the fluid phase (Fairchild et al., 2000; Treble et al., 2015). For example, in the case of calcite, the distribution coefficients of Mg and Sr, calculated by Huang and Fairchild (2001) at 15 °C, are *DMg* = 0.019 ± 0.003 and *DSr* = 0.072 ± 0.01. For aragonite, *DMg* is orders of magnitude smaller than for calcite (i.e. *DMg* = 0.0007 ± 0.0001, Zhong and Mucci, 1989; and 0.0017 ± 0.0003, Gaetani and Cohen, 2006) and *DSr* is several orders of magnitude higher than calcite (1.1 ± 0.1, Kitano et al., 1971 and 1.2 ± 0.03, Dietzel et al., 2004). Using the trace-element data from modern drip-waters (Table 2.2) and recent aragonite precipitates from the top of the stalagmite (Table 2.4) I estimate the distribution coefficients for Mg and Sr to be: *DMg* = 0.00349 ± 0.00106 and *DSr* = 1.12 ± 0.041 at ~18 °C which are in broad agreement with estimates by Gaetani and Cohen (2006) and Kitano et al. (1971). Therefore, a significant removal of Ca relative to Mg and Sr from seepage water during the PCP process at DeSoto

Caverns will increase both Mg/Ca and Sr/Ca ratios in the cave drip-waters.

Table 2.4. Trace element concentrations of recently formed aragonites from top of an actively stalagmite growing underneath drip #6. Uncertainties are standard error of the mean (1σ).

Sample	Ca^{2+} (mM/l)	Mg^{2+} (mM/l)	Sr^{2+} (mM/l)	Mg^{2+}/Ca^{2+}	Sr^{2+}/Ca^{2+} ($\times 10^3$)
D6A	9646.3	44	3.6	0.0046	0.3732
D6B	9496.8	16.7	3.8	0.0018	0.4001
D6C	9694.8	65.8	3.7	0.0068	0.3816
D6D	9684.5	21.8	4.0	0.0023	0.4130
DATA SUMMARY	9631 ±46	37.1 ±11.3	3.78 ±0.17	0.00384 ±0.00116	0.3920 ±0.0899

According to Tooth and Fairchild (2003) and McDonald et al. (2007), PCP occurs mostly during low-rainfall periods because of CO_2 degassing from infiltrated waters in the ventilated pore spaces. Thus, relatively low Ca, Mg and Sr concentrations (Fig. 2.7) and high Mg/Ca and Sr/Ca ratios (Fig. 2.8) during 2012 in comparison with 2013 likely document the transition from a “dry” to a “wet” year. Specifically, during 2012 elemental concentrations were lower by a factor of 1.5 and the trace-element ratios were higher by a factor of 1.2 relative to 2013 (Figs. 2.7 and 2.8). Finally, the observed positive linear relationship between Sr and Mg concentrations (Fig. 2.9) offers additional evidence of PCP activity in the epikarst causing Ca removal and coeval Sr and Mg enrichment in the drip-waters.

6. CONCLUSIONS

Figure 2.10 summarizes the findings of this investigation aiming to provide insights into hydroclimate proxies contrast between years with distinctly different amount of rainfall. The principal conclusions of the study are as follows.

1. Over the two-year study, cave air temperature was stable and relative humidity was >95 % at DeSoto Caverns In contrast, rainfall amounts differed substantially between the years. Drip-water $\delta^{18}O$ and δD values increased during the dry year and decreased during the wet year while

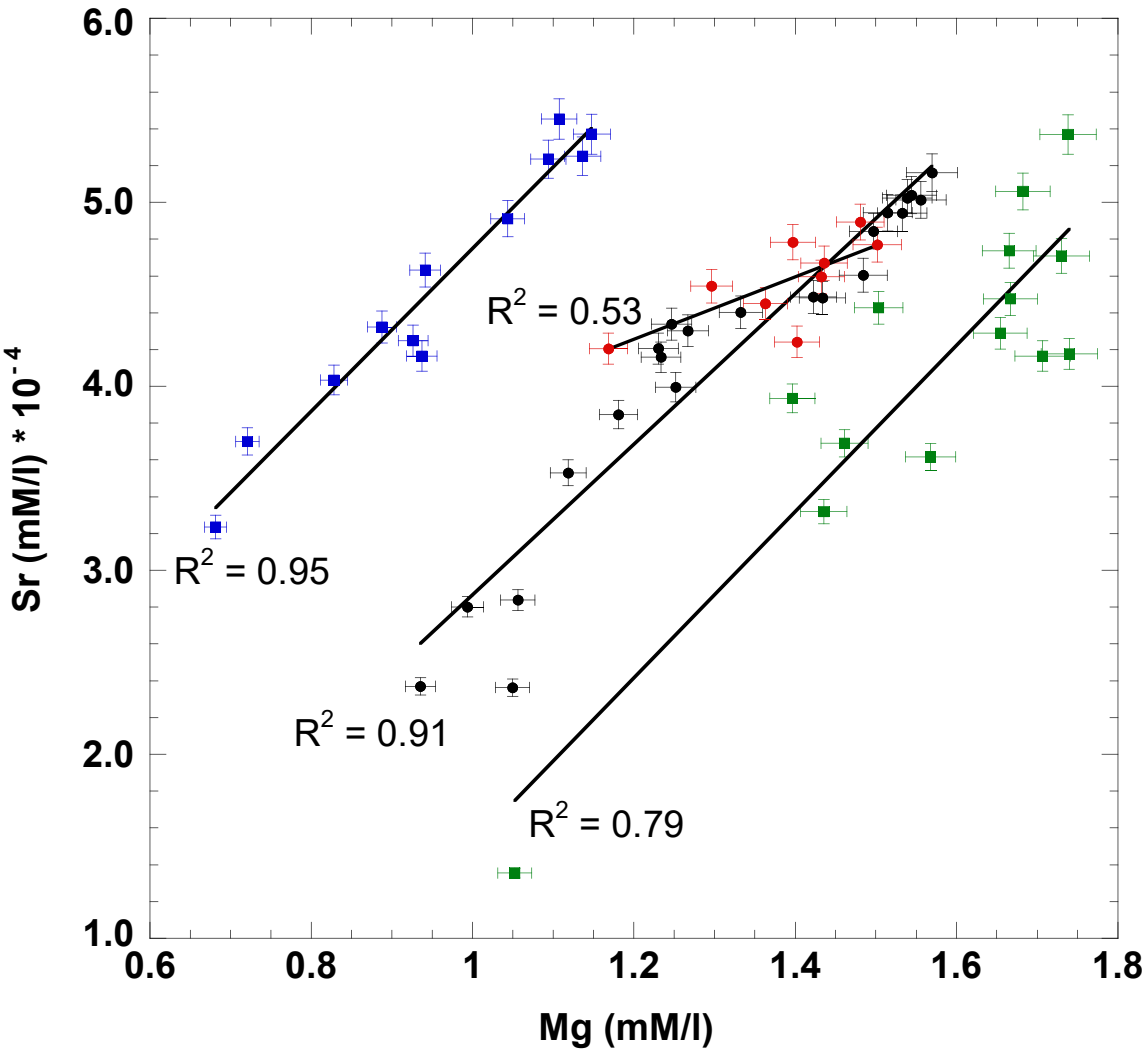

Fig. 2.9. Cross plots of Sr vs. Mg concentrations in DeSoto Caverns drip-water. Symbols representing drip-water sites as in Figure 2.1. Regression lines of individual drip sites exhibit statistically significant positive correlations between Sr and Mg, suggesting prior carbonate precipitation (PCP) upstream of the drips that are feeding the stalagmites.

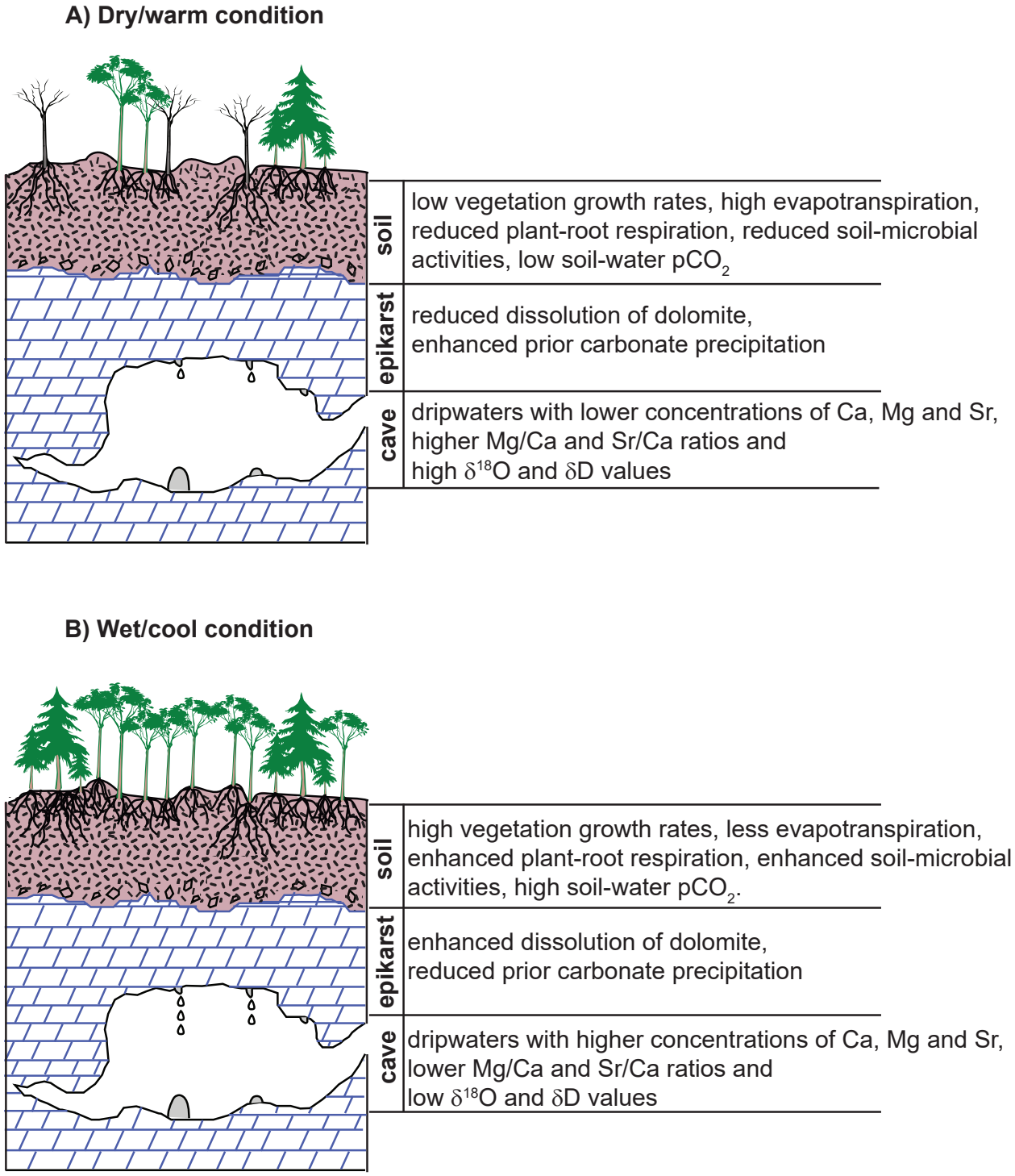

Fig. 2.10. Cartoon of the karst landscape at DeSoto Caverns summarizing the factors controlling the geochemistry of cave drip-water, and speleothems. (A) Factors controlling the geochemistry of drip- water during warm/dry conditions, and (B) Factors controlling the geochemistry of drip-water during cool/wet conditions.

trace- element concentrations decreased (increased) and their ratios increased (decreased) during the dry (wet) year.

2. Observed interannual variability in trace-element concentrations and Mg/Ca and Sr/Ca ratios are likely controlled by variation in amount of rainfall. This finding corroborates the results of Tremaine and Froelich (2013) at Hollow Ridge Cave. They reported the dependency of Mg/ Ca and Sr/ Ca ratios on rainfall amount, using farmed calcite underlying active drips.

3. Drip-water stable isotope and trace-elemental data reported here have important implications for speleothem-based paleo-hydroclimate interpretations because the hydroclimate proxies are likely to be archived in the speleothems deposited underneath the drips (Cruz et al., 2007; Mattey et al., 2010; Wong et al., 2011).

ACKNOWLEDGEMENTS

I thank Tim Lacy and Allen Mathis III for providing me free access to the cave for observations and samples collection; graduate and undergraduate students who assisted me in fieldwork. I am very much thankful to Dr. Joe Lambert for giving me wise advice and assisting me in the lab work. Trace element measurements were performed by Dr. Sidhartha Bhattacharyya at the University of Alabama. This study was funded by the Gulf Coast Association of Geological Societies (GCAGS faculty and student grants) and multiple University of Alabama student and research grants.

REFERENCES

Aharon, P. and Dhungana, R. 2017: Ocean-atmosphere interactions as drivers of mid-to-late Holocene rapid climate changes: Evidence from high-resolution stalagmite records at DeSoto Caverns, Southeast USA. Quat. Sci. Rev. Vol. 170, 69-81.

Baigorria, G.A., Jones, J.W., Shin, D.W., Mishra, A. and O'Brien, J.J. 2007: Assessing uncertainties in crop model simulations using daily bias-corrected Regional Circulation Model outputs. Clim. Res. Vol. 34, 211-222.

Banner, J.L. and Hanson, G.N. 1990: Calculation of simultaneous isotopic and trace element variations during water-rock interaction with applications to carbonate diagenesis. Geochem. et Cosmochim. Acta, Vol. 54, 3123-3137.

Burns, S.J., Flietmann, D., Matter, A., Neff, U. and Mangini, A. 2001: Speleothem evidence from Oman for continental pluvial events during interglacial periods. Geology, Vol. 29, No. 723-626.

Burns, S.J., Fleitmann, D., Mudelsee, M., Neff, U., Matter, A. and Mangini, A. 2002: A 780-year annually resolved record of Indian Ocean monsoon precipitation from a speleothem from south Oman. Jour. of Geophys. Res., Vol. 107, No. D20, 4434.

Craig, H. 1961: Isotopic Variations in Meteoric Waters. Science, New Ser., Vol. 133, No. 3465, 1702-1703.

Craig, H. 1961: Standard for Reporting Concentration of Deuterium and Oxygen-18 in Natural Waters. Science, New Ser., Vol. 133, No. 3467, 1833-1834.

Cruz, F.W., Karmann, I., Viana, O., Burns, S. J., Ferrari, J. A., Vuille, M., Sial, A.N. and Moreira, M. Z. 2005: Stable isotope study of cave percolation waters in subtropical Brazil: Implications for paleoclimate interferences from speleothems, Chem, Geology, Vol. 220, 245-262.

Cruz, F.W., Burns, S. J., Jercinovic, M., Karmann, I., Sharp, W.D., and Vuille, M. 2007: Evidence of rainfall variations in Southern Brazil from trace element ratios (Mg/Ca and Sr/Ca) in a Late Pleistocene stalagmite. Geochem. et Cosmochim. Acta, Vol. 71, Issue 9, 2250-2263.

Dietzel, M., Gussone, N. and Eisenhauer, A. 2004: Co-precipitation of Sr^{2+} and Ba^{2+} with aragonite by membrane diffusion of CO2 between 10 and 50 °C. Chem. Geol., Vol. 203, Issues 1-2, 139- 151.

Epstein, S. and Mayeda, T. 1953: Variation of ^{18}O content of waters from natural sources. Geochem. et Cosmochim. Acta, Vol. 5, Issue 5, 213-224.

Fairchild, I.J., Borsato, A., Tooth, A.F., Frisia, S., Hawkesworth, C.J., Huang, Y., McDermott, F. and Spiro, B. 2000: Controls on trace element (Sr-Mg) compositions of carbonate cave waters: implications for speleothem climatic record. Chem. Geology, Vol. 166, Issues 3-4, 255-269.

Fairchild, I.J. and Treble, P.C. 2009: Trace elements in speleothems as recorders of environmental change. Quat. Sci. Rev., Vol. 28, Issues 5-6, 449-468.

Fairchild, I.J. and Baker, A. 2012: Speleothem science: from process to past environments. John Wiley & Sons.

Feng, S., Hu, Q., Wu, Q. and Mann, M.E. 2013: A Gridded Reconstruction of Warm Season Precipitation for Asia Spanning the Past Half Millennium. Jour. of Climate, Vol. 26, 2192-2204.

Fleitmann, D., Burns, S.J., Mudelsee, M., Neff, U., Kramers, H., Mangini, A. and Matter, A. 2003a: Holocene Forcing of the Indian Monsoon Recorded in a Stalagmite from Southern Oman. Science, Vol. 300, 1737-1739. Hendy, C.H. 1971: The isotopic geochemistry of speleothems 1. The calculation of the effects of different modes of formation on the isotopic composition of speleothems and their applicability as palaeoclimatic indicators. Geochem. et Cosmochim. Acta, Vol. 35, Issue 8, 801-824.

Gat, J.R., Shemesh, A., Tziperman, Eli., Hecht, A., Georgopoulos, D. and Basturk, O. 1996: The stable isotope composition of waters of the eastern Mediterranean Sea. Jour. of Geophys. Res. Vol. 101, No. C3, 6441-6451.

Gaetani, G.A. and Cohen, A.L. 2006: Element partitioning during precipitation of aragonite from seawater: A framework for understanding paleoproxies. Geochem. et Cosmochim. Acta, Vol. 70, Issue 18, 4617-4634.

Guan, H., Zhang, X., Skrzypek, G., Sun, Z. and Xu, X. 2013: Deuterium excess variations of rainfall events in a coastal area of South Australia and its relationship with synoptic weather systems and atmospheric moisture sources. Jour. of Geophys. Res, Vol. 118, 1123-1138.

Horita, J. 1988. Hydrogen isotope analysis of natural waters using an H_2 – water equilibrium method: a special application to brines. Chem. Geol (Iso. Geosc. Sec), Vol. 72, 89-94.

Hendy, C.H. 1971: The isotopic geochemistry of speleothems-I. The calculation of the effects of different modes of formation on the isotopic composition of speleothems and their applicability as paleoclimatic indicators. Geochem. et Cosmochim. Acta, Vol. 35, Issue 8, 801-824.

Huang, Y. and Fairchild, I.J. 2001: Partitioning of Sr^{2+} and Mg^{2+} into calcite under karst-

analogue experimental conditions. Geochem. Cosmochim. Acta, Vol. 65, No.1, 47-62.

Johnson, K.R., Hu, C., Belshaw, N.S., Henderson, G.M. 2006: Seasonal trace-element and stable- isotope variations in a Chinese speleothem: The potential for high-resolution paleomonsoon reconstruction. Earth and Planet. Sci. Lett., Vol. 244, Issues 1-2, 394-407.

Karmann, I., Cruz, F.W., Viana, O., and Burns, S.J. 2007: Climate influence on geochemistry parameters of waters from Santana-Pérolas cave system, Brazil. Vol. 244, Issues 1-2, 232-247.

Kitano, Y., Kanamori, N. and Oomori, T. 1971: Measurements of distribution coefficients of strontium and barium between carbonate precipitate and solution – Abnormally high values of distribution coefficients measured at early stages of carbonate formation. Geochem. Jour., Vol. 4, 183-206. Lachniet. M.S. 2009: Climatic and environmental controls on speleothem oxygen-isotope values. Quat. Sci. Rev., Vol. 28, Issues 5-6, 412-432.

Lambert, W.J. and Aharon, P. 2010: Oxygen and hydrogen isotopes of rainfall and drip-water at DeSoto Caverns (Alabama, USA): Key to understanding past variability of moisture transport from the Gulf of Mexico. Geochem. Cosmochim. Acta, Vol. 74, 846-861.

Luo, W., Wang, S., Xie, X. 2012: A comparative study on the stable isotopes from precipitation to speleothems in four caves of Guizhou, China. Chemie der Erde- Geochem, Vol. 73, Issue 2, 205- 215.

McDonald, J., Drysdale, R., Hill, D., Chisari, R. and Wong, H. 2007: The hydrochemical response of cave drip-waters to sub-annual and inter-annual climate variability, Wombeyan Caves, SE Australia. Chem. Geology, Vol. 244, Issues 3-4, 605-623.

Mattey, D., Lowry, D., Duffet, J., Fisher, R., Hodge, E. and Frisai, S. 2008: A 53 year seasonally resolved oxygen and carbon isotope record from a modern Gibraltar speleothem: Reconstructed drip-water and relationship to local precipitation. Earth Planet. Sci. Lett., Vol 269, 80-95.

Mattey, D.P., Fairchild, I.J., Atkinson, T.C., Latin, J.P., Ainsworth, M. and Durell, R. 2010: Seasonal microclimate control of calcite fabrics, stable isotopes and trace elements in modern speleothem from Michaels Cave, Gibraltar. Geol. Soci. London, Spec. Pub. Vol. 336, 323-344.

Nelson, S.T. 2000: A simple, practical methodology for routine VSMOW/SLAP normalization of water samples analyzed by continuous flow methods. Rapid Commun. Mass Spectrum, Vol. 14, 1044-1046.

Oster, J.L., Montañez, I.P. and Kelley, N.P. 2012: Response of a modern cave system to large seasonal precipitation variability. Geochem. et Cosmochim. Acta, Vol. 91, 92-108.

Rozanski, K., Araguás-Araguás, L. and Gonfiantini, R. 1993: Isotopic Patterns in Modern Global

Precipitation, in Climate Change in Continental Isotopic Records. Geophysical Monograph, Vol 78, Americal Geophysical Union. 1-36.

Samani, Z. 2000: Estimating solar radiation and evapotranspiration using minimum climatological data. J. Irrig. Drain. Eng. Vol. 126, 265-267.

Schroeder, M. J., Glovinsky M., Henricks, V.F., Hood, F.C. and Hull, M.K. 1964: Synoptic weather types associated with critical fire weather. Defense Documentation Center for Scientific and Technical Information, Cameron Station Alexandria, VA, 492 pp.

Sinclair, D.J. 2011: Two mathematical models of Mg and Sr partitioning into solution during incongruent calcite dissolution. Implications for drip-water and speleothem studies. Chem, Geol. Vol. 283, 119-133.

Tooth, A.F. and Fairchild, I.J. 2003: Soil and karst aquifer hydrological controls on the geochemical evolution of speleothem-forming drip-waters, Crag Cave, southwest Ireland. Jour. of Hydro. Vol. 273, Issues 1-4, 51-68.

Treble, P.C., Fairchild, I.J., Griffiths, A., Baker, A., Meredith, K.T., Wood, A. and McGuire, E. 2015: Impacts of cave air ventilation and in-cave prior calcite precipitation on Golgotha Cave drip-water chemistry, southwest Australia. Quat. Sci. Rev, Vol. 127, 61-72.

Tremaine, D.M., Froelich, P.N. and Wang, Y. 2011: Speleothem calcite farmed in situ: Modern calibration of $\delta^{18}O$ and $\delta^{13}C$ paleoclimate proxies in a continuously-monitored natural cave system. Geochem. et Cosmochim. Acta, Vol. 75, Issue 17, 4929-4950.

Tremaine, D.M. and Froelich, P.N. 2013: Speleothem trace element signatures: A hydrologic geochemical study of modern cave drip-waters and farmed calcite. Geochem. et Cosmochim. Acta, Vol. 121, 522-545.

Wang, Y., Cheng, H., Edwards, L.R., Kong, X., Shao, X., Chen, S., Wu, J., Jiang, X., Wang, X. and An, Z. 2008: Millennial- and orbital-scale changes in the East Asian monsoon over the past 224,000 years. Nature Lett. Vol. 451, 1090-1093.

Wong, C.I., Banner, J.L., Musgrove, M. 2011: Seasonal drip-water Mg/Ca and Sr/Ca variations driven by cave ventilation: Implications for and modeling of speleothem paleoclimate records. Geochem. et Cosmochim. Acta, Vol. 75, Issue 12, 3514-3529.

Zhong, S. and Mucci, A. 1989: Calcite and aragonite precipitation from seawater solutions of various salinities: Precipitation rates and overgrowth compositions. Chem. Geol., Vol. 78, 283- 299.

CHAPTER 3

VENTILATION EFFECTS ON CAVE AIR pCO_2 AND VARIATION IN DRIP-WATER CARBONATE CHEMISTRY AT DESOTO CAVERNS (ALABAMA, USA)

ABSTRACT

Paleoclimatic interpretation of speleothem $\delta^{13}C$ values is under-utilized owing to the complexity of carbon transport and isotope fractionation in the karst system. Here I present the results of a 2-year monitoring study at DeSoto Caverns aiming to understand how cave ventilation affects seasonal cave-air pCO_2, drip-water dissolved inorganic carbon [DIC], $\delta^{13}C_{DIC}$, pH, alkalinity, Saturation Index of aragonite (SI_{AR}), and subsequent growth rates and $\delta^{13}C$ of stalagmites. The highest cave air pCO_2 of 5.0 (atm × 10^3) with the lowest $\delta^{13}C_{cave\ air\ CO2}$ (-22.9 ‰V-PDB) and $\delta^{18}O_{cave\ air\ CO2}$ (37.8 ‰ V-SMOW) were measured in summer, when substantially warmer external air relative to cave air leads to cave air stagnation. In contrast, the lowest cave-air pCO_2 of 0.48 (atm × 10^3) with the highest $\delta^{13}C_{CO2}$ (-12.0 ‰ V-PDB) and $\delta^{18}O_{CO2}$ (46.1 ‰ V-SMOW) were measured in winter when substantial cooling of the external air relative to the cave air leads to vigorous ventilation.

[DIC] and $\delta^{13}C_{DIC}$ of drip waters range from 1.2 to 4.2 mM and -11.4 to -3.4 (‰ V-PDB) respectively. [DIC] and $\delta^{13}C_{DIC}$ show seasonal variability and are inversely related. Drip-waters pH and SI_{AR} range from 7.04 to 8.53 and -0.55 to 0.76 respectively, and exhibit seasonal coherency with cave air pCO_2. Alkalinity of drip waters ranges from 6.88 to 2.25 meq/l and is highest during March-April. These data suggest that winter-summer contrast in cave ventilation exerts a dominant control on carbonate chemistry. Rapid aragonite deposition is predicted during

late winter/early spring at DeSoto Caverns.

1. INTRODUCTION

Interpretation of speleothem $\delta^{13}C$ time series is traditionally limited to climate-induced processes above the cave, such as the ratio of C3 to C4 plant species (Dorale et al., 1992; Denniston et al., 1999) and the relative contribution of soil CO_2 versus atmospheric CO_2 to dissolved inorganic carbon (Genty et al., 2001). One critical assumption concerning the validity of such interpretations is that the cave deposits are precipitated in a stable cave atmosphere. Hence, changes in the carbon chemistry of the deposits would be controlled primarily by environmental variability (e.g., rainfall amount, vegetation type, etc.) outside the cave. Recent advances in cave monitoring, however, have demonstrated unequivocally that the atmosphere within a cave does not remain stable as previously thought. During the winter months, those caves whose entrances are topographically higher than the cave chambers may be ventilated vigorously when there is exchange between external cold and dense air, and relatively warm and less dense cave air. During the summer months ventilation may weaken considerably because of stagnation of the relatively cool and dense cave air (Frisia et al., 2000; Baldini et al., 2006; Banner et al., 2007).

A number of researchers (e.g., Spötl et al., 2005; Banner et al., 2007; Baldini et al., 2008; Kowalczk and Froelich, 2010) suggested that in order for speleothem deposition to occur the cave atmosphere must be ventilated with the external atmosphere. These authors (op. cit.) argued that strong cave ventilation lowers the level of cave air CO_2 concentrations, enhances CO_2 degassing from drip waters, and consequently increases saturation level of carbonate, thus promoting deposition of the speleothems. Other authors (e.g., Cai et al., 2011) proposed that variations in drip flow rates control cave air pCO_2 and demonstrated that during rainy periods,

CO_2 flux into the cave is high due to increased drip rates whereas during dry periods, CO_2 flux is relatively low due to decreased drip rates.

Drip water and speleothem carbon chemistry measurements were previously acquired over a 3-year period (June-2005 to May-2008) by Lambert and Aharon (2011) from the thickly (~ 40 m) capped back chamber at DeSoto Caverns (Fig. 3.1). These authors (op. cit.) proposed a cave- ventilation model for DeSoto Caverns in the absence of critical cave air pCO_2 data to support their interpretation. Here I present the results and interpretation of a 2-year (January 2012 to December 2013) cave-monitoring program at DeSoto Caverns that document carbon chemistry of both cave air and drip water collected from the thinly (~ 10 m) capped front chamber of the cave. Specifically, this study addresses how changes in cave ventilation affect the interaction of carbon in the cave air, cave drip-water, and speleothem deposition. The 2–year cave monitoring study was designed to (i) examine the temporal and spatial variability of dissolved inorganic carbon and $\delta^{13}C_{DIC}$ in drip waters; (ii) compare drip-water carbon-chemistry with the results acquired from the thickly capped back chamber of the cave (Lambert and Aharon, 2011); (iii) investigate cave air pCO_2, $\delta^{13}C_{CO2}$ and $\delta^{18}O_{CO2}$ variation and their influence on drip water carbon chemistry, and (iv) test the cave air ventilation model proposed by Lambert and Aharon (2011).

2. STUDY SITE AND REGIONAL CLIMATE

DeSoto Caverns (86°16’36” W, 33°18’26” N) is located on the outskirts of Childersburg, AL in the foothills of the Appalachian Mountains. The cave lies within an Upper Ordovician dolomite karst system and is separated from, the Gulf of Mexico, the major moisture source, by 365 km of low-elevation coastal plains (Fig. 3.1, inset). The cave, situated at an elevation of 70 m, is approximately 150 m long and has two contiguous segments: i) a large 70 m long by 50 m

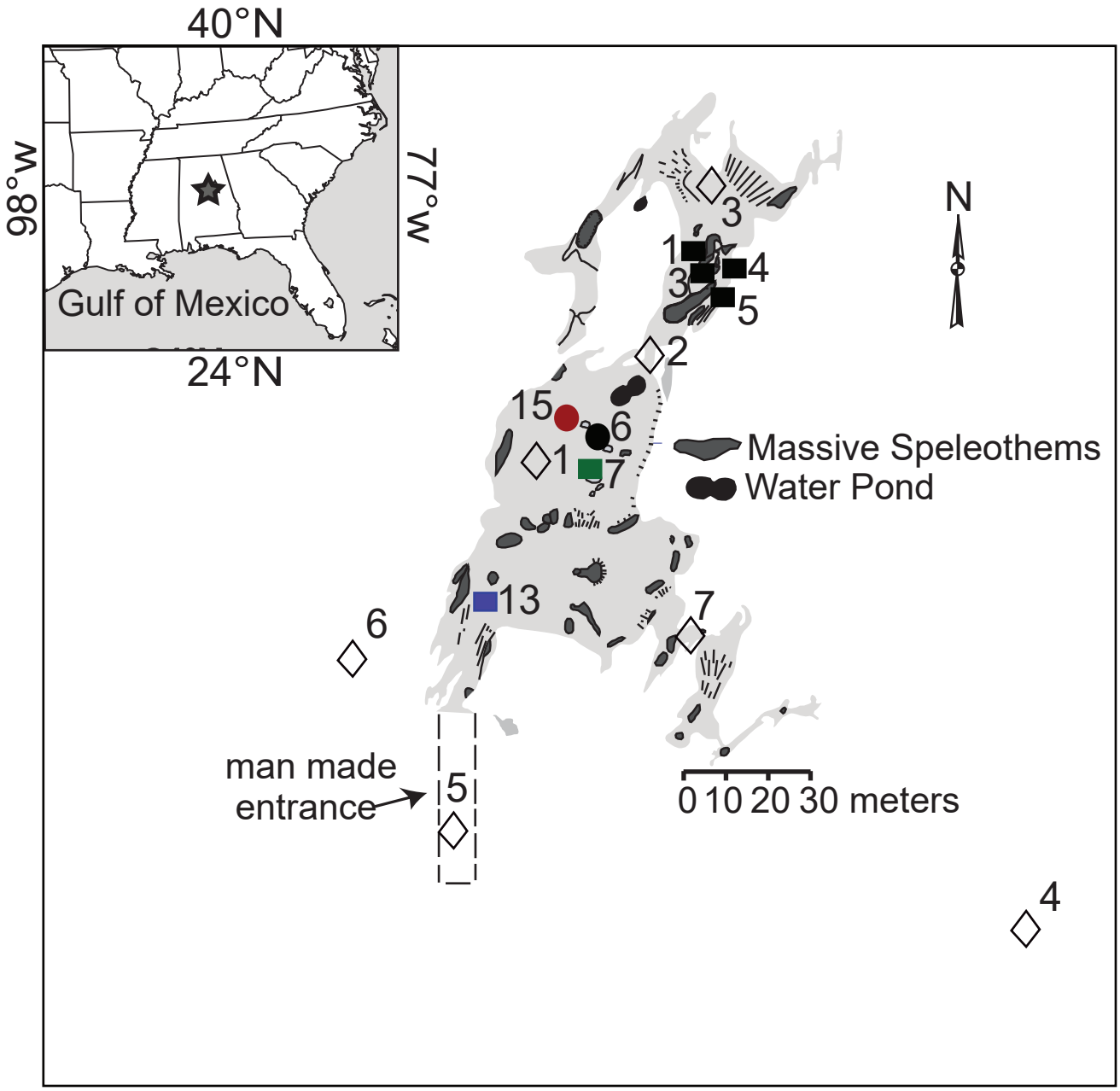

Fig. 3.1. Plan view of DeSoto Caverns (modified after Lambert and Aharon, 2010) showing four drip-water sampling locations: site 6 (solid black circle), site 7 (solid green square), site 13 (solid blue square) and site 15 (solid red circle). Five air-sampling sites within the cave and two atmospheric air-sampling sites outside the cave (empty diamonds). Sampling locations of drips studied by Lambert and Aharon (2010; 2011) in the small back chambers of the cave are shown by solid black squares. The inset shows the map of southeastern US with the location of DeSoto Caverns (solid green star).

wide front chamber with 10 m thick overlying bedrock, and ii) small chambers in the back of the cave with relatively thick (30-40 m) overlying bedrock. The cave entrance is at a topographically higher position than cave chambers with an elevation difference of ~16m. The cave is contains all six common types of speleothems: stalactites, stalagmites, flowstone, soda straw, column and draperies. Both fossil and active speleothems found within the cave were/are deposited as aragonite (Lambert and Aharon, 2010; Aharon and Dhungana, 2017).

The climate of the study area is humid sub-tropical and rainfall occurs throughout the year (Cotton et al., 1974). The area experiences a mean annual air temperature of 17.2 °C and an average annual rainfall total of 1417 mm based on 1958-2004 data (www.ncdc.noaa.gov). Present climate is typified by a moderate seasonality with average monthly air temperatures ranging from ~7°C (January) to ~27°C (July) while average monthly rainfall ranges from ~80 mm (October) to ~150 mm (March) (Lambert and Aharon, 2010). Rainfall is usually well distributed throughout the year with two distinct modes. In winter the collision of opposing cold and warm air masses often results in rain-producing storm systems that are carried eastward by the polar jet stream (Baigorria et al., 2007). In contrast, summer rainfall is typically derived by convection-style thunderstorms whose frequency is influenced by the east-west position of the Bermuda High pressure cell (Schroeder et al., 1964).

3. METHODS

The cave system was monitored monthly for 2 years (Jan. 2012 – Dec. 2013). The air and drip-waters were sampled for geochemical analysis with the goal of unraveling the dominant factors controlling the system's carbon chemistry and resultant $\delta^{13}C$ of speleothems.

3.1. FIELD METHODS

3.1.1. AIR pCO_2

The air parameters analyzed include pCO_2, $\delta^{13}C_{CO2}$ and $\delta^{18}O_{CO2}$ of cave-air at five stations and external-air at two stations (Fig. 3.1). Sampling locations were chosen carefully in order to understand how cave-air CO_2 concentration and stable carbon isotope chemistry of the cave air CO_2 varies from the entrance to the back of the cave. Sample vials consisted of 12 ml borosilicate Labco Exetainers, which can be sealed easily by hand using plastic caps with an internal rubber septum. For each study site location, three sample vials were used and the results averaged in order to obtain the desired data. Vials were opened for ~5 minutes and recapped after gas exchange. Spötl (2004) demonstrated that this sampling technique allows for adequate storage of gas samples for at least 14 days.

3.1.2. CAVE DRIP-WATERS

The cave drip-water parameters analyzed include dissolved inorganic carbon [DIC], $\delta^{13}C_{DIC}$, pH, alkalinity and aragonite saturation index (SI_{AR}). Drip water was collected from four locations in the front chamber of the cave (Fig. 3.1) where the cap rock is relatively thin and drip falling distance is ~25 m. Among the four sampling drips, drips 6, 7 and 15 are stalagmite-precipitating drips that lie at the center of the chamber whereas drip 13 does not precipitate a stalagmite and lies close to the entrance of the cave. Drip water was accumulated in clean plastic bags that were placed in 1000 ml nalgene bottles. 15-cm diameter funnels were used to direct the falling drips into the plastic bags. Aliquots of drip water for alkalinity and trace-element measurements were stored in 125 ml nalgene bottles and acid-washed 60 ml nalgene bottles, respectively. In both cases High Density Polyethylene (HDPE) nalgene bottles were used. The pH and temperature of drip-waters were measured in the field using an Orion StarTM A121

portable pH-temperature meter with an accuracy of ± 0.01 and ± 0.1°C, respectively.

With the exception below, drip-water samples for [DIC] and $\delta^{13}C_{DIC}$ were stored in 15 ml septum-capped airtight glass serum bottles. The exception occurred during the period December 2012-September 2013 when 8 ml Low Density Polyethylene (LDPE) nalgene bottles were used. In both cases bottles were completely filled to avoid headspace and a few grains of $HgCl_2$ were added in order to prevent microbial activity. Most drip-water samples collected in LDPE nalgene bottles during the second monitoring year were found to yield erroneous DIC and $\delta^{13}C_{DIC}$ results because of poor gas retention and were subsequently discarded. Drip flow rates were estimated by measuring the fluid volume collected over a known time interval.

3.1.3. CAVE AIR TEMPERATURE AND RELATIVE HUMIDITY

Cave-air temperature and relative humidity were monitored between January and March 2012 and November 2012 to Dec 2013 using an HTAB-176 Certified Hygro/Temp Indicator and between April and October 2012 using an HOBO Pro v2 Temp/RH Data Logger.

3.2. LABORATORY METHODS

3.2.1. AIR-CO_2 ISOTOPE ANALYSIS

Cave- and external air CO_2 were measured using a Delta V-plus Gasbench following a method described by Spötl (2004). Air-CO_2 samples were analyzed within a few days (typically the following day) of collection. A calibration curve was derived based on two end-members: (i) Air-CO_2 collected in open air was assumed a CO_2 value of 400 ppm (Baumann et al., 2012), and (ii) He/CO_2 tank with a known CO_2 concentration of 2930 ppm. Analytical precision of the CO_2 measurement is better than 2% based on sample repeats. Five repeats of CO_2 released by reaction with orthophosphoric acid from the NBS-19 standard were measured within each batch of samples to calibrate the $\delta^{13}C_{CO2}$ values to the V-PDB scale. Analytical precisions for $\delta^{13}C_{CO2}$

and $\delta^{18}O_{CO2}$ measurements are ±0.1‰ and ±0.4‰ respectively, based on sample repeats. In this study, $\delta^{18}O$ values of cave air CO_2 are used to better understand cave ventilation processes. Because oxygen isotope ratios of cave air CO_2 were not measured by dissolving calcite in orthophosphoric acid at 25 °C (according to the definition of PDB standard) and the fractionation factor for the phosphoric acid extraction of CO_2 from calcite is 10.2‰ (Sharma and Clayton, 1965; Kim et al., 2007), $\delta^{18}O$ values of cave air CO_2 are reported here as V-SMOW using the relationship between PDB and SMOW as follows:

$$\delta^{18}O_{CO2}\ (‰\ V-SMOW) = 1.04143\ [\delta^{18}O_{(CO2-PDB)} + 10.2 + 41.92906] \quad (1)$$

3.2.2. DETERMINATION OF CAVE DRIP-WATER CARBONATE ALKALINITY, DIC, CA^{2+} AND $\delta^{13}C_{DIC}$

Carbonate alkalinity measurements were performed using the Gran titration method (Gran, 1952). Drip-water was titrated with 0.1 N HCl within 24 hours of collection and reported as meq/ liter. Titrations were done in a 1000 ml Machlett Buret (Fisher Scientific) that has an acid drop accuracy of ± 0.05 ml. Reproducibility of the alkalinity measurements is ±0.08 meq/l or better.

Aragonite saturation index (SI_{AR}) of drip waters was calculated using the computer program PHREEQCI (Parkhurst and Appelo 1999; Charlton and Parkhurst, 2002) where water temperature, pH, HCO_3^-, and Ca^{2+} were used as the major input parameters. For Ca^{2+} measurements the drip-water samples were filtered through 0.2-µm filters and acidified with nitric acid. Analyses were performed using a Perkin Elmer Optima 3000 DV ICP-OES (Inductively Coupled Plasma – Optical Emission Spectrometer). Solute was calibrated using multiple element standards from CPI International Inc. and quality-control standards from High Purity Inc. Errors for Ca^{2+} measurements are reported to be better than 2% based on standard analysis.

The measurements of [DIC] and $\delta^{13}C_{DIC}$ of the drip-waters were performed on a Gasbench online with a CF-IRMS (modified Delta-plus). Both [DIC] and $\delta^{13}C_{DIC}$ data were derived from one sample aliquot (0.7 ml volume; method adapted from Spötl, 2005). [DIC] concentrations are expressed as mM/l, and carbon-isotope data are reported relative to V-PDB standard calibrated through the NBS-19 standard. Multiple DIC standards were produced between 0 and 6 mM by dissolving Na_2CO_3 into a known volume of distilled water. Calibration curves, derived from these known DIC concentrations relative to mass 44 beam intensity, were used to determine [DIC] of sample fluids. Errors for [DIC] measurements are reported to be better than 4% based on standard repeats. Analytical precisions for the $\delta^{13}C_{DIC}$ measurements are ±0.2‰, based on standard repeats.

pCO_2 of drip-water was estimated using the following equation derived from measured [DIC] and pH values (modified from Faust and Aly, 1981).

$$pCO_2 = \frac{[DIC]\times[\alpha H_2CO_3]}{K_H} \quad (2)$$

where, [DIC] concentrations are expressed in moles, the $[\alpha H_2CO_3]$ variable is a function of pH of drip-waters and K_H are temperature-dependent Henry's law constants for CO_2(g) solubility in water and expressed in mole/l/atm.

4. RESULTS

4.1. DRIP FLOW-RATE TIME SERIES

The monthly rainfall records reported here are from the town of Childersburg, 7 km away from DeSoto Caverns. The rainfall record indicates that total annual precipitation in 2012 (1428 mm) was lower by about 30% relative to 2013 (1936 mm) (Fig. 3.2 A). The monthly water budget exhibits a 6-month long moisture-deficit in 2012 compared to only 2 months in 2013 (Fig 3.2 B). The cave drip-water flow rates were substantially higher in 2013 than in 2012; this

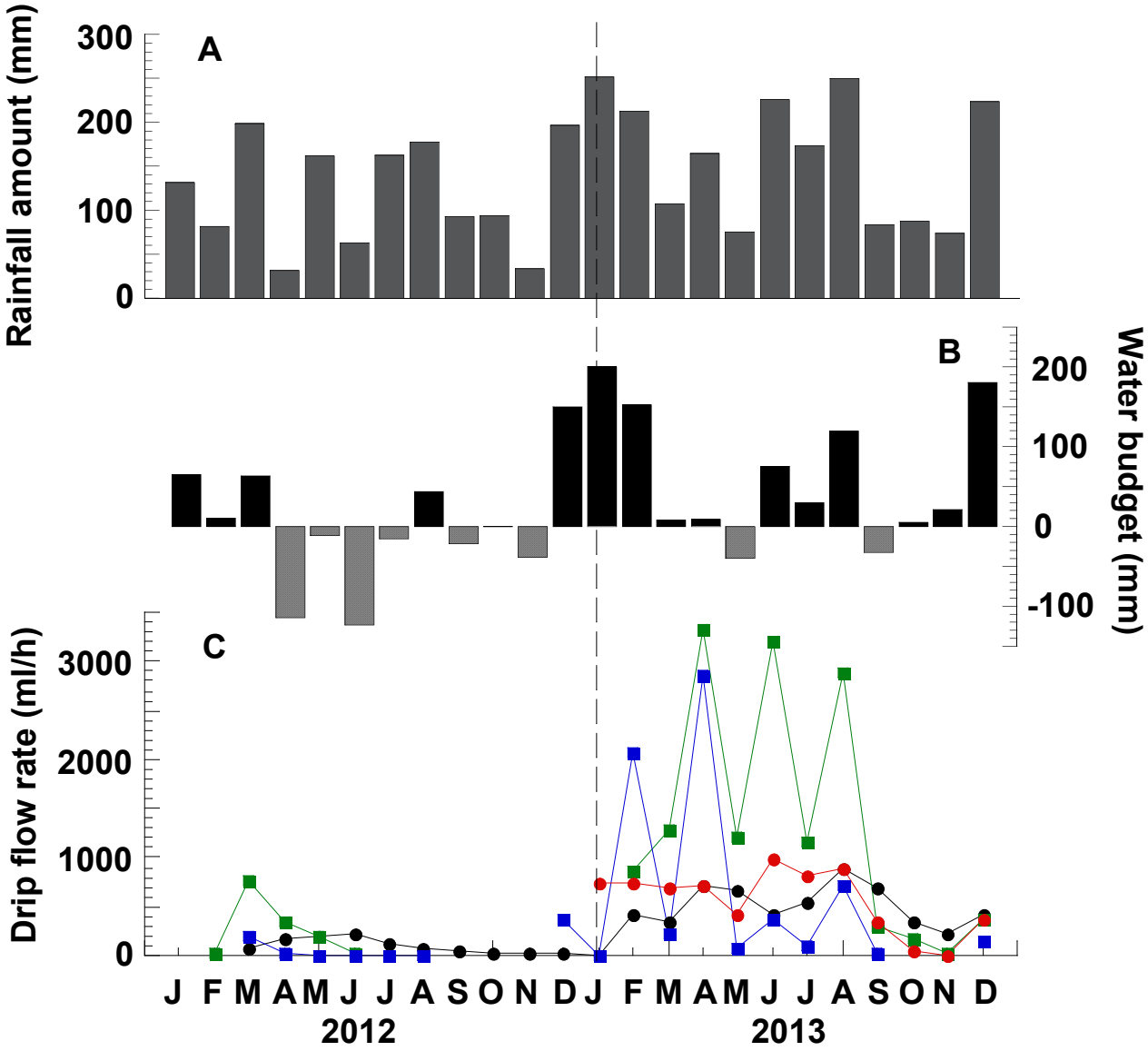

Fig. 3.2. Drip-flow rates are compared to coeval rainfall amount and monthly water budget. (A) Monthly rainfall record at Childersburg water plant station from January 2012 to December 2013 (www.ncdc.noaa.gov). (B) Soil-moisture budget was calculated using the equation from Samani (2000) including local Precipitation and Evapo-Transpiration (P-ET).(C) Drip-flow rate (ml/h) time series for all four drips. Refer to Fig. 3.1 for drip site locations and symbols.

difference corresponds to variation in water budget. A lag of 1-3 months is observed between the start of positive monthly water budgets and the initiation of high drip flow rates (Figs. 3.2, B and C). The relatively lower (higher) rainfall and higher (lower) evapotranspiration during 2012 as compared to 2013 reduced (enhanced) the drip-water discharge into the cave. Among four sampled drip sites, only drip site 6 had continuous drip-water discharge throughout the two-year study period. The average drip flow rate at site 6 was substantially higher by a factor of ~4.8 in 2013 (471.3 ml/h) than in 2012 (97.3 ml/h). The lowest monthly drip flow rate of 3.0 ml/h was observed at site 13 in June 2012 whereas the highest drip flow rate of 3330 ml/h was observed at site 7 in April 2013 (Figs. 3.1 and 3.2 C).

4.2. CAVE AIR DYNAMICS

The seasonality observed in the cave air parameters has been summarized in Table 3.1. The monthly cave air temperature at DeSoto Caverns fluctuated between 17 °C and 19.2 °C with a mean temperature of 18.2 ± 0.1 °C occurring between January 2012 and December 2013 (Fig. 3.3 A). The relative humidity inside the cave was always > 95% over the study period (Table 3.1; Appendix 3.1). The CO_2 concentrations at all sampling sites within the cave increased in summer (May-Oct) and decreased in winter (Nov-Apr) (Figure 3.3 B; Appendix 3.2). The lowest pCO_2 of 0.48 (atm × 10^3) was measured near the entrance (site 5) in January 2012 and the highest of 5.0 (atm × 10^3) was measured at the back of the cave (site 3) in August 2012. The average cave air CO_2 concentration during peak summer months (Jun-Sept) of 2013 was about 21% lower than during the same months in 2012. The average pCO_2 measured outside the cave at sites 4 and 6 were 0.39 (atm × 10^3) and 0.41 (atm × 10^3) respectively, which are close to the current atmospheric pCO_2 level of 0.4 (atm × 10^3; Baumann et al., 2012). The $\delta^{13}C_{cave\ air\ CO2}$ values decrease during summer and increase during winter and are inversely related to cave

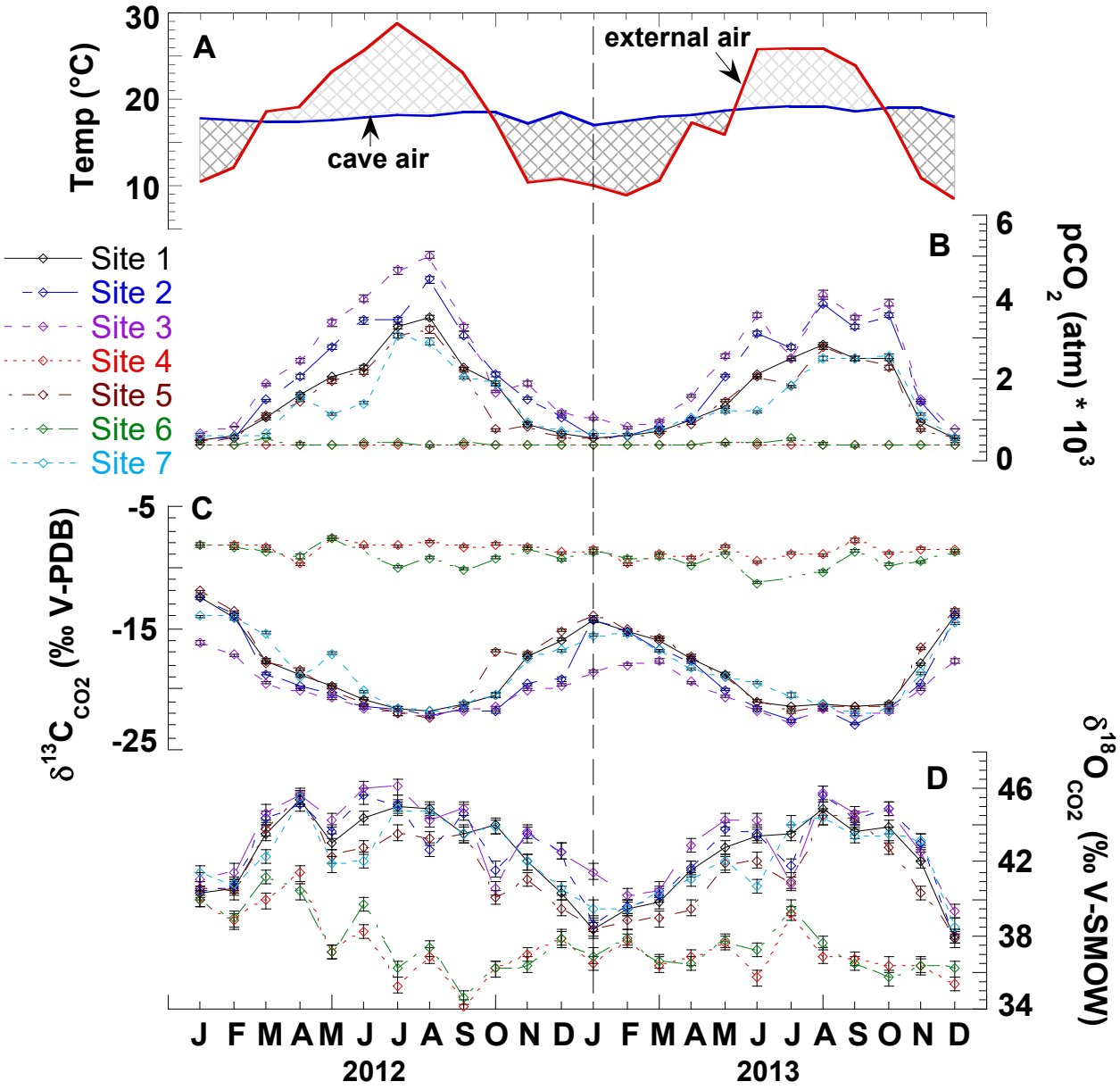

Fig. 3.3. Time series of cave-air monitoring data. (A) Monthly mean air temperature record at Childersburg water plant station (www.ncdc.noaa.gov) and cave-air temperature. (B) Cave- and atmospheric air CO_2 concentrations within and outside the cave. (C) Carbon -isotope composition of air CO_2. (D) Oxygen-isotope composition of air CO_2. Vertical bars represent standard error (1σ). Refer to Fig. 3.1 for drip site locations and symbols.

Table 3.1. Seasonality in cave air parameters. Uncertainties are standard error of the mean (1σ).

Period	Cave T (°C)	RH (%)	Cave Air pCO_2 (atm × 10^3)	$\delta^{13}C_{cave\ air\ CO_2}$ (‰ VPDB)	$\delta^{18}O_{cave\ air\ CO_2}$ (‰ VSMOW)
2-Year Mean	18.2 ± 0.1 (n=24)	100 (n=24)	1.6 ± 0.2 (n=24)	-18.4±0.6 (n=24)	42.4±0.4 (n=24)
Summer	18.5 ± 0.1 (n=12)	100 (n=12)	2.4 ± 0.2 (n=12)	-20.9±0.3 (n=24)	43.9±0.2 (n=24)
Winter	17.8 ± 0.2 (n=12)	100 (n=12)	0.8 ± 0.1 (n=12)	-16.0±0.6 (n=24)	41.0±0.6 (n=24)

pCO_2 (Fig. 3.3 C). The lowest $\delta^{13}C_{cave\ air\ CO2}$ value of -22.9 (‰ V-PDB) was observed at site 2 (i.e., narrow passage that connects the large front chamber to the small back chambers of the cave) in September 2013 and the highest value of -12.0 (‰ V-PDB) was observed at site 5 (i.e., near the cave entrance) in January 2012. The average $\delta^{13}C$ values of CO_2 measured outside the cave at sites 4 and 6 were -8.6 ± 0.1 and -9.5 ± 0.2 (‰ V-PDB) respectively, that are close to the average $\delta^{13}C$ value of -9.4 ± 0.3 (‰ V-PDB) of atmospheric CO_2 (Widory and Javoy, 2003). The $\delta^{18}O_{cave\ air\ CO2}$ was higher during summer (up to 46.1 ‰ V-SMOW at site 3 in July 2012) and lower (down to 37.8 ‰ V-SMOW at site 1 in December 2013) during winter (Fig. 3.3 D). The average $\delta^{18}O$ values of air CO_2 (between September 2012 and December 2013) outside the cave at sites 4 and 6 were 36.9 ± 0.3 (‰ V-SMOW) and 37.1 ± 0.3 (‰ V-SMOW) respectively, which are near the average $\delta^{18}O$ value (34.3 ‰ V-SMOW) of atmospheric CO_2 (Ciais et al., 1997). However, between March and September 2012 the outside cave $\delta^{18}O$ air CO_2 decreased from ~ 41 to 34 ‰ (V-SMOW) at sites 4 and 6 and this trend is likely caused by the warm/dry weather condition during this time interval.

According to Francey and Tans (1987) and Flanagan et al. (1993), the isotopic composition of plant leaf water is the $\delta^{18}O$ primary controlling factor of atmospheric CO_2. Hence, during warm/dry conditions the stomatal closure of the leaves to retain water limits the

isotopic exchange between relatively ^{18}O-enriched leaf water and ^{18}O-depleted atmospheric CO_2, which likely decreases the atmospheric $\delta^{18}O$ value.

Cave air pCO_2 and $\delta^{13}C_{cave\ air\ CO2}$ exhibit a significant negative correlation (Fig. 3.4 A) with the y- intercept of -23.6 ± 0.09 (‰ V-PDB) being close to the $\delta^{13}C$ of soil-CO_2 (-21.7 ‰ V-PDB, Lambert and Aharon, 2011). The negative relationship is likely the result of mixing of two end-member components: (i) atmospheric pCO_2 (0.41 ± 0.01 atm × 10^3) with $\delta^{13}C$ = -9 ±0.1 (‰ V-PDB) (n = 48), and (ii) ^{13}C- depleted soil-CO_2 inclusive of CO_2 degassed from groundwater, respired from plant roots and generated from decay of soil organic matter. Respired soil CO_2 most likely represents the lightest end-member $\delta^{13}C$ values of the cave air (Mattey et al., 2010). $\delta^{18}O_{cave\ air\ CO2}$ shows a significant positive correlation with cave air pCO_2 (Fig. 3.4 B) and its y- intercept value of 45.1 ± 0.2 (‰ V-SMOW) is close to the global mean oxygen-isotope composition of soil-CO_2 (47 ‰ V-SMOW, Ciais et al., 1997). Hence the "Keeling" plots (Keeling, 1958) in Figure 3.4 offer compelling evidence that atmospheric and soil-respired pCO_2 are the dominant end-member components that contribute to the CO_2 cave air at DeSoto Caverns.

4.3. CAVE DRIP-WATER CARBONATE CHEMISTRY

Drip-water CO_2 concentration is generally higher than that of cave air CO_2 and the two parameters are positively correlated (Fig. 3.5). The 2- year time series of hydrochemical parameters monitored at four different drip sites (sites 6, 7, 13 and 15) in the front chamber of DeSoto Caverns (see Appendix 3.3 for the data) are graphed in Figure 3.6. The seasonality observed in drip-water chemistry has been summarized in Table 3.2. Alkalinity was higher during late winter/early spring with an average of 5.8 ± 0.2 meq/l (n = 22) and relatively lower during the summer peak months (Jun-Sept) with an average of 3.7 ± 0.2 meq/l (n = 17).

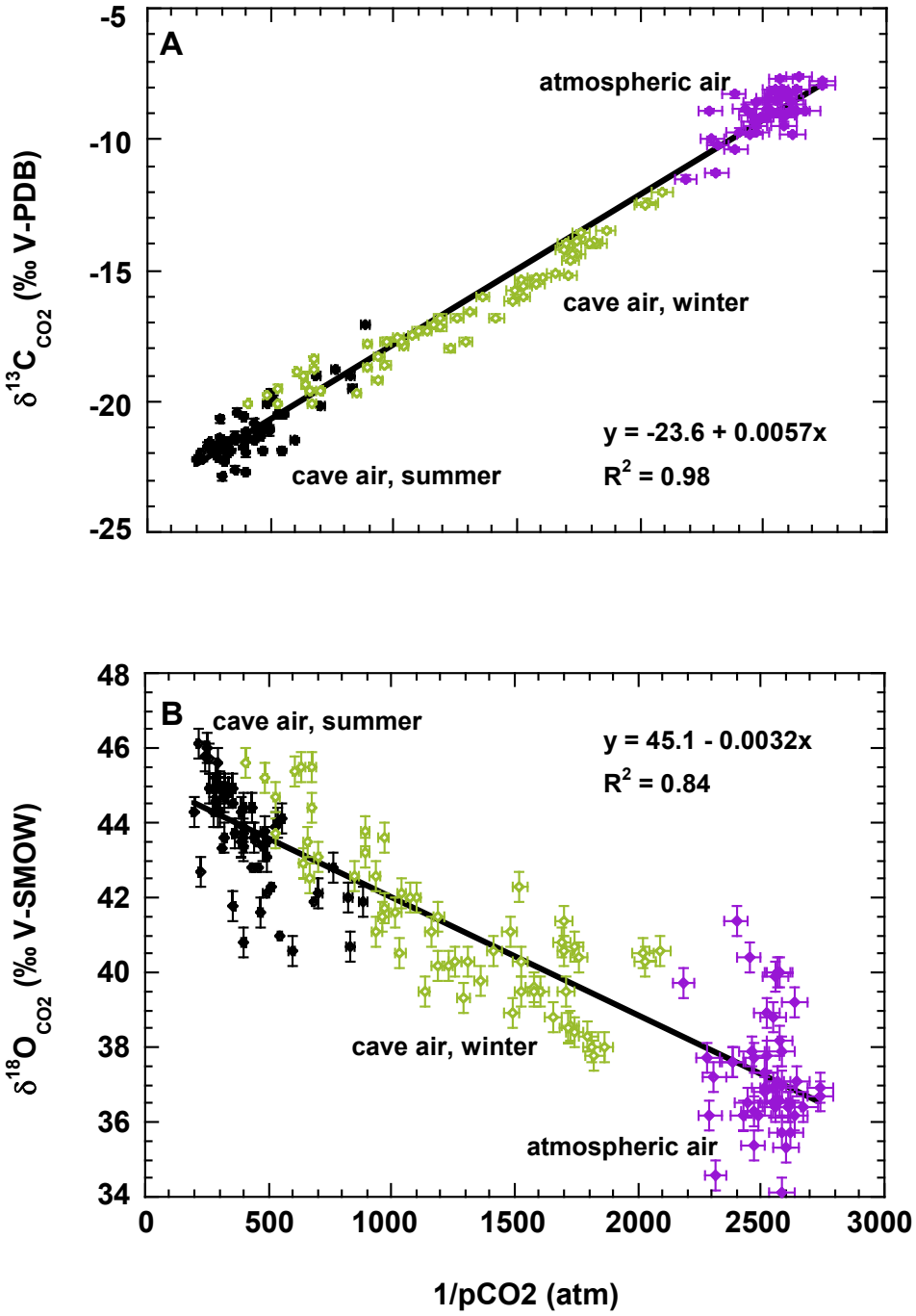

Fig. 3.4. Cross plots of $\delta^{13}C$ and $\delta^{18}O$ measurements vs the reciprocal pCO_2 in cave and atmospheric air CO_2. Horizontal and vertical bars are standard error (1σ). (A) $\delta^{13}C$; (B) $\delta^{18}O$. The significant negative correlation between air pCO_2 and $\delta^{13}C$ air CO_2 is represented by the following best fit equation: $\delta^{13}C_{air\ CO2} = (0.0057 \times 1/pCO_2) - 23.6$ ($r^2 = 0.98$). The $\delta^{18}O_{air\ pCO2}$ shows a significant positive correlation with air pCO_2 and is represented by the following best-fit equation; $\delta^{18}O_{air\ CO2} = (-0.0032 \times 1/pCO_2) + 45.1$ ($r^2 = 0.84$). The best-fit lines represent end-member mixing between two CO_2 sources in the cave atmosphere: atmospheric CO_2 and soil CO_2 (see text).

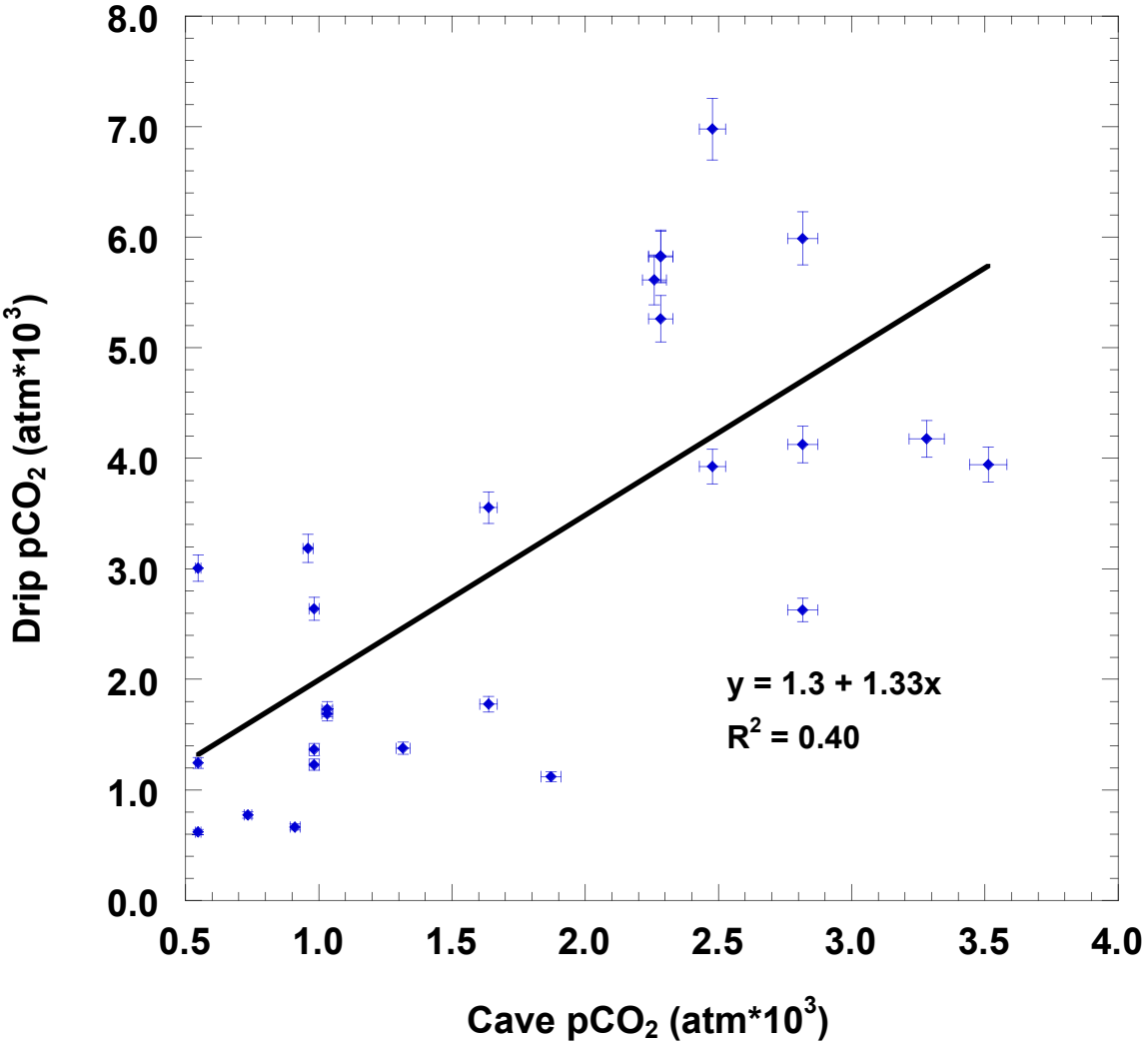

Fig. 3.5. Cross plot of drip-water pCO_2 and cave-air pCO_2. Bars represent standard error (1σ). Drip-water is richer in CO_2 than coeval cave air and the two parameters obey the following linear relationship: drip pCO_2 = (1.33 × cave-air pCO_2) + 1.3 (r^2=0.4).

Table 3.2. Seasonality in cave drip water parameters. Uncertainties are std. error of the mean.

Period	pH	Alkalinity (meq/l)	Ca^{2+} (mM/l)	SI_{AR}	DIC (mM)	$\delta^{13}C_{DIC}$ (‰ VPDB)
2-Year Mean	7.7 ± 0.1 (n=22)	4.6 ± 0.3 (n=17)	1.2 ± 0.1 (n=22)	-0.1 ± 0.1 (n=19)	1st monitoring year (Mean)	
					2.8±0.2 (n= 10)	-8.1±0.5 (n=10)
Summer	7.5 ± 0.1 (n=11)	4.2 ± 0.2 (n=10)	1.3 ± 0.1 (n=12)	-0.2 ± 0.1 (n=11)	2.9±0.3 (n=6)	-8.5±0.8 (n=6)
Winter	7.9 ± 0.1 (n=11)	5.3 ± 0.6 (n=7)	1.1 ± 0.1 (n=10)	0.08 ± 0.1 (n=8)	2.5±0.4 (n=4)	-7.5±0.8 (n=4)

However, alkalinity was exceptionally low in October, November and December 2013 with an average of 2.8 ± 0.1 meq/l (n = 17) (Fig. 3.6 A). The drip-water pH time series exhibit seasonality with an average high of 8.04 ± 0.1 (n=32) and an average low of 7.7 ± 0.1 (n = 31) during winter and summer months, respectively (Fig. 3.6 B). The pH was exceptionally high in December 2013 at all drip sites.

The SI_{AR} of drip-waters ranges from - 0.55 to + 0.76 (Fig. 3.6 C). Drip-water at sites 6 and 7 is under-saturated with respect to aragonite during summer (but in August 2013 drip-water at both drip sites was slightly above the saturation line) and supersaturated during winter. Drip-water at sites 13 and 15 is supersaturated nearly year-round with respect to aragonite. Saturation index is higher exhibits seasonality such that higher during winter and lower during summer.

Drip-water pCO_2 (Fig. 3.6 D) is highest during summer (maximum values up to 6.9 (atm $\times 10^3$)) and lowest (down to near atmospheric CO_2 level) during winter (November and December 2013 are exceptions, where drip pCO_2 values are up to 14.7 and 8.3 (atm $\times 10^3$), respectively) and show an inverse relationship with pH and SI_{AR}. Cave drip-water [DIC] and $\delta^{13}C_{DIC}$ time series are shown in Figures 3.6 E and F, respectively. During the first monitoring year, both parameters varied seasonally (Table 3.1) with summer months exhibiting higher

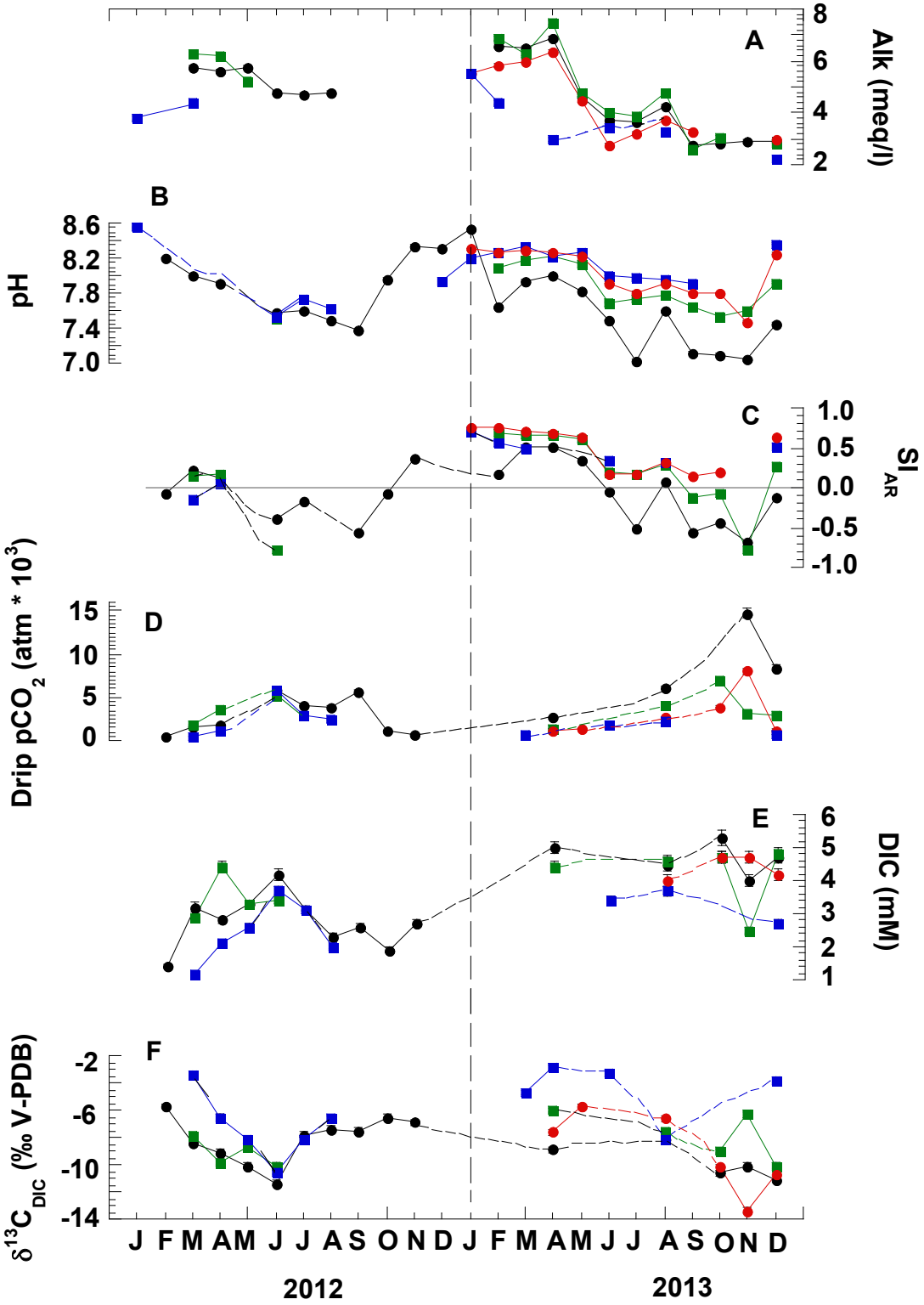

Fig. 3.6 Time series of hydrochemical parameters measured in drip waters at DeSoto Caverns.(A) Alkalinity; (B) pH; (C) Aragonite Saturation Index; (D) Drip water pCO_2; (E) DIC, and (F) $\delta^{13}C$ of DIC. Refer to Fig. 3.1 for drip site locations and symbols.

[DIC] and lower $\delta^{13}C_{DIC}$ values (up to 4.2 mM and down to -11.4 ‰ V-PDB, respectively) and winter months the reverse (down to 1.2 mM and up to -3.4 ‰ V-PDB, respectively). However, during the relatively wet late fall/early winter months of the second monitoring year drip-water showed exceptionally high [DIC] and low $\delta^{13}C_{DIC}$ values. Importantly, $\delta^{13}C_{DIC}$ values show an inverse relationship with drip pCO_2 suggesting that drip-water pCO_2 enrichment derives from external ^{13}C-depleted sources (Fig. 3.7). The seasonal variability discerned here in drip-water [DIC] and $\delta^{13}C_{DIC}$ is consistent with results of drip-water [DIC] and $\delta^{13}C_{DIC}$ measurements made over a 3-yr period (2005 to 2008) in the back chamber of the cave (Lambert and Aharon, 2011).

Carbonate alkalinity and DIC are defined as the sum of charged carbonate species and the sum of all inorganic carbon species in a solution, respectively (Deffeyes, 1965). The major differences between the two definitions are the occurrence of neutral CO_2 in DIC and the doubling of dissolved carbonate in Carbonate Alkalinity, as follows:

$$\text{Carb Alk} = [HCO_3^-] + 2[CO_3^{2-}] \quad (3)$$

$$\text{DIC} = [CO_2]aq + [HCO_3^-] + [CO_3^{2-}] \quad (4)$$

An alkalinity versus [DIC] cross-plot, also known as a Deffeyes diagram (Deffeyes, 1965) (Fig. 3.8) aims to unravel the dominant factors that affect the carbon chemistry of drip-waters. Viewed this way, drip-waters sampled in winter exhibits a trend with a slope of 2:1, suggesting that the dominant dissolved carbon species in the drip-water is $[CO_3^{2-}]$ whereas drip-water sampled in summer show a trend with a slope near 1:1 suggesting the dominant dissolved carbon species is $[HCO_3^-]$. Samples collected during late fall/early winter 2013 show a nearly horizontal distribution indicating that $[CO_2]aq$ is the dominant dissolved carbon species in these samples.

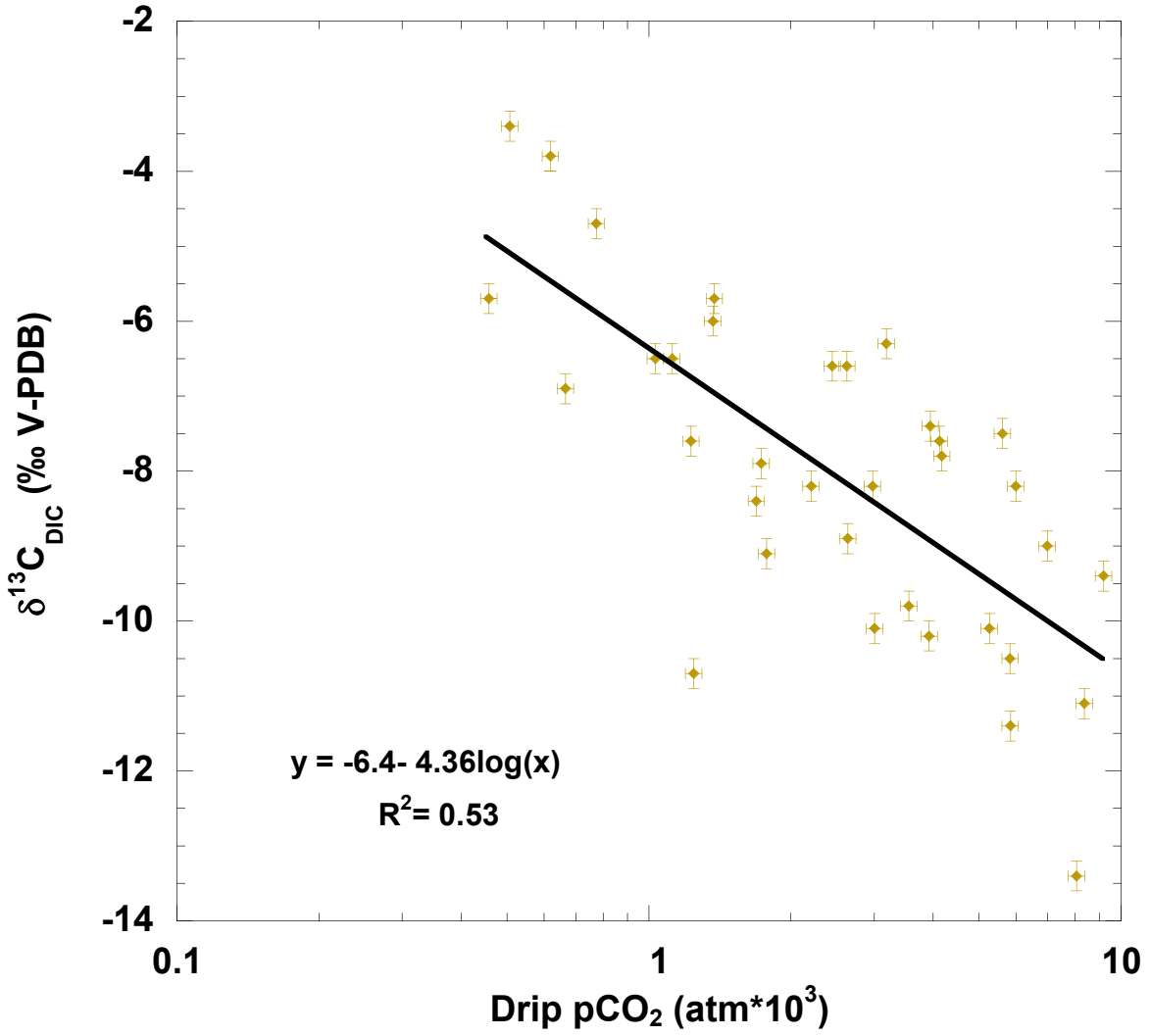

Fig. 3.7. Cross plot of drip-water pCO_2 and $\delta^{13}C_{DIC}$. $\delta^{13}C_{DIC}$ is inversely related to drip pCO_2; i.e., higher degassing of CO_2 from drip-water increases drip-water $\delta^{13}C_{DIC}$ values and vice versa.

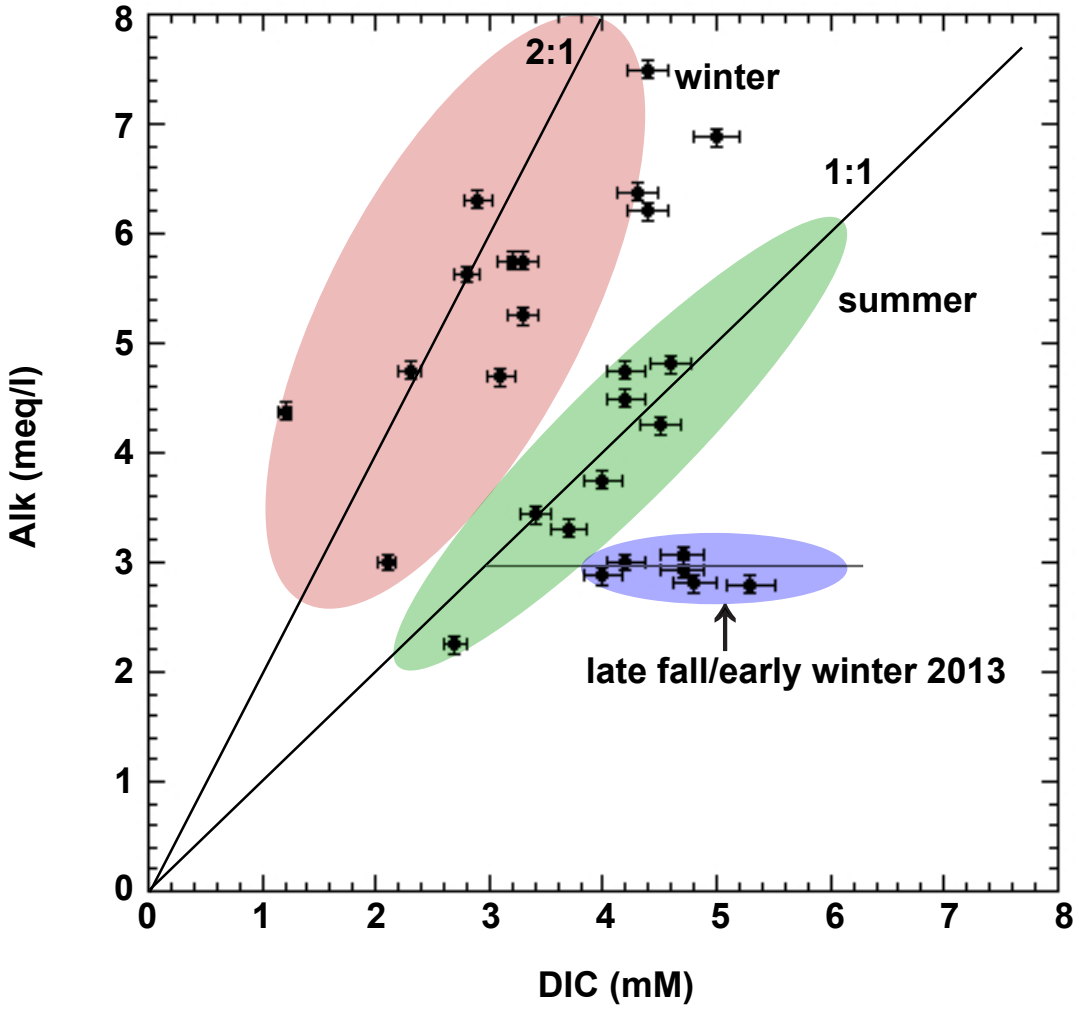

Fig. 3.8. Deffeyes diagram showing the variability in the dominance of CO_3^{2-}, HCO_3^- and CO_2 in cave drip-water. Note that the winter drip-water samples cluster around the 2:1 line indicating the major source of carbon in drip-water samples is CO_3^{2-}, the summer drip-water samples cluster around the 1:1 line indicating the major source of carbon in these samples is HCO_3^-, and late fall/early winter 2013 drip-water samples cluster around a horizontal line indicating the major source of carbon in these samples is CO_2.

5. DISCUSSION

Interpretation of $\delta^{13}C$ variation in speleothems has been linked to changes in (i) $\delta^{13}C$ of atmospheric CO_2 (Baskaran and Krishnamurthy, 1993); (ii) vegetation type overlying caves (i.e., C3- and C4- type plants; Dorale et al., 1992; 1998); (iii) soil biological activity such as plant root respiration and decomposition of soil organic matter by microbial respiration above caves (Baker et al., 2011), and (iv) inorganic processes related to dissolution of the host rock (Hendy, 1971; Fairchild et al., 2006). . More recently, however, a number of investigators have proposed that exchange of cave air with the surface atmosphere (ventilation) on a seasonal time scale directly affects the drip-water carbonate chemistry (Spötl et al., 2005; Banner et al., 2007). In the sections below I discuss the evidence supporting seasonal ventilation as the principal factor controlling carbonate chemistry of drip-water and thereby that of speleothems at DeSoto Caverns.

5.1. EFFECTS OF SEASIONAL CAVE VENTILATION ON CAVE-AIR pCO_2 AND ISOTOPE COMPOSITIONS

Cave air pCO_2, $\delta^{13}C_{air\ CO2}$ and $\delta^{18}O_{air\ CO2}$ vary seasonally (Figs. 3.4 A and B). The observed seasonality in cave air CO_2 concentrations and its carbon and oxygen isotopic composition has been attributed to temperature-dependent density-driven cave ventilation. Figures 3.9 A and B illustrate the relationship of cave air pCO_2 and $\delta^{13}C_{cave\ air\ CO2}$ with the temperature differences (ΔT) between external air and cave air. The observed temperature differences of up to 10.5 °C between external air and cave air cause density differences, which control seasonally reversing air flows. During summer, the outside temperature is high relative to cave air, creating a negative pressure gradient, which leads to stagnation of the cave air owing to diminished reverse air flow. Summer cave-air stagnation causes pCO_2 to increase as CO_2 is continuously delivered to the cave via drip-waters from the soil horizon and epikarst. pCO_2

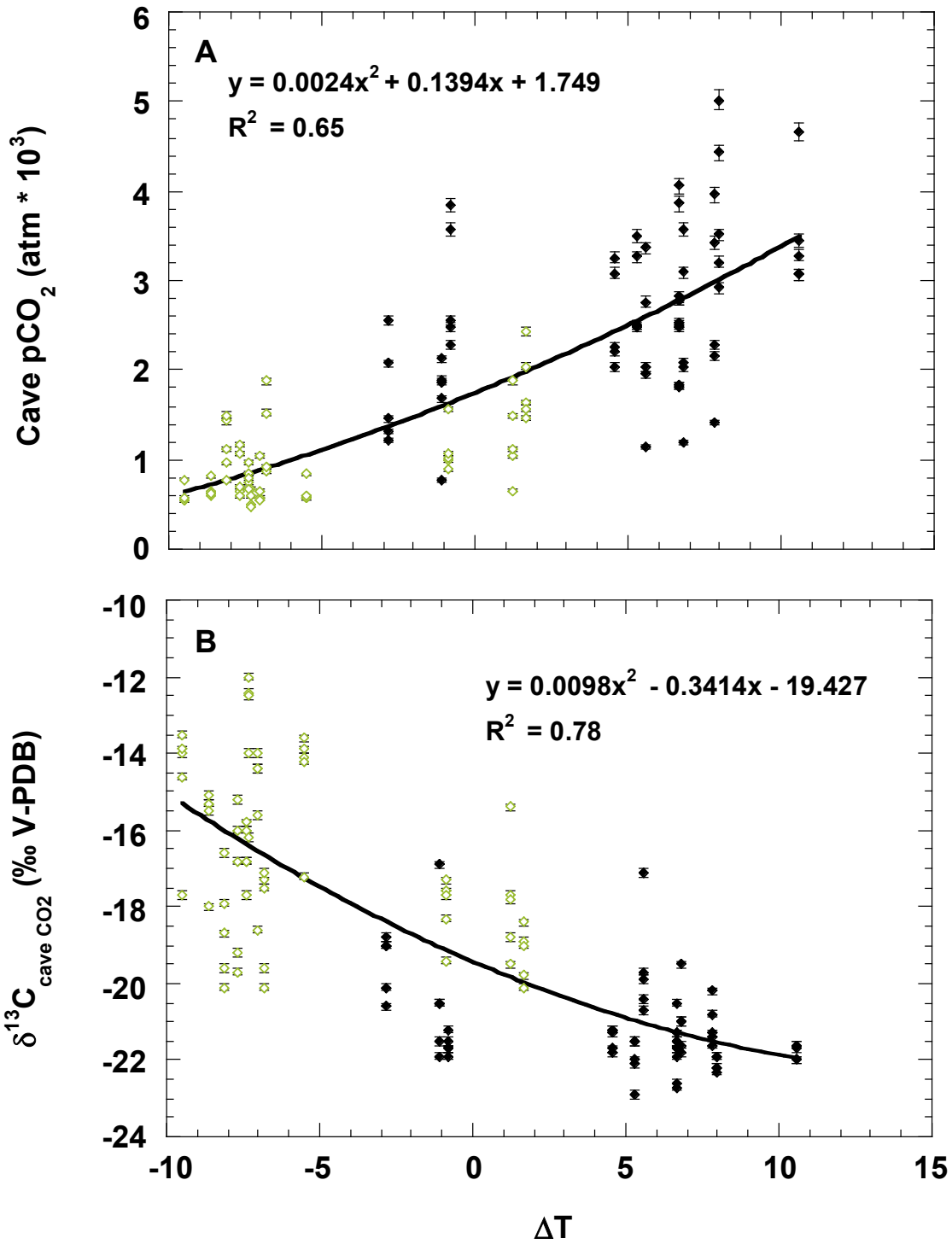

Fig. 3.9. Plots of (A) cave air pCO_2 and (B) $\delta^{13}C$ of cave air CO_2 against cave air temperature difference from outside temperature. Solid black diamonds represent summer season whereas empty green diamonds represent winter season.

levels reach as high as 5.0 (atm × 10^3). The $\delta^{13}C$ values of summer cave air CO_2 are relatively depleted and close to the $\delta^{13}C$ value of soil CO_2, reflecting the carbon contribution from overlying soil. ^{13}C-depleted $\delta^{13}C$ summer cave air CO_2 is least diluted by the outside atmosphere, owing to the stagnant mode of the cave chamber in summer. This represents one end member (i.e., soil CO_2) of the mixing components. Conversely, during winter, the outside temperature is low relative to that of cave air, causing the pressure gradient to be reversed. This allows outside air to descend from cave entrances that are topographically higher than cave chambers and enhance cave ventilation. Consequently, mixing of cave air with atmospheric air decreases cave air CO_2 concentration and pCO_2 levels approach the atmospheric level. Furthermore, ventilation driven-mixing of isotopically light cave air CO_2 with isotopically heavy atmospheric CO_2 elevates the $\delta^{13}C$ values of winter cave CO_2 (as high as -12.0‰). The $\delta^{18}O_{\text{cave air CO2}}$, on the other hand shows a strong positive correlation with cave air pCO_2. The $\delta^{18}O$ values of cave air CO_2 are higher and close to the $\delta^{18}O$ value of soil CO_2, which is one end component of cave air. Elevated $^{18}O_{\text{cave air CO2}}$ values during summer are likely linked to ^{18}O enrichment of moisture in the overlying soil due to enhanced evaporation (Gorczyca et al., 2003). In contrast, winter $\delta^{18}O$ values of cave air CO_2 are likely due to ventilation-driven mixing of isotopically heavy cave air CO_2 with relatively light atmospheric CO_2.

Some studies have suggested a positive relationship between drip flow rate and cave air pCO_2 (Kowaczk and Froelich, 2010; Cai et al., 2011). However, at DeSoto Caverns cave air pCO_2 is likely correlated with temperature differences between external air and cave air, rather than drip flow rate. At DeSoto Caverns, cave air pCO_2 was ~21 % lower in summer 2013 than in summer 2012. Relatively high cave air pCO_2 (up to 5.0 (atm × 10^3)) during summer 2012 coincided with increased temperature differences (max 10.5 °C between external air and cave

air) and decreased average drip flow rate (46 ml/h). Conversely, decreased cave air pCO_2 (down to 4.0 (atm × 10^3)) during summer 2013 coincided with decreased temperature differences (max 6.6 °C) and increased average drip flow rate (613 ml/h). If the drip flow rate was a dominant source of CO_2 to the cave, summer 2013 would have displayed higher cave air CO_2 concentrations than did summer 2012. Average drip flow rate during summer 2013 was ~ 13 times greater than that of summer 2012. Compared with summer 2012, the reduced temperature differences during the relatively cool summer of 2013 may have partially alleviated cave-air stagnation and thereby decreased cave air pCO_2.

5.2. EFFECTS OF SEASONAL CAVE VENTILATION ON DRIP-WATER CARBONATE GEOCHEMISTRY

Seasonal variation in the concentration of CO2 in cave air owing to ventilation/stagnation of a cave chamber can affect the carbonate geochemistry of the drip-water and hence the carbon isotopic composition of speleothems (James et al., 2015; Breitenbach et al., 2015). Over the study period, high pH, SI_{AR}, alkalinity, $\delta^{13}C_{DIC}$, and low pCO_2 and [DIC] values were observed in drip- water during winter. By contrast, low pH, SI_{AR}, alkalinity, $\delta^{13}C_{DIC}$, and high pCO_2 and [DIC] values are observed during summer when cave air pCO_2 is high. This seasonal alteration in pCO_2 controls drip- water carbonate chemistries at DeSoto Caverns. During summer, the relatively high cave air pCO_2 reduces CO_2 degassing from drip-water owing to a reduced cave air/drip-water pCO_2 gradient, resulting in high pCO_2 and consequently low alkalinity, SI_{AR} and pH values in drip-water. By contrast, during winter the relatively low pCO_2 in cave air facilitates CO_2 degassing from drip-water owing to the high cave air/drip-water pCO_2 gradient, associated high alkalinity, SI_{AR} and pH values in drip-water (Spötl et al., 2005; Banner et al., 2007). Because the drip-water is highly alkaline and super-saturated with respect to aragonite, rapid calcium- carbonate precipitation is expected in the cave during winter. This hypothesis is

supported by the clustering of most winter drip-water samples around the line of 2:1 slope in the Deffeyes diagram (Fig. 3.8). The major source of carbon in drip-water samples that fall on the 2:1-slope line is $CO3^{2-}$ (Deffeyes, 1965). A high concentration of $CO3^{2-}$ in drip-water favors carbonate precipitation (Given and Wilkinson 1985, Duan et al. 2012). During summer, the alkalinity is relatively low and the dominant source of carbon in the drip-water is $HCO3^{-}$, as summer drip-water samples mostly fall on or near the 1:1 slope in Deffeyes diagram (Deffeyes, 1965). Because the dominant presence of HCO3 in drip-water inhibits calcium-carbonate precipitation (Duan et al., 2012), the rate of calcium-carbonate precipitation is relatively low during summer. The relatively low pH and SI_{AR} values in summer drip-water further indicate reduced calcium-carbonate precipitation in summer at DeSoto Caverns. However, drip-water samples that were collected during late fall/early winter of wet year 2013 show exceptionally low alkalinity and these samples fall on the horizontal line in the Deffeyes diagram, indicating that CO_2 is the major source of carbon in the drip-water. The high production of CO_2 during this period is likely due to the enhanced soil-microbial activities (Atkinson, 1977; Mattey et al., 2010). Additions of CO_2 in drip-water results in low pH and SIAR values and consequently low rates of carbonate precipitation in the cave. The slow degassing of CO_2 from drip-waters during summer owing to high concentrations of cave CO_2, leads the isotope fractionation between cave air pCO_2 and drip pCO_2 to near equilibrium under Rayleigh conditions, which resulted in elevation of [DIC] and depletion of ^{13}C in drip-water. In contrast, the low concentration of cave CO_2 during winter enhanced drip-water degassing, which resulted in reduction of [DIC] and enrichment of $\delta^{13}C$ in drip-water. However, drip-water samples of the late fall/early winter months of the wet year 2013 show exceptionally high [DIC] and low $\delta^{13}C_{DIC}$ values. Similarly, drip-water pCO_2 values reached as high as 14.7 (atm × 10^3). Hence, it is likely that exceptionally

high production of CO_2 due to enhanced soil-metabolic activities resulted in high [DIC] and low $\delta^{13}C_{DIC}$ values in the drip-waters during this period.

The lowest $\delta^{13}C_{DIC}$ value (-11.4‰) obtained in this study during summer is in good agreement with the predicted initial $\delta^{13}C_{DIC}$ value (-12.0 ‰) of drips at DeSoto Caverns under isotopic equilibrium conditions (Lambert and Aharon, 2011). However, the winter $\delta^{13}C_{DIC}$ values are substantially higher (range -8.4‰ to -3.4‰) than the predicted $\delta^{13}C_{DIC}$ value. There are two major factors that can elevate the $\delta^{13}C$ in drip-water during winter: (i) increase in $\delta^{13}C_{soil\ CO2}$ following a drop in biogenic soil CO_2 production owing to low temperature (Spötl et al., 2005; Banner et al, 2007; Frisia et al., 2011) and (ii) kinetically enhanced carbon-isotope fractionation due to strong cave ventilation (Lambert and Aharon, 2011). The latter actor plays a more prominent role than the former to further elevate the $\delta^{13}C$ in drip-water during winter, especially in DeSoto Caverns, which has (i) temperature gradients of up to 10 °C between the external air and the cave air, and (ii) cave air pCO_2 that varies seasonally by about a factor of 10, between 5.0 (atm × 10^3) in summer to 0.5 (atm × 10^3) in winter. The relatively low cave air pCO_2 during winter enhances CO_2 degassing from drip-water, and thus causing kinetic isotope fractionation, i.e., ^{13}C enrichment, in cave drip- water.

5.3. CARBON-ISOTOPE FRACTIONATION BETWEEN DRIP DIC AND CAVE-AIR CO_2

In order to understand whether the isotope fractionation accompanying CO_2 degassing and carbonate deposition is controlled by equilibrium or kinetic processes, I use the following linear form of the Rayleigh fractionation equation (modified after Matthews and Kolodny, 1978; Bar- Matthews et al., 1996):

$$(\delta^{13} + 1000) = (\delta^{13}C_0 + 1000) + ln(\alpha - 1)f \quad (5)$$

where, f is the fraction of [DIC] remaining in the drips and, $\delta^{13}C_t$ and $\delta^{13}C_0$ are the carbon

isotope ratios of the [DIC] at time (*t*) and initially (0). The value of f is calculated by assuming the highest [DIC] value (5.3 mM) equals that of the drip-water as it first emerged on the cave ceiling; thus, *ft* becomes equal to [DIC]t/5.3 and *f0* becomes equal to 1 (Bar-Matthews et al., 1996; Lambert and Aharon., 2011). CO_2 - degassing and calcium-carbonate precipitation can be represented by the following equation:

$$Ca^{2+}_{aq} + 2HCO^{-}_{3(aq)} = CaCO_{3(s)} + CO_{2(g)} + H_2O_{(aq)} \quad (6)$$

in which under the Rayleigh equilibrium model the carbon of dissolved bicarbonate is split equally between two phases: $CaCO_3$ and CO_2. The appropriate fractionation factors used here are 1000 $ln\alpha_{(CO2-HCO3^-)}$ = −8.6‰ (Zhang et al., 1995) and 1000 $ln\alpha_{(CaCO3(AR)-HCO3^-)}$ = 2.7‰ (Romanek et al., 1992). Because the carbon is equally partitioned between two phases, the theoretical fractionation factor is the mean of these two values:

$$1000\ ln\alpha_{[(CO2-HCO3^-)+(CaCO3(AR)-HCO3^-)]/2} = -3.0‰ \quad (7)$$

Hence, under Rayleigh equilibrium the data plotted on a graph of ($\delta^{13}C_t$ + 1000) vs. lnf in Fig. 3.10 A would follow the theoretical line whose slope is – 3.0‰. Instead, the drips data from the large front chamber of the cave follow the line whose slope is – 4.1‰ indicating kinetically enhanced isotopic fractionation is dominant during winter months. Similar results were obtained using drip data from the small back chamber of the cave. However, in this case drip data follow the line whose slope is –6.7‰ (Fig. 3.10 B) (Lambert and Aharon, 2011). The more negative slope of the modeled fractionation line in the back chamber of the cave is most likely due to the very short falling distance (<10 cm) of drips of sampled drip-waters compared to the long falling path (>25 m) of drips in the front chamber. The observation of relatively enriched ^{13}C values in drip-waters in the front chamber is consistent with the findings of Meyer et al. (2014) in central Texas caves. According to Meyer et al. (2014), long drip flow paths in caves allow greater CO_2

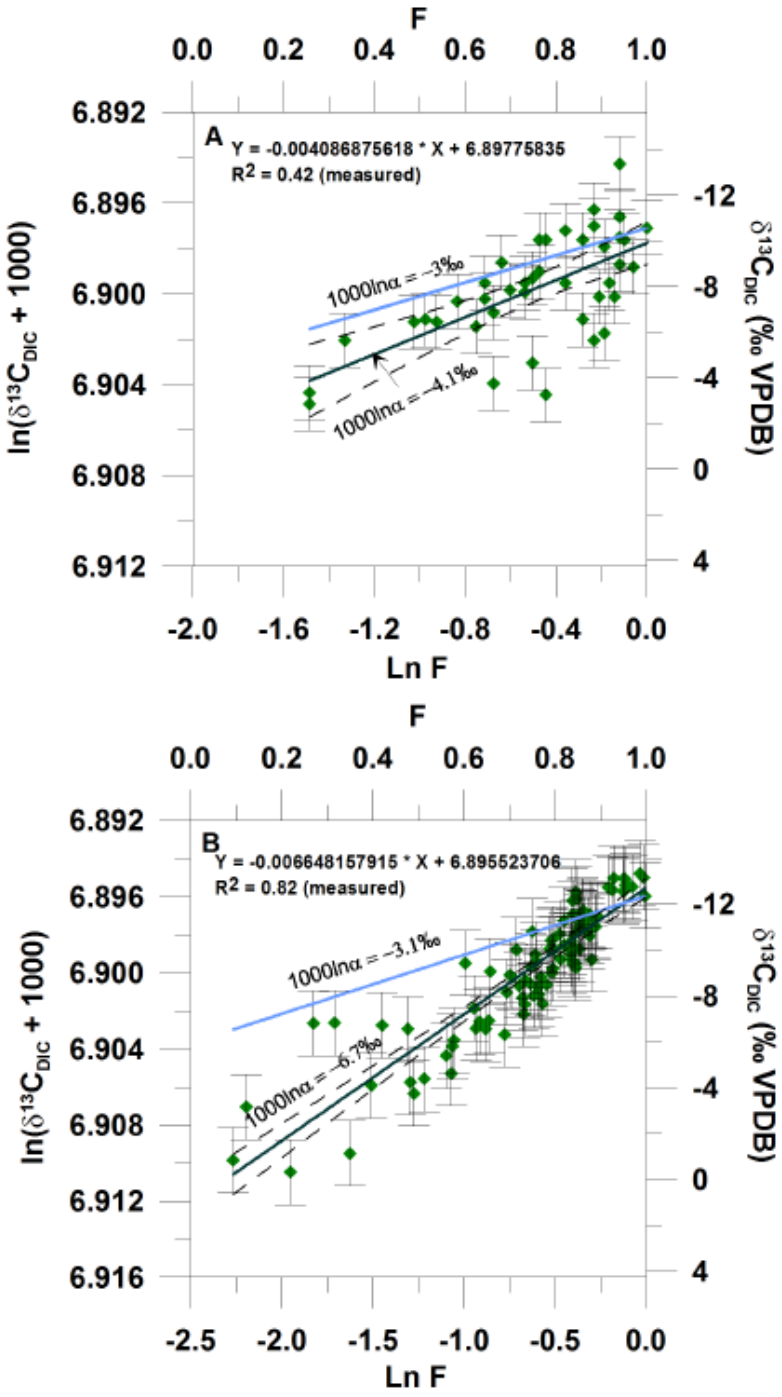

Fig. 3.10. Rayleigh fractionation plots modeling the ^{13}C fractionation by CO_2 degassing and precipitation of carbonate using (A) data from the large front chamber of the cave (this study) and (B) data from the small back chamber of the cave (Lambert and Aharon, 2011). Note the deviation of modeled slope (linear fit with 95% CL) from the theoretical equilibrium slope (blue line) in both cases.

degassing and yield consistently higher $\delta^{13}C_{DIC}$ values. Furthermore, the back chamber of the cave, which is comparatively farther from the entrance, has a less pronounced ventilation effect than the front chamber. The relatively weak ventilation reduced degassing and lowered drip-water $\delta^{13}C$ values in the back chamber of the cave.

6. CONCLUSIONS

Figure 3.11 summarizes the findings of this 2-year monitoring study providing insights into control of ventilation on drip-water carbonate geochemistry at DeSoto Caverns. Based on the results of this study, I draw the following conclusions.

1. The cave is well ventilated, showing prominent seasonal ventilation regimes with highest pCO_2 during summer and lowest pCO_2 level during winter. Summer cave air stagnation allows CO_2 to increase within the cave chamber, as CO_2 delivery to the cave continues via drip-water from the soil horizon and epikarst. By contrast, during winter, the cold and dense outside air poor in CO_2 descends through the cave entrance (which is topographically higher than the cave chambers) and displaces warmer and CO_2-rich air, thus lowering the CO_2 concentration in the cave.

2. The exchange between cave and surface air during winter months is validated using a keeling plot, which shows negative and positive relationship of cave pCO_2 with $\delta^{13}C_{CO2}$ and $\delta^{18}O_{CO2}$, respectively. The strong relationship of $\delta^{18}O_{CO2}$ with cave air CO_2 concentrations indicates that $\delta^{18}O$ values of cave air CO_2 can be used as a proxy for cave ventilation.

3. The pCO_2 level in the cave is likely controlled by external/cave air temperature gradients rather than drip flow rate.

4. Seasonally varying cave-air pCO_2 likely controls the drip-water pCO_2, pH, SI_{AR}, alkalinity, $\delta^{13}C_{DIC}$, and [DIC].

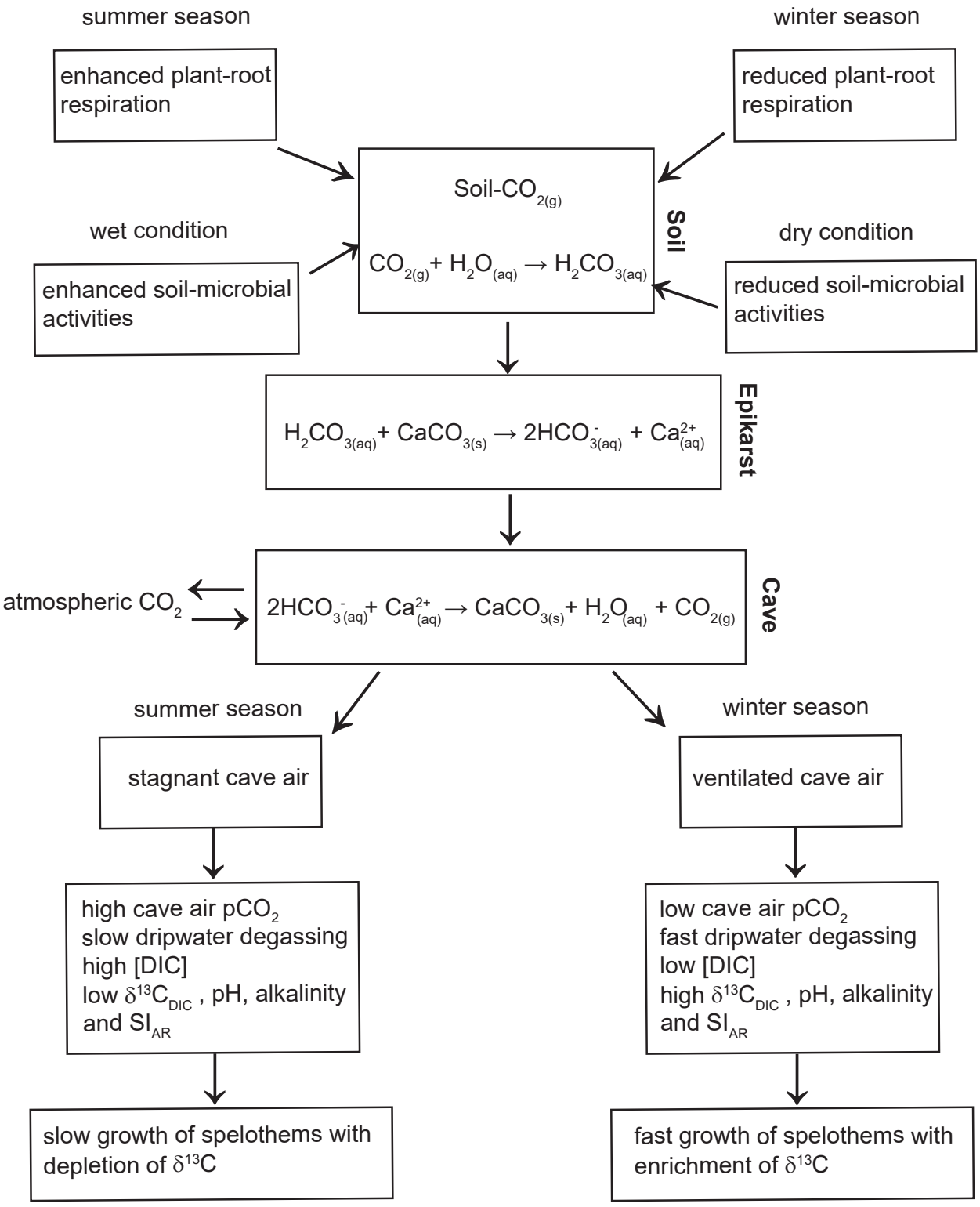

Fig. 3.11. Pathways by which carbon enters into the cave atmosphere and affects growth rates as well as carbon-isotopic compositions of speleothems.

5. Drip-water is highly alkaline and super-saturated with respect to aragonite during winter, indicating precipitation of speleothem aragonite is favored during the winter months at DeSoto Caverns.

6. The findings of this study agree with the results of Mattey et al. (2008) and Banner at al. (2007), who suggested that ventilation-led seasonal variability of cave-air pCO_2 likely affect the $\delta^{13}C$ and growth rate of speleothems.

ACKNOWLEDGEMENTS

I thank Tim Lacy and Allen Mathis III for providing me free access to the cave for observations and samples collection; graduate and undergraduate students who assisted me in fieldwork. I am very much thankful to Dr. Joe Lambert for giving me wise advice and assisting me in the lab work. Trace-element measurements were performed by Dr. Siddhartha Bhattacharyya at the University of Alabama. This study was funded by the Gulf Coast Association of Geological Societies (GCAGS faculty and student grants) and multiple University of Alabama student and research grants.

REFERENCES

Aharon, P. and Dhungana, R. 2017: Ocean-atmosphere interactions as drivers of mid-to-late Holocene rapid climate changes: Evidence from high-resolution stalagmite records at DeSoto Caverns, Southeast USA. Quat. Sci. Rev. Vol. 170, 69-81.

Atkinson, T.C. 1977: Carbon dioxide in the atmosphere of the unsaturated zone: An important control of groundwater hardness in the limestone. Jour. of hydrol. Vol. 35, 111-123.

Baldini, J.U.L., Baldini, L.M., McDermott, F. and Nicholas, C. 2006: Carbon dioxide sources, sinks, and spatial variability in shallow temperate zone caves: evidence from Ballynamintra cave, Ireland. J. cave and karst Stud. Vol. 68, No. 1, 4-11.

Baldini, J.U.L., McDermott, F., Hoffmann, D.L., Richards, D.A. and Clipson, N. 2008: Very high- frequency and seasonal cave atmosphere pCO_2 variability: Implications for stalagmite growth and oxygen isotope-based paleoclimate records. Earth Planet. Sci. Lett., Vol. 272, 118-129.

Banner, J.L., Guilfoyle, A., James, E.W., Stern, L.A. and Musgrove, M.L. 2007: Seasonal Variations in Modern Speleothem Calcite Growth in Central Texas, U.S.A. J. Sediment. Res., Vol. 77, No. 8, 615-622.

Baigorria, G.A., Jones, J.W., Shin, D.W., Mishra, A. and O'Brien, J.J. 2007: Assessing uncertainties in crop model simulations using daily bias-corrected Regional Circulation Model outputs. Clim. Res. Vol. 34, 211-222.

Baker, A., Wilson, R., Fairchild, I.J., Franke, J., Spötl, C., Mattey, D., Trouet, V. and Fuller, L. 2011: High resolution $\delta^{18}O$ and $\delta^{13}C$ records from an annually laminated Scottish stalagmite and relationship with last millennium climate. Global Planet. Change, Vol. 79, Issues 3-4, 303-311.

Bar-Matthews, M., Ayalon, A., Matthews, A., Sass, E. and Halicz, L. 1996: Carbon and oxygen isotope study of the active water-carbonate system in a karstic Mediterranean cave: implications for paleoclimate research in semiarid regions. Geochim. Cosmochim. Acta, Vol. 60, 332-347.

Baskaran, M. and Krishnamurthy, R.V. 1993: Speleothems as proxy for the carbon isotope composition of atmospheric CO_2, Geophys. Res. Lett., Vol. 20. Issue 24, 2905-2908.

Baumann, H., Talmage, S.C. and Gobler, C.J. 2012: Reduced early life growth and survival in a fish in direct response to increased carbon dioxide. Nature Clim. Change, Vol. 2, 38-42.

Breitenbach, S., Lechleitner, F. A., Meyer, H., Diengdoh, G., Mattey, D., Marwan, N. 2015: Cave ventilation and rainfall signals in drip-water in a monsoonal setting - a monitoring study from NE India: Chem. Geol. Vol. 402, 111-124.

Cai, B., Zhu, J., Ban, F. and Tan, M. 2011: Intra-annual variation of the calcite deposition rate of drip-water in Shinhua Cave, Beijing, China and its implications for palaeoclimatic reconstructions. Boreas, Vol. 40, 525-535.

Charlton, S.R., and Parkhurst, D.L., 2002, PhreeqcI--A graphical user interface to the geochemical model PHREEQC: U.S. Geological Survey Fact Sheet FS-031-02, April 2002, 2 p.

Ciais, P., Denning, A.S., Tans, P.P., Berry, J.A., Randall, D.A., Collatz, G.J., sellers, P.J., White, J.W.C., Troilier, M., Meijer, H.A.J., Francey, R.J., Monfray, P. and Heimann, M. 1997: A three- dimensional synthesis study of $\delta^{18}O$ in atmosphere CO_2: 1. Surface fluxces. J. Geophys. Res., Vol. 102, 5857-5872.

Deffeyes, K.S. 1965: Carbonate Equilibria: A Graphic and Algebraic Approach. Limnol. Oceanogr.
Vol. 10, 412-426.

Denniston, R.F., González, L.A., Baker, R.G., Asmerom, Y., Reagan, M.K., Edwards, R.L. and Alexander, E.C. 1999: The Holocene, Vol. 9, No. 6 671-676.

Dorale, J.A., González, L.A., Reagan, M.K., Pickett, D.A., Murrell, M.T. and Baker, R.G. 1992: A High-Resolution Record of Holocene Climate Change in Speleothems Calcite from Cold Water Cave, Northeast Iowa. Science, Vol. 258, No. 5088, 1626-1630.

Dorale, J.A., Edwards, R.L., Ito, E. and González, L.A. 1998: Climate and Vegetation History of the Midcontinent from 75 to 25 ka: A Speleothem Record from Crevice Cave, Missouri, USA. Science, Vol. 282, 1871-1874.

Duan, W., Cai, B., Tan, M., Liu, H. and Zhang, Y. 2012: The growth mechanism of the aragonitic stalagmite laminae from Yunnan Xianren Cave, SW China revealed by cave monitoring. Boreas, Vol. 41, 113-123.

Fairchild, I.J., Smith, C.L., Baker, A., Fuller, L., Spötl, C., Mattey, D., McDermott, F. and E.I.M.F. 2006: Modification and preservation of environmental signals in speleothems. Earth-Sci. Rev. Vol. 75, Issues, 1-4, 105-153.

Faust, S.D. and Aly, O.M. 1981: Chemistry of natural waters. Butterworths, Boston MA. An Ann Arbor Science Book. 1981. 400.

Flanagan, L.B., Marshall, J.D., Ehleringer, J.R. 1993. Photosynthetic gas exchange and the stable isotope composition of leaf water: comparison of xylem-tapping mistletoe and its host. Plant, Cell and Environ, Vol. 16, 623-631.

Francey, R.J. and Tans, P.P. 1987: Latitudinal variation in oxygen-18 of atmospheric CO_2. Nature, Vol. 327, 495-497.

Frisia, S., Borsato, A., Fairchild, I.J. and McDermott, F. 2000: Calcite Fabrics, Growth Mechanisms, and Environments of Formation in Speleothems from the Italian Alps and Southwestern Ireland. Jour. of Sed. Res, Vol. 70, No. 5, 1183-1196.

Frisia, S., Fairchild, I.J., Fohlmeister, J., Miorandi, R., Spötl, C. and Borsato, A. 2011: Carbon mass- balance modeling and carbon isotope exchange processes in dynamic caves. Geochim. Cosmochim. Acta, Vol. 75, 380-400.

Genty, D., Baker, A., Massault, M., Proctor, C., Gilmour, M., PonsBranchu, E. and Hamelin, B. 2001: Dead carbon in stalagmites: Carbonate bedrock paleodissolution vs. ageing of soil organic matter. Implications for 13C variations in speleothems. Geochim. Cosmochim. Acta, Vol. 65, 3443–3457

Given, R.K. and Wilkinson, B.H. 1985: Kinetic control of morphology, composition, and mineralogy of abiotic sedimentary carbonates. Jour. of Sed. Petr, Vol. 55, no. 1, 109-119.

Gorczyca, Z., Rozanski, K., Kuc, T. and Michalec, B. 2003: Seasonal variability of the soil CO_2 flux and its isotopic composition in southern Poland. Nukleonika, Vol. 48, No. 4, 187-196.

Gran, G. 1952: Determination of the equivalent point in potentiometric titrations, Part 2. Analyst 77, 661-671.

Hendy, C.H. 1971: The isotopic geochemistry of speleothems-I. The calculation of the effects of different modes of formation on the isotopic composition of speleothems and their applicability as palaeoclimatic indicators. Geochim. Cosmochim. Acta, Vol. 35, Issue 8, 801-824.

James, E.W., Banner, J.L. and Hardt, B. 2015: A global model for cave ventilation and seasonal bias in speleothem paleoclimate records. Geochem. Geophys. Geosyst. Vol. 16, 1044-1051.

Keeling, C.D. 1958: The concentration and isotopic abundances of atmospheric carbon dioxide in rural areas. Geochim. Cosmochim. Acta, Vol. 13, 322-334.

Kim, S.T., Mucci, A. and Taylor, B.E. 2007: Phosphoric acid fractionation factors for calcite and aragonite between 25 and 75 °C: Revisited. Chem. Geol. Vol. 246, 135-146.

Kowalczk, A.J. and Froelich, P.N. 2010: Cave air ventilation and CO_2 outgassing by radon-222 modeling: how fast do caves breathe? Earth Planet. Sci. Lett., Vol. 289, 209-219.

Lambert, W.J. and Aharon, P. 2010: Oxygen and hydrogen isotopes of rainfall and drip-water at DeSoto Caverns (Alabama, USA): Key to understanding past variability of moisture transport from the Gulf of Mexico. Geochem. Cosmochim. Acta, Vol. 74, 846-861.

Lambert, W.J. and Aharon, P. 2011: Controls on dissolved inorganic carbon and $\delta^{13}C$ in cave waters from DeSoto Caverns: Implications for speleothem $\delta^{13}C$ assessments. Geochem. Cosmochim.Acta, Vol. 75, 753-768.

Mattey, D., Lowry, D., Duffet, J., Fisher, R., Hodge, E. and Frisai, S. 2008: A 53 year seasonally resolved oxygen and carbon isotope record from a modern Gibraltar speleothem: Reconstructed drip-water and relationship to local precipitation. Earth Planet. Sci. Lett., Vol 269, 80-95.

Mattey, D.P., Fairchild, I.J., Atkinson, T.C., Latin, J.P., Ainsworth, M. and Durell, R. 2010: Seasonal microclimate control of calcite fabrics, stable isotopes and trace elements in modern speleothem from Michaels Cave, Gibraltar. Geol. Soci. London, Spec. Pub. Vol. 336, 323-344.

Matthews, A. and Kolodny, Y. 1978: Oxygen isotope fractionation in decarbonation metamorphism: the Mottled Zone event. Earth Planet. Sci. Lett. Vol. 39, 179-192.

Meyer, K.W., Feng, W., Breecker, D.O., Banner, J.L. and Guilfoyle, A. 2014: Interpretation of speleothem calcite δ13C variations: Evidence from monitoring soil CO_2, drip-water, and modern speleothem calcite in central Texas. Geochem. Cosmochim. Acta, Vol. 142, 281-298.

Parkhurst, D.L. and Appelo, C.A.J. 1999: User's guide to PHREEQC (version 2): A computer program for speciation, batch-reaction, one-dimensional transport, and inverse geochemical calculations: U.S. Geol. Surv. Water-Res. Invest. Rep. 99-4259, 312 p.

Romanek, C.S., Grossman, E.L. and Morse, J.W. 1992: Carbon isotopic fractionation in synthetic aragonite and calcite: Effects of temperature and precipitation rate. Geochim. Cosmochim. Acta, Vol. 56, 419-430.

Samani, Z. 2000: Estimating solar radiation and evapotranspiration using minimum climatological data. J. Irrig. Drain. Eng. Vol. 126, 265-267.

Schroeder, M. J., Glovinsky M., Henricks, V.F., Hood, F.C. and Hull, M.K. 1964: Synoptic weather types associated with critical fire weather. Defense Documentation Center for Scientific and Technical Information, Cameron Station Alexandria, VA, 492 pp.

Sharma, T. and Clayton, R.N. 1965: Measurement of $^{18}O/^{16}O$ ratios of total oxygen of carbonates.Geochem. Cosmochim. Acta, Vol. 29, 1347-1353.

Spötl, C. 2004: A simple method of soil gas stable carbon isotope analysis. Rapid Commun. Mass Spectrom, Vol. 18 pp.1239-1242.

Spötl, C. 2005: A robust and fast method of sampling and analysis of $\delta^{13}C$ of dissolved inorganic carbon in ground waters. Isot. Environ. Health Stud. Vol 41. 3, 217-221.

Spötl, C., Fairchild, I.J. and Tooth, A.F. 2005: Cave air control on drip-water geochemistry, Obir Caves (Austria): Implications for speleothem deposition in dynamically ventilated caves. Geochim. Cosmochim. Acta, Vol. 69, 2451-2468.

Widory, D. and Javoy, M. 2003: The carbon isotope composition of atmospheric CO_2 in Paris. Earth Planet. Sci. Lett. Vol. 215, 289-298.

Zhang, J., Quay, P.D. and Wilbur, D.O. 1995: Carbon isotope fractionation during gas-water exchange and dissolution of CO_2. Geochim. Cosmochim. Acta, Vol. 59, No.1, 107-114.

CHAPTER 4

OCEAN-ATMOSPHERE INTERACTIONS AS DRIVERS OF MID-TO-LATE HOLOCENE RAPID CLIAMATE CHANGES: EVIDENCE FROM HIGH-RESOLUTION STALAGMITE RECORDS AT DESOTO CAVERNS, SOUTHEASTERN USA

ABSTRACT

Oxygen- and carbon- isotope time series derived from an actively growing aragonitic stalagmite in DeSoto Caverns exhibit with unusual clarity rapid hydroclimate changes in the mid-to-late Holocene. Data consist of 1884 paired $\delta^{18}O$ and $\delta^{13}C$ measurements whose chronology is anchored by 35 $^{230}Th/^{234}U$ absolute dates in the interval 6.0-1.1 cal ka BP. Exceptional ^{18}O- and ^{13}C enrichment centered at 4.8 ± 0.14 cal ka BP likely record the effects of a severe drought. Isotope cycles from 4.7 to 1.3 cal ka BP, exhibit a dominant periodicity of 68 ±4 yrs. A gradual cooling trend of ~0.6 °C/10^3 yrs is attributed to a declining seasonal contrast in insolation. The synchronicity of the mega-drought in the southeastern US with (1) the termination of the African Humid Period; (ii) the abrupt reduction of North Atlantic Deep Water production, and (iii) rapid sea-ice expansion in the polar regions of both Hemispheres testifies to the global extent and rapidity of the "5 ka" event and points to variable production of North Atlantic Deep Water as the likely controlling factor. The multidecadal cycles are consistent with alternating dry and wet summers occurring during a long-term switch in the seasonal rainfall pattern from winter-dominated to summer-dominated. Correspondence between periodic summer droughts in the southeastern US and weakening of summer monsoons in Central China support climate models that predict profound hydroclimate changes in the late Holocene governed by the Atlantic Multidecadal Oscillation. The relatively rapid hydroclimate phase

transitions documented in this study complicate correlation of late Holocene drought events that had significant societal impacts.

1. INTRODUCTION

The climate of the mid-to-late Holocene appears relatively stable when viewed in the context of the large, rapid swings of the last deglaciation, but a number of significant abrupt hydroclimate events occupied during the last 5000 years. The most dramatic such climate events occurred in or near the mid-Holocene. The first "5 ka" event occurred at the transition from the relatively warm Hypsithermal to the relatively cool Neoglacial (H/N transition) and its extent is considered global (Davis and Thompson, 2006; Hodell et al., 2001; Keigwin, 1996; Thompson et al., 2006). An other occurred during the early part of the late Holocene: the “4.2 ka” event. Its global extent, expression and whether it represents a single event or multiple events are subject to debate (Booth et al., 2005; Finné et al., 2011).

Two aspects of the prominent 5 ka and 4.2 ka climate shifts are particularly controversial: (i) their timing and duration, and (ii) the controlling factors (Arz et al., 2006; Bar-Matthews and Ayalon, 2011; Booth et al., 2005; Cullen et al., 2000; Davis and Thompson, 2006; Dixit et al., 2014; Drysdale et al., 2006; Yang et al., 2015).

The precise timing and duration of the 5 ka and 4.2 ka events are equivocal because most dates are either based on the radiocarbon time scale using reservoir corrections with large uncertainties (Arz et al., 2006; Cullen et al., 2000; Dixit et al, 2014; Russell and Johnson, 2005), or on questionable correlations (Gasse, 2002). The speleothem archives from caves in Corchia, Italy (Drysdale et al., 2006), Soreq, Israel (BarMatthews and Ayalon, 2011), and Mawmluh, Northeast India (Berkelhammer et al. 2012) are exceptional, whose age models were derived from absolute U/Th dates.

The factors controlling climate variability at multi-century but sub-Milankovitch time-scales are poorly constrained (Wanner et al., 2008). A number of studies proposed solar variability as a possible forcing mechanism (Bond et al., 2001; Wanner et al., 2008) while others implicate the Atlantic Multidecadal Oscillation (AMO; Knudsen et al., 2011), a northward-southward shift of the Westerlies (Zanchetta et al., 2014), or El-Niño-Southern Oscillation (ENSO) variability (Booth et al., 2005; Donders et al., 2005).

This study presents the results of a stalagmite investigation (DSSG-5) from DeSoto Caverns in the Inner Gulf Coast (IGC), southeastern US (SEUS) (Fig. 4.1 A), spanning the time interval from 6.0 to 1.1 cal ka BP. The stalagmite, whose chronology is anchored by 35 precise $^{230}Th/^{234}U$ absolute dates, yields stable oxygen- and carbon-isotope time series at a resolution of 2-8 yrs that exhibit with unusual clarity the climate changes that occurred during the mid-to-late Holocene. The geographic location of the cave in the IGC offers unusual opportunities to study hydroclimate variability in the mid-to-late Holocene because: (i) it is located at the southern limit of the winter polar jet-stream; (ii) it receives moisture predominantly from the Gulf of Mexico (GoM), which occupies a central position in the Atlantic Warm Pool (AWP), the second largest oceanic warm pool on Earth (Wang and Enfield, 2001); (iii) The GoM is a significant source of moisture fueling the North American rainfall at present and its moisture-controlling role likely extended back in the Holocene and beyond, and (iv) global atmospheric circulation patterns, such as ENSO and the Bermuda High (BH), govern the interannual $\delta^{18}O$-isotope trends discerned in cave drip-waters (Lambert and Aharon, 2010). This study provides detailed climate-proxy records whose chronology is well constrained, and assesses the dominant drivers of climate variability in mid-to-late Holocene in the SEUS where high-resolution continental paleo-climate records,

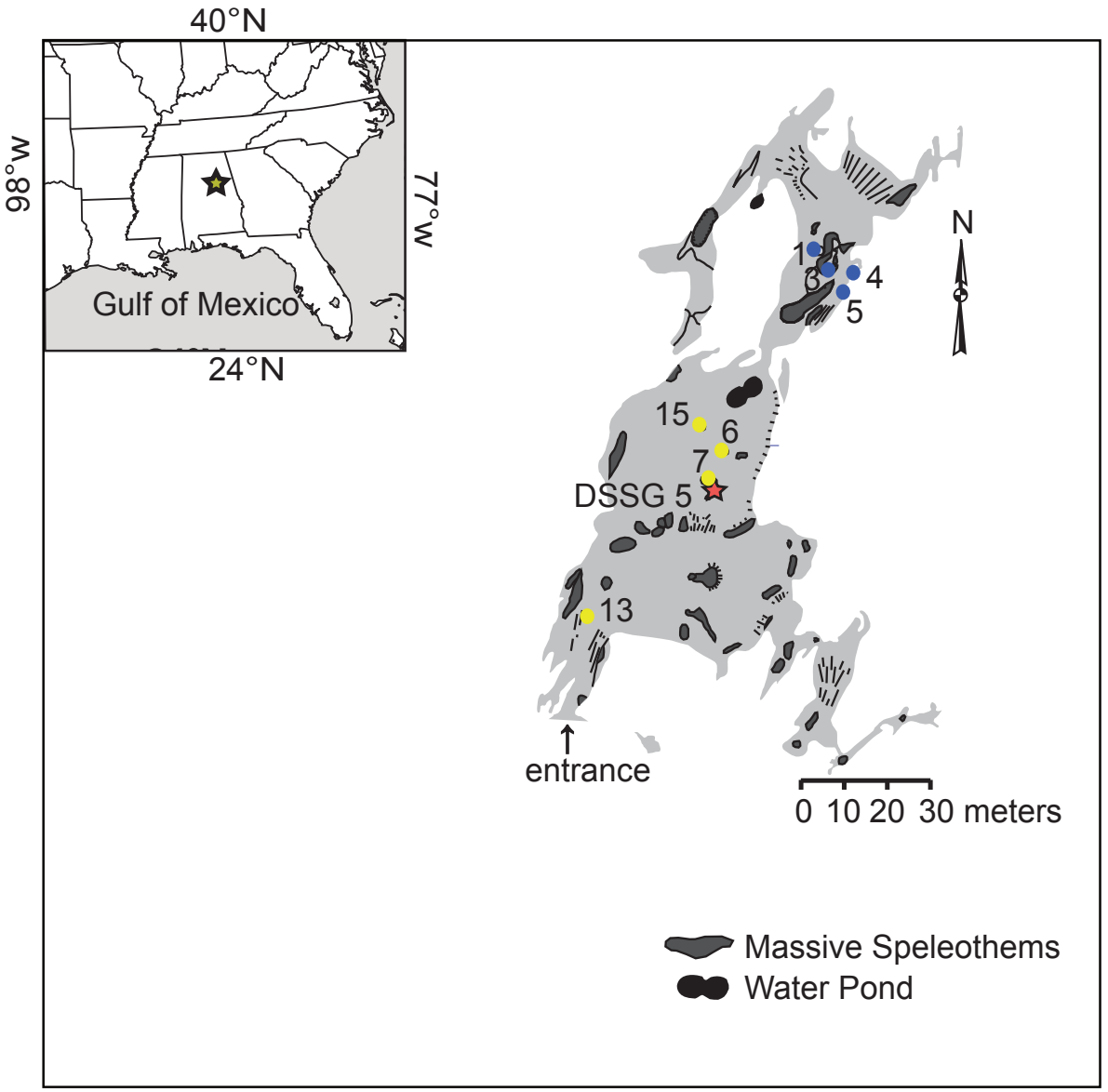

Fig. 4.1. Inset: Map of the southeastern US (SEUS) and the Inner Gulf Coast (IGC) showing the location of DeSoto Caverns(solid star). Plan-view map of DeSoto Caverns (modified from Lambert and Aharon, 2010) showing the locations of the DSSG-5 stalagmite (red star) in the front chamber of the cave. Blue dots mark the location of drips studied by Lambert and Aharon (2010, 2011) in the back chamber of the cave. Yellow dots mark the locations of drips in the front chamber whose isotope chemistry is discussed in this study.

such as those from speleothems, are notably lacking.

2. STUDY SITE AND REGIONAL CLIMATE

DeSoto Caverns (86°16’36’’ W, 33°18’26’’N) is located on the outskirts of Childersburg, AL in the IGC, and is separated from its major moisture source in the GoM by 365 km of low-lying coastal plains (Fig. 4.1, inset). Details of the cave geomorphology can be found in Lambert and Aharon (2010; 2011). Pristine fossil and active speleothems within the cave consist primarily of metastable aragonite (Lambert and Aharon, 2010; 2011).

The study area experiences a mean annual air temperature of 17.2 °C and an average annual rainfall total of 1338 ±70 mm (1σ Standard Error of the Mean (SEM), n=10) based on rainfall gauge data over the period 2005-2015 (Table 4.1). The question of seasonality is important in the interpretation of proxy climate data and therefore warrants further attention.

Present climate is typified by a moderate seasonality with average monthly air temperatures ranging from ~7 ℃ in January to ~27 ℃ in July. Average monthly rainfall ranges from ~80 mm in October to ~150 mm in March (Lambert and Aharon, 2010). Winter precipitation is greater than summer precipitation (fw>fs) by a factor of 1.3 (fw=0.56 ±0.08; fs=0.44 ±0.08, 1σ SEM, n=10).

Rainfall occurs throughout the year with two distinct modes. In winter, the collision of opposing cold and warm air masses often results in rain-producing storm systems that are carried eastward by the polar jet-stream (Baigorria et al., 2007). In contrast, summer rainfall is typically derived by convection-style thunderstorms whose frequency is impacted by the east-west position of the BH pressure cell (Li et al., 2011). Ten years (2005-2015) of weekly rainfall isotope measurements (Table 4.1) yield a seasonal $\delta^{18}O$ contrast of 1.1‰ (based on

weighted monthly means) between a mean winter rainfall value of -5.1 ±0.3‰ and a mean

Table 4.1. Summary of monitoring data at DeSoto Caverns relevant to this study. Uncertainties are listed as standard error of the mean (1σ).

Period	Rainfall (mm)	$\delta^{18}O$ (rainfall) (‰VSMOW)	$\delta^{2}H$ (rainfall) (‰VSMOW)	Cave T (^{o}C)	RH (%)	$\delta^{18}O$ (drips) (‰VSMOW)	$\delta^{2}H$ (drips) (‰VSMOW)
Annual	1338 ±70 (n=10)	-4.6 ±0.2 (n=126)	-23.3 ±4 (n=126)	18.2 ±0.7 (n=24)	100 (n=24)	-4.7 ±0.3 (n=23)	-24.3 ±2.7 (n=22)
Summer	583 ±14 (n=10)	-4.0 ±0.2 (n=10)	-20.3 ±1.5 (n=10)	18.5 ±0.5 (n=12)	100 (n=12)	-4.8 ±0.2 (n=12)	-25.4 ±2.7 (n=11)
Winter	755 ±37 (n=10)	-5.1 ±0.3 (n=10)	-25.6 ±2.5 (n=10)	17.8 ±0.6 (n=12)	100 (n=12)	-4.6 ±0.4 (n=11)	-21.8 ±4.9 (n=11)

summer rainfall value of -4.0 ±0.2‰ (1σ SEM, n=10). Exceptions are rainfalls associated with tropical storms that yield anomalous ^{18}O-depletions down to -8.3‰ (e.g., five severe tropical storms encountered in the summer of 2005) and interannual ^{18}O enrichment trends of up to 1‰ associated with regional droughts (e.g., drought of 2006-2007; Lambert and Aharon, 2010).

Monthly monitoring of DeSoto Caverns air parameters temperature and humidity, drip-water flow rates, stable isotopes and elemental chemistry occurred during two time intervals. Five drip-water sites were monitored in the back chamber of the cave (Fig. 4.1, cave map) over a three- year period (2005-2008) (Lambert and Aharon, 2010, 2011). Four drip-water sites were subsequently monitored in this study over a two-year period (2012-2013) in the cave front-chamber above and immediately adjacent to the DSSG-5 stalagmite (Fig. 4.1, cave map). The complete results of the second monitoring phase are the subject of a separate manuscript (in prep.) and only measurements relevant to this study are summarized in Table 4.1.

3. METHODS

An actively growing stalagmite, located in the center of the cave front chamber, was cored along the growth axis (core dimensions: 75 cm long, 4 cm diameter) without causing permanent damage to the whole formation (DSSG-5, Fig. 4.2 A). The uppermost 40 mm of the stalagmite contains several hiatuses reported by Aharon et al. (2012) and therefore the paleoclimate reconstruction in this study focuses on the stalagmite interval below 40 mm. In the laboratory the core was cut in two halves; after cleaning with weak HCl and deionized water in a sonicator, one half was used for U/Th dating and stable-isotope analysis and the other half was used to prepare thin sections. These thin sections were used to examine the carbonate fabrics under a Nikon SMZ800 optical microscope equipped with a Spot Insight QE Camera. Spot Advanced software was used to acquire photomicrographs and to measure crystal sizes.

Thirty-five pristine aragonite samples (sampling locations in Fig. 4.2 A) with weights in the range of 35-40 mg were acquired for U/Th dating using a Nu multicollector inductively coupled plasma mass spectrometer (MC-ICPMS) at the University of Melbourne, Australia (Hellstrom, 2003). Samples with weights ranging from 60-100 µg were drilled for stable-isotope analysis along the stalagmite growth axis using a computer-controlled micro-milling machine. A sampling interval from 100 to 500 µm varied according to the growth rate of the stalagmite with the aim to acquire highly resolved (2-8 yrs) $\delta^{18}O$ and $\delta^{13}C$ time series. Limited areas of aragonite neomorphism to calcite (green and blue-shaded intervals in Fig. 4.2 A) were avoided as much as possible during samples collection for U/Th dating and isotope analysis because (i) replacement calcite might fail to preserve the isotopic signatures of the precursor mineral (Frisia et al., 2002; Lachniet, 2015), and (ii) loss of Uranium [U] during recrystallization of aragonite to secondary calcite is likely to make the $^{230}Th/^{234}U$ dates unreliable (Lachniet et al., 2012, but see

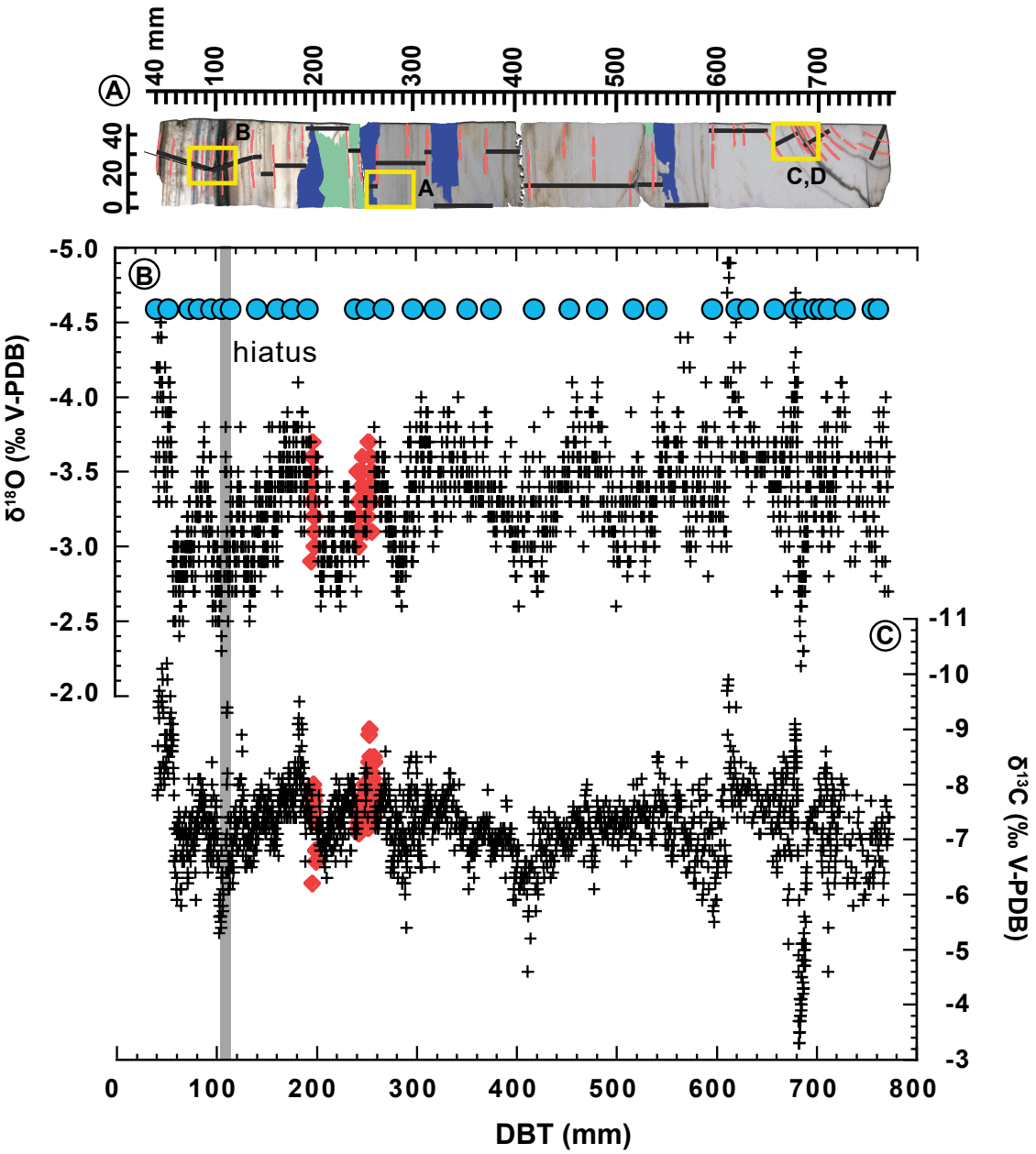

Fig. 4.2. (A) Cored stalagmite oriented horizontally to conform the orientation of the isotope plots; Yellow rectangles next to letters indicate the position of thin sections whose microphotographs are shown in Fig. 4.4. Aragonite mineralogy is shown in natural color; Massive neomorphic calcites replacing aragonite are shown in green (equant) and blue (columnar) shades. Red strips and black-lines mark the sampling locations of U/Th dates and the sampling profile for stable-isotope measurements, respectively. Dark, black layer between 106.3 and 112.6 mm Depth Below Top (DBT) has been identified as a hiatus (see text). (B & C) $\delta^{18}O$ and $\delta^{13}C$ determinations graphed against DBT. Isotope values derived from secondary calcites (red diamonds) have been corrected to equivalent aragonite values according to Phillips (2011) (see text). Note the coherency between calcite- corrected values and that of the adjacent pristine aragonites; U/Th sampling positions are marked by blue-filled circles.

Domnguez-Villar et al., 2017).

Oxygen- and carbon-isotope measurements were performed on a modified Delta-plus Continuous Flow-Isotope Ratio Mass Spectrometer (CF-IRMS). Samples were reacted with 100% phosphoric acid at 50 °C and the released CO_2 was separated from other interfering gases in a GasBench II online with the IRMS. Fifteen standards of NBS-19 were measured randomly with every eighty samples. Because the standard is calcite whereas the stalagmite samples are aragonite, a correction of – 0.34‰ at 50 °C was applied to the oxygen-isotope values of the measured samples according to Kim et al. (2007). The isotope ratios are reported in the conventional delta (δ) notation in per mil (‰) relative to Vienna-Pee Dee Belemnite (V-PDB). Analytical precision for both oxygen and carbon, based on standards and sample repeats, is ± 0.1‰ (1σ).

4. RESULTS

4.1. STABLE OXYGEN AND CARBON ISOTOPES

X-ray diffraction analysis coupled with petrographic observations reveal that the DSSG-5 stalagmite consists predominantly of aragonite. Its dominance is attributed to the relatively high Mg^{2+} concentrations (Mg/Ca >1.1 mol/mol threshold of aragonite precipitation (Rossi and Lozano, 2016)) derived from dissolution of the dolomitic host rock (Phillips, 2011). $\delta^{18}O$ and $\delta^{13}C$ measurements, graphed against depth below 40 mm of stalagmite (Figs. 4.2, B and C), consist of 1884 samples of which 97% are primary aragonite (n=1828) and 3% (n=56) are replacement calcites. Philips (2011) documented two neomorphic calcite fabrics replacing aragonite in the DSSG-5 stalagmite (Fig. 4.2 A): (i) equant, and (ii) columnar. Equant calcite typically inherits the textural and chemical features of the primary aragonite whereas columnar calcite is fabric destructive. Areas of massive neomorphic calcite in the intervals between

188-269, 325-352 and 545-566 mm were avoided during sampling as indicated by the vertical lines for stable isotopes (black) and horizontal lines (red) for U/Th dating (Fig. 4.2 A). In the intervals 195 to 199 mm and 251 to 258 mm respectively, where sampling the calcite was unavoidable, the isotope values of the calcites were normalized to aragonite according to the corrections derived by Phillips (2011) as follows (i) the $\delta^{18}O$ and $\delta^{13}C$ values derived from columnar calcite were corrected by -0.6‰ and -2‰, respectively, and (ii) the $\delta^{18}O$ values derived from equant calcite were corrected by -0.1‰ and no correction was needed for $\delta^{13}C$ values. The veracity of the normalization can be judged on the basis of the coherence exhibited between adjacent aragonite-calcite samples (Figs. 4.2, B and C).

4.2. U-SERIES ISOTOPES, AGE DATING AND STALAGMITE GROWTH RATES

Radiometric dating results are based on [U] and [Th] isotope determinations of tightly spaced samples (n=35, Figs. 4.2 A and B) (Table 4.2). With the exception of two samples to be discussed later, the aragonites closely approximate closed-system conditions and yield highly precise ages for the past ~6 cal ka BP yrs (Fig. 4.3 A) on the basis of their (i) relatively high [U] concentrations varying from 0.9 ppm to 4.3 ppm (mean: 2.11 ±0.96 ppm, n=33); (ii) generally $^{230}Th/^{232}Th>100$ activity ratios; (iii) low scatter of $^{234}U/^{238}U$ initial ratios, and (iv) conformable stratigraphic ages in an age-depth trend (Fig. 4.3 A). The generally high [U] concentrations in aragonite relative to a calcite mineralogy is explained by the favorable accommodation of UO_2 in the aragonite lattice (Railsback et al., 2002) thus improving the reliability of the radiometric dating from mg-size samples (Lachniet, 2015). Exceptions are two samples at 617 and 685 mm depth (Table 4.2) whose [U] concentrations of 0.45 and 0.31 ppm, respectively, are substantially below the mean [U] concentration of 2.11 ppm. This [U] loss may have occurred during partial replacement of the aragonite botryoids by neomorphic columnar calcite thus violating the

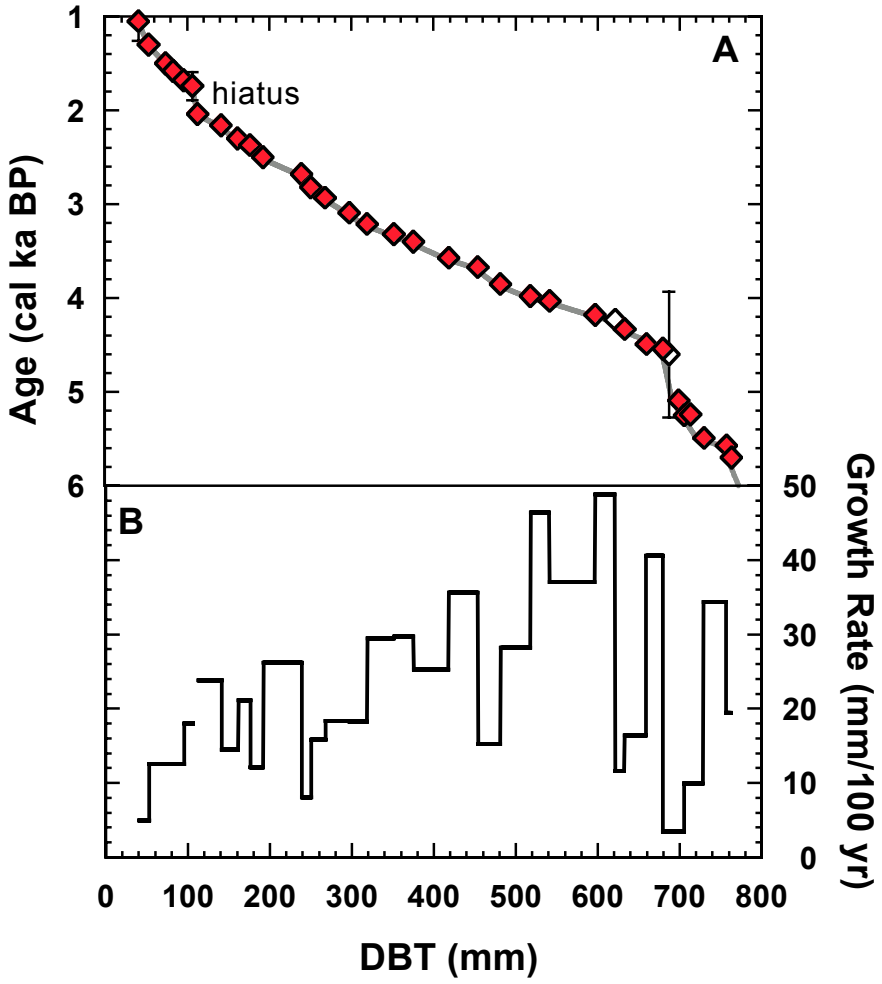

Fig. 4.3. (A) Age-depth profile of the stalagmite DSSG-5 derived from the $^{230}Th/^{234}U$ dates listed in Table 2. Red-filled diamonds are radiometric dates of pristine aragonite. Vertical bars are 2σ error. Two samples (5-36 and 5-27) represented by empty diamonds were excluded from the age model because of potential [U] leakage during partial replacement of aragonite by neomorphic calcite. The age model delineated by the gray line was derived from the Ager software application of the ARAND Time Series Analysis package (Howell et al., 2006). Record of variable growth rates graphed against depth in core using the age model in (A) (see text).

assumption of a closed- system. However, the two samples yield stratigraphically coherent ages (Table 4.2) suggesting that the partial replacement may have occurred close to the time of deposition. Similar complications in dating calcite replacements of aragonite were encountered in the U-Series dating study of an aragonitic stalagmite from Mexico (Lachniet et al., 2012).

U/Th isotope data listed in Table 4.2 yield a robust age model (Fig. 4.3 A) exhibiting stalagmite sections with variable growth rates (Fig. 4.3 B): (i) a lower, short section from 6.0 to 5.1 cal ka BP characterized by a growth rate of up to 34 mm/100 yrs that is succeeded by an exceptionally slow growth-rate interval of 3.5 mm/100 yr from 5.1 to 4.54 cal ka BP; (ii) a long middle section from 4.54 to 2.04 cal ka BP exhibiting a growth-rate peak of 48 mm/100 yrs and alternating fast and slow growth rates superimposed on a progressive decline to 24 mm/100 yrs; (iii) an offset in U/Th dates between 2.04 and 1.74 cal ka BP corresponding to a prominent dark, black layer (Fig. 4.3 B), and (iv) a rapid decline of growth rates to ~5 mm/100 yrs in the interval 1.74 to 1.1 cal ka BP.

The question arises whether the cored stalagmite investigated here (Fig. 4.2 A) contains any noticeable discontinuities, given their presence in the uppermost 40 mm of the DSSG-5 stalagmite, excluded from this study (Aharon et al., 2012). Assessment of the closely spaced U/ Th dates in conjunction with detailed petrographic observations (next section) offer the means to identify discontinuities in stalagmites. A ~6 mm thick, dark layer centered at 106 mm DBT (Fig. 4.2 A) exhibits an offset between two closely spaced U/Th dates at 2.04 ±0.05 and 1.74 ±015 cal ka BP (Table 4.2) and likely represents a depositional discontinuity. Additionally, the interval between 691 and 678 mm across a ~5 mm thick gray layer and centered at 685 mm DBT (Fig. 4.2 A) requires close scrutiny to evaluate whether it represents a hiatus or an exceptionally slow grow rate bracketed by three closely spaced U/Th dates of 5.1, 4.6 and 4.5 cal ka BP.

Table 4.2. U-Series isotopes and dating results of stalagmite DSSG-5.

ID	[a]DBT (mm)	[U] (ppm)	[Th] (ppb)	$^{230}Th/^{238}U$	$^{234}U/^{238}U$	$^{232}Th/^{238}U$	$^{230}Th/^{232}Th$	Age (cal ka BP) (uncorrected)	[b]Age (cal ka BP) (corrected)	$^{c}\delta^{234}U_i$ (‰)
5-28	40.5	1.707 ±0.128	11.29 ±0.85	0.0199 ±0.0002	1.6398 ±0.0031	0.002178 ±0.000004	9.1 ±0.1	1.33 ±0.01	1.05 ±0.21	641.8 ±1.2
5-1	52.9	3.147 ±0.236	0.92 ±0.07	0.0201 ±0.0004	1.6086 ±0.0027	0.0000097 ±0.000001	207.5 ±4.9	1.36 ±0.03	1.30 ±0.03	610.8 ±1.0
5-13	73.8	1.645 ±0.124	0.47 ±0.04	0.0237 ±0.0004	1.6590 ±0.0032	0.000095 ±0.000003	250.2 ±8.7	1.57 ±0.03	1.50 ±0.03	661.8 ±1.3
5-14	83.0	2.605 ±0.196	0.27 ±0.02	0.0241 ±0.0003	1.6055 ±0.0028	0.000034 ±0.000001	715.5 ±20.1	1.64 ±0.02	1.58 ±0.02	608.2 ±1.1
5-15	95.5	2.244 ±0.169	0.86 ±0.07	0.0258 ±0.0003	1.6221 ±0.0027	0.000126 ±0.000005	205.0 ±8.0	1.74 ±0.02	1.68 ±0.02	625.1 ±1.0
5-29	106.3	1.405 ±0.105	6.62 ±0.50	0.0291 ±0.0003	1.6341 ±0.0031	0.001552 ±0.000003	18.7 ±0.2	1.95 ±0.02	1.74 ±0.15	637.3 ±1.2
5-16	112.6	1.048 ±0.079	1.56 ±0.13	0.0315 ±0.0007	1.6291 ±0.0028	0.000491 ±0.000013	64.1 ±2.3	2.12 ±0.05	2.04 ±0.05	632.8 ±1.1
5-17	138.7	1.694 ±0.128	0.95 ±0.08	0.0331 ±0.0004	1.6329 ±0.0028	0.000185 ±0.000005	179.3 ±5.6	2.23 ±0.03	2.16 ±0.03	636.8 ±1.1
5-2	159.2	1.866 ±0.140	0.35 ±0.03	0.0350 ±0.0007	1.6301 ±0.0029	0.000062 ±0.000003	562.2 ±27.3	2.36 ±0.05	2.30 ±0.05	634.1 ±1.1
5-30	174.0	2.402 ±0.180	5.15 ±0.39	0.0373 ±0.0003	1.6461 ±0.0030	0.000706 ±0.000002	52.8 ±0.4	2.49 ±0.02	2.37 ±0.07	650.6 ±1.2
5-23	189.5	4.068 ±0.306	0.45 ±0.06	0.0375 ±0.0003	1.6149 ±0.0031	0.000037 ±0.000004	1025.8 ±114.9	2.55 ±0.02	2.50 ±0.02	619.4 ±1.2
5-18	236.2	3.733 ±0.282	1.26 ±0.11	0.0409 ±0.0005	1.6379 ±0.0029	0.000111 ±0.000005	367.5 ±16.3	2.75 ±0.04	2.68 ±0.03	642.8 ±1.1
5-31	247.6	4.263 ±0.320	0.20 ±0.02	0.0429 ±0.0003	1.6421 ±0.0032	0.000015 ±0.00000	2819.0 ±43.2	2.87 ±0.02	2.82 ±0.02	647.4 ±1.3

5-3	265.3	3.960 ±0.297	0.25 ±0.02	0.0445 ±0.0004	1.6426 ±0.0028	0.000021 ±0.000001	2114.4 ±87.3	2.99 ±0.03	2.93 ±0.03	648.0 ±1.1
5-32	294.6	3.611 ±0.271	0.28 ±0.02	0.0477 ±0.0004	1.6710 ±0.0031	0.000036 ±0.000001	1858.5 ±41.7	3.14 ±0.03	3.09 ±0.03	677.0 ±1.3
5-4	314.7	2.912 ±0.219	0.31 ±0.02	0.0488 ±0.0007	1.6454 ±0.0028	0.000035 ±0.000001	1395.3 ±37.7	3.27 ±0.05	3.21 ±0.05	651.3 ±1.1
5-33	347.1	2.647 ±0.199	2.31 ±0.17	0.0511 ±0.0004	1.6594 ±0.0028	0.000287 ±0.000001	178.0 ±1.4	3.40 ±0.03	3.32 ±0.04	665.7 ±1.1
5-5	371.0	2.304 ±0.173	0.55 ±0.05	0.0522 ±0.0009	1.6619 ±0.0027	0.000078 ±0.000004	669.6 ±33.8	3.46 ±0.06	3.40 ±0.06	668.2 ±1.1
5-6	413.7	1.502 ±0.113	0.76 ±0.06	0.0564 ±0.0009	1.7114 ±0.0028	0.000167 ±0.000004	338.3 ±9.1	3.64 ±0.06	3.57 ±0.06	718.6 ±1.2
5-34	449.3	1.624 ±0.122	1.96 ±0.15	0.0571 ±0.0003	1.6786 ±0.0034	0.000397 ±0.000001	143.9 ±0.9	3.76 ±0.02	3.67 ±0.04	685.8 ±1.4
5-7	476.7	1.732 ±0.130	0.91 ±0.07	0.0604 ±0.0010	1.7070 ±0.0028	0.000174 ±0.000006	347.8 ±12.5	3.91 ±0.07	3.85 ±0.07	714.7 ±1.2
5-35	513.4	1.024 ±0.077	0.35 ±0.03	0.0628 ±0.0005	1.7188 ±0.0035	0.000113 ±0.000001	558.3 ±7.0	4.04 ±0.03	3.98 ±0.04	727.1 ±1.5
5-8	536.8	1.785 ±0.134	5.05 ±0.41	0.0634 ±0.0011	1.7008 ±0.0031	0.000931 ±0.000031	68.1 ±2.5	4.12 ±0.07	4.03 ±0.07	708.9 ±1.3
5-9	592.3	1.465 ±0.110	0.50 ±0.04	0.0656 ±0.0007	1.7102 ±0.0035	0.000113 ±0.000004	580.2 ±23.3	4.25 ±0.05	4.18 ±0.05	718.6 ±1.5
5-36	616.1	0.451 ±0.034	0.30 ±0.02	0.0668 ±0.0009	1.7188 ±0.0036	0.000216 ±0.000001	309.2 ±5.0	4.30 ±0.06	4.23 ±0.06	727.6 ±1.5
5-24	624.8	1.952 ±0.147	0.41 ±0.19	0.0670 ±0.0007	1.6948 ±0.0037	0.000070 ±0.000031	963.0 ±189.0	4.37 ±0.04	4.33 ±0.05	703.5 ±1.5
5-37	656.0	1.594 ±0.120	0.17 ±0.01	0.0690 ±0.0004	1.7079 ±0.0029	0.000034 ±0.00000	2020.0 ±24.6	4.47 ±0.03	4.43 ±0.03	717.0 ±1.2

5-10	677.8	2.323 ±0.008	0.27 ±0.02	0.0734 ±0.0006	1.7663 ±0.0029	0.000038 ±0.000001	1919.0 ±64.7	4.60 ±0.04	4.54 ±0.04	776.3 ±1.3
5-27	684.7	0.307 ±0.023	6.82 ±0.52	0.0844 ±0.013	1.7611 ±0.0035	0.007314 ±0.000044	11.5 ±0.2	5.33 ±0.08	4.60 ±0.67	771.2 ±1.7
5-25	691.1	0.884 ±0.067	0.38 ±0.10	0.0804 ±0.0011	1.7398 ±0.0043	0.000142 ±0.000037	564.7 ±146.0	5.13 ±0.07	5.09 ±0.07	750.6 ±1.9
5-38	702.7	1.253 ±0.094	0.23 ±0.02	0.0842 ±0.0005	1.7652 ±0.0034	0.000062 ±0.00000	1368.7 ±14.0	5.30 ±0.03	5.25 ±0.03	776.8 ±1.5
5-19	710.0	1.886 ±0.142	0.62 ±0.05	0.0844 ±0.0007	1.7682 ±0.0031	0.000108 ±0.000002	782.2 ±18.0	5.30 ±0.05	5.24 ±0.05	779.7 ±1.4
5-26	721.0	1.017 ±0.077	1.09 ±0.13	0.0895 ±0.0009	1.7949 ±0.0038	0.000353 ±0.000034	253.8 ±24.4	5.55 ±0.06	5.49 ±0.06	807.5 ±1.7
5-39	752.1	1.405 ±0.105	1.64 ±0.12	0.0904 ±0.0006	1.7818 ±0.0040	0.000385 ±0.000001	234.9 ±1.7	5.65 ±0.04	5.57 ±0.05	794.3 ±1.8
5-11	758.2	0.884 ±0.066	0.35 ±0.03	0.0915 ±0.0013	1.7641 ±0.0032	0.000131 ±0.000008	695.5 ±45.5	5.76 ±0.08	5.70 ±0.08	776.5 ±1.4

Note: All ratios are activity ratios and uncertainties are 2σ error. Two ID samples listed in bold Italics (***5-36*** and ***5-27***) were excluded from the age model in Figure 3 A because of potential [U] loss during partial replacement of aragonite to columnar calcite (see text) [a] Distance below top of stalagmite.

[b] U/Th dates are conventionally corrected for external ($^{230}Th/^{232}Th$) assuming an initial activity ratio of 0.81 ±0.4 for a contaminant at secular equilibrium and with an arbitrary uncertainty of 50%. Here we used a slightly lower activity ratio of 0.65 ±0.3 that was acquired from Monte Carlo determinations of stratigraphically constrained ($^{230}Th/^{232}Th$) best fit value for the DSSG-5 stalagmite following the method of Hellstrom (2006). [c] $\delta^{234}U_A=[(^{234}U/^{238}U)_A -1]*10^3$; initial $(\delta^{234}U)_i$ values were back-calculated from present day using the corrected ages as follows: $\delta^{234}U_i$ (^{o}/oo)= $\delta^{234}U_A$ *e^(λ_{234}*t_{corr}) ; $\lambda_{234} = 2.8263*10^{-6}$ yr^{-1} ; t is the corrected age in years (column b).

4.3. THIN-SECTIONS ANALYSIS

Typical fabric in the DSSG-5 stalagmite consists of densely packed rows of aragonite botryoids (Fig. 4.4 A): (i) fanning upward; (ii) normal to the growth surface, and (iii) are generally between 200 and 600 μm across. Botryoidal aragonite was described by Bertaux et al. (2002) as a fibrous fabric in which adjacent crystals have the same crystallographic orientation under an optical microscope.

The dark layer at ~106 mm DBT (Fig. 4.4 B) exhibits (i) a succession of closely spaced interruptions, ~0.1 to ~0.2 mm thick, between the rows of botryoidal aragonite; (ii) truncation of the botryoid tips preceding the gaps; (iii) disruption of ordered deposition by dissolution and cavity filling by dark, fine detritus, and (iv) optical discontinuity between botryoid rows bordering the depositional gaps. These markers, typical of disconformities in stalagmite deposition (Fig. 5 in Aharon et al., 2012) are consistent with the occurrence of a hiatus within the dark, black layer (Fig. 4.4 B). The layers below and above the hiatus contain aragonite botryoids that are larger by a factor of three than their typical size (Fig. 4.4 A) suggesting deposition from drip-water ponded on the stalagmite top and experiencing slow CO_2 degassing (Frisia et al., 2002).

Whether the gray layer centered at 685 mm DBT represents a hiatus or an exceptionally low growth rate of ~4 mm/100 yrs (Fig. 4.3) has been investigated in detail. The following evidence supports a low growth rate: (i) unlike the hiatus at ~106 mm DBT (Fig. 4.4 B), no discontinuities are discerned between the rows (Figs. 4.4 C and D); (ii) large aragonite botryoids (> 1mm in size) that are tightly packed show optical continuity across the seasonal layers (Fig. 4.4 D); (iii) the most prominent $\delta^{18}O$ and $\delta^{13}C$ positive excursions discerned in Figures 4.2 B and C occur entirely within the high birefringence layer that lacks evidence of

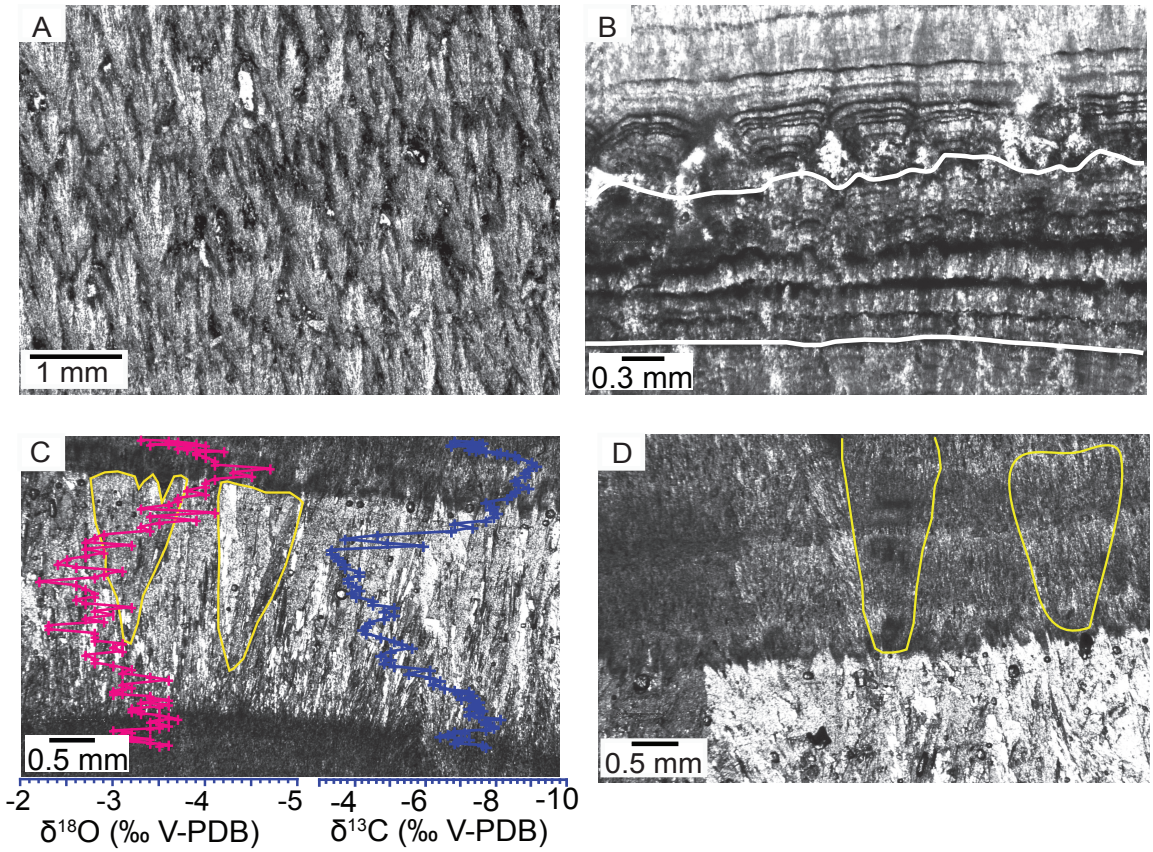

Fig. 4. 4. Photomicrographs in plane-polarized light from thin sections shown in Fig.2 A, illustrating aragonite fabrics in stalagmite DSSG-5. (A) Typical fabric of densely packed rows of aragonite botryoids with their long axes oriented in the direction of growth. (B) Fabric of the dark layer at ~106 mm DBT (see Fig. 2 A), showing disruptions in otherwise ordered deposition, indicating a hiatus in the interval delineated by white lines: (i) "shaved" tops of botryoids; (ii) depositional gaps, ~0.1-0.2 mm wide, filled by dark, fine detritus, and (iii) optical discontinuity between botryoid rows. (C & D) Close-up images of the gray layer centered at 685 mm DBT. Exceptionally large aragonite botryoids, up to 3.5 mm long and ~0.5 mm wide, rugged tops of botryoids displaying optical continuity, and anomalous ^{18}O and ^{13}C enrichment entirely within an uninterrupted row of botryoids argue in favor of an exceptionally low growth rate. Unusually large aragonite botryoids are considered indicators of deposition under dry-climate conditions (Frisia et al., 2002).

discontinuity (Fig. 4.4 C). Frisia et al. (2002) established that aragonite botryoids with length- to-width ratio exceeding 6:1 are typically enriched in ^{18}O and ^{13}C, indicating deposition under drought conditions. The petrographic analysis and isotope data (see below) are consistent with this interpretation.

4.4. $\delta^{18}O$ AND $\delta^{13}C$ TIME SERIES

Stable-isotope time series spanning the mid-to-late Holocene are shown in Figure 4.5 (see Appendix 4.1 for data) with the chronology based on the age model in Figure 4.3 A. The time series exhibit significant variability and contain a number of distinct positive and negative departures from the mean values of -3.3 ±0.4‰ and -7.3 ±0.8‰ for $\delta^{18}O$ and $\delta^{13}C$, respectively (n=1884). With one exception, $\delta^{18}O$ and $\delta^{13}C$ profiles are coherent on interdecadal and intercentennial time scales. The exception is the long-term positive$\delta^{18}O$ trend that has no counterpart in the $\delta^{13}C$ record (Fig. 4.5).

The most prominent among the $\delta^{18}O$ and $\delta^{13}C$ isotope excursions are the positive shifts to -2.3‰ and -3.6‰, respectively, centered at 4.8 cal ka BP (marked #1 in Fig. 4.5). $\delta^{18}O$ and $\delta^{13}C$ reversals to about modern values at ~4.6 cal ka BP constitute the first of a succession of alternating positive and negative isotope excursions of about 0.9‰ to 1.2‰ amplitudes (positive isotope shifts at about 4.5, 4.1, 3.8, 3.5, 3.0, 2.6, 2.1 and 1.4 cal ka BP, and negative isotope shifts in between) extending to the top of the series (marked #2 in Fig. 4.5). A hiatus centered at ~1.8 cal ka BP of 100-300 yrs duration precedes the last positive isotope excursion in the series. These isotope excursions are superimposed on an ^{18}O long-term enrichment trend of ~0.52‰ (marked #3 in Fig. 4.5). Although both $\delta^{18}O$ and $\delta^{13}C$ records exhibit interdecadal periodicities after the 4.8 cal ka BP isotope event, the $\delta^{13}C$ cycles are proportionally smaller in amplitude, and the long-term trend is noticeably absent.

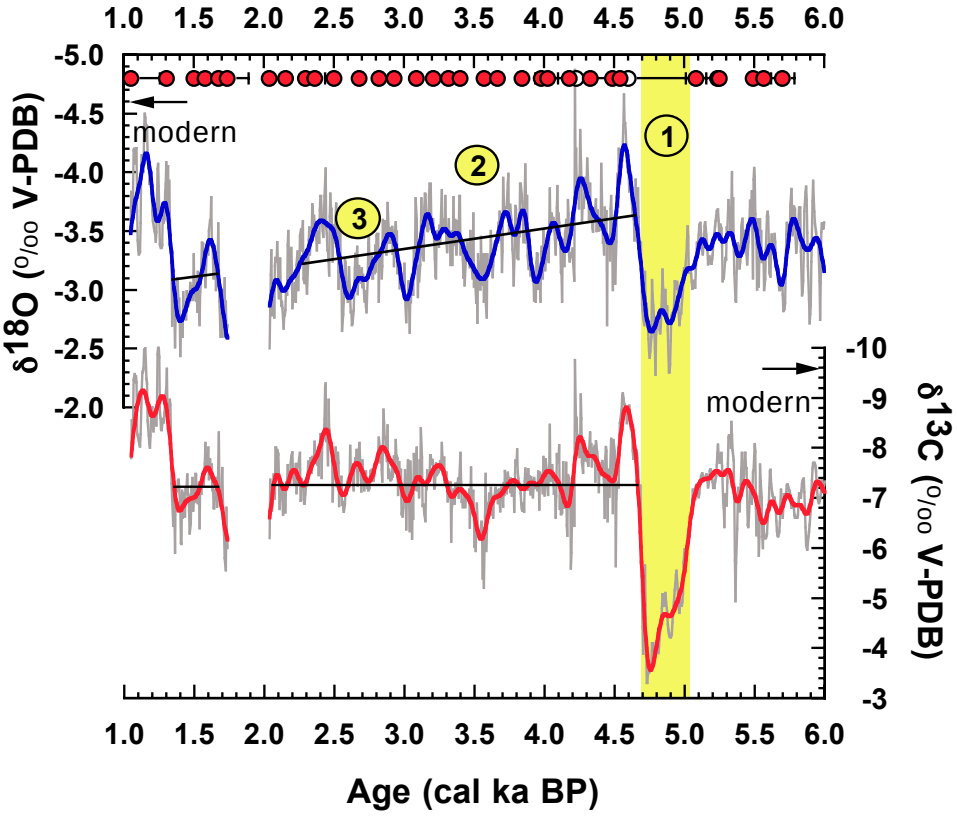

Fig. 4.5. $\delta^{18}O$ and $\delta^{13}C$ time-series graphed against the age model derived in Fig. 3 A on the basis of 33 precise $^{230}Th/^{234}U$ dates (red filled circles on top). Arrows mark the $\delta^{18}O$ and $\delta^{13}C$ values of modern pristine aragonites (n = 12). Thin gray lines connect measured isotope values (n = 1884) at 5 yrs resolution. ARAND software application (Howell et al., 2006) was used to smooth the $\delta^{18}O$ and $\delta^{13}C$ time series (thick blue and red lines, respectively) with a 60-yr low pass filter (LPF) using a Δt = 5 yrs. Three prominent isotope events documented in the isotope time series are marked by numbers as follows: (1) exceptional ^{18}O and ^{13}C-enrichments at 4.8 cal ka BP ("5 ka" event); (2) recovery of the isotopes to almost modern level at 4.6 cal ka BP followed by inter centennial $\delta^{18}O$ and $\delta^{13}C$ synchronous cycles, and (3) millennial ^{18}O-enrichment trend that is absent in the contemporaneous $\delta^{13}C$ time series.

4.5. A TEST OF ISOTOPE HOMOGENEITY AND EQUILIBRIUM

The necessary avoidance of sampling neomorphic calcite forced us to shift occasionally the sampling path laterally from the central axis of growth by few cm (Fig. 4.2 A). In order to test for isotope homogeneity of the 4 cm wide core, samples for $\delta^{18}O$ and $\delta^{13}C$ determinations were acquired along two growth increments at 82 and 299 mm depths, respectively, using the conventional "Hendy tests" (Hendy, 1971). The results, graphed in Figure 4.6 A, offer compelling evidence that the pristine aragonite is isotopically homogenous across the core along the growth layers (Fig. 4.6 A). Additionally, an absence of correlation between the oxygen and carbon isotopes (Fig. 4.6 B) suggests that isotopic equilibrium between aragonite and drip-water source was maintained (Hendy, 1971).

5. DISCUSSION

5.1. PALEOCLIMATE IMPLICATIONS OF THE $\delta^{18}O$ AND $\delta^{13}C$ TIME SERIES

The isotope time series in Figure 4.5 beg the question of their paleoclimate significance. Three prominent isotope events need to be address: (i) the exceptional ^{18}O and ^{13}C-enrichments at ~4.8 cal ka BP (the "5 ka" event); (ii) the recovery of the isotopes to almost modern levels at ~4.6 cal ka BP followed by interdecadal and intercentennial $\delta^{18}O$ and $\delta^{13}C$ synchronous cycles, and (iii) the millennial ^{18}O-enrichment trend that is absent in the contemporaneous $\delta^{13}C$ time-series. I will first evaluate the climate-driven factors that govern the variability observed in the $\delta^{18}O$ time series, follows by those controlling the $\delta^{13}C$ time series.

5.2. CLIMATE FACTORS CONTROLLING THE OXYGEN-ISOTOPE VARIATION

Oxygen-isotope excursions in stalagmites are generally controlled by a number of factors (McDermott, 2004; Lachniet, 2009, 2015), including changes in: (i) ambient cave air temperature that mimics on the average annual air temperature outside the cave; (ii) rainfall amount; (iii)

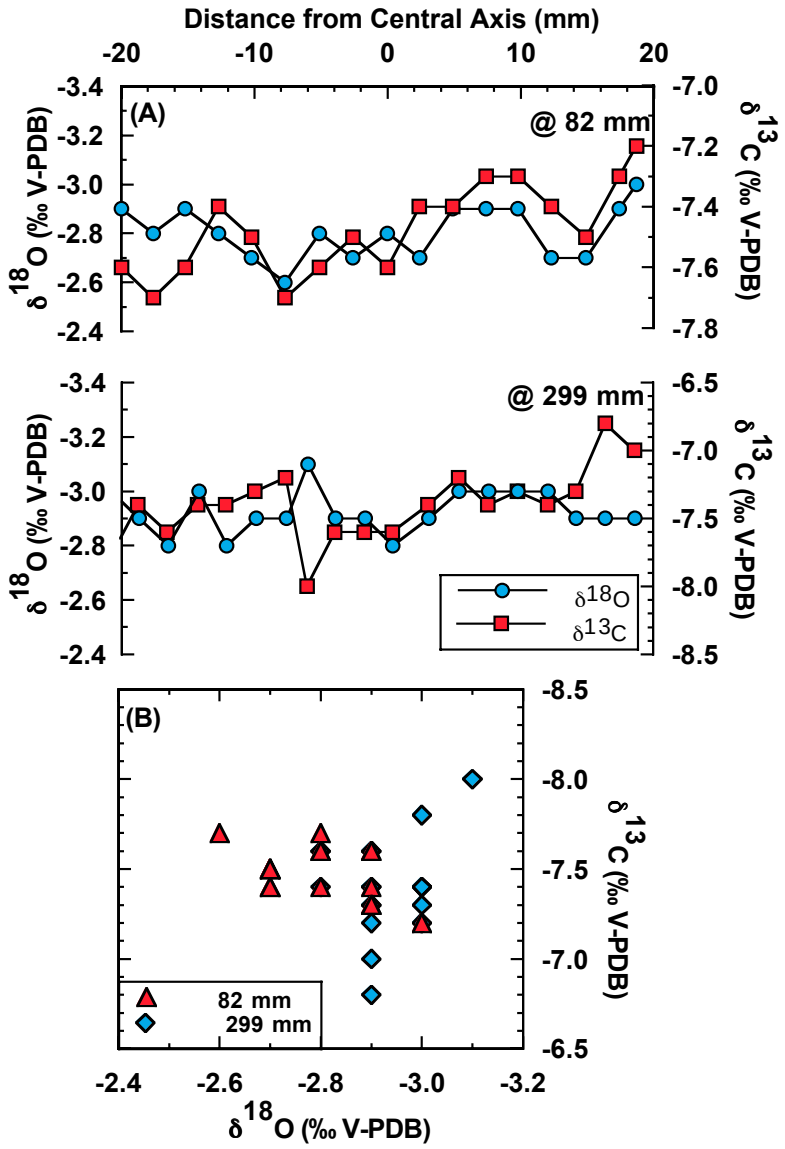

Fig. 4.6. Tests of isotope homogeneity and isotope equilibrium state using conventional "Hendy tests" (Hendy, 1971). (A) $\delta^{18}O$ and $\delta^{13}C$ values of samples acquired along growth layers at 82 mm and 299 mm DBT; absence of statistically significant deviations from the mean along the growth layers offers evidence of isotope homogeneity away from the axis of maximum growth. (B) Cross plot of oxygen and carbon isotopes acquired along the growth increments; the absence of correlation displayed by the isotopes favors aragonite deposition in isotope equilibrium with the drips.

combined air-temperature and rainfall variability; (iv) seasonal shift in rainfall dominance without a substantial air-temperature change, and (v) kinetic isotope fractionation that are attributed to evaporation on the stalagmite tops during severe droughts.

Figure 4.7 depicts an envelope encompassing the temperature-dependence of $\delta^{18}O$ fractionation between aragonite and water based on published equations. Aragonite $\delta^{18}O$ values falling within the area of the envelope are considered to have been deposited in isotope equilibrium whereas values outside the envelope were not. Thin aragonite layers shaved from the tops of active stalagmites next to DSSG-5, likely representing several years of deposition, yield $\delta^{18}O_{ar}$=-4.6 ±0.1 (‰V-PDB or 26.2 ‰V-SMOW; 1σ SEM, n=12). Given an annual drip-water mean $\delta^{18}O$ of -4.7 (‰ V-SMOW) (Table 4.1), a $\delta^{18}O$ difference between the modern aragonite and drip-water of ($\delta^{18}O_{ar}$ - $\delta^{18}O_{dw}$) =30.9 (‰V-SMOW or -0.04 ±0.5 ‰ V-PDB) and an annual mean cave air temperature of 18.2 ±0.7 °C indicate that recently formed aragonites at DeSoto Caverns grew in isotopic equilibrium (Fig. 4.6).

Were ambient temperature change the dominant factor controlling the rapid $\delta^{18}O$ positive shifts documented in Figure 4.5 in the absence of change in drip-water $\delta^{18}O$, then the maximum ($\delta^{18}O_{ar}$ - $\delta^{18}O_{dw}$) excursions of 2.3‰ at ~4.8 cal ka BP and 1.8‰ mean shift during the interval 4.73-1.14 cal ka BP relative to the modern value would correspond to ~6 to ~13 °C and ~4 to ~11°C cooling relative to present (Fig. 4.7). Such low cave-air temperatures are unlikely in the mid-to-late Holocene (Kim et al., 2004; Marcott et al., 2013). With one exception to be discussed later, the long-term seasonal rainfall switch from winter to summer and occurrence of severe summer droughts likely controlled the isotope cycles and extreme isotope excursions (Figure. 4.5).

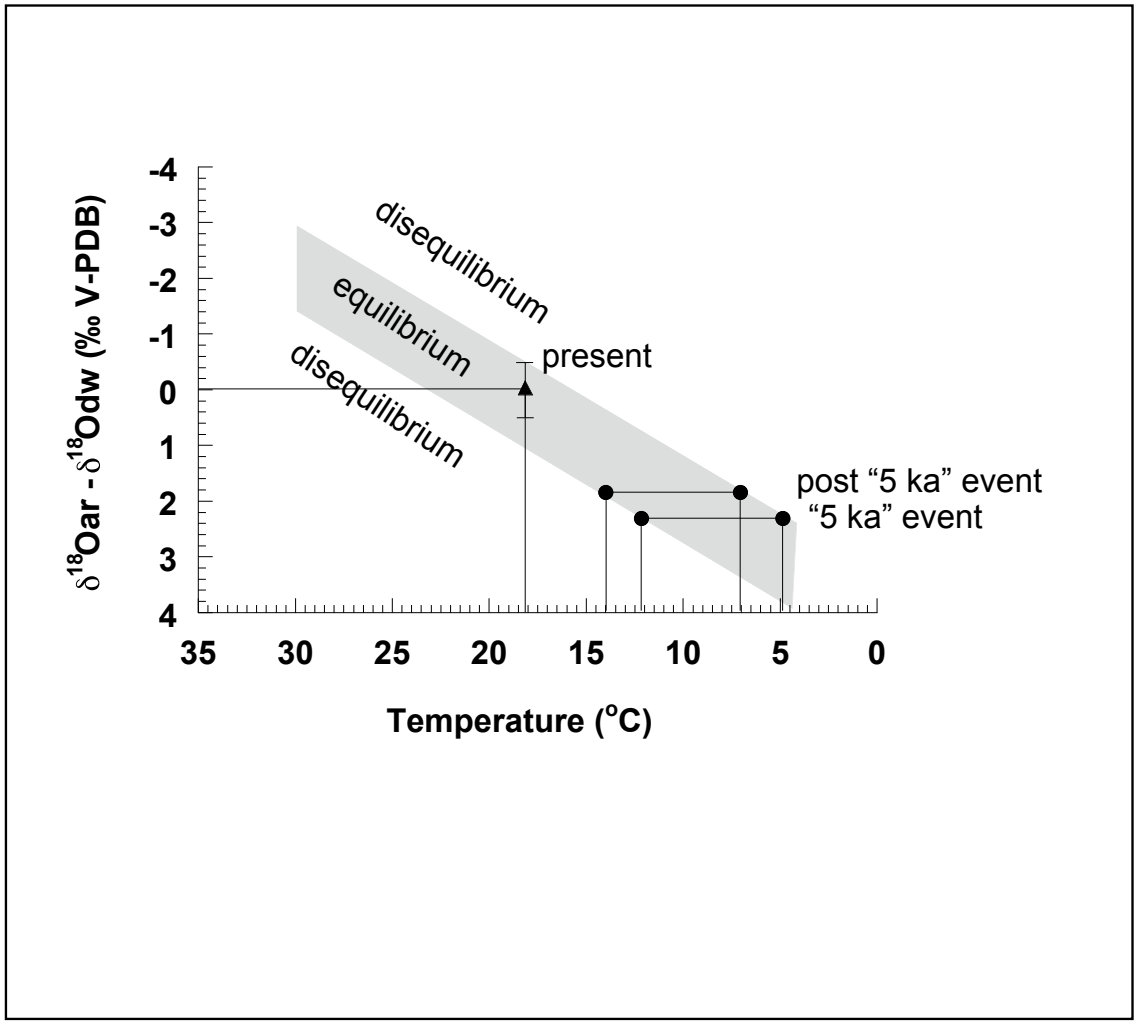

Fig. 4.7. Temperature-dependency of oxygen isotope fractionation between aragonite and drips. The “isotope equilibrium” field (grey-shaded polygon) is defined by $\delta^{18}O$ thermometers derived on the basis of published equations (Aharon and Chappell, 1983; Grossman and Ku, 1986; Thorrold et al., 1997; Radtke et al., 1998; White et al., 1999; Böhm et al., 2000; Kim et al., 2007). The intersection of Modern aragonites $\delta^{18}O$ minus annual mean drip water $\delta^{18}O$ values (filled triangle, $\delta^{18}O_{ar} - \delta^{18}O_{dw}$ = 30.9‰ V-SMOW or -0.04 ± 0.5‰ V-PDB) at the present mean annual cave temperature of 18.2 ± 0.7 °C (Table 1) falls within the isotope equilibrium field. On the premise that all other factors except air cave temperature remained unchanged in the past, the maximum $\delta^{18}O$ positive excursion during the “5 ka” event and the mean $\delta^{18}O$ positive shift during the interval 4.73 - 1.14 cal ka BP yield a cooling relative to present that is highly unlikely for the mid-to-late Holocene (see text).

5.3. SWITCH IN RAINFALL SEASONALITY OR CHANGES IN WATER-VAPOR SOURCES?

Two distinct climate factors may explain the positive and negative $\delta^{18}O$ cycles documented in Figure 4.5: (i) switch in the rainy season from winter to summer (accompanied by summer droughts), and (ii) periodic changes in water-vapor sources.

Rainfall $\delta^{18}O$ interannual variation has been interpreted as resulting from changes in ground air temperature since the pioneering work of Dansgaard (1964). More recent studies based on multi-decadal precipitation records have demonstrated that $\delta^{18}O$ interannual variability can better be explained by changes in the seasonal distribution of rainfall, a finding that has important paleo-hydroclimate implications (Henderson et al., 2010; Vachon et al., 2007). ENSO variability and the variable position of BH in the North Atlantic, the latter being controlled by the variable pressure differential between the Icelandic low and the Azores high, were proposed by Lambert and Aharon (2010) as the main drivers of present-day droughts and wet spells for SEUS and the IGC. Paleo-hydroclimate results (Hardt et al., 2010) as well as models simulating the present hydroclimate in the SEUS (Folland et al., 2009; Knight et al., 2006; Ortegren et al., 2011) support Lambert and Aharon's (2010) contention. These studies (op. cit.) have indicated that on interdecadal time scales hydroclimate extremes are only weakly controlled by ENSO whereas the Southern North Atlantic Oscillation (SNAO) in general, and BH west-east summer migration specifically, play a key role in generating hydroclimate extremes. Both SNAO and BH indices are strongly associated with the pattern of the North Atlantic sea-surface temperature (SST) shifts, known as the Atlantic Multidecadal Oscillation (AMO; Kerr, 2005). A warm AMO phase is associated with dry summers whereas a cool AMO phase is associated with wet summer regimes (Baines and Folland, 2007; Ortegren et al., 2011). The simple numerical model below illustrates how a change in seasonal rainfall dominance can impact the interannual $\delta^{18}O$ of the

drips, and consequently that of the aragonite stalagmites from DeSoto Caverns.

Under the present hydroclimate conditions, Alabama rainfall exhibits a winter excess over summer of 1.3 ($f_w > f_s$) and $\delta^{18}O$ differential between the two main seasons of 1.1‰ (V-SMOW) (Table 4.1). On the other hand the seasonal $\delta^{18}O$ differential in drip-waters is statistically insignificant, suggesting mixing of seasonal waters in the epikarst (Table 4.1) whose fractions can be estimated using a simple mass balance equation as follows:

$$\delta_w f_w + \delta_s f_s = \delta_{dw} (f_w + f_s) \qquad (1)$$

where, $\delta_w f_w$ and $\delta_s f_s$ are the $\delta^{18}O$ and fractions of winter and summer rainfall, respectively, and δ_{dw} is the annual mean of $\delta^{18}O$ of drip-waters. Using the $\delta^{18}O$ values listed in Table 4.1 and ($f_w + f_s$) =1, estimation of annual drips consists of a mixture of 62% winter and 38% summer rainfall (f_w=0.62; f_s=0.38). Because the annual differential between aragonite and drip-waters (($\delta^{18}O_{ar} - \delta^{18}O_{dw}$) =-0.04 ±0.5 (‰ V-PDB)) is constant in the absence of a cave air temperature change, then a $\delta^{18}O_{ar}$ =-2.7 (‰ V-PDB) (the mean ^{18}O-enrichment in the late Holocene cycles, Fig. 4.5) will yield a $\delta^{18}O_{dw}$ = -2.7 (‰ V-SMOW). Assuming an unchanged winter rainfall of $\delta^{18}O_w$=-5.1 (‰ V-SMOW) and a $\delta^{18}O_s$=-1.3 (‰ V-SMOW), a value typical of July-August normal rainfall, then using the mass-balance expression in (1) above the $\delta^{18}O$ positive excursions during "event #2" (Fig. 4.5) can be explained by a reversal of the dominant rainfall from winter to summer in the epikarst ($f_s \geq f_w$; f_s=0.63; f_w=0.37) and summer rainfall variability. Extreme ^{18}O-enrichment in summer rainfall is not unusual under the present hydroclimate conditions; for example, monthly rainfall>100 mm typically yields $\delta^{18}O$ weighted mean values that are up to 3.3 ‰ enriched in ^{18}O relative to the annual weighted mean (Table 4.1).

Changes in water vapor sourcing offers an alternative explanation for $\delta^{18}O$ cycles (Figure. 4.5). Simulations by LeGrande and Schmidt (2009) for the Northern Hemisphere predict

$\delta^{18}O$ enrichment in summer rainfall during the Mid-to-Late Holocene relative to modern. They attributed this result to alteration of water-vapor transport from the tropical ocean onto land. However, the synchronization of fluctuations in $\delta^{13}C$ and $\delta^{18}O$ supports a reversal of the seasonal distribution of rainfall as the controlling driver of the observed mid-to-late Holocene $\delta^{18}O$ cyclicity (Fig. 4.5). This is because changes in water-vapor sourcing will affect the $\delta^{18}O$ of rainfall, and ultimately the stalagmite proxy $\delta^{18}O$ record, but will not impact the $\delta^{13}C$ record. In contrast, a switch in the seasonal distribution of rainfall will be manifested in both proxy records, as described below.

Lambert and Aharon (2011) have identified a number of above-cave and in-cave processes affecting the Dissolved Inorganic Carbon (DIC) and ^{13}C variation in drips and stalagmites at DeSoto Caverns. The above-cave processes include the degree of water availability to C3 plants and water percolation rates through the vadose zone. The in- cave processes include the rate and degree of CO_2 degassing that are a function of drip flow-rates and seasonal changes in ventilation affecting pCO_2 changes in the cave atmosphere. On the basis of a radiocarbon mass-balance of carbon delivered annually by drips to the aragonite stalagmites at DeSoto Caverns, Lambert and Aharon (2011) established that ~77% of the carbon is derived from ^{13}C-depleted soil CO_2 and the remainder from dissolution of ^{13}C-enriched dolomite bedrock. Variation in summer rainfall would impact stalagmite $\delta^{13}C$ values because of (i) substantially higher evapotranspiration in summer months and (ii) its effect on biomass productivity. Dry summers will reduce water availability in the soil during the growing season that in turn would elevate the $\delta^{13}C$ of soil CO_2 reaching the cave (Lambert and Aharon, 2010; 2011).

5.4. SEVERE DROUGHT EVENTS

Two severe drought events affected the southeast while the stalagmite was growing. One event, centered at 4.8 ±0.14 (2 σ) cal ka BP (the "5 ka" event), exhibits ^{18}O and ^{13}C enrichments of 2.3‰ and 6‰, respectively, relative to modern values, and is associated with an anomalously slow growth rate (Fig. 4.3 B). The other event, centered at ~1.8 cal ka BP and associated with a hiatus (Fig. 4.4 B), is bounded by layers with ^{18}O and ^{13}C enrichments of 2‰ and 4‰ relative to modern, respectively. These values are the highest late-Holocene positive excursions measured on the stalagmite (Fig. 4.5). The isotope data and the associated features of the two events above suggest severe drought. Exceptional isotope enrichments in stalagmites is typically caused by kinetic effects (Lachniet, 2015) associated with long residence time of drip-water on stalagmite tops. This promotes enhanced evaporation and occurs during significant slow-down or complete cessation of dripping. Second, petrographic observations of the intervals containing the two events show unusually large aragonite botryoids (> 1mm in size; Figs. 4.4 B and D), which are diagnostic of deposition under dry conditions (Frisia et al., 2002).

The positive $\delta^{18}O$ trend of ~0.52‰ (event #3 in Fig. 4.5), coupled with the absence of a contemporaneous positive trend in $\delta^{13}C$, offers compelling evidence of gradual cooling (~0.6 °C/10^3 yrs) over the time interval 4.7 to 1.3 cal ka BP (total of ~2 °C) given a $\delta^{18}O$ temperature dependency of 0.23‰ °C-1. $\delta^{13}C$ is insensitive to cave-air temperature changes (carbon isotope fractionation of 0.035‰ °C-1 between solid carbonate and bicarbonate, Emrich et al., 1970) and is consistent with independently estimated cooling of ~2 °C from 7 cal ka BP to ~0.1 cal ka BP for extratropical Northern Hemisphere sites (30° to 90 °N) (Marcott et al., 2013).

5.5. LINKING CLIMATE EVENTS AND OCEAN-ATMOSPHERE DYNAMICS IN THE MID-TO-LATE HOLOCENE

In order to gauge whether the documented isotope variation in the DeSoto stalagmite (Fig.

4.5) reflects regional or global climate change, the findings of this study are compared with contemporaneous proxy records from elsewhere.

The most prominent positive-isotope excursions documented at DeSoto Caverns (Fig. 4.8 A), centered at 4.8 ±0.14 cal ka BP (the "5 ka" event), exhibit rapid inception and termination, and likely a severe drought that lasted about 300-yrs duration. The exceptional hydroclimate event in SEUS is synchronous with the abrupt termination of the African Humid Period (AHP) in both West and East Africa, dated by radiocarbon at 4.9 ±0.4 cal ka BP and 4.96 ±0.07 cal ka BP, respectively, (Fig. 4.8 B). The transition between humid and dry phase is estimated to have taken between 280 and 490 yrs (Tierney and deMenocal, 2013). The SEUS severe drought and the initiation of North African aridification were synchronous with (i) a major $\delta^{13}C$ negative excursion in benthic foraminifera (Fig. 4.8 C) indicating a large reduction in the North Atlantic Deep Water (NADW) formation associated with extreme wintry conditions and expansion of sea-ice (Oppo et al., 2003), and (ii) an abrupt increase in lithic fragments in the South Atlantic sector of the Southern Ocean (Fig. 4.8 D) indicating contemporaneous sea-ice advances in the Southern Hemisphere (Hodell et al., 2001). The "5 ka" climate event also left indelible marks on tropical ice caps in both hemispheres. Ice cores from the Kilimanjaro ice cap in eastern Africa exhibit a substantial reduction of ice deposition accompanied by a thick layer of dust suggesting a severe drought event coinciding with the rapid retreat of the Quelccaya ice cap in the southeastern Andes of Peru (Thompson et al., 2006). The correspondence of the abrupt hydroclimate changes in the tropics and subtropics with SST cooling and sea-ice advances in the polar regions of the Atlantic Ocean offer compelling evidence of an abrupt climate change of global extent involving complex ocean-atmosphere interactions. The event marks the termination of the Hypsithermal and the initiation of the Neoglacial phase of the Holocene

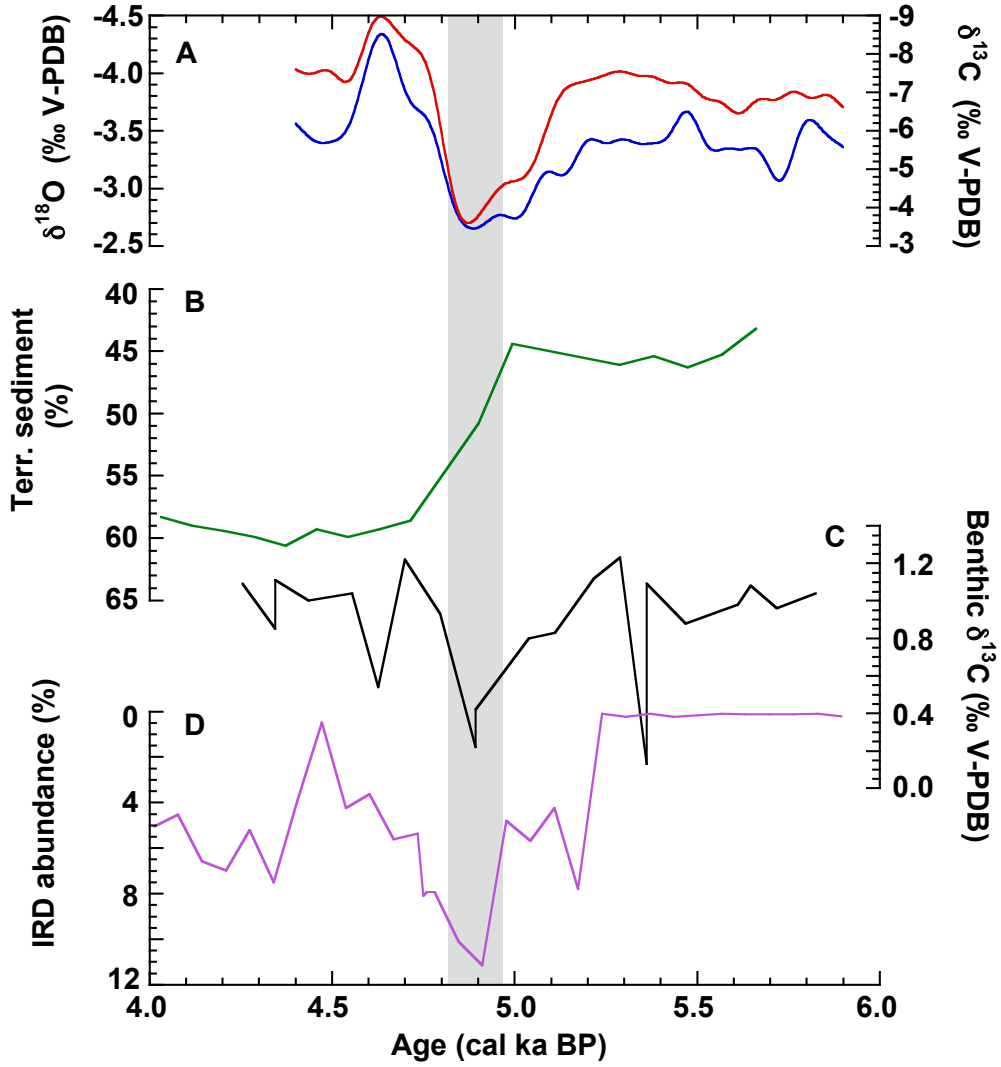

Fig. 4.8. Comparison of the "5 ka" mega-drought event at DeSoto Caverns with coeval mid-Holocene climate records. (A) The mega-drought centered at 4.8 ± 0.14 cal ka B.P (2σ) is manifested at Desoto Caverns by the exceptional $\delta^{18}O$ and $\delta^{13}C$ positive excursions. (B) Abrupt increase in % eolian sediment at ODP site 658C off Northwest African margin corresponds with the transition between humid and dry phase modes that caused the termination of the African Humid Period (AHP) and the initiation of the North African desertification (deMenocal et al., 2000). The original age model was recalculated using the revised phase transition age of 4.9 ± 0.4 cal ka BP (Tierney and DeMenocal, 2013). (C) Benthic foraminifera $\delta^{13}C$ record from the subpolar North Atlantic ODP 980 site serving as a proxy for the North Atlantic Deep Water (NADW) production variability (Oppo et al., 2003). The abrupt negative $\delta^{13}C$ excursion coeval with the "5 ka" event corresponds to a slowdown in NADW production and a cooling in Greenland. (D) Abundance variability in Ice-Rafted Detritus (IRD) from the Subantarctic South Atlantic offers evidence for a rapid sea-ice expansion in the Southern Ocean during the "5 ka" event (Hodell et al., 2001).

followed by a gradual cooling of ~2 °C from mid-to-late Holocene.

The recovery from the "5 ka" drought was succeeded by prominent century-long $\delta^{18}O$ and $\delta^{13}C$ cycles. The most severe of the periodic summer droughts is associated with a hiatus centered between 2.04 and 1.74 cal ka BP (or 90 BC and 210 AD). The succession of nine century-long droughts events is consistent in time and amplitude with $\delta^{18}O$ time series from stalagmites at the Jiuxian Cave in central China that record summer monsoon wet and dry modes (Cai et al., 2010).

Manifestation of long-term hydroclimate changes in the mid-to-late Holocene (published reports summarized by Wanner et al., 2008), is attributed to a decrease in insolation differential between summer and winter in the Northern Hemisphere (Holmes, 2008) (Fig. 4.9 B). The documented correlation between SEUS and central China stalagmite records is consistent with the model prediction of strong links between SNAO, BH and AMO (Baines and Folland, 2007; Folland et al., 2009; Henderson and Vega, 1996; Ortegren et al., 2011) and the subtropical North Atlantic response to changes in the Asian Summer Monsoon (ASM) (Lu et al., 2006; Rodwell and Hoskins, 2001).

Modelers seeking to establish the climate impacts of the AMO on the basis of instrumental climate records have suggested warm to cold phase shifts of 60-80 yrs periodicity in the North Atlantic (Kerr, 2000; 2005; Minobe, 1997; Schlesinger and Ramankutty, 1994). The shortness of the instrumental climate records (1861-2010), however, limits the confidence of the proposed periodicity. The dominant periodicity of 68 ±4 yrs exhibited by the DeSoto stalagmite $\delta^{18}O$ time series (Fig. 4.9 C) is consistent with the modern AMO phase shift periodicity and strengthens the argument that AMO played a dominant role in the hydroclimate changes documented in the late Holocene.

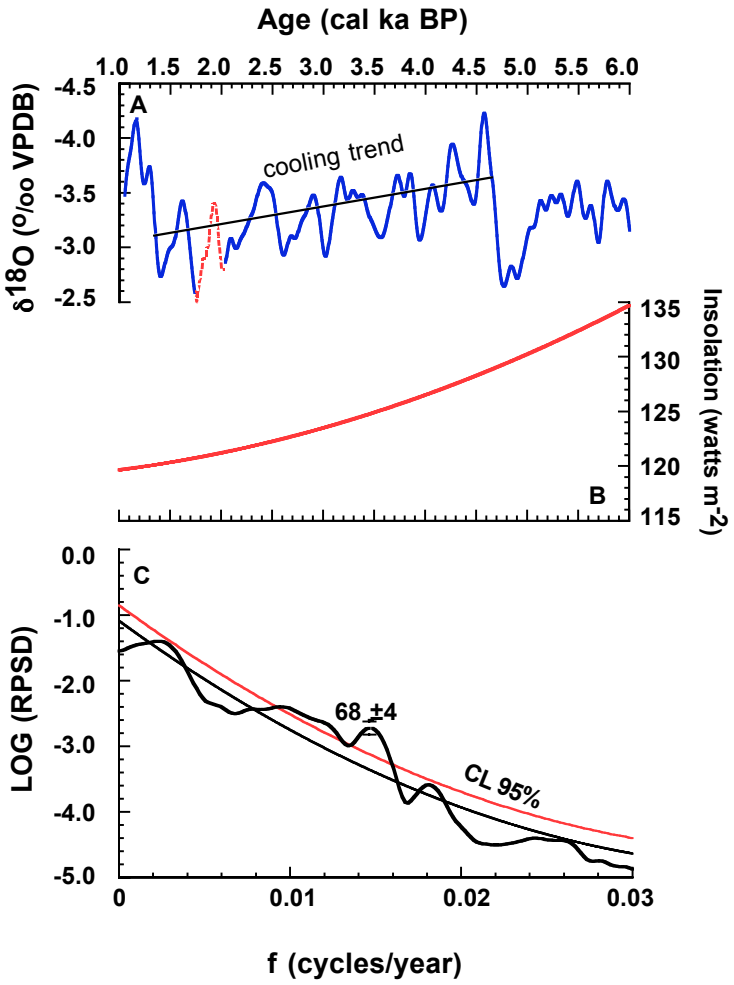

Fig. 4.9. (A) Mid-to-Late Holocene $\delta^{18}O$ time series exhibiting a millennial ^{18}O-enrichment trend corresponding to a gradual cooling of ~2 °C. Missing values (dashed red lines) during the hiatus between 2.04 and 1.74 cal ka BP ("porous time-series") were estimated using Excel software (Honaker and King, 2010). (B) Gradual reduction in seasonal insolation contrast (summer minus winter) at 30°N during mid-to-late Holocene (Berger and Loutre,1991). (C) Power Spectra Density (PSD) of $\delta^{18}O$ time series from stalagmite DSSG-5 in the interval 4.73 to 1.135 cal ka BP derived by ARAND software application (Howell et al., 2006). Pre-whitening at $f \leq 0.0333$ yrs was used to remove the high frequencies that would otherwise impair the fidelity of the PSD analysis (Gilman et al., 1963). Thin black and red lines correspond to spectral background and 95% confidence interval, respectively. The input parameters that were used to derive the PSD output are as follows: (i) Number of samples (N = 720); (ii) Time lags (M = 144); (iii) Number of frequencies (Nf = 288); (iv) Degrees of freedom (Ndf = 13), and (v) Bandwidth (B = 0.00185139). The units on the ordinate are the logarithm of the Relative Power Spectra Density (RPSD) and the frequency units on the abscissa are cycles/ year. The dominant periodicity of 68 ± 4 yrs exceeds the 95%confidence level and is consistent with the AMO periodicity of 60 - 80 yrs (Minobe, 1997; Kerr, 2005; Knight et al., 2005).

The late Holocene hydroclimate events have long attracted the attention of scientists from a variety of disciplines because of the likely societal impact of droughts on the declining and subsequent fading of ancient civilizations in the Levant, India and Asia (Clark et al., 2016; Staubwasser and Weiss, 2006). Whereas the majority of the drought events seem to cluster around 4.5-4.0 cal ka BP (Booth et al., 2005; Bar-Matthews and Ayalon, 2011; Cullen et al.,2000; Davis and Thompson, 2006; Dixit et al., 2014; Liu and Feng, 2012; Meijer et al., 2012; Stanley et al., 2003; Wang et al., 2016; Weiss et al., 1993; Welc and Marks, 2014; Zanchetta et al., 2016, among others) it is evident that discrete droughts started centuries before (e.g., 4.7 cal ka BP in a central Tibetan ice core, Thompson et al., 2006) and continued periodically to the last millennium (Russell and Johnson, 2005).

Although it is generally accepted that manifestations of drought during the late Holocene occurred in widely separated geographic locations, some sites offer proxy evidence of wetter conditions; e.g., pollen evidence in lake sediments from central Brazil dated at 4.6 cal ks BP (Salgado-Labouriau et al., 1998), Northern Mexico lake levels over the time interval 4.3 to 3.8 cal ka BP (Castiglia and Fawcett, 2006) and sediment cores from the Central Everglades, Florida dated at 4.6 to 2.8 cal ka BP (Glasser et al., 2013). Therefore, it is apparent that late Holocene exhibits climate complexities dictated by data resolution, spatial distribution and the accuracy and precision of the chronology.

6. CONCLUSIONS

1. Investigation of an actively forming stalagmite at DeSoto Caverns by thin-sections petrography, stable oxygen- and carbon-isotopes and high precision $^{230}Th/^{234}U$ radiometric dating of pristine aragonites yield proxy hydroclimate time series at interannual resolution and afford an assessment of the dominant climate drivers in the time interval 6.0-1.1 cal ka BP.

2. Prior monitoring of the cave ambient environment, isotope chemistry determinations of multiple drips, decade-long weekly rainfall $\delta^{18}O$ and $\delta^{2}H$ data and isotope determinations of actively forming aragonites provide a solid frame of reference for identifying of the factors exerting the strongest influence on the hydroclimate, documented by the stalagmite-based $\delta^{18}O$ and $\delta^{13}C$.

3. Four prominent isotope excursions were identified: (i) a rapid positive shift centered at 4.8 ± 0.14 cal ka BP carrying the imprint of a severe drought is consistent with the "5 ka" event elsewhere; (ii) a succession of multiple negative and positive cyclic isotope excursions of 0.9‰ to 1.2‰ in the interval 4.6 to 1.1 cal ka BP having a dominant periodicity of 68 ±4 yrs and representing alternating sets of years with wet and dry summers superimposed on a long-term switch of rainfall dominance from winter to summer; (iii) a severe drought between 2.04 and 1.74 cal ka BP associated with a hiatus, and (iv) a long-term ^{18}O-enrichment trend of 0.52‰ representing an equivalent cooling of ~2 °C.

4. The severe drought at 4.8 cal ka BP matches well in timing and rate with the phase transition from humid to dry climate in northern Africa and the expansion of sea-ice in the polar regions. The synchrony and abruptness of the documented climate changes at 5 ka suggest close climate links between the tropics, subtropics and polar regions and point to a major episode of NADW production disturbance as the cause of the "5 ka" global event.

5. Gradual cooling of ~2 °C from the Mid-to-Late Holocene is consistent with the contemporaneous reduction in the Northern Hemisphere summer minus winter insolation.

6. The data interpretation of a long-term change in dominant seasonal rainfall from winter to summer, accompanied by years with alternating dry and wet summers during the late Holocene, is supported both by paleohydroclimate reconstructions from southern West Virginia

speleothems (Hardt et al., 2010) and model results indicating that the relative impact of the Bermuda High on summer rainfall variation driven by AMO is strong (Baines and Folland, 2007; Ortegren et al., 2011).

7. Consistency between the DeSoto speleothem records and coeval central China speleothem records that respond to the Asian Summer Monsoon support model predictions of strong links between the subtropical North Atlantic and changes in the ASM.

8. The relatively short and rapid wet and dry phase mode transitions documented by the DeSoto speleothem archive pose a major challenge to attempts to correlate with the periodic drought events that had significant societal impacts in the Levant, India and Asia. The cyclic hydroclimate variability in the late Holocene is likely controlled by AMO but additional records with improved dating precision and higher resolution are needed in order to confirm or confute this hypothesis.

9. The timing and duration of the short wet/dry summer rainfall cycles are constrained by 28 $^{230}Th/^{234}U$ dates with <1% (2σ) errors thus establishing the continuous late Holocene proxy hydroclimate record from DeSoto Caverns as one of the best dated and highly resolved (~5yrs mean resolution) time series of the period. The phase shifts documented in the stalagmite demonstrates that late Holocene hydroclimate variability was cyclic.

ACKNOWLEDGMENTS

I am thankful Tim Lacy and Allen Mathis III for providing me free access to the cave for observations and sampling of speleothems. The study of the mid-to-late Holocene stalagmite from DeSoto Caverns was funded by grants to Dr. Paul Aharon from the Alabama State Climatologist Office. It was also funded by the Geological Sciences Advisory Board (GSAB) and multiple University of Alabama student and research grants. U-series measurements were performed under contract by John Hellstrom at the School of Earth Sciences, University of Melbourne, Australia. I am thankful to present and former members of the SPELEOTEAM research group (Joe Lambert, David Aldridge and Hunter Phillips) for assistance with thin sections analysis, mass spectrometry and fruitful discussions.

REFERENCES

Aharon, P. and Chappell, J. 1983: Carbon and oxygen isotope probes of reef environment histories. In Barnes D. J., (ed) Perspectives on coral reefs: 1–15. Austral. Instit. Marine Sci., Bryan Clouston Publ, Canberra, Australia.

Aharon, P., Aldridge, D. and Hellstrom, J. 2012: Rainfall variability and the rise and collapse of the Mississippian chiefdomes: Evidence from a DeSoto caverns stalagmite; in: Giosan, L., Fuller, D. Q., Nicol, K., Flad, R. K., Clift, P. D. (Eds.), Climates, Landscapes and Civilizations. Geoph. Monog. Series 198, Am. Geophys. Union, Washington DC, pp. 35-41, 10.1029/2012GM001203.

Arz, H.W., Lamy, F. and Pätzold, J. 2006: A pronounced dry event recorded around 4.2 ka in brine sediments from the northern Red Sea. Quat. Res. 66 (3), 432–441.

Baigorria, G.A., Jones, J.W. and O'Brien, J. J. 2007: Understanding rainfall spatial variability in southeast USA at different timescales. Int. J. Clim. 27 (6), 749–760.

Baines, P. G. and Folland, C. K. 2007: Evidence for a rapid global climate shift across the late 1960s. J. Clim. 20, 2721-2744, doi: 10.1175/JCLI4177.1.

Bard, E. 2013: Out of Africa humid period. Science 342, 808-809, doi: 10.1126/science.1246519.

Bar-Matthews, M. and Ayalon, A. 2011: Mid-Holocene climate variations revealed by high-resolution speleothem records from Soreq Cave, Israel and their correlation with cultural changes. The Holocene 21 (1), 163-171.

Berger, A. and Loutre, M. F. 1991: Insolation values for the climate of the last 10 million years. Quat. Sci. Rev. 10, 297-317.

Berkelhammer, M., Sinha, A., Stott, L., Cheng, H., Pausata, F. S. R. and Yoshimura, K. 2012: An abrupt shift in the Indian monsoon 4000 years ago, in: Giosan, L., Fuller, D. Q., Nicol, K., Flad, R. K., Clift, P. D. (Eds.), Climates, Landscapes and Civilizations. Geoph. Monog. Series 198, Am. Geophys. Union, Washington DC, pp. 75-87, 10.1029/2012GM001207.

Bertaux, J., Sondag, F., Santos, R., Soubiès, F., Causse, C., Plagnes, V., Cornec, F.L. and Seidel, A. 2002: Paleoclimatic record of speleothems in a tropical region: study of laminated sequences from a Holocene stalagmite in Central-west Brazil. Quat. Int. 89, 3–16.

Böhm, F., Joachimski, M. M., Dullo, W. C., Eisenhauer, A., Lehnert, H., Reitner, J., and

Wörheide, G. 2000: Oxygen isotope fractionation in marine aragonite of coralline sponges. Geochim. Cosmochim. Acta, 64 (10), 1695–1703.

Bond, G., Kromer, B., Beer, J., Muscheler, R., Evans, M.N., Showers, W., Hoffmann, S., Bond, R. L., Hajdas, I., and Bonani, G. 2001: Persistent solar influence on North Atlantic climate during the Holocene. Science 294, 2130–2136.

Booth, R.K., Jackson, S.T., Forman, S. L., Kutzbach, J. E., Bettis III., E. A., Kreigs, J. and Wright, D. K. 2005: A severe centennial-scale drought in mid continental North America 4200 years ago and apparent global linkages. The Holocene 15 (3), 321–328.

Cai, Y., Tan, L., Cheng, H., An, Z., Edwards, R. L., Kelly, M. J., Kong, X. and Wang, X. 2010: The variation of summer monsoon precipitation in central China since the last deglaciation. Earth Planet. Sc. Lett. 291, 21-31.

Castiglia, P. J. and Fawcett, P. J. 2006: Large Holocene lakes and climate change in the Chihuahuan desert. Geology 34 (2), 113-116, doi: 10.1130/G22036.1.

Clarke, J. Brooks, N., Banning, E. B., Bar-Matthews, M., Campbell, S., Clare, L., Cremaschi, M., di Lernia, S., Drake, N., Gallinaro, M., Manning, S., Nicoll, K., Philip, G., Rosen, S., Shoop, U-D., Tafuri, M. A., Weninger, B. and Zerboni, A. 2016: Climatic changes and social transformations in the Near East and North Africa during the “long” 4th millennium BC: A comparative study of environmental and archaeological evidence. Quat. Sci. Rev. 136, 96-121.

Cullen, H.M., deMenocal, P.B., Hemming, S., Hemming, G., Brown, F.H., Guilderson, T. and Sirocko, F. 2000: Climate change and the collapse of the Akkadian empire: Evidence from the deep sea. Geology 28 (4), 379–382.

Dansgaard, W. 1964: Stable isotopes in precipitation. Tellus 16, 436-468.

Davis, M.E. and Thompson, L.G. 2006: An Andean ice-core record of a Middle Hlocene mega-drought in North Africa and Asia. Annals Glaciol. 43, 34–41.

deMenocal, P., Ortiz, J., Guilderson, T., Adkins, J., Sarnthein, M., Baker, L. and Yarusinsky, M. 2000: Abrupt onset and termination of the African humid Period: rapid climate responses to gradual insolation forcing. Quat. Sci. Rev. 19 (1-5), 347–361.

deMenocal, P. 2008: Africa on the edge. Nat. Geosci. 1, 650-651.

Dixit, Y., Hodell, D. A. and Petrie, C. A. 2014: Abrupt weakening of the summer monsoon in Northweast India ~4100 yr ago. Geology 42 (4), 339-342, doi: 10.1130/G35236.1.

Domínguez-Villar, D., Krklec, K., Pelicon, P., Fairchild, I. J., Cheng, H. and Edwards, L. R. 2017: Geochemistry of speleothems affected by aragonite to calcite recrystallization - Potential inheritance from the precursor mineral. Geochim. Cosmochim. Acta 200, 310-329,

http:// dx.doi.org/10.1016/j.gca.2016.11.040.

Donders, T. H., Wagner, F., Dlicher, D. L. and Visscher, H. 2005: Mid-to-late Holocene El-Niño- Southern Oscillation dynamics reflected in the subtropical terrestrial realm. PNAS 102 (31), 10904-10908.

Drysdale, R., Zanchetta, G., Hellstrom, J., Maas, R., Fallik, A., Pickett, M., Cartwright, I. and Piccini, L. 2006: Late Holocene drought responsible for the collapse of Old orld civilizations is recorded in an Italian cave flowstone. Geology 34 (2), 101-104.

Emrich, K., Ehhalt, D. H. and Vogel, J. C. 1970: Carbon isotope fractionation during the precipitation of calcium carbonate. Earth. Planet. Sc. Lett. 8, 363-371.

Finné, M., Holmgren, K. Sundqvist, H.S., Weiberg, E. and Lindblom, M. 2011: Climate in the Eastern Mediterranean and adjacent regions during the past 6000 years – A review. J. Archeol. Sci. 38, 3153–3173.

Folland, C. K., Knight, J., Linderholm, H. W., Fereday, D., Ineson, S. and Hurrell, J. W. 2009: The summer North Atlantic Oscillation: Past, present, and future. J. Clim. 22, 1082-1103, doi: 10.1175/2008JCLI2459.1.

Frisia, S., Borsato, A., Fairchild, I.J., McDermott, F. and Selmo, E.M. 2002: Aragonite-calcite relationships in speleothems (Grotte de Clamouse, France): Environment, fabrics, and carbonate geochemistry. J. Sedim. Res. 72 (5), 687–699.

Gasse, F. 2000: Hydrological changes in the Africa tropics since the Last Glacial Maximum. Quat. Sci. Rev. 19 (1-5), 189–211.

Gill, R. B. 2001: The Great Mayan Droughts. Water, Life and Death.

Gilman, D. L., Fuglister, F. J. and Mitchell, J. M. 1963: On the power spectrum of “red noise”. J. Atmos. Sci. 20, 182-184.

Glaser, P. H., Hansen, C. S., Donovan, J. J., Givnish, T. J., Stricker, C. A. and Volin, J. C. 2013: Holocene dynamics of the Florida Everglades with respect to climate, dustfall, and tropical storms. PNAS 110 (43), 17211-17216, doi: 10.1073/pnas.1222239110.

Grossman, E.L. and Ku, T.L. 1986: Oxygen and carbon isotope fractionation in biogenic aragonite: temperature effects. Chem. Geol. 59, 59–74.

Hardt, B., Rowe, H. D., Springer, G. S., Cheng, H. and Edwards, R. L. 2010: The seasonality of East-Central North American precipitation based on three coeval Holocene speleothems from Southern West Virginia. Earth. Planet. Sc. Lett, 295, 342-348.

Hellstrom, J. 2003: Rapid and accurate U/Th dating using parallel ion-counting multi-collector ICP-MS. J. Analyt. Atom. Spect. 18, 1346–1351.

Hellstrom, J. 2006: U/Th dating of speleothems with high initial ^{230}Th using stratigraphical constraint. Quat. Geochronol. 1, 289-295.

Henderson, K. G. and Vega, A. J. 1996: Regional precipitation variability in the southern United States. Phys. Geogr. 17 (2), 93-112.

Henderson, A. K., Nelson, D. M., Sheng-Hu., F., Huang, Y., Shuman, B. N., and Williams, J. W. 2010: Holocene precipitation seasonality captured by a dual hydrogen and oxygen isotope approach at Steel lake, Minnesota. Earth Planet. Sc. Lett. 300, 205-214.

Hendy, C.H. 1971: The isotopic geochemistry of speleothems 1. The calculation of the effects of the different modes of formation on the isotopic composition of speleothems and their applicability as palaeoclimatic indicators. Geochim. Cosmochim. Acta 35, 801–824.

Hodell, D. A., Kanfoush, L., Shemesh, A., Crosta, X., Charles, C. D. and Guilderson, T. P. 2001: Abrupt Cooling of Antarctic Surface Waters and Sea Ice Expansion in the South Atlantic Sector of the Sothern Ocean at 5000 cal yr B.P. Quat. Res. 56, 191–198.

Honaker, J. and King, G. 2010: What to do about missing values in time series cross-section data? Am. J. Pol. Sci. 54 (2), 561-581.

Holmes, J. A. 2008: How the Sahara became dry. Science 320, 752-753.

Howell, P., Pisias, N., Balance, J., Baughman, J. and Ochs, L. 2006: ARAND time series analysis software, Brown University, Providence RI.

Keigwin, L.D. 1996: The Little Ice Age and Medieval Warm Period in the Sargasso Sea. Science 274 (5292), 1504–1508.

Kerr, R. A. 2000: A North Atlantic climate pacemaker for the centuries. Science 288 (5473), 1984-1985, doi: 10.1126/science.288.5473.1984.

Kerr, R.A. 2005: Atlantic climate pacemaker for millennia past, decades hence? Science 309, 41-42.

Kim, J.H., Rimbu, N., Lorenz, S.J., Lohmann, G., Nam, S-II., Schouten, S., Rühlemann, C. and Schneider, R.R. 2004: North Pacific and North Atlantic sea-surface temperature variability during the Holocene. Quat. Sci. Rev. 22 (20-22), 2141–2154.

Kim, S. T., O'Neil, J. R., Hillaire-Marcel, C. and Mucci, A. 2007: Oxygen isotope fractionation between synthetic aragonite and water: Influence of temperature and Mg2+ concentration. Geochim. Cosmochim. Acta 71, 4704–4715.

Knight, J. R., Allan, R. J., Folland, C. K., Vellinga, M. and Mann, M. E. 2005: A signature of persistent natural thermohaline circulation cycles in observed climate. Geophys. Res. Let. 32, L20708, 1-4, doi: 10.1029/2005GL024233.

Knight, J. R., Folland, C. K., and Scaife, A. A. 2006: Climate impacts of the Atlantic Multidecadal Oscillation. Geophys. Res. Lett. 33, L17706, doi: 10.1029/2006GL026242.

Knudsen, M.F., Seidenkrantz, M.S., Jacobsen, B.H. and Kuijpers, A. 2011: Tracking the Atlantic Multidecadal Oscillation through the last 8,000 years. Nature Commun. 2 (178), 1–8.

Lachniet, M. S. 2009: Climatic and environmental controls on speleothem oxygen isotope values. Quat. Sci. Rev. 28, 412-432, doi: 10.1016/j.quascirev.2008.10.021.

Lachniet, M. S., Bernal, J. P., Asmerom, Y. and Polyak, V. 2012: Uranium loss and aragonite-calcite age discordance in a calcitized aragonite stalagmite. Quat. Geochron. 14, 26-37.

Lachniet, M. S. 2015: Are aragonite stalagmites reliable paleoclimate proxies? Tests for oxygen isotopes time series replication and equilibrium. GSA Bull. 127 (11/12), 1521-1533, doi: 10.1130/B31161.1.

Lambert, W.J. and Aharon, P. 2010: Oxygen and hydrogen isotopes of rainfall and drip-water at DeSoto Caverns (Alabama, USA): Key to understanding past variability of moisture transport from the Gulf of Mexico. Geochim. Cosmochim. Acta 74, 846–861.

Lambert, W.J. and Aharon, P. 2011: Controls on dissolved inorganic carbon and $\delta^{13}C$ in cave waters from DeSoto caverns: Implications for speleothem $\delta^{13}C$ assessments. Geochim. Cosmochim. Acta 75, 753-768.

LeGrande, A. N. and Schmidt, G. A. 2009: Sources of Holocene variability of oxygen isotopes in paleoclimate archives. Clim. Past, 441-455.

Liu, F. and Feng, Z. 2012: A dramatic climatic transition at ~4000 cal. Yr BP and its cultural responses in Chinese cultural domains. The Holocene 22 (10), 1181-1197.

Lu, R., Dong, B. and Ding, H. 2006: Impact of the Atlantic Multidecadal Oscillation on the Asian summer monsoon. Geophys. Res. Lett. 33, L24701, doi: 10.1029/2006GL027655.

Marcott, S.A., Shakun, J.D., Clark, P.U. and Mix, A.C. 2013: A reconstruction of regional and global temperature for the past 11,300 years. Science 339 (6124), 1198–1201.

McDermott, F. 2004: Paleo-climate reconstruction from stable isotope variations in speleothems: a review. Quat. Sci. Rev. 23, 901–918.

Meijer, H. J. M., Gill, A., deLouw, P. G. B., Van Den Hoek Ostende, L. W., Hume, J. P. and Rijsdijk, K. F. 2012; Dodo remains from an in situ context from Mare aux Songes, Mauritius. Naturwissenschften 99, 177-184.

Minobe, S. 1997: A 50-70 year climatic oscillation over the North Pacific and North America. Geophys. Res. Let. 24 (6), 683-686.

Morley, A., Rosnethal, Y. and deMenocal, P. 2014: Ocean-atmosphere climate shift during the mid- to-late Holocene transition. Earth. Planet. Sc. Lett. 388, 18-26, doi: 10.1016/epsl2013.11039.

Oppo, D. W., Mcmanus, J. F. and Cullen, J. L. 2003: Deepwater variability in the Holocene epoch. Nature 422, 277–278.

Ortegren, J. T., Knapp, P. A., Maxwell, J. T., Tyminski, W. P. and Soulé, P. T. 2011: Ocean-atmopshere influences on low-frequency warm-season drought variability in the Gulf Coast and Southeastern Unites States. J. Appl. Meteorol. Clim., 1177-1186, doi: 10.1175/2010JAMC2566.1.

Phillips IV, J.H. 2011: Insights into aragonite digenesis as evidenced from spelean carbonate. M.S. Thesis, University of Alabama, 66 pp.

Radtke, R.L., Showers, W., Moksness, E. and Lenz, P. 1998: Environmental information stored in otoliths: insights from stable isotopes. Marine Biol. 132, 347–348.

Railsback, L.B., Dabous, A.A., Osmond, J.K. and Fleisher, C.J. 2002: Petrographic and geochemical screening of speleothems for U-series dating: An example from recrystallized speleothems from Wadi Sannur Caverns, Egypt. J. Cave Karst stud. 64 (2), 108–116.

Rodwell, M. J., Hoskins and B. J. 2001: Subtropical anticyclones and summer monsoons. J. Clim.14 (15), 3192-3211.

Rossi, C. and Lozano, R. P. 2016: Hydrochemical controls on aragonite versus calcite precipitation in cave drip-waters. Geochim. Cosmochim. Acta 192, 70-96.

Russell, J. M. and Johnson, T. C. 2005: A high-resolution geochemical record from lake Edward, Uganda Congo and the timing and causes of tropical African drought during the late Holocene. Quat. Sci. Rev. 24, 1375-1389.

Salgado-Labouriau, M. L., Barberi, M., Ferraz-Vicentini, K. R. and Parizzi, M. G. 1998: A dry climate event during the late Quaternary of tropical Brazil. Rev. Paleobot. Palyno. 99, 115-129.

Schlesinger, M. E. and Ramankutty, N. 1994: An oscillation in the global climate system of period 65-70 years. Nature 367, 723-726, doi: 10.1038/367723a0.

Stanley, J. D., Krom, M. D., Cliff, R. A. and Woodward, J. 2003: Short Contribution: Nile failure at the end of the Old Kingdom, Egypt: Strontium isotopic and petrologic evidence. Geoarcheol. 18 (3), 395-402.

Staubwasser, M. and Weiss, H. 2006: Holocene climate and cultural evolution in late prehistoric-early historic West Asia. Quat. Res. 66 (3), 372–387.

Stocker, T.F., Tarasov, P., Wagner, M. and Widmann, M. 2008: Mid- to Late Holocene climate change: an overview. Quat. Sci. Rev. 27 (19-20), 1791–1828.

Thompson, L.G., Thompson, E.M., Breher, H., Davis, M., León, B., Les, D., Lin, P.N., Mashiotta, T. and Mountain, K., 2006: Abrupt tropical climate change: Past and present. PNAS 103 (28), 10536–10543.

Thorrold, S.R., Campana, S.E., Jones, C.M. and Swart, P.K. 1997: Factors determining $\delta^{13}C$ and $\delta^{18}O$ fractionation in aragonitic otoliths of marine fish. Geochim. Cosmochim. Acta 61 (14), 2909–2919.

Tierney, J. E. and deMenocal, P. B. 2013: Abrupt shifts in Horn of Africa hydroclimate since the last glacial maximum. Science 342, 843-846.

Vachon, R. W., White, J. W. C., Gutmann, E. and Welker, J. M., 2007: Amount-weighted annual isotopic (^{18}O) values are affected by the seasonality of precipitation. Geophys. Res. Lett. 34, L21707, doi: 10.1029/2007GL030547.

Wang, C. and Enfield, D. B. 2001: The tropical Western hemisphere warm pool. Geophys. Res. Lett. 28 (8), 1635-1638.

Wang, J., Sun, L., Chen, L., Xu, L., Wang, Y. and Wang, X. 2016: The abrupt climate change near 4,400 yr BP on the cultural transition in Yuchisi, China and its global linkage. Sci. Rep. 27723, doi: 10.1038/srep27723.

Wanner, H., Beer, J., Bütikofer, J., Crowley, T.J., Cubasch, U., Flückiger, J., Goosse, H., Grosjean, M., Joos, F., Kaplan, J.O., Küttel, M., Müller, S.A., Prentice, I.C., Solomina, O., Stocker, T.F., Tarasov, P., Wagner, M. and Widmann, M. 2008: Mid- to Late Holocene climate change: an overview. Quat. Sci. Rev. 27 (19-20), 1791–1828.

Weiss, H., Courty, M.A., Wetterstrom, W., Guichard, F., Senior, L., Meadow, R. and Curnow, A. 1993: The genesis and collapse of third millennium north Mesopotamian civilization. Science 261 (5124), 995–1004.

Welc, F. and Marks, L. 2014: Climate change at the end of the old Kingdom in Egypt around 4200 BP: New geoarcheological evidence. Quat. Int. 324, 124-133.

White, R.M.P., Dennis, P.F. and Atkinson, T.C. 1999: Experimental calibration and field investigation of the oxygen isotopic fractionation between biogenic aragonite and water. Rapid Commun. Mass Spec. 13, 1242–1247.

Yang, X., Scuderi, L. A., Wang, X., Scuderi, L. J., Zhang, D., Li, H., Forman, S., Xu, Q., Wang R., Huang, W. and Yang, S. 2015: Groundwater sapping as the cause of irreversible desertification of Hunshandake sand lands, Inner Mongolia, Northern China. PNAS 112 (3), 702-706.

Zanchetta, G., Bar-Matthews, M., Drysdale, R. N., Lionello, P., Ayalon, A., Hellstrom, J. C., Isola, I., and Regattieri, E. 2014: Coeval dry events in the central and eastern Mediterranean basin at 5.2 and 5.6 ka recorded in Corchia (Italy) and Soreq caves. Global Planet. Chang. 122, 130-139.

Zanchetta, G., Regattieri, E., Isola, I., Drysdale, R. N., Bini, M., Baneschi, I. and Hellstrom, J. C. 2016: The so-called “4.2 event” in the central Mediterranean and its climatic teleconnections. Alpine. Mediterr. Quat. 29 (1), 5-17.

CHAPTER 5

CONCLUSIONS

This work provides valuable insights into dominant controls of hydroclimate proxies of cave drip-waters at Desoto Caverns, which improved interpretation of hydroclimatic conditions affecting the Southeast US during the mid-to-late Holocene. The rainwater isotope records show slight interannual ^{18}O and ^{2}H depletion trends, which correspond to observed increases in rainfall. However, coeval drip-water $\delta^{18}O$ and δD values exhibit significant interannual negative trends from warm/dry to cool/wet conditions. The substantial reduction of drip-water isotope values relative to rainwater is likely due to mixing of fresh- with residual evaporated water in the epikarst zone. Drip-water elemental concentrations decreased and their ratios increased during dry years, whereas elemental concentrations increased and their ratios decreased during wet years. Observed interannual variation in trace-element concentrations and Mg/Ca and Sr/Ca ratios are likely controlled by rainfall amount.

Unlike drip-water $\delta^{18}O$, $\delta^{13}C$ of dissolved inorganic carbon of cave drip-water has strong seasonal variation, with depleted values during summer and enriched values during winter. Seasonal coherence of $\delta^{13}C_{DIC}$, and [DIC] of drip-water with cave air pCO_2 indicates that seasonal ventilation/stagnation mode of the cave chamber controls the drip-water carbonate chemistry. The summer cave air stagnation allows CO_2 to reach the pCO_2 levels up to 5.0 (atm × 10^3), as CO_2 delivery to the cave continues via drip-water from the soil horizon and epikarst. The high concentration of CO_2 within DeSoto Caverns in summer inhibits degassing of CO_2 from drip-water, accompanied by quasi-equilibrium isotopic fractionation. This decreases the $\delta^{13}C_{DIC}$

values. By contrast, during winter, cold and dense outside air with low CO_2 descends through the cave entrance (which is topographically higher than the cave chambers) and displaces warmer and CO_2-rich air. This lowers the CO_2 concentration in the cave and pCO_2 levels reach close to the atmospheric level. The low cave air pCO_2 during winter increases CO_2 degassing from drip-water DIC, which causes kinetic isotope fractionation, i.e., ^{13}C enrichment in cave drip-water. The drip-water is highly alkaline and super-saturated with respect to aragonite during winter. Hence, precipitation of speleothem aragonite is favored during winter at DeSoto Caverns.

The investigation of an actively growing stalagmite at DesSoto Caverns by means of petrography, stable isotopes ($\delta^{18}O$ and $\delta^{13}C$) and high precision U/Th dating provides high-resolution (2-8 yrs) climate proxy records and assesses the major drivers of climate variation in the mid-to-late Holocene (6.0-1.1 cal ka BP) in the southeastern US. Four prominent climatic events have been documented in the isotope data. Two severe drought events ocurred, one centered at 4.8 ±0.14 (2σ) and the other centered at 1.8 cal ka BP. The severe drought centered at 4.8 ±0.14 cal ka BP, represented by rapid positive shifts in $\delta^{18}O$ and $\delta^{13}C$ data is consistent with the "5 ka" event recognized elsewhere. The synchrony of the documented abrupt climate changes at ~5 ka in DeSoto Caverns with the abrupt end of the African Humid Period and expansion of sea-ice in the polar regions suggests that the major disturbance of NADW production was the cause of the "5 ka" global event. The long-term positive $\delta^{18}O$ shift of ~0.52‰ coupled with the absence of a contemporaneous positive trend in $\delta^{13}C$, offer compelling evidence for gradual cooling of ~ 2 °C over the time interval 4.7 to 1.3 cal ka BP. This gradual cooling is consistent with the contemporaneous reduction in the difference between Northern Hemisphere summer and winter insolation. A simple numerical model based on the modern rain water- and drip-water- $\delta^{18}O$ data suggests that a switch of seasonal rainfall dominance from

winter to summer was the controlling driver of the observed mid-to-late Holocene $\delta^{18}O$ cyclicity in the speleothem. This interpretation of a long-term change in the rainy season from winter to summer during the late Holocene is supported by paleohydroclimate reconstructions from Southern West Virginia speleothems (Hardt et al., 2010). The DeSoto stalagmite $\delta^{18}O$ time series exhibits a dominant periodicity of 68 ±4 yrs, which is consistent with the modern Atlantic Multidecadal Oscillation phase shift periodicity suggesting that AMO played a dominant role in the hydroclimate changes documented in the late Holocene.

REFERENCES

Asmerom, Y., Polyak, V.J. and Burns, S.J. 2010: Variable winter moisture in the southwestern United States linked to rapid glacial climate shifts. Nat. Geosc., Vol. 3, 114-117.

Baker, A., Asrat, A., Fairchild, I.J., Leng, M.J., Wynn, P.M., Bryant, C., Genty, D. and Umer, M. 2007: Analysis of the climate signal contained within $\delta^{18}O$ and growth rate parameters in two Ethiopian stalagmites. Geochem. Cosmochim. Acta, Vol. 71, Issues 12, 2975-2988.

Burns, S.J., Fleitmann, D., Mudelsee, M., Neff, U., Matter, A. and Mangini, A. 2002: A 780-year annually resolved record of Indian Ocean monsoon precipitation from a speleothem from south Oman. Jour. of Geophys. Res., Vol. 107, No. D20, 4434.

Cosford, J., Qing, H., Mattey, D., Eglington, B. and Zhang, M. 2009: Climatic and local effects on stalagmite $\delta^{13}C$ values at Lianhua Cave, China. Paleogeo. Paleoclimate. Paleoeco., Vol. 280, Issues 1-2, 235-244.

Cruz, F.W., Karmann, I., Viana, O., Burns, S. J., Ferrari, J. A., Vuille, M., Sial, A.N. and Moreira, M. Z. 2005: Stable isotope study of cave percolation waters in subtropical Brazil: Implications for paleoclimate interferences from speleothems, Chem, Geology, Vol. 220, 245-262.

Delcourt, P. A. 1980: Goshen Springs: Late Quaternary Vegetation Record for Southern Alabama. Ecol., 78 Vol. 61, 371–386.

Donders, T.H., Wagner, F., Dilcher, D.L. and Vischer, H. 2005: Mid- to Late-Holocene El Niño-Southern Oscillation dynamics reflected in the subtropical terrestrial realm. Proceed. of the Nat. Acad. of Sci., Vol. 102, No. 31, 10904-10908.

Fairchild, I.J. and Treble, P.C. 2009: Trace elements in speleothems as recorders of environmental change. Quat. Sci. Rev., Vol. 28, Issues 5-6, 449-468.

Tremaine, D.M. and Froelich, P.N. 2013: Speleothem trace element signatures: A hydrologic geochemical study of modern cave drip-waters and farmed calcite. Geochem. et Cosmochim. Acta, Vol. 121, 522-545.

Hardt, B., Rowe, H.D., Springer, G.S., Cheng, H., Edwards, R.L. 2010: The seasonality of east central North American precipitation based on three coeval Holocene speleothems from southern West Virginia. Earth. and Planet. Sci. Lett., Vol. 295, Issues 3-4, 342-348.

Hodell, D.A., Curtis, J.H., Jones, G.A., Gundy, A.H., Brenner, M., Binford, M.W. and Dorsey,

K.T. 1991: Reconstruction of Caribbean climate change over the past 10,500 years. Nature, Vol. 352, 790-793.

Hodge, E.J., Richards, D.A., Smart, P.L., Andreo, B., Hoffmann, D.L., Mattey, D.P. and Ramón, A.G. 2008: Effective precipitation in southern Spain (~ 266 to 46 ka) based on a speleothem stable carbon isotope record. Quat. Res., Vol. 69, Issue 3, 447-457.

Karl, T.R. and Young, P.J. 1987: The 1986 Southeast Drought in Historical Perspective. Bull. Americ. Meteorolog. Soc., Vol. 68, No. 7. 773-778.

Lachniet, M.S. 2009: Climatic and environmental controls on speleothem oxygen isotope values. Quat. Sci. Rev., Vol. 28, Issues 5-6, 412-432.

Lambert, W.J. and Aharon, P. 2010: Oxygen and hydrogen isotopes of rainfall and drip-water at DeSoto Caverns (Alabama, USA): Key to understanding past variability of moisture transport from the Gulf of Mexico. Geochem. Cosmochim. Acta, Vol. 74, 846-861.

Maxwell, J.T. and Soulé, P.T. 2009: United States drought of 2007: historical perspectives. Clim. Res., Vol. 38, 95-104.

McDermott, F. 2004: Paleo-climate reconstruction from stable isotope variations in speleothems: a review. Quat. Sci. Rev., Vol. 23, Issues 7-8, 901-918.

Neff, U., Burns, S.J., Mangini, A., Mudelsee, M., Fleitmann, D. and Matter, A. 2001: Strong coherence between solar variability and the monsoon in Oman between 9 and 6 kyr ago. Nature, Vol. 411, 290-293.

Ortegren, J.T., Knapp, P.A., Maxwell, J.T., Tyminski, W.P. and Soulé, P.T. 2011: Ocean-Atmosphere Influences on Low-Frequency Warm-Season Drought Variability in the Gulf Coast and Southeastern United States. Jour. of Appl. Meteorol. and Clim., Vol. 50, 1177-1186.

Poore, R. Z., Dowsett, H. J., Verardo, S. and Quinn, T. M. 2003: Millennial- to century-scale variability in Gulf of Mexico Holocene climate records. Paleocean., Vol.18, Issue 2, 1048.

Schroeder, M.J., Glovinsky, M., Henricks, V.F., Hood, F.C. and Hull, M.K. 1964: Synoptic weather types associated with critical fire weather. Defense Documentation Center for Scientific and Technical Information, Cameron Station Alexandria, VA, 492 pp.

Seager, R., Tzanova, A. and Nakamura, J. 2009: Drought in the Southeastern United States: Causes, Variability over the Last Millennium, and the Potential for Future Hydroclimate Change. Jour. of Clim., Vol. 22, 5021-5045.

Stahle D. W. and Cleaveland M. K. 1994: Tree-ring reconstructed rainfall over the southeastern U.S.A. during the Medieval Warm Period and Little Ice Age. Clim. Change, Vol. 2, No. 26, 199-212.

Stahle, D. W., Fye, F. K., Cook, E. R., and Griffin, R.D. 2007: Tree-ring reconstructed megadroughts over North America since A. D. 1300, Clim. Change, Vol. 83, Issues 1-2, 133–149.

Wang, H., Fu, R., Kumar, A. and Li, W. 2010: Intensification of Summer Rainfall Variability in the Southeastern United States During Recent Decades. Jour. of Hydrometeor., Vol. 11, 1007-1018.

Willard, D.A., Bernhardt, E., Korejwo, D.A. and Meyers, S.R. 2005: Impact of millennial-scale Holocene climate variability on eastern North American terrestrial ecosystems: pollen-based climatic reconstruction. Global and Planet. Change, Vol. 47, 17-35.

Wong, C.I., Banner, J.L., Musgrove, M. 2011: Seasonal drip-water Mg/Ca and Sr/Ca variations driven by cave ventilation: Implications for and modeling of speleothem paleoclimate records. Geochem. et Cosmochim. Acta, Vol. 75, Issue 12, 3514-3529.

Xinggong, K., Yongjin, W., Jiangying, W.U., Hai, C., Edwards, R.L. and Xianfeng, W. 2005: Complicated responses of stalagmite $\delta^{13}C$ to climate change during the last glaciation from Hulu Cave, Nanjing, China.

APPENDIX 2.1.

(RAINWATER ISOTOPE DATA)

Month	Rainfall (mm)	$\delta^{18}O_{rain}$ (‰ VSMOW)	$\delta^{2}H_{rain}$ (‰ VSMOW)	d-ecxess (‰)
1/2012	152.7	-4.2	-16.9	16.7
2/2012	170.3	-5.4	-33.0	10.2
3/2012	123.3	-4.9	-28.2	11.0
4/2012	15.8	-1.2	-4.0	5.6
5/2012	149.9	-4.6	-22.2	14.6
6/2012	34.4	-6.2	-37.7	11.9
7/2012	77.1	-2.3	-10.6	7.8
8/2012	139.5	-3.1	-15.6	9.2
9/2012	201.5	-4.2	-22.9	10.7
10/2012	76.8	-4.9	-23.8	15.4
11/2012	32.0	-5.7	-31.5	14.1
12/2012	231.6	-5.9	-29.0	18.2
1/2013	208.3	-3.9	-18.6	12.6
2/2013	168.4	-3.9	-17.6	13.6
3/2013	145.1	-3.6	-13.7	15.1
4/2013	141.7	-4.5	-25.6	10.4
5/2013	37.0	-3.7	-22.6	7.0
6/2013	217.6	-6.0	-41.6	6.4
7/2013	133.6	-4.9	-31.4	7.8
8/2013	157.3	-2.6	-11.8	9.0
9/2013	46.5	-6.1	-39.9	8.9
10/2013	40.7	-3.2	-12.3	13.3
11/2013	88.8	-6.4	-29.0	22.2
12/2013	220.6	-4.7	-26.5	11.1

APPENDIX 2.2.

(DRIPWATER ISOTOPE DATA)

Drip Site #6

Sampling date	Drip rate (ml/h)	$\delta^{18}O_{drip}$ (‰ VSMOW)	$\delta^{2}H_{drip}$ (‰ VSMOW)	d-ecxess (‰)	Temp (°C)
1/19/2012	-	-	-	-	-
2/20/2012	-	-4.0	-22.2	9.8	17.6
3/19/2012	86.0	-4.6	-22.1	14.7	18.3
4/20/2012	165.0	-4.8	-23.7	14.7	18.3
5/21/2012	207.9	-4.7	-22.8	14.8	-
6/19/2012	218.3	-4.7	-	-	18.9
7/20/2012	123.7	-4.7	-25.6	12.0	19.1
8/17/2012	73.5	-4.8	-19.6	18.8	19.1
9/21/2012	39.9	-4.8	-24.4	14.0	19.1
10/19/2012	25.9	-4.6	-23.7	13.1	19.0
11/20/2012	17.6	-4.1	-20.8	12.0	18.9
12/20/2012	14.9	-4.2	-19.1	14.5	18.6
1/18/2013	10.2	-4.1	-21.1	11.7	18.0
2/22/2013	408.8	-4.9	-26.7	12.5	17.8
3/22/2013	335.7	-5.0	-25.5	14.5	18.0
4/19/2013	718.5	-4.8	-23.8	14.6	18.3
5/17/2013	656.6	-5.1	-28.6	12.2	19.0
6/21/2013	422.9	-5.1	-24.7	16.1	19.2
7/19/2013	537.8	-5.2	-27.5	14.1	19.8
8/20/2013	879.0	-5.0	-26.3	13.7	18.9
9/19/2013	693.1	-4.7	-28.2	9.4	18.9
10/17/2013	352.9	-4.6	-28.1	8.7	19.0
11/18/2013	219.0	-5.0	-24.2	15.8	18.6
12/18/2013	421.0	-4.6	-24.8	12.0	18.3

Drip Site #7

Sampling date	Drip rate (ml/h)	$\delta^{18}O_{drip}$ (‰ VSMOW)	$\delta^{2}H_{drip}$ (‰ VSMOW)	d-ecxess (‰)	Temp (°C)
1/19/2012	-	-	-	-	-
2/20/2012	23.6	-	-	-	-
3/19/2012	760.6	-4.3	-25.1	9.3	18.7
4/20/2012	352.6	-4.9	-25.0	14.2	18.9
5/21/2012	194.4	-4.7	-25.5	12.1	-
6/19/2012	28.6	-4.6	-	-	18.8
7/20/2012	-	-	-	-	-
8/17/2012	-	-	-	-	-
9/21/2012	-	-	-	-	-
10/19/2012	-	-	-	-	-
11/20/2012	-	-	-	-	-
12/20/2012	-	-	-	-	-
1/18/2013	-	-	-	-	-
2/22/2013	867.4	-5.0	-26.3	13.7	17.8
3/22/2013	1277.1	-4.7	-17.0	20.6	17.9
4/19/2013	3330.0	-4.8	-25.0	13.4	18.1
5/17/2013	1220.0	-4.7	-26.4	11.2	18.5
6/21/2013	3202.5	-5.0	-27.9	12.1	19.4
7/19/2013	1171.6	-5.0	-26.3	13.7	19.8
8/20/2013	2887.5	-4.9	-21.8	17.4	18.7
9/19/2013	303.6	-4.9	-26.2	13.0	18.7
10/17/2013	176.4	-4.5	-25.9	10.1	18.9
11/18/2013	18.5	-3.8	-17.6	12.8	18.6
12/18/2013	382.0	-4.5	-23.2	12.8	17.9

Drip Site #13

Sampling date	Drip rate (ml/h)	$\delta^{18}O_{drip}$ (‰ VSMOW)	$\delta^{2}H_{drip}$ (‰ VSMOW)	d-ecxess (‰)	Temp (°C)
1/19/2012	-	-3.1	-	-	17.7
2/20/2012	-	-	-	-	
3/19/2012	186.5	-3.9	-19.9	11.3	18.1
4/20/2012	32.6	-3.9	-17.0	14.2	18.1
5/21/2012	10.3	-4.0	-	-	-
6/19/2012	5.0	-4.6	-	-	19.9
7/20/2012	8.1	-4.4	-	-	18.8
8/17/2012	9.7	-4.5	-	-	18.9
9/21/2012	-	-	-	-	-
10/19/2012	-	-	-	-	-
11/20/2012	-	-	-	-	-
12/20/2012	360.0	-3.8	-16.8	13.6	19.1
1/18/2013	8.2	-3.9	-20.1	11.1	18.2
2/22/2013	2076.9	-3.9	-18.2	13.0	17.8
3/22/2013	219.4	-3.7	-9.9	19.7	17.6
4/19/2013	2853.3	-3.8	-20.1	10.3	18.0
5/17/2013	81.0	-	-	-	-
6/21/2013	368.0	-5.1	-22.0	18.8	18.9
7/19/2013	88.9	-4.9	-19.6	19.6	19.2
8/20/2013	720.0	-4.6	-23.5	13.3	18.7
9/19/2013	13.8	-4.3	-24.6	9.8	18.6
10/17/2013	-	-	-	-	-
11/18/2013	-	-	-	-	-
12/18/2013	142.2	-3.2	-13.9	11.7	18.0

Drip Site #15

Sampling date	Drip rate (ml/h)	$\delta^{18}O_{drip}$ (‰ VSMOW)	$\delta^{2}H_{drip}$ (‰ VSMOW)	d-ecxess (‰)	Temp (°C)
1/18/2013	748.3	-5.0	-28.4	11.6	18.2
2/22/2013	733.7	-5.0	-23.2	16.8	17.7
3/22/2013	700.0	-4.8	-30.5	7.9	17.8
4/19/2013	720.0	-5.0	-29.4	10.6	18.1
5/17/2013	421.4	-5.3	-25.7	16.7	18.5
6/21/2013	980.0	-4.3	-	-	18.8
7/19/2013	820.0	-5.0	-18.0	22.0	19.8
8/20/2013	879.0	-5.0	-25.7	14.3	18.7
9/19/2013	351.3	-4.9	-22.0	17.2	18.6
10/17/2013	57.4	-4.9	-20.8	18.4	18.7
11/18/2013	2.6	-3.6	-14.2	14.6	19.0
12/18/2013	367.2	-4.9	-23.2	16.0	18.1

APPENDIX 2.3.

(TRACE ELEMENT CHEMISTRY)

Drip Site #6

Sampling date	Ca^{2+} (mM/l)	Mg^{2+} (mM/l)	Sr^{2+} (mM/l × 10^4)	Mg^{2+}/ Ca^{2+}	Sr^{2+}/ Ca^{2+} (× 10^3)
1/19/2012	-	-	-	-	-
2/20/2012	0.77	0.99	2.80	1.28	0.36
3/19/2012	1.14	1.25	4.00	1.10	0.35
4/20/2012	1.21	1.27	4.30	1.05	0.36
5/21/2012	1.17	1.23	4.21	1.05	0.36
6/19/2012	0.55	0.94	2.37	1.71	0.43
7/20/2012	1.19	1.25	4.34	1.05	0.36
8/17/2012	1.16	1.23	4.16	1.07	0.36
9/21/2012	1.05	1.18	3.85	1.12	0.37
10/19/2012	0.97	1.12	3.53	1.16	0.36
11/20/2012	0.79	1.06	2.84	1.33	0.36
12/20/2012	0.67	1.05	2.36	1.57	0.35
1/18/2013	-	-	-	-	-
2/22/2013	1.17	1.33	4.40	1.14	0.38
3/22/2013	1.27	1.48	4.60	1.17	0.36
4/19/2013	1.54	1.53	4.94	0.99	0.32
5/17/2013	1.49	1.50	4.84	1.00	0.32
6/21/2013	1.56	1.56	5.01	1.00	0.32
7/19/2013	1.53	1.54	5.04	1.01	0.33
8/20/2013	1.59	1.57	5.16	0.99	0.32
9 /19/2013	1.54	1.54	5.02	0.99	0.33
10/17/2013	1.50	1.51	4.94	1.01	0.33
11/18/2013	1.35	1.42	4.49	1.05	0.33
12/18/2013	1.40	1.43	4.48	1.03	0.32

Drip Site #7

Sampling date	Ca^{2+} (mM/l)	Mg^{2+} (mM/l)	Sr^{2+} (mM/l × 10^4)	Mg^{2+}/ Ca^{2+}	Sr^{2+}/ Ca^{2+} (× 10^3)
1/19/2012	-	-	-	-	-
2/20/2012	-	-	-	-	-
3/19/2012	1.14	1.40	3.93	1.23	0.35
4/20/2012	1.08	1.46	3.69	1.35	0.34
5/21/2012	0.93	1.44	3.32	1.54	0.36
6/19/2012	0.30	1.05	1.35	3.50	0.45
7/20/2012	-	-	-	-	-
8/17/2012	-	-	-	-	-
9/21/2012	-	-	-	-	-
10/19/2012	-	-	-	-	-
11/20/2012	-	-	-	-	-
12/20/2012	-	-	-	-	-
1/18/2013	-	-	-	-	-
2/22/2013	1.28	1.50	4.43	1.18	0.35
3/22/2013	1.15	1.65	4.29	1.44	0.37
4/19/2013	1.45	1.67	4.74	1.14	0.33
5/17/2013	1.36	1.67	4.47	1.22	0.33
6/21/2013	1.59	1.68	5.06	1.06	0.32
7/19/2013	1.45	1.73	4.71	1.19	0.32
8/20/2013	1.71	1.74	5.37	1.01	0.31
9 /19/2013	1.28	1.71	4.17	1.33	0.33
10/17/2013	1.25	1.74	4.18	1.39	0.33
11/18/2013	0.36	1.63	1.21	4.53	0.34
12/18/2013	1.07	1.57	3.62	1.47	0.34

Drip Site #13

Sampling date	Ca^{2+} (mM/l)	Mg^{2+} (mM/l)	Sr^{2+} (mM/l × 10^4)	Mg^{2+}/ Ca^{2+}	Sr^{2+}/ Ca^{2+} (× 10^3)
1/19/2012	-	-	-	-	-
2/20/2012	-	-	-	-	-
3/19/2012	1.01	0.89	4.32	0.88	0.43
4/20/2012	1.03	0.94	4.63	0.91	0.45
5/21/2012	1.20	1.10	5.45	0.92	0.46
6/19/2012	-	-	-	-	-
7/20/2012	-	-	-	-	-
8/17/2012	-	-	-	-	-
9/21/2012	-	-	-	-	-
10/19/2012	-	-	-	-	-
11/20/2012	-	-	-	-	-
12/20/2012	0.85	0.72	3.70	0.84	0.43
1/18/2013	1.23	1.04	4.91	0.85	0.40
2/22/2013	0.97	0.83	4.04	0.86	0.42
3/22/2013	0.10	0.94	4.17	0.94	0.42
4/19/2013	0.80	0.68	3.23	0.85	0.40
5/17/2013	-	-	-	-	-
6/21/2013	1.42	1.43	4.73	1.01	0.33
7/19/2013	1.28	1.15	5.37	0.90	0.42
8/20/2013	1.35	1.09	5.24	0.81	0.39
9 /19/2013	1.22	1.14	5.25	0.93	0.43
10/17/2013	-	-	-	-	-
11/18/2013	-	-	-	-	-
12/18/2013	1.11	0.93	4.25	0.83	0.38

Drip Site #15

Sampling date	Ca^{2+} (mM/l)	Mg^{2+} (mM/l)	Sr^{2+} (mM/l × 10^4)	Mg^{2+}/ Ca^{2+}	Sr^{2+}/ Ca^{2+} (× 10^3)
1/18/2013	1.14	1.17	4.21	1.03	0.37
2/22/2013	1.25	1.30	4.54	1.04	0.36
3/22/2013	0.96	1.40	4.24	1.46	0.44
4/19/2013	1.35	1.43	4.60	1.06	0.34
5/17/2013	1.37	1.44	4.67	1.05	0.34
6/21/2013	1.23	1.07	4.93	0.86	0.40
7/19/2013	1.42	1.48	4.89	1.04	0.34
8/20/2013	1.45	1.40	4.78	0.96	0.33
9 /19/2013	1.43	1.50	4.77	1.05	0.33
10/17/2013	1.18	1.46	4.17	1.24	0.35
11/18/2013	-	-	-	-	-
12/18/2013	1.31	1.36	4.45	1.04	0.34

APPENDIX 3.1.

(RELATIVE HUMIDITY AND TEMP DATA)

Sampling date	RH (%)	Cave air T (°C)	External air temp (°C)
1/19/2012	100.0	17.8	10.5
2/202012	100.0	17.6	12.1
3/19/2012	99.8	17.4	18.6
4/20/2012	99.8	17.4	19.1
5/21/2012	100.0	17.6	23.2
6/19/2012	99.7	17.9	25.7
7/20/2012	100.0	18.2	28.8
8/17/2012	100.0	18.1	26.1
9/21/2012	100.0	18.5	23.1
10/19/2012	100.0	18.5	17.4
11/20/2012	100.0	17.2	10.4
12/20/2012	100.0	18.5	10.8
1/18/2013	100.0	17.0	10.0
2/22/2013	100.0	17.5	8.9
3/22/2013	100.0	18.0	10.6
4/19/2013	100.0	18.2	17.3
5/17/2013	100.0	18.7	15.9
6/21/2013	100.0	19.0	25.8
7/19/2013	100.0	19.2	25.9
8/20/2013	100.0	19.2	25.9
9/19/2013	100.0	18.6	23.9
10/17/2013	100.0	19.0	18.2
11/18/2013	100.0	19.0	10.9
12/18/2013	100.0	18.0	8.5

APPENDIX 3.2.

(CAVE AIR ISOTOPE DATA)

Site #1

Sampling date	pCO_2 (atm * 10^3)	$\delta^{13}C_{CO2}$ (‰ V-PDB)	$\delta^{18}O_{CO2}$ (‰ V-SMOW)
1/19/2012	0.493	-12.4	40.3
2/20/2012	0.587	-14.1	40.6
3/19/2012	1.032	-17.7	43.6
4/20/2012	1.638	-18.9	45.4
5/21/2012	2.031	-19.7	43.1
6/19/2012	2.284	-20.8	44.4
7/20/2012	3.282	-21.6	45.0
8/17/2012	3.513	-21.9	44.9
9/21/2012	2.260	-21.2	43.6
10/19/2012	1.872	-20.5	44.0
11/20/2012	0.911	-17.3	42.0
12/20/2012	0.656	-16.0	40.3
1/18/2013	0.573	-14.4	38.4
2/22/2013	0.622	-15.3	39.5
3/22/2013	0.734	-16.0	39.8
4/19/2013	0.983	-17.6	41.6
5/17/2013	1.317	-18.8	42.8
6/21/2013	2.087	-21.0	43.4
7/19/2013	2.478	-21.5	43.6
8/20/2013	2.817	-21.3	44.9
9/19/2013	2.478	-21.5	43.7
10/17/2013	2.478	-21.2	43.9
11/18/2013	0.960	-17.9	42.1
12 /18/2013	0.548	-14.0	37.8

Site #2

Sampling Date	pCO_2 (atm * 10^3)	$\delta^{13}C_{CO2}$ (‰ V-PDB)	$\delta^{18}O_{CO2}$ (‰ V-SMOW)
1/19/2012	0.495	-12.5	40.5
2/20/2012	0.574	-13.9	40.7
3/19/2012	1.483	-18.8	44.4
4/20/2012	2.046	-19.8	45.2
5/21/2012	2.765	-20.4	43.7
6/19/2012	3.420	-21.4	45.6
7/20/2012	3.454	-21.7	45.2
8/17/2012	4.437	-22.2	42.7
9/21/2012	3.080	-21.7	44.7
10/19/2012	2.122	-21.9	41.6
11/20/2012	1.523	-19.6	43.5
12/20/2012	1.072	-19.2	42.6
1/18/2013	0.580	-14.4	38.6
2/22/2013	0.635	-15.3	39.6
3/22/2013	0.843	-16.8	40.2
4/19/2013	1.030	-17.7	41.7
5/17/2013	2.073	-20.1	43.8
6/21/2013	3.098	-21.6	43.6
7/19/2013	2.782	-22.6	41.8
8/20/2013	3.858	-21.7	45.7
9/19/2013	3.264	-22.9	44.3
10/17/2013	3.565	-21.7	44.9
11/18/2013	1.427	-19.6	43.1
12 /18/2013	0.551	-13.9	38.0

Site #3

Sampling date	pCO_2 (atm * 10^3)	$\delta^{13}C_{CO2}$ (‰ V-PDB)	$\delta^{18}O_{CO2}$ (‰ V-SMOW)
1/19/2012	0.676	-16.2	41.1
2/20/2012	0.839	-17.2	41.5
3/19/2012	1.875	-19.5	44.7
4/20/2012	2.428	-20.1	45.6
5/21/2012	3.365	-20.7	44.3
6/19/2012	3.959	-21.6	46.0
7/20/2012	4.657	-22.0	46.1
8/17/2012	5.021	-22.2	44.3
9/21/2012	3.257	-21.8	44.9
10/19/2012	1.681	-21.5	40.6
11/20/2012	1.884	-20.1	43.7
12/20/2012	1.177	-19.7	42.6
1/18/2013	1.035	-18.6	41.5
2/22/2013	0.814	-18.0	40.2
3/22/2013	0.966	-17.7	40.5
4/19/2013	1.564	-19.4	42.9
5/17/2013	2.550	-20.6	44.3
6/21/2013	3.563	-21.8	44.3
7/19/2013	2.523	-22.7	40.8
8/20/2013	4.061	-21.7	45.8
9/19/2013	3.492	-22.1	44.6
10/17/2013	3.852	-21.9	44.9
11/18/2013	1.497	-20.1	42.5
12 /18/2013	0.773	-17.7	39.3

Site #4

Sampling date	pCO_2 (atm * 10^3)	$\delta^{13}C_{CO2}$ (‰ V-PDB)	$\delta^{18}O_{CO2}$ (‰ V-SMOW)
1/19/2012	0.388	-8.1	40.0
2/20/2012	0.392	-8.1	38.8
3/19/2012	0.391	-8.3	39.9
4/20/2012	0.417	-9.7	41.4
5/21/2012	0.389	-7.7	37.1
6/19/2012	0.388	-8.2	38.2
7/20/2012	0.384	-8.2	35.3
8/17/2012	0.365	-7.9	36.9
9/21/2012	0.387	-8.3	34.1
10/19/2012	0.379	-8.1	36.2
11/20/2012	0.387	-8.3	37.0
12/20/2012	0.396	-8.8	37.8
1/18/2013	0.392	-8.5	36.5
2/22/2013	0.404	-9.7	37.7
3/22/2013	0.383	-8.9	36.4
4/19/2013	0.397	-9.2	36.8
5/17/2013	0.420	-8.3	37.6
6/21/2013	0.387	-9.5	35.7
7/19/2013	0.379	-8.9	39.2
8/20/2013	0.392	-9.0	36.9
9/19/2013	0.365	-7.8	36.7
10/17/2013	0.374	-8.9	36.4
11/18/2013	0.383	-8.5	36.4
12 /18/2013	0.405	-8.6	35.4

Site #5

Sampling date	pCO_2 (atm * 10^3)	$\delta^{13}C_{CO2}$ (‰ V-PDB)	$\delta^{18}O_{CO2}$ (‰ V-SMOW)
1/19/2012	0.478	-12.0	40.6
2/20/2012	0.568	-13.6	40.4
3/19/2012	1.121	-17.8	43.8
4/20/2012	1.471	-18.4	45.5
5/21/2012	1.951	-19.9	42.3
6/19/2012	2.157	-21.3	42.8
7/20/2012	3.072	-22.0	43.6
8/17/2012	3.205	-22.3	43.3
9/21/2012	2.210	-21.3	43.5
10/19/2012	0.767	-16.9	40.1
11/20/2012	0.860	-17.1	41.1
12/20/2012	0.584	-15.2	39.5
1/18/2013	0.556	-14.0	38.3
2/22/2013	0.604	-15.1	38.8
3/22/2013	0.672	-15.8	38.9
4/19/2013	0.882	-17.3	39.5
5/17/2013	1.454	-19.0	41.9
6/21/2013	2.036	-21.0	42.1
7/19/2013	1.826	-21.9	41.0
8/20/2013	2.777	-21.5	44.5
9/19/2013	2.494	-21.5	44.4
10/17/2013	2.285	-21.5	42.8
11/18/2013	0.765	-16.6	40.3
12 /18/2013	0.537	-13.5	38.0

Site #6

Sampling date	pCO_2 (atm * 10^3)	$\delta^{13}C_{CO2}$ (‰ V-PDB)	$\delta^{18}O_{CO2}$ (‰ V-SMOW)
1/19/2012	0.390	-8.2	40.0
2/20/2012	0.396	-8.4	38.9
3/19/2012	0.574	-8.7	41.2
4/20/2012	0.408	-9.1	40.4
5/21/2012	0.378	-7.6	37.1
6/19/2012	0.458	-11.5	39.7
7/20/2012	0.436	-10.0	36.2
8/17/2012	0.398	-9.2	37.3
9/21/2012	0.432	-10.2	34.6
10/19/2012	0.402	-9.2	36.2
11/20/2012	0.391	-8.5	36.4
12/20/2012	0.406	-9.3	37.9
1/18/2013	0.398	-8.8	36.9
2/22/2013	0.387	-9.2	37.9
3/22/2013	0.388	-9.1	36.6
4/19/2013	0.409	-9.8	36.5
5/17/2013	0.438	-8.9	37.7
6/21/2013	0.433	-11.3	37.2
7/19/2013	0.534	-13.1	39.5
8/20/2013	0.419	-10.4	37.6
9/19/2013	0.382	-8.7	36.5
10/17/2013	0.382	-9.8	35.7
11/18/2013	0.405	-9.5	36.3
12 /18/2013	0.412	-8.8	36.2

Site #7

Sampling date	pCO_2 (atm * 10^3)	$\delta^{13}C_{CO2}$ (‰ V-PDB)	$\delta^{18}O_{CO2}$ (‰ V-SMOW)
1/19/2012	0.588	-14.0	41.4
2/20/2012	0.591	-14.2	40.8
3/19/2012	0.657	-15.4	42.3
4/20/2012	1.574	-19.0	45.5
5/21/2012	1.134	-17.1	41.9
6/19/2012	1.416	-20.2	42.1
7/20/2012	3.075	-21.6	44.9
8/17/2012	2.917	-21.9	44.8
9/21/2012	2.035	-21.2	43.5
10/19/2012	1.890	-20.5	43.9
11/20/2012	0.927	-17.5	42.0
12/20/2012	0.706	-16.8	40.6
1/18/2013	0.655	-15.6	39.5
2/22/2013	0.633	-15.5	39.5
3/22/2013	0.797	-16.8	40.3
4/19/2013	1.063	-18.3	41.1
5/17/2013	1.218	-19.0	42.0
6/21/2013	1.201	-19.5	40.7
7/19/2013	1.814	-20.5	44.1
8/20/2013	2.494	-21.3	44.4
9/19/2013	2.501	-22.0	43.4
10/17/2013	2.548	-21.7	43.5
11/18/2013	1.121	-18.7	43.2
12 /18/2013	0.583	-14.6	38.5

APPENDIX 3.3.

(DRIP WATER CARBONATE CHEMISTRY DATA)

Drip Site #6

Sampling date	DIC (mM/l)	$\delta^{13}C_{DIC}$ (‰ VPDB)	Alkalinity (meq/l)	$pCO2_{drip}$ (atm * 10^3)	SI_{AR}	pH	Temp (°C)
1/19/2012	-	-	-	-	-	-	-
2/20/2012	1.4	-5.7		0.513	-0.060	8.20	17.6
3/19/2012	3.2	-8.4	5.75	1.869	0.230	8.00	18.3
4/20/2012	2.8	-9.1	5.63	1.959	0.120	7.92	18.3
5/21/2012	3.3	-10.1	5.75	-	-	-	-
6/19/2012	4.2	-11.4	4.75	6.439	-0.390	7.57	18.9
7/20/2012	3.1	-7.8	4.69	4.564	-0.180	7.59	19.1
8/17/2012	2.3	-7.4	4.75	4.293	-	7.48	19.1
9/21/2012	2.6	-7.5	-	6.124	-0.550	7.37	19.1
10/19/2012	1.9	-6.5	-	1.277	-0.070	7.96	19.0
11/20/2012	2.7	-6.9	-	0.727	0.370	8.34	18.9
12/20/2012	-	-	-	-	-	8.31	18.6
1/18/2013	-	-	-	-	-	8.53	18.0
2/22/2013	-	-	6.56	-	0.180	7.64	17.8
3/22/2013	-	-	6.50	-	0.510	7.94	18.0
4/19/2013	5.0	-8.9	6.88	2.920	0.520	8.00	18.3
5/17/2013	-	-	4.61	-	0.350	7.83	19.0
6/21/2013	-	-	3.75	-	-0.050	7.49	19.2
7/19/2013	-	-	3.69	-	-0.510	7.03	19.8
8/20/2013	4.5	-8.2	4.25	6.606	0.080	7.59	18.9
9/19/2013	-	-	2.75	-	-0.550	7.12	18.9
10/17/2013	5.3	-10.6	2.80	24.079	-0.450	7.1	19.0
11/18/2013	4.0	-10.1	2.88	16.096	-0.690	7.04	18.6
12/18/2013	4.7	-11.1	2.94	9.235	-0.120	7.45	18.3

Drip Site #7

Sampling date	DIC (mM/l)	$\delta^{13}C_{DIC}$ (‰ VPDB)	Alkalinity (meq/l)	$pCO2_{drip}$ (atm * 10^3)	SI_{AR}	pH	Temp (°C)
1/19/2012	-	-	-	-	-	-	-
2/20/2012	-	-	-	-	-	-	-
3/19/2012	2.9	-7.9	6.31	1.907	0.140	7.95	18.7
4/20/2012	4.4	-9.8	6.20	3.887	0.160	7.82	18.9
5/21/2012	3.3	-8.7	5.25	-	-	-	-
6/19/2012	3.4	-10.1	-	5.798	-0.790	7.52	18.8
7/20/2012	-	-	-	-	-	-	-
8/17/2012	-	-	-	-	-	-	-
9/21/2012	-	-	-	-	-	-	-
10/19/2012	-	-	-	-	-	-	-
11/20/2012	-	-	-	-	-	-	-
12/20/2012	-	-	-	-	-	-	-
1/18/2013	-	-	-	-	-	-	-
2/22/2013	-	-	6.86	-	0.680	8.10	17.8
3/22/2013	-	-	6.25	-	0.670	8.17	17.9
4/19/2013	4.4	-6.0	7.50	1.514	0.670	8.23	18.1
5/17/2013	-	-	4.75	-	0.610	8.14	18.5
6/21/2013	-	-	4.00	-	0.190	7.70	19.4
7/19/2013	-	-	3.86	-	0.170	7.73	19.8
8/20/2013	4.6	-7.6	4.81	4.530	0.300	7.77	18.7
9/19/2013	-	-	2.63	-	-0.130	7.65	18.7
10/17/2013	4.7	-9.0	3.06	7.689	-0.060	7.54	18.9
11/18/2013	2.5	-6.3	-	3.497	-0.770	7.61	18.6
12/18/2013	4.8	-10.1	2.81	3.340	0.270	7.92	17.9

Drip Site #13

Sampling date	DIC (mM/l)	$\delta^{13}C_{DIC}$ (‰ VPDB)	Alkalinity (meq/l)	$pCO2_{drip}$ (atm * 10^3)	SI_{AR}	pH	Temp (°C)
1/19/2012	-	-	3.81	-	-	-	17.7
2/20/2012	-	-	-	-	-	-	-
3/19/2012	1.2	-3.4	4.38	0.596	-	8.07	18.1
4/20/2012	2.1	-6.5		1.142	-	8.03	18.1
5/21/2012	2.6	-8.2	-	-	-	-	-
6/19/2012	3.7	-10.5	-	6.281	-	7.53	19.9
7/20/2012	3.1	-8.2	-	3.268	-	7.74	18.8
8/17/2012	2.0	-6.6	-	2.690	-	7.63	18.9
9/21/2012	-	-	-	-	-	-	-
10/19/2012	-	-	-	-	-	-	-
11/20/2012	-	-	-	-	-	-	-
12/20/2012	-	-	-	-	-	7.94	19.1
1/18/2013	-	-	5.50	-	0.700	8.21	18.2
2/22/2013	-	-	4.38	-	0.570	8.27	17.8
3/22/2013	3.2	-4.7	-	0.869	0.500	8.33	17.6
4/19/2013	1.2	-2.9	3.00	0.412	-	8.23	18.0
5/17/2013	-	-	-	-	-	-	-
6/21/2013	3.4	-3.3	3.44	2.048	0.340	7.99	18.9
7/19/2013	-	-	-	-	-	7.97	19.2
8/20/2013	3.7	-8.2	3.31	2.433	0.320	7.95	18.7
9/19/2013	-	-	-	-	-	7.92	18.6
10/17/2013	-	-	-	-	-	-	-
11/18/2013	-	-	-	-	-	-	-
12/18/2013	2.7	-3.8	2.25	0.687	0.510	8.36	18.0

Drip Site #15

Sampling date	DIC (mM/l)	$\delta^{13}C_{DIC}$ (‰ VPDB)	Alkalinity (meq/l)	$pCO2_{drip}$ (atm * 10^3)	SI_{AR}	pH	Temp (°C)
1/18/2013	-	-	5.50	-	0.76	8.31	18.2
2/22/2013	-	-	5.81	-	0.76	8.26	17.7
3/22/2013	-	-	6.00	-	0.70	8.30	17.8
4/19/2013	4.3	-7.6	6.38	1.35	0.68	8.27	18.1
5/17/2013	4.2	-5.7	4.50	1.49	0.63	8.22	18.5
6/21/2013	-	-	2.75	-	0.16	7.92	18.8
7/19/2013	-	-	3.19	-	0.17	7.81	19.8
8/20/2013	4.0	-6.6	3.75	2.88	0.33	7.91	18.7
9/19/2013	-	-	3.25	-	0.15	7.80	18.6
10/17/2013	4.7	-10.2	-	4.33	0.20	7.80	18.7
11/18/2013	4.7	-13.4	-	8.95	-	7.47	19.0
12/18/2013	4.2	-10.7	3.00	1.38	0.64	8.25	18.1

APPENDIX 4.1.

(DSSG-5 STABLE ISOTOPE DATA)

DBT (mm)	Model Age (cal ka BP)	$\delta^{18}O$ (‰ V-PDB) (Ar)	$\delta^{13}C$ (‰ V-PDB) (Ar)
40.5	1.050	-3.5	-7.8
40.8	1.056	-3.9	-8.7
41.1	1.062	-3.6	-7.9
41.5	1.070	-4.2	-9.4
41.8	1.076	-4.2	-9.5
42.1	1.082	-4.0	-9.2
42.4	1.088	-4.4	-9.7
42.7	1.094	-3.7	-8.3
43.0	1.100	-3.4	-8.2
43.4	1.108	-3.3	-8.1
43.7	1.115	-3.3	-8.0
44.0	1.121	-3.6	-8.3
44.3	1.127	-4.2	-9.5
44.6	1.133	-4.1	-9.5
45.0	1.141	-4.0	-9.6
45.3	1.147	-4.5	-10.1
45.6	1.153	-4.5	-9.9
45.9	1.159	-4.4	-9.4
46.2	1.165	-4.4	-9.3
46.5	1.171	-4.1	-8.4
46.9	1.179	-4.1	-8.1
47.2	1.185	-3.9	-8.0
47.5	1.191	-4.0	-8.3
47.8	1.197	-4.0	-8.9
48.1	1.203	-3.7	-8.7
48.4	1.209	-3.6	-8.3
48.8	1.217	-3.5	-8.7
49.1	1.223	-3.5	-8.7
49.4	1.229	-3.4	-8.4
49.7	1.235	-3.5	-8.9
50.0	1.242	-4.2	-10.2
50.4	1.250	-3.9	-9.9
50.7	1.256	-3.6	-8.6
51.0	1.262	-3.3	-8.6
51.3	1.268	-3.4	-8.2
51.6	1.274	-3.3	-8.6
51.9	1.280	-3.7	-8.5
52.3	1.288	-3.5	-8.6
52.6	1.294	-3.8	-8.9

DBT (mm)	Model Age (cal ka BP)	$\delta^{18}O$ (‰ V-PDB) (Ar)	$\delta^{13}C$ (‰ V-PDB) (Ar)
52.9	1.300	-3.9	-9.2
53.2	1.303	-3.9	-9.1
53.4	1.305	-4.1	-9.6
53.7	1.308	-3.9	-9.3
54.0	1.311	-3.6	-8.6
54.3	1.313	-3.8	-8.6
54.5	1.315	-4.1	-8.9
54.8	1.318	-3.7	-8.7
55.1	1.321	-3.6	-8.7
55.3	1.323	-4.0	-8.6
55.6	1.326	-3.9	-9.1
55.9	1.329	-3.7	-8.9
56.2	1.332	-3.6	-8.8
56.4	1.333	-3.3	-8.3
56.7	1.336	-3.5	-8.1
57.0	1.339	-3.5	-7.8
57.2	1.341	-2.9	-6.6
57.5	1.344	-2.8	-7.2
57.8	1.347	-2.5	-6.6
58.1	1.350	-2.9	-6.4
58.3	1.352	-2.7	-6.8
58.6	1.355	-3.0	-7.2
58.9	1.357	-3.0	-7.2
59.1	1.359	-3.0	-6.7
59.4	1.362	-2.9	-6.1
59.7	1.365	-2.5	-5.9
60.0	1.368	-2.5	-6.3
60.2	1.370	-2.8	-7.1
60.5	1.373	-2.7	-7.3
60.8	1.376	-3.0	-7.1
61.0	1.378	-2.9	-7.2
61.3	1.380	-3.0	-7.2
61.6	1.383	-3.1	-7.1
61.9	1.386	-3.1	-7.5
62.1	1.388	-3.1	-7.3
62.4	1.391	-2.8	-7.4

DBT (mm)	Model Age (cal ka BP)	$\delta^{18}O$ (‰ V-PDB) (Ar)	$\delta^{13}C$ (‰ V-PDB) (Ar)
62.7	1.394	-2.8	-7.4
62.9	1.396	-3.0	-7.1
63.2	1.399	-2.8	-7.0
63.5	1.401	-2.7	-6.7
63.8	1.404	-2.4	-6.1
64.0	1.406	-2.5	-6.1
64.3	1.409	-2.6	-5.8
64.6	1.412	-2.8	-6.7
64.8	1.414	-2.7	-7.1
65.1	1.417	-2.9	-7.2
65.4	1.420	-2.6	-6.6
65.7	1.422	-2.6	-6.6
65.9	1.424	-3.0	-6.8
66.2	1.427	-2.9	-7.1
66.5	1.430	-2.8	-7.1
66.7	1.432	-3.0	-6.9
67.0	1.435	-2.8	-6.6
67.3	1.438	-2.9	-7.4
67.6	1.441	-2.7	-7.1
67.8	1.443	-2.5	-7.1
68.1	1.445	-2.8	-7.1
68.4	1.448	-2.9	-7.2
68.6	1.450	-3.0	-7.5
68.9	1.453	-2.8	-7.2
69.2	1.456	-3.0	-7.0
69.5	1.459	-2.8	-7.0
69.7	1.461	-2.9	-7.1
70.0	1.464	-2.8	-6.7
70.3	1.467	-3.0	-6.8
70.5	1.468	-2.9	-6.4
70.8	1.471	-3.0	-6.2
71.1	1.474	-3.0	-6.3
71.4	1.477	-3.2	-7.0
71.6	1.479	-2.8	-6.7
71.9	1.482	-3.1	-8.1
72.2	1.485	-3.0	-7.1

DBT (mm)	Model Age (cal ka BP)	$\delta^{18}O$ (‰ V-PDB) (Ar)	$\delta^{13}C$ (‰ V-PDB) (Ar)
72.4	1.487	-3.2	-7.2
72.7	1.489	-3.0	-7.4
73.0	1.492	-3.1	-7.4
73.3	1.495	-2.9	-6.7
73.5	1.497	-3.0	-6.6
73.8	1.500	-3.3	-7.1
74.1	1.503	-3.3	-7.2
74.4	1.505	-3.0	-6.9
74.7	1.508	-3.0	-7.4
74.9	1.510	-3.0	-7.4
75.2	1.512	-3.0	-7.9
75.5	1.515	-2.9	-7.5
75.8	1.517	-3.0	-6.9
76.1	1.520	-3.1	-7.0
76.4	1.523	-3.0	-6.8
76.7	1.525	-2.8	-6.9
77.0	1.528	-2.8	-6.9
77.2	1.530	-3.2	-7.1
77.5	1.532	-2.9	-6.8
77.8	1.535	-3.0	-7.3
78.1	1.537	-2.9	-7.3
78.4	1.540	-2.7	-6.4
78.7	1.543	-2.7	-5.9
79.0	1.545	-3.0	-7.3
79.3	1.548	-2.7	-7.1
79.5	1.550	-3.1	-7.1
79.8	1.552	-2.8	-7.0
80.1	1.555	-3.2	-7.3
80.4	1.557	-3.2	-7.4
80.7	1.560	-3.4	-7.4
81.0	1.563	-3.3	-7.5
81.3	1.565	-3.4	-7.5
81.6	1.568	-3.5	-8.1
81.8	1.570	-3.2	-7.2
82.1	1.572	-3.2	-7.5
82.4	1.575	-3.3	-7.7

DBT (mm)	Model Age (cal ka BP)	$\delta^{18}O$ (‰ V-PDB) (Ar)	$\delta^{13}C$ (‰ V-PDB) (Ar)
82.7	1.577	-3.2	-7.6
83.0	1.580	-3.2	-8.1
83.3	1.582	-2.9	-7.8
83.6	1.585	-3.0	-7.7
83.8	1.586	-3.2	-7.8
84.1	1.589	-3.2	-7.9
84.4	1.591	-3.4	-7.3
84.7	1.594	-3.2	-7.6
84.9	1.595	-3.4	-7.8
85.2	1.598	-3.4	-7.8
85.5	1.600	-3.3	-8.0
85.8	1.602	-3.4	-7.7
86.1	1.605	-3.3	-7.4
86.3	1.606	-3.3	-7.2
86.6	1.609	-3.5	-7.5
86.9	1.611	-3.5	-7.6
87.2	1.614	-3.5	-7.6
87.4	1.615	-3.6	-7.8
87.7	1.618	-3.1	-7.4
88.0	1.620	-3.6	-7.4
88.3	1.622	-3.7	-7.4
88.6	1.625	-3.8	-7.7
88.8	1.626	-3.7	-7.4
89.1	1.629	-3.4	-7.1
89.4	1.631	-3.4	-7.2
89.7	1.634	-3.4	-7.4
89.9	1.635	-3.4	-7.3
90.2	1.638	-2.9	-6.6
90.5	1.640	-3.1	-6.8
90.8	1.642	-3.1	-6.4
91.1	1.645	-3.2	-6.8
91.3	1.646	-2.8	-6.7
91.6	1.649	-3.3	-7.0
91.9	1.651	-3.3	-7.3
92.2	1.654	-3.4	-7.4
92.4	1.655	-3.3	-7.1

DBT (mm)	Model Age (cal ka BP)	$\delta^{18}O$ (‰ V-PDB) (Ar)	$\delta^{13}C$ (‰ V-PDB) (Ar)
92.7	1.658	-3.2	-7.0
93.0	1.660	-3.0	-7.4
93.3	1.662	-3.0	-6.8
93.6	1.665	-3.1	-6.8
93.8	1.666	-3.1	-7.0
94.1	1.669	-3.1	-6.6
94.4	1.671	-3.3	-7.4
94.7	1.674	-3.3	-7.7
94.9	1.675	-3.6	-8.4
95.2	1.678	-3.6	-8.0
95.5	1.680	-3.2	-7.1
95.8	1.682	-3.2	-7.3
96.0	1.683	-2.8	-6.7
96.3	1.684	-2.7	-6.6
96.5	1.686	-3.1	-7.8
96.8	1.687	-2.9	-7.2
97.0	1.688	-2.5	-6.9
97.3	1.690	-2.6	-6.9
97.6	1.692	-3.0	-7.4
97.8	1.693	-2.6	-7.0
98.1	1.694	-2.9	-7.1
98.3	1.696	-3.0	-7.2
98.6	1.697	-3.0	-7.6
98.8	1.698	-3.0	-7.6
99.1	1.700	-3.0	-7.6
99.4	1.702	-3.0	-7.7
99.6	1.703	-2.8	-7.4
99.9	1.704	-2.5	-6.7
100.1	1.706	-2.7	-7.1
100.4	1.707	-2.6	-7.1
100.6	1.708	-2.7	-7.0
100.9	1.710	-2.7	-6.5
101.2	1.712	-2.8	-6.7
101.4	1.713	-3.0	-6.6
101.7	1.714	-3.0	-6.6
101.9	1.716	-2.9	-5.9

DBT (mm)	Model Age (cal ka BP)	$\delta^{18}O$ (‰ V-PDB) (Ar)	$\delta^{13}C$ (‰ V-PDB) (Ar)	
102.2	1.717	-2.5	-5.3	
102.4	1.718	-2.7	-5.6	
102.7	1.720	-3.1	-5.8	
103.0	1.722	-2.8	-6.0	
103.2	1.723	-2.7	-5.6	
103.5	1.724	-2.7	-5.6	
103.7	1.726	-2.5	-5.5	
104.0	1.727	-2.6	-5.6	
104.2	1.728	-2.9	-5.4	
104.5	1.730	-2.9	-6.8	
104.8	1.732	-2.8	-6.3	
105.0	1.733	-2.9	-6.4	
105.3	1.734	-2.7	-6.3	
105.5	1.736	-2.6	-6.1	
105.8	1.737	-2.3	-5.8	
106.0	1.738	-2.4	-5.7	
106.3	1.740	-2.7	-6.0	**Hiatus**
112.6	2.040	-2.5	-6.2	
112.9	2.041	-2.7	-6.7	
113.2	2.043	-2.7	-7.0	
113.5	2.044	-2.9	-7.3	
113.8	2.046	-2.8	-7.4	
114.1	2.047	-3.0	-6.6	
114.3	2.048	-2.8	-6.5	
114.6	2.049	-2.9	-6.6	
114.9	2.051	-3.3	-7.0	
115.2	2.052	-3.2	-6.7	
115.5	2.053	-3.5	-6.9	
115.8	2.055	-3.4	-6.9	
116.1	2.056	-3.1	-6.2	
116.4	2.057	-3.2	-6.5	
116.7	2.059	-2.7	-6.4	
117.0	2.060	-2.8	-7.0	
117.2	2.061	-3.3	-7.5	
117.5	2.063	-3.1	-7.0	
117.8	2.064	-3.0	-7.3	

DBT (mm)	Model Age (cal ka BP)	$\delta^{18}O$ (‰ V-PDB) (Ar)	$\delta^{13}C$ (‰ V-PDB) (Ar)
118.1	2.065	-3.0	-7.2
118.4	2.067	-3.0	-7.4
118.7	2.068	-3.0	-7.2
119.0	2.069	-3.1	-7.6
119.3	2.071	-2.9	-7.3
119.6	2.072	-3.0	-7.0
119.9	2.074	-2.7	-6.8
120.1	2.074	-2.8	-7.1
120.4	2.076	-2.7	-6.8
120.7	2.077	-2.9	-7.3
121.0	2.079	-2.7	-6.8
121.3	2.080	-3.2	-8.0
121.6	2.081	-3.3	-7.3
121.9	2.083	-3.0	-8.0
122.2	2.084	-3.4	-8.0
122.5	2.086	-3.2	-8.0
122.8	2.087	-3.5	-8.1
123.0	2.088	-2.9	-6.9
123.3	2.089	-3.3	-7.6
123.6	2.091	-3.2	-7.4
123.9	2.092	-3.4	-7.4
124.2	2.093	-3.4	-8.1
124.5	2.095	-3.3	-7.7
124.8	2.096	-3.8	-8.9
125.1	2.097	-3.4	-8.6
125.4	2.099	-3.0	-7.7
125.7	2.100	-3.3	-7.9
125.9	2.101	-3.1	-7.1
126.2	2.103	-3.1	-6.7
126.5	2.104	-3.1	-7.8
126.8	2.105	-3.0	-7.3
127.1	2.107	-3.0	-6.9
127.4	2.108	-3.2	-7.5
127.7	2.109	-3.1	-7.0
128.0	2.111	-2.7	-6.5
128.3	2.112	-2.8	-7.3

DBT (mm)	Model Age (cal ka BP)	$\delta^{18}O$ (‰ V-PDB) (Ar)	$\delta^{13}C$ (‰ V-PDB) (Ar)
128.6	2.114	-2.9	-7.4
128.8	2.114	-3.3	-7.5
129.1	2.116	-3.2	-6.7
129.4	2.117	-3.2	-7.0
129.7	2.119	-2.9	-6.5
130.0	2.120	-3.0	-7.3
130.3	2.121	-2.9	-6.9
130.6	2.123	-2.8	-7.0
130.9	2.124	-2.8	-7.3
131.2	2.126	-2.9	-7.0
131.5	2.127	-2.8	-6.6
131.7	2.128	-2.8	-7.2
132.0	2.129	-2.9	-6.9
132.3	2.131	-2.9	-7.0
132.6	2.132	-2.9	-7.0
132.9	2.133	-3.0	-6.9
133.2	2.135	-2.8	-6.6
133.5	2.136	-3.0	-6.9
133.8	2.137	-2.6	-6.6
134.1	2.139	-2.5	-6.9
134.4	2.140	-2.7	-7.1
134.6	2.141	-2.6	-6.5
134.9	2.143	-3.2	-7.5
135.2	2.144	-2.7	-7.0
135.5	2.145	-2.8	-7.3
135.8	2.147	-2.9	-7.3
136.1	2.148	-2.8	-7.1
136.4	2.149	-2.7	-6.8
136.7	2.151	-2.9	-6.6
137.0	2.152	-3.1	-7.2
137.3	2.154	-3.0	-7.8
137.5	2.154	-2.9	-7.4
137.8	2.156	-2.7	-6.8
138.1	2.157	-2.9	-7.4
138.4	2.159	-2.9	-7.4
138.7	2.160	-3.0	-7.3

DBT (mm)	Model Age (cal ka BP)	$\delta^{18}O$ (‰ V-PDB) (Ar)	$\delta^{13}C$ (‰ V-PDB) (Ar)
139.0	2.162	-2.8	-7.0
139.3	2.164	-2.7	-6.8
139.5	2.165	-3.1	-7.6
139.8	2.168	-3.3	-7.1
140.1	2.170	-3.4	-7.7
140.4	2.172	-3.3	-7.5
140.7	2.174	-3.4	-7.4
140.9	2.175	-3.5	-7.3
141.2	2.177	-3.1	-7.0
141.5	2.179	-3.2	-7.3
141.8	2.181	-3.4	-7.6
142.1	2.183	-3.2	-7.7
142.4	2.185	-3.1	-7.2
142.6	2.187	-2.9	-7.2
142.9	2.189	-3.1	-7.6
143.2	2.191	-3.1	-7.7
143.5	2.193	-3.3	-7.6
143.8	2.195	-3.4	-7.8
144.0	2.196	-3.1	-7.9
144.3	2.198	-3.1	-8.0
144.6	2.200	-3.2	-7.9
144.9	2.202	-3.3	-7.9
145.2	2.204	-2.8	-7.2
145.4	2.206	-2.9	-7.8
145.7	2.208	-2.9	-7.3
146.0	2.210	-2.9	-7.4
146.3	2.212	-3.2	-7.3
146.6	2.214	-3.2	-7.5
146.8	2.215	-2.9	-7.2
147.1	2.217	-3.3	-7.7
147.4	2.219	-3.0	-7.5
147.7	2.221	-3.2	-7.3
148.0	2.224	-3.1	-7.6
148.2	2.225	-2.9	-7.7
148.5	2.227	-3.0	-7.2
148.8	2.229	-2.9	-7.1

DBT (mm)	Model Age (cal ka BP)	$\delta^{18}O$ (‰ V-PDB) (Ar)	$\delta^{13}C$ (‰ V-PDB) (Ar)
149.1	2.231	-2.9	-7.1
149.4	2.233	-3.4	-7.6
149.7	2.235	-3.2	-7.3
149.9	2.236	-3.2	-7.4
150.2	2.239	-3.4	-7.6
150.5	2.241	-3.3	-7.7
150.8	2.243	-2.9	-7.5
151.1	2.245	-3.0	-7.7
151.3	2.246	-3.0	-7.4
151.6	2.248	-3.4	-7.9
151.9	2.250	-3.2	-7.8
152.2	2.252	-3.0	-7.2
152.5	2.254	-2.9	-7.5
152.7	2.256	-3.4	-8.2
153.0	2.258	-3.3	-7.5
153.3	2.260	-3.4	-6.8
153.6	2.262	-3.8	-7.8
153.9	2.264	-3.6	-7.4
154.1	2.265	-3.5	-6.9
154.4	2.267	-3.4	-7.0
154.7	2.269	-3.3	-7.3
155.0	2.271	-3.4	-7.5
155.3	2.273	-3.5	-7.6
155.5	2.275	-3.5	-7.2
155.8	2.277	-3.5	-7.6
156.1	2.279	-3.3	-6.9
156.4	2.281	-3.8	-7.4
156.7	2.283	-3.4	-7.2
157.0	2.285	-3.1	-6.9
157.2	2.286	-3.0	-7.0
157.5	2.288	-2.9	-6.8
157.8	2.290	-3.1	-6.9
158.1	2.292	-3.1	-7.2
158.4	2.295	-3.2	-7.0
158.6	2.296	-3.2	-7.2
158.9	2.298	-3.3	-7.3

DBT (mm)	Model Age (cal ka BP)	$\delta^{18}O$ (‰ V-PDB) (Ar)	$\delta^{13}C$ (‰ V-PDB) (Ar)
159.2	2.300	-3.3	-7.3
159.5	2.301	-3.4	-6.9
159.7	2.302	-3.2	-6.9
160.0	2.304	-3.2	-7.4
160.2	2.305	-3.1	-7.3
160.5	2.306	-2.9	-7.1
160.8	2.308	-3.1	-7.7
161.0	2.309	-3.1	-7.4
161.3	2.310	-3.0	-7.4
161.5	2.311	-2.7	-6.7
161.8	2.312	-3.1	-8.1
162.1	2.314	-2.9	-7.5
162.3	2.315	-3.2	-7.7
162.6	2.316	-3.4	-7.8
162.8	2.317	-3.2	-7.5
163.1	2.318	-3.4	-7.7
163.4	2.320	-3.4	-7.7
163.6	2.321	-3.6	-7.5
163.9	2.322	-3.8	-7.9
164.1	2.323	-3.8	-7.7
164.4	2.325	-3.5	-7.4
164.7	2.326	-3.6	-8.0
164.9	2.327	-3.5	-8.1
165.2	2.328	-3.3	-8.0
165.4	2.329	-3.4	-7.7
165.7	2.331	-3.2	-7.9
165.9	2.332	-3.4	-8.1
166.2	2.333	-3.4	-7.9
166.5	2.335	-3.4	-7.8
166.7	2.335	-3.5	-7.7
167.0	2.337	-3.5	-7.8
167.2	2.338	-3.6	-7.7
167.5	2.339	-3.5	-7.6
167.8	2.341	-3.4	-7.4
168.0	2.342	-3.6	-7.6
168.3	2.343	-3.8	-7.9

DBT (mm)	Model Age (cal ka BP)	$\delta^{18}O$ (‰ V-PDB) (Ar)	$\delta^{13}C$ (‰ V-PDB) (Ar)
168.5	2.344	-3.8	-7.6
168.8	2.345	-3.7	-7.9
169.1	2.347	-3.8	-7.9
169.3	2.348	-3.7	-7.5
169.6	2.349	-3.7	-7.8
169.8	2.350	-3.7	-7.7
170.1	2.352	-3.4	-7.4
170.4	2.353	-3.5	-7.4
170.6	2.354	-3.5	-7.7
170.9	2.355	-3.5	-7.8
171.1	2.356	-3.6	-7.8
171.4	2.358	-3.8	-8.2
171.7	2.359	-3.9	-8.3
171.9	2.360	-3.6	-8.1
172.2	2.361	-3.4	-8.0
172.4	2.362	-3.2	-7.5
172.7	2.364	-3.4	-7.9
173.0	2.365	-3.5	-7.9
173.2	2.366	-3.2	-7.4
173.5	2.368	-3.5	-7.4
173.7	2.369	-3.7	-8.2
174.0	2.370	-3.5	-7.7
174.3	2.373	-3.6	-7.7
174.5	2.374	-3.5	-7.7
174.8	2.377	-3.3	-7.8
175.0	2.378	-3.4	-7.6
175.3	2.381	-3.3	-7.7
175.5	2.383	-3.4	-7.8
175.8	2.385	-3.5	-7.9
176.1	2.388	-3.5	-7.7
176.3	2.389	-3.5	-7.4
176.6	2.392	-3.4	-7.6
176.8	2.393	-3.4	-7.7
177.1	2.396	-3.4	-7.8
177.4	2.399	-3.5	-8.1
177.6	2.400	-3.7	-8.3

DBT (mm)	Model Age (cal ka BP)	$\delta^{18}O$ (‰ V-PDB) (Ar)	$\delta^{13}C$ (‰ V-PDB) (Ar)
177.9	2.403	-3.6	-8.2
178.1	2.404	-3.8	-8.4
178.4	2.407	-3.8	-7.7
178.6	2.409	-3.8	-7.4
178.9	2.411	-3.8	-7.4
179.2	2.414	-3.8	-7.9
179.4	2.415	-3.5	-8.1
179.7	2.418	-3.4	-8.0
179.9	2.419	-3.5	-8.2
180.2	2.422	-3.5	-7.9
180.4	2.424	-3.5	-8.2
180.7	2.426	-3.4	-8.2
181.0	2.429	-3.7	-9.1
181.2	2.430	-3.6	-8.4
181.5	2.433	-3.6	-8.9
181.7	2.435	-3.8	-9.2
182.0	2.437	-3.8	-9.1
182.3	2.440	-4.1	-9.5
182.5	2.441	-3.8	-8.6
182.8	2.444	-3.6	-8.0
183.0	2.445	-3.5	-8.2
183.3	2.448	-3.6	-8.4
183.5	2.450	-3.5	-8.2
183.8	2.452	-3.3	-7.5
184.1	2.455	-3.3	-7.6
184.3	2.456	-3.5	-7.9
184.6	2.459	-3.4	-8.7
184.8	2.461	-3.3	-9.1
185.1	2.463	-3.2	-9.0
185.3	2.465	-3.1	-8.4
185.6	2.467	-3.4	-8.1
185.9	2.470	-3.6	-8.4
186.1	2.471	-3.8	-7.7
186.4	2.474	-3.7	-7.7
186.6	2.476	-3.9	-8.1
186.9	2.478	-3.9	-8.3

DBT (mm)	Model Age (cal ka BP)	$\delta^{18}O$ (‰ V-PDB) (Ar)	$\delta^{13}C$ (‰ V-PDB) (Ar)
187.2	2.481	-3.6	-7.8
187.4	2.482	-3.6	-7.5
187.7	2.485	-3.7	-7.9
187.9	2.487	-3.5	-7.9
188.2	2.489	-3.4	-7.3
188.4	2.491	-3.1	-6.6
188.7	2.493	-3.3	-7.1
189.0	2.496	-3.6	-7.5
189.2	2.497	-3.2	-7.4
189.5	2.500	-3.4	-7.6
189.8	2.501	-3.5	-7.7
190.1	2.502	-3.4	-7.9
190.4	2.503	-3.5	-7.7
190.7	2.505	-3.7	-7.9
190.9	2.505	-3.4	-7.4
191.2	2.507	-3.4	-7.6
191.5	2.508	-3.5	-7.6
191.8	2.509	-3.5	-7.6
192.1	2.510	-3.5	-8.0
192.4	2.511	-3.3	-7.3
192.7	2.512	-3.5	-7.9
193.0	2.513	-3.5	-7.3
193.3	2.515	-3.7	-7.4
193.6	2.516	-3.8	-7.2
193.9	2.517	-3.7	-7.4
194.2	2.518	-3.5	-7.5
194.5	2.519	-3.5	-7.3
194.8	2.520	-3.5	-7.2
195.1	2.522	-3.7	-7.8
195.4	2.523	-2.9	-6.2
195.6	2.524	-3.3	-7.6
195.9	2.525	-3.3	-7.9
196.2	2.526	-3.4	-7.9
196.5	2.527	-3.6	-8.0
196.8	2.528	-3.7	-7.8
197.1	2.529	-3.6	-7.7

DBT (mm)	Model Age (cal ka BP)	$\delta^{18}O$ (‰ V-PDB) (Ar)	$\delta^{13}C$ (‰ V-PDB) (Ar)
197.4	2.530	-3.5	-7.7
197.7	2.532	-3.2	-7.8
198.0	2.533	-3.3	-7.5
198.3	2.534	-3.1	-7.3
198.6	2.535	-3.0	-6.8
198.9	2.536	-3.0	-6.6
199.2	2.537	-3.2	-6.6
199.5	2.539	-3.5	-7.2
199.8	2.540	-3.3	-7.2
200.1	2.541	-3.5	-7.2
200.3	2.542	-3.6	-7.3
200.6	2.543	-3.6	-7.0
200.9	2.544	-3.4	-7.1
201.2	2.545	-3.5	-7.3
201.5	2.546	-3.5	-7.1
201.8	2.547	-3.6	-7.8
202.1	2.549	-3.4	-7.1
202.4	2.550	-3.2	-7.6
202.7	2.551	-2.9	-6.9
203.0	2.552	-3.0	-7.2
203.3	2.553	-3.3	-7.4
203.6	2.554	-3.1	-6.8
203.9	2.556	-3.2	-6.9
204.2	2.557	-3.0	-7.2
204.5	2.558	-2.8	-7.2
204.8	2.559	-2.7	-6.9
205.0	2.560	-2.6	-6.8
205.3	2.561	-2.8	-7.3
205.6	2.562	-2.9	-7.2
205.9	2.563	-2.8	-7.1
206.2	2.564	-2.9	-7.1
206.5	2.566	-2.7	-6.6
206.8	2.567	-2.8	-6.9
207.1	2.568	-3.0	-7.1
207.4	2.569	-3.0	-7.0
207.7	2.570	-2.9	-6.7

DBT (mm)	Model Age (cal ka BP)	$\delta^{18}O$ (‰ V-PDB) (Ar)	$\delta^{13}C$ (‰ V-PDB) (Ar)
208.0	2.571	-2.8	-6.5
208.3	2.572	-2.9	-6.9
208.6	2.574	-2.9	-6.8
208.9	2.575	-3.0	-6.9
209.2	2.576	-3.1	-6.8
209.4	2.577	-3.0	-7.0
209.7	2.578	-3.0	-6.7
210.0	2.579	-3.0	-6.3
210.3	2.580	-3.3	-7.3
210.6	2.581	-3.3	-7.0
210.9	2.582	-3.4	-7.0
211.2	2.584	-3.5	-7.2
211.5	2.585	-3.3	-7.2
211.8	2.586	-2.9	-7.0
212.1	2.587	-3.1	-7.3
212.4	2.588	-2.9	-7.5
212.7	2.589	-3.1	-7.3
213.0	2.591	-2.9	-6.9
213.3	2.592	-3.2	-7.1
213.6	2.593	-3.2	-7.2
213.9	2.594	-3.4	-7.6
214.1	2.595	-3.1	-7.4
214.4	2.596	-2.9	-6.8
214.7	2.597	-2.9	-7.1
215.0	2.598	-2.7	-7.3
215.3	2.599	-2.9	-7.4
215.6	2.601	-2.9	-7.4
215.9	2.602	-3.2	-7.7
216.2	2.603	-3.0	-6.8
216.5	2.604	-3.1	-7.3
216.8	2.605	-3.0	-7.2
217.1	2.606	-3.0	-7.1
217.4	2.608	-3.2	-7.8
217.7	2.609	-3.0	-6.9
218.0	2.610	-3.2	-7.5
218.3	2.611	-3.1	-6.9

DBT (mm)	Model Age (cal ka BP)	$\delta^{18}O$ (‰ V-PDB) (Ar)	$\delta^{13}C$ (‰ V-PDB) (Ar)
218.6	2.612	-3.0	-6.6
218.8	2.613	-3.0	-7.4
219.1	2.614	-3.0	-7.8
219.4	2.615	-2.9	-8.1
219.7	2.616	-2.8	-7.3
220.0	2.618	-2.8	-7.0
220.3	2.619	-2.8	-7.0
220.6	2.620	-2.8	-7.6
220.9	2.621	-2.9	-7.3
221.2	2.622	-2.7	-7.7
221.5	2.623	-2.9	-7.8
221.8	2.624	-2.9	-7.5
222.1	2.626	-2.7	-7.2
222.4	2.627	-2.8	-8.0
222.7	2.628	-2.8	-7.4
223.0	2.629	-2.7	-7.8
223.3	2.630	-2.7	-7.5
223.5	2.631	-2.7	-7.1
223.8	2.632	-2.7	-6.8
224.1	2.633	-2.7	-6.8
224.4	2.635	-2.8	-7.3
224.7	2.636	-2.6	-7.3
225.0	2.637	-2.8	-7.7
225.3	2.638	-3.0	-7.5
225.6	2.639	-2.9	-7.6
225.9	2.640	-2.8	-7.0
226.2	2.641	-3.1	-7.4
226.5	2.643	-2.9	-7.3
226.8	2.644	-3.0	-7.7
227.1	2.645	-3.0	-7.6
227.4	2.646	-3.0	-7.5
227.7	2.647	-3.0	-7.2
228.0	2.648	-3.0	-7.1
228.2	2.649	-3.4	-7.8
228.5	2.650	-3.1	-7.8
228.8	2.651	-3.3	-7.6

DBT (mm)	Model Age (cal ka BP)	$\delta^{18}O$ (‰ V-PDB) (Ar)	$\delta^{13}C$ (‰ V-PDB) (Ar)
229.1	2.653	-3.1	-6.6
229.4	2.654	-3.2	-7.6
229.7	2.655	-3.3	-7.7
230.0	2.656	-3.4	-7.6
230.3	2.657	-3.4	-7.8
230.6	2.658	-3.2	-7.8
230.9	2.660	-3.2	-8.1
231.2	2.661	-3.0	-7.7
231.5	2.662	-3.0	-7.1
231.8	2.663	-3.4	-7.9
232.1	2.664	-3.3	-7.5
232.4	2.665	-3.4	-7.6
232.7	2.667	-3.2	-7.9
232.9	2.667	-3.4	-8.0
233.2	2.668	-3.0	-7.6
233.5	2.670	-3.0	-7.5
233.8	2.671	-2.9	-6.8
234.1	2.672	-3.1	-7.6
234.4	2.673	-2.8	-6.8
234.7	2.674	-3.2	-8.1
235.0	2.675	-3.1	-7.9
235.3	2.677	-3.1	-7.5
235.6	2.678	-3.2	-7.8
235.9	2.679	-3.1	-7.7
236.2	2.680	-3.2	-8.1
236.5	2.684	-3.2	-7.7
236.9	2.689	-3.1	-7.9
237.2	2.692	-3.0	-7.2
237.5	2.696	-3.1	-7.1
237.9	2.701	-3.2	-7.9
238.2	2.705	-3.0	-7.4
238.5	2.708	-3.2	-7.7
238.9	2.713	-3.0	-7.2
239.2	2.717	-2.9	-7.1
239.6	2.722	-2.9	-7.7
239.9	2.725	-3.0	-7.5

DBT (mm)	Model Age (cal ka BP)	$\delta^{18}O$ (‰ V-PDB) (Ar)	$\delta^{13}C$ (‰ V-PDB) (Ar)
240.2	2.729	-2.9	-7.3
240.6	2.734	-2.7	-7.2
240.9	2.738	-3.1	-7.2
241.2	2.741	-3.1	-7.3
241.6	2.746	-3.5	-7.1
241.9	2.750	-3.5	-7.2
242.2	2.754	-3.1	-7.4
242.6	2.759	-3.3	-7.5
242.9	2.762	-3.0	-7.6
243.2	2.766	-3.2	-7.4
243.6	2.771	-3.3	-7.6
243.9	2.775	-3.1	-7.4
244.2	2.778	-3.1	-7.3
244.6	2.783	-3.1	-7.4
244.9	2.787	-3.4	-7.5
245.2	2.791	-3.1	-7.6
245.6	2.795	-3.4	-7.7
245.9	2.799	-3.1	-7.7
246.3	2.804	-3.4	-7.8
246.6	2.808	-3.6	-7.7
246.9	2.811	-3.4	-7.8
247.3	2.816	-3.5	-8.0
247.6	2.820	-2.9	-8.2
247.9	2.822	-3.1	-7.5
248.3	2.824	-3.3	-7.9
248.6	2.826	-3.2	-8.0
248.9	2.828	-3.3	-8.3
249.2	2.830	-3.2	-7.7
249.6	2.832	-3.1	-7.9
249.9	2.834	-3.3	-7.9
250.2	2.836	-3.3	-8.2
250.5	2.838	-3.1	-7.4
250.9	2.841	-3.1	-7.6
251.2	2.842	-3.2	-7.4
251.5	2.844	-3.2	-7.2
251.9	2.847	-3.2	-7.6

DBT (mm)	Model Age (cal ka BP)	$\delta^{18}O$ (‰ V-PDB) (Ar)	$\delta^{13}C$ (‰ V-PDB) (Ar)
252.2	2.849	-3.3	-8.4
252.5	2.850	-3.7	-8.9
252.8	2.852	-3.7	-9.0
253.2	2.855	-3.4	-8.5
253.5	2.857	-3.4	-8.4
253.8	2.859	-3.3	-8.2
254.2	2.861	-3.5	-8.2
254.5	2.863	-3.4	-8.1
254.8	2.865	-3.6	-8.2
255.1	2.867	-3.5	-8.2
255.5	2.869	-3.4	-8.2
255.8	2.871	-3.4	-7.9
256.1	2.873	-3.1	-8.1
256.4	2.875	-3.3	-7.7
256.8	2.877	-3.3	-8.0
257.1	2.879	-3.4	-8.5
257.4	2.881	-3.5	-8.4
257.8	2.883	-3.4	-7.4
258.1	2.885	-3.8	-7.4
258.4	2.887	-3.3	-7.2
258.7	2.889	-3.5	-7.6
259.1	2.891	-3.5	-7.5
259.4	2.893	-3.4	-7.5
259.7	2.895	-3.4	-7.5
260.1	2.898	-3.3	-7.3
260.4	2.900	-3.5	-7.3
260.7	2.901	-3.6	-7.5
261.0	2.903	-3.5	-7.2
261.4	2.906	-3.4	-7.6
261.7	2.908	-3.5	-7.2
262.0	2.909	-3.4	-7.3
262.3	2.911	-3.4	-7.6
262.7	2.914	-3.6	-7.6
263.0	2.916	-3.5	-7.8
263.3	2.918	-3.5	-7.8
263.7	2.920	-3.3	-7.4

DBT (mm)	Model Age (cal ka BP)	$\delta^{18}O$ (‰ V-PDB) (Ar)	$\delta^{13}C$ (‰ V-PDB) (Ar)
264.0	2.922	-3.2	-7.6
264.3	2.924	-3.7	-7.9
264.6	2.926	-3.4	-7.8
265.0	2.928	-3.2	-7.6
265.3	2.930	-3.2	-7.8
265.6	2.932	-3.3	-7.7
265.9	2.933	-3.3	-7.6
266.2	2.935	-3.4	-7.7
266.5	2.937	-3.5	-7.7
266.8	2.938	-3.6	-8.0
267.1	2.940	-3.6	-8.2
267.4	2.941	-3.4	-7.8
267.6	2.943	-3.5	-7.5
267.9	2.944	-3.5	-7.8
268.2	2.946	-3.4	-7.9
268.5	2.947	-3.6	-8.6
268.8	2.949	-3.6	-8.0
269.1	2.951	-3.4	-7.6
269.4	2.952	-3.3	-7.9
269.7	2.954	-3.2	-7.0
270.0	2.956	-3.1	-7.1
270.3	2.957	-3.2	-7.2
270.6	2.959	-3.2	-7.3
270.9	2.961	-3.3	-7.3
271.2	2.962	-3.4	-7.7
271.5	2.964	-3.4	-8.1
271.7	2.965	-3.2	-7.7
272.0	2.967	-3.3	-7.9
272.3	2.968	-3.1	-7.3
272.6	2.970	-3.0	-7.2
272.9	2.972	-3.2	-7.8
273.2	2.973	-3.1	-7.0
273.5	2.975	-3.2	-7.6
273.8	2.976	-3.3	-7.3
274.1	2.978	-3.1	-6.4
274.4	2.980	-3.1	-6.6

DBT (mm)	Model Age (cal ka BP)	$\delta^{18}O$ (‰ V-PDB) (Ar)	$\delta^{13}C$ (‰ V-PDB) (Ar)
274.7	2.981	-3.3	-7.0
275.0	2.983	-3.0	-6.5
275.3	2.985	-3.1	-6.6
275.6	2.986	-3.2	-7.0
275.8	2.987	-3.1	-7.5
276.1	2.989	-2.9	-6.5
276.4	2.991	-3.1	-6.7
276.7	2.992	-2.9	-6.4
277.0	2.994	-3.1	-6.6
277.3	2.996	-3.0	-6.9
277.6	2.997	-3.0	-6.8
277.9	2.999	-3.1	-7.4
278.2	3.000	-3.0	-7.1
278.5	3.002	-3.0	-7.0
278.8	3.004	-3.3	-7.7
279.1	3.005	-3.2	-7.5
279.4	3.007	-3.0	-7.3
279.7	3.009	-3.1	-7.4
280.0	3.010	-2.9	-7.4
280.2	3.011	-2.8	-7.3
280.5	3.013	-2.8	-7.2
280.8	3.015	-2.7	-6.3
281.1	3.016	-2.8	-6.6
281.4	3.018	-2.8	-6.8
281.7	3.020	-2.9	-7.0
282.0	3.021	-2.8	-7.0
282.3	3.023	-2.8	-7.4
282.6	3.024	-2.9	-7.9
282.9	3.026	-2.9	-7.4
283.2	3.028	-2.7	-7.1
283.5	3.029	-2.9	-7.1
283.8	3.031	-2.9	-6.7
284.1	3.033	-3.0	-7.4
284.3	3.034	-3.6	-6.7
284.6	3.035	-2.9	-7.0
284.9	3.037	-2.8	-7.0

DBT (mm)	Model Age (cal ka BP)	$\delta^{18}O$ (‰ V-PDB) (Ar)	$\delta^{13}C$ (‰ V-PDB) (Ar)
285.2	3.039	-2.8	-6.9
285.5	3.040	-2.6	-6.2
285.8	3.042	-2.6	-6.3
286.1	3.044	-2.9	-7.2
286.4	3.045	-3.0	-7.8
286.7	3.047	-2.9	-7.6
287.0	3.048	-2.8	-6.8
287.3	3.050	-2.9	-7.1
287.6	3.052	-3.1	-6.9
287.9	3.053	-2.9	-6.0
288.2	3.055	-3.1	-6.2
288.4	3.056	-3.2	-6.8
288.7	3.058	-3.1	-6.9
289.0	3.059	-3.2	-7.1
289.3	3.061	-3.0	-6.6
289.6	3.063	-2.8	-5.4
289.9	3.064	-3.0	-6.5
290.2	3.066	-2.9	-6.7
290.5	3.068	-3.2	-6.8
290.8	3.069	-3.2	-7.6
291.1	3.071	-3.5	-8.2
291.4	3.073	-3.3	-7.8
291.7	3.074	-3.1	-7.2
292.0	3.076	-3.5	-7.9
292.3	3.077	-3.7	-8.4
292.5	3.079	-3.3	-7.7
292.8	3.080	-3.3	-7.1
293.1	3.082	-3.2	-6.4
293.4	3.083	-3.4	-6.8
293.7	3.085	-3.8	-7.9
294.0	3.087	-3.7	-8.5
294.3	3.088	-3.7	-7.8
294.6	3.090	-3.6	-8.0
294.9	3.092	-3.4	-7.5
295.2	3.094	-3.4	-7.0
295.5	3.095	-3.2	-7.2

DBT (mm)	Model Age (cal ka BP)	$\delta^{18}O$ (‰ V-PDB) (Ar)	$\delta^{13}C$ (‰ V-PDB) (Ar)
295.8	3.097	-2.9	-7.1
296.1	3.099	-3.0	-7.6
296.4	3.101	-2.9	-7.3
296.7	3.103	-2.9	-7.1
297.0	3.104	-3.2	-6.9
297.3	3.106	-3.2	-7.2
297.6	3.108	-3.4	-7.4
297.9	3.110	-3.1	-7.9
298.1	3.111	-3.0	-7.3
298.4	3.113	-3.1	-7.5
298.7	3.114	-3.1	-7.2
299.0	3.116	-3.5	-7.8
299.3	3.118	-3.4	-8.5
299.6	3.120	-3.5	-8.4
299.9	3.122	-3.4	-8.2
300.2	3.123	-3.6	-7.9
300.5	3.125	-3.8	-7.8
300.8	3.127	-3.6	-7.6
301.1	3.129	-3.3	-6.7
301.4	3.131	-3.6	-6.9
301.7	3.132	-3.3	-7.3
302.0	3.134	-3.3	-6.7
302.3	3.136	-3.3	-7.1
302.6	3.138	-3.2	-6.8
302.9	3.140	-3.3	-6.9
303.2	3.141	-3.1	-6.7
303.5	3.143	-3.4	-6.5
303.8	3.145	-3.7	-6.7
304.1	3.147	-3.7	-6.5
304.4	3.149	-3.9	-6.7
304.7	3.150	-3.8	-6.5
304.9	3.151	-3.6	-7.2
305.2	3.153	-4.0	-7.3
305.5	3.155	-3.8	-7.3
305.8	3.157	-3.7	-7.4
306.1	3.159	-3.6	-7.1

DBT (mm)	Model Age (cal ka BP)	$\delta^{18}O$ (‰ V-PDB) (Ar)	$\delta^{13}C$ (‰ V-PDB) (Ar)
306.4	3.160	-3.7	-7.2
306.7	3.162	-3.5	-7.1
307.0	3.164	-3.4	-7.5
307.3	3.166	-3.6	-7.6
307.6	3.168	-3.4	-7.5
307.9	3.169	-3.5	-7.3
308.2	3.171	-3.5	-7.5
308.5	3.173	-3.7	-7.4
308.8	3.175	-3.5	-7.4
309.1	3.177	-3.7	-7.8
309.4	3.178	-3.7	-7.6
309.7	3.180	-3.8	-7.4
310.0	3.182	-3.7	-7.8
310.3	3.184	-3.9	-8.0
310.6	3.186	-3.9	-7.8
310.9	3.187	-3.8	-7.6
311.2	3.189	-3.9	-7.7
311.4	3.190	-3.9	-7.9
311.7	3.192	-3.7	-7.4
312.0	3.194	-3.6	-7.5
312.3	3.196	-3.5	-7.8
312.6	3.197	-3.5	-7.5
312.9	3.199	-3.5	-7.8
313.2	3.201	-3.7	-7.7
313.5	3.203	-3.7	-8.5
313.8	3.205	-3.5	-7.6
314.1	3.206	-3.6	-7.7
314.4	3.208	-3.6	-8.0
314.7	3.210	-3.6	-7.5
315.2	3.212	-3.6	-7.6
315.7	3.213	-3.3	-7.0
316.2	3.215	-3.4	-7.2
316.7	3.217	-3.4	-7.2
317.2	3.218	-3.0	-6.5
317.7	3.220	-3.3	-7.3
318.2	3.222	-3.2	-7.7

DBT (mm)	Model Age (cal ka BP)	$\delta^{18}O$ (‰ V-PDB) (Ar)	$\delta^{13}C$ (‰ V-PDB) (Ar)
318.7	3.224	-3.2	-7.2
319.2	3.225	-3.1	-7.8
319.7	3.227	-3.2	-7.5
320.2	3.229	-3.1	-7.3
320.7	3.230	-3.1	-7.5
321.2	3.232	-3.2	-7.2
321.7	3.234	-3.4	-7.2
322.2	3.235	-3.5	-7.6
322.7	3.237	-3.5	-7.4
323.2	3.239	-3.5	-7.6
323.7	3.241	-3.5	-7.5
324.2	3.242	-3.8	-7.7
324.7	3.244	-3.5	-7.7
325.2	3.246	-3.4	-7.4
325.7	3.247	-3.7	-7.9
326.2	3.249	-3.6	-7.7
326.7	3.251	-3.2	-7.5
327.2	3.252	-3.5	-7.5
327.6	3.254	-3.9	-7.6
328.1	3.255	-3.4	-7.8
328.6	3.257	-3.3	-7.4
329.1	3.259	-3.4	-7.8
329.6	3.261	-3.4	-7.6
330.1	3.262	-3.3	-7.1
330.6	3.264	-3.7	-7.3
331.1	3.266	-3.7	-7.9
331.6	3.267	-3.8	-7.8
332.1	3.269	-3.9	-8.2
332.6	3.271	-3.8	-8.0
333.1	3.272	-3.9	-8.2
333.6	3.274	-3.6	-7.1
334.1	3.276	-3.4	-7.9
334.6	3.278	-3.2	-7.3
335.1	3.279	-3.5	-7.6
335.6	3.281	-3.6	-7.6
336.1	3.283	-3.5	-8.0

DBT (mm)	Model Age (cal ka BP)	$\delta^{18}O$ (‰ V-PDB) (Ar)	$\delta^{13}C$ (‰ V-PDB) (Ar)
336.6	3.284	-3.6	-7.7
337.1	3.286	-3.6	-8.0
337.6	3.288	-3.3	-6.8
338.1	3.289	-3.4	-7.2
338.6	3.291	-3.7	-7.5
339.1	3.293	-3.4	-7.2
339.6	3.295	-3.8	-7.6
340.1	3.296	-3.8	-7.3
340.6	3.298	-3.5	-7.5
341.1	3.300	-3.5	-7.5
341.6	3.301	-3.6	-7.5
342.1	3.303	-4.0	-8.0
342.6	3.305	-3.4	-7.2
343.1	3.306	-3.4	-7.3
343.6	3.308	-3.3	-7.1
344.1	3.310	-3.3	-6.9
344.6	3.312	-3.5	-7.2
345.1	3.313	-3.7	-7.3
345.6	3.315	-3.5	-7.0
346.1	3.317	-3.5	-6.9
346.6	3.318	-3.5	-7.3
347.1	3.320	-3.6	-7.2
347.6	3.322	-3.6	-7.3
348.1	3.323	-3.7	-7.2
348.6	3.325	-3.4	-7.3
349.1	3.327	-3.6	-7.4
349.6	3.328	-3.6	-7.3
350.1	3.330	-3.4	-7.3
350.6	3.332	-3.5	-6.8
351.1	3.333	-3.4	-6.5
351.6	3.335	-3.2	-6.1
352.1	3.337	-3.4	-6.5
352.6	3.338	-3.4	-6.8
353.1	3.340	-3.5	-6.8
353.6	3.342	-3.4	-6.9
354.1	3.343	-3.4	-6.7

DBT (mm)	Model Age (cal ka BP)	$\delta^{18}O$ (‰ V-PDB) (Ar)	$\delta^{13}C$ (‰ V-PDB) (Ar)
354.6	3.345	-3.2	-6.9
355.1	3.347	-3.3	-6.7
355.6	3.348	-3.4	-6.7
356.0	3.350	-3.5	-7.2
356.5	3.351	-3.3	-6.9
357.0	3.353	-3.3	-6.3
357.5	3.355	-3.8	-7.0
358.0	3.356	-3.7	-6.7
358.5	3.358	-3.7	-7.1
359.0	3.360	-3.4	-6.9
359.5	3.362	-3.3	-6.8
360.0	3.363	-3.4	-6.9
360.5	3.365	-3.6	-7.3
361.0	3.367	-3.5	-7.1
361.5	3.368	-3.4	-7.2
362.0	3.370	-3.4	-7.1
362.5	3.372	-3.3	-7.1
363.0	3.373	-3.3	-7.1
363.5	3.375	-3.3	-7.3
364.0	3.377	-3.3	-7.2
364.5	3.378	-3.3	-7.2
365.0	3.380	-3.4	-7.3
365.5	3.382	-3.3	-7.0
366.0	3.383	-3.3	-7.0
366.5	3.385	-3.6	-7.4
367.0	3.387	-3.3	-7.2
367.5	3.388	-3.4	-7.2
368.0	3.390	-3.5	-7.0
368.5	3.392	-3.9	-7.3
369.0	3.393	-3.7	-7.2
369.5	3.395	-3.8	-7.4
370.0	3.397	-3.9	-7.3
370.5	3.398	-3.7	-7.3
371.0	3.400	-3.8	-7.9
371.5	3.402	-3.4	-7.0
372.0	3.404	-3.2	-7.2

DBT (mm)	Model Age (cal ka BP)	$\delta^{18}O$ (‰ V-PDB) (Ar)	$\delta^{13}C$ (‰ V-PDB) (Ar)
372.5	3.406	-3.4	-7.4
372.9	3.408	-3.3	-7.1
373.4	3.410	-3.5	-7.0
373.9	3.412	-3.2	-6.6
374.4	3.414	-3.2	-6.8
374.9	3.416	-3.4	-7.0
375.4	3.418	-3.4	-7.1
375.8	3.419	-3.3	-6.9
376.3	3.421	-3.2	-6.7
376.8	3.423	-3.2	-6.8
377.3	3.425	-3.1	-6.9
377.8	3.427	-3.2	-6.7
378.3	3.429	-3.4	-7.1
378.8	3.431	-3.4	-6.9
379.2	3.433	-3.1	-7.0
379.7	3.435	-3.0	-6.8
380.2	3.437	-3.2	-6.9
380.7	3.439	-3.1	-7.0
381.2	3.441	-3.3	-7.0
381.7	3.443	-3.3	-7.1
382.2	3.445	-3.3	-7.1
382.6	3.446	-3.3	-7.0
383.1	3.448	-3.4	-7.0
383.6	3.450	-3.3	-7.0
384.1	3.452	-3.5	-7.2
384.6	3.454	-3.4	-7.1
385.1	3.456	-3.4	-6.9
385.5	3.458	-3.2	-6.7
386.0	3.460	-3.3	-6.9
386.5	3.462	-3.2	-7.2
387.0	3.464	-3.2	-7.1
387.5	3.466	-3.3	-7.2
388.0	3.468	-3.2	-7.1
388.5	3.470	-3.1	-6.3
388.9	3.471	-3.6	-6.9
389.4	3.473	-3.5	-7.7

DBT (mm)	Model Age (cal ka BP)	$\delta^{18}O$ (‰ V-PDB) (Ar)	$\delta^{13}C$ (‰ V-PDB) (Ar)
389.9	3.475	-3.5	-7.6
390.4	3.477	-3.2	-7.0
390.9	3.479	-3.2	-7.0
391.4	3.481	-3.3	-6.9
391.9	3.483	-3.3	-7.0
392.3	3.485	-3.2	-7.0
392.8	3.487	-3.2	-7.1
393.3	3.489	-3.1	-7.2
393.8	3.491	-3.1	-7.0
394.3	3.493	-3.1	-6.8
394.8	3.495	-3.7	-7.2
395.2	3.496	-3.3	-6.8
395.7	3.498	-3.2	-6.7
396.2	3.500	-3.0	-5.9
396.7	3.502	-3.1	-6.1
397.2	3.504	-3.3	-6.9
397.7	3.506	-2.9	-6.3
398.2	3.508	-3.0	-6.4
398.6	3.510	-3.1	-5.9
399.1	3.512	-2.8	-6.8
399.6	3.514	-3.0	-6.3
400.1	3.516	-2.8	-6.5
400.6	3.518	-3.0	-6.6
401.1	3.520	-3.1	-6.9
401.6	3.522	-3.1	-6.8
402.0	3.523	-3.2	-6.8
402.5	3.525	-2.6	-6.1
403.0	3.527	-3.0	-6.1
403.5	3.529	-3.3	-6.2
404.0	3.531	-3.3	-6.3
404.5	3.533	-3.3	-6.4
404.9	3.535	-3.2	-6.2
405.4	3.537	-2.9	-6.3
405.9	3.539	-3.4	-6.3
406.4	3.541	-3.1	-6.3
406.9	3.543	-3.1	-6.1

DBT (mm)	Model Age (cal ka BP)	$\delta^{18}O$ (‰ V-PDB) (Ar)	$\delta^{13}C$ (‰ V-PDB) (Ar)
407.4	3.545	-3.0	-6.3
407.9	3.547	-3.1	-6.4
408.3	3.549	-3.3	-6.6
408.8	3.550	-3.5	-6.5
409.3	3.552	-3.6	-6.6
409.8	3.554	-3.2	-6.3
410.3	3.556	-3.2	-6.0
410.8	3.558	-3.2	-4.6
411.3	3.560	-3.0	-5.6
411.7	3.562	-3.2	-5.7
412.2	3.564	-3.2	-6.3
412.7	3.566	-3.4	-6.5
413.2	3.568	-3.5	-6.5
413.7	3.570	-2.9	-5.2
414.2	3.571	-3.0	-6.5
414.7	3.573	-3.3	-6.6
415.3	3.574	-2.9	-6.5
415.8	3.576	-3.0	-6.9
416.3	3.577	-3.6	-7.1
416.8	3.579	-3.3	-7.4
417.4	3.580	-3.3	-7.5
417.9	3.582	-3.8	-6.4
418.4	3.583	-3.0	-6.1
418.9	3.585	-2.8	-5.7
419.5	3.586	-3.3	-6.7
420.0	3.588	-2.8	-6.2
420.5	3.589	-2.7	-6.1
421.0	3.591	-2.8	-6.3
421.6	3.592	-2.7	-6.0
422.1	3.594	-3.1	-7.3
422.6	3.595	-3.3	-6.9
423.1	3.596	-3.4	-7.1
423.7	3.598	-3.6	-7.4
424.2	3.599	-3.3	-6.7
424.7	3.601	-2.8	-6.9
425.2	3.602	-2.9	-6.9

DBT (mm)	Model Age (cal ka BP)	$\delta^{18}O$ (‰ V-PDB) (Ar)	$\delta^{13}C$ (‰ V-PDB) (Ar)
425.8	3.604	-3.1	-6.8
426.3	3.605	-3.2	-7.2
426.8	3.607	-3.0	-6.5
427.3	3.608	-2.8	-6.3
427.8	3.610	-3.1	-6.8
428.4	3.611	-3.5	-7.3
428.9	3.613	-3.1	-6.8
429.4	3.614	-3.2	-6.9
429.9	3.616	-3.3	-6.6
430.5	3.617	-3.1	-6.5
431.0	3.619	-3.0	-7.1
431.5	3.620	-3.5	-7.2
432.0	3.621	-3.9	-7.5
432.6	3.623	-3.5	-7.0
433.1	3.624	-3.4	-6.7
433.6	3.626	-3.1	-6.6
434.1	3.627	-3.0	-6.3
434.7	3.629	-3.3	-6.7
435.2	3.630	-3.2	-7.1
435.7	3.632	-3.4	-6.7
436.2	3.633	-3.3	-6.4
436.8	3.635	-3.1	-6.6
437.3	3.636	-3.2	-6.6
437.8	3.638	-3.5	-7.4
438.3	3.639	-3.4	-7.3
438.9	3.641	-3.2	-6.8
439.4	3.642	-3.1	-6.9
439.9	3.644	-3.3	-7.2
440.4	3.645	-3.3	-7.0
440.9	3.646	-3.2	-7.3
441.5	3.648	-3.4	-7.0
442.0	3.649	-3.4	-7.2
442.5	3.651	-3.4	-7.2
443.0	3.652	-3.4	-7.1
443.6	3.654	-3.4	-7.2
444.1	3.655	-3.4	-7.1

DBT (mm)	Model Age (cal ka BP)	$\delta^{18}O$ (‰ V-PDB) (Ar)	$\delta^{13}C$ (‰ V-PDB) (Ar)
444.6	3.657	-3.4	-7.0
445.1	3.658	-3.4	-7.1
445.7	3.660	-3.4	-7.0
446.2	3.661	-3.5	-6.8
446.7	3.663	-3.6	-7.2
447.2	3.664	-3.6	-7.3
447.8	3.666	-3.4	-7.0
448.3	3.667	-3.5	-6.9
448.8	3.669	-3.4	-6.7
449.3	3.670	-3.4	-6.9
449.8	3.673	-3.7	-7.3
450.4	3.677	-3.4	-7.0
450.9	3.681	-3.5	-6.9
451.4	3.684	-3.7	-6.7
451.9	3.687	-3.6	-6.8
452.4	3.690	-3.4	-7.1
453.0	3.694	-3.5	-7.2
453.5	3.698	-3.3	-7.2
454.0	3.701	-3.1	-6.9
454.5	3.704	-3.3	-6.8
455.0	3.707	-3.4	-6.9
455.5	3.711	-4.1	-7.4
456.1	3.715	-3.6	-7.0
456.6	3.718	-3.8	-7.6
457.1	3.721	-3.6	-7.5
457.6	3.725	-3.7	-7.4
458.1	3.728	-3.7	-7.1
458.6	3.731	-3.7	-7.1
459.2	3.735	-3.7	-7.3
459.7	3.738	-3.9	-7.5
460.2	3.742	-3.9	-7.5
460.7	3.745	-4.0	-7.4
461.2	3.748	-3.6	-7.3
461.7	3.751	-3.4	-7.3
462.3	3.755	-3.5	-7.1
462.8	3.759	-3.8	-7.5

DBT (mm)	Model Age (cal ka BP)	$\delta^{18}O$ (‰ V-PDB) (Ar)	$\delta^{13}C$ (‰ V-PDB) (Ar)
463.3	3.762	-3.6	-7.2
463.8	3.765	-3.6	-7.3
464.3	3.769	-3.5	-7.0
464.8	3.772	-3.5	-7.1
465.4	3.776	-3.3	-7.2
465.9	3.779	-3.3	-7.3
466.4	3.782	-3.2	-7.3
466.9	3.786	-3.0	-6.6
467.4	3.789	-3.3	-7.1
467.9	3.792	-3.5	-7.6
468.5	3.796	-3.8	-7.8
469.0	3.799	-3.7	-7.6
469.5	3.803	-3.6	-7.9
470.0	3.806	-3.5	-8.0
470.5	3.809	-3.3	-7.6
471.0	3.813	-3.2	-7.2
471.6	3.816	-3.3	-7.5
472.1	3.820	-3.5	-7.3
472.6	3.823	-3.4	-7.2
473.1	3.826	-3.5	-7.3
473.6	3.830	-3.9	-7.1
474.1	3.833	-3.9	-7.1
474.7	3.837	-3.9	-6.7
475.2	3.840	-3.8	-6.8
475.7	3.843	-3.6	-6.5
476.2	3.847	-3.9	-7.0
476.7	3.850	-3.6	-6.9
477.2	3.852	-3.2	-6.1
477.8	3.854	-3.1	-6.6
478.3	3.856	-3.6	-6.8
478.8	3.857	-3.5	-7.3
479.3	3.859	-3.6	-7.3
479.8	3.861	-3.6	-7.4
480.4	3.863	-4.0	-7.7
480.9	3.865	-4.1	-7.6
481.4	3.867	-3.5	-7.4

DBT (mm)	Model Age (cal ka BP)	$\delta^{18}O$ (‰ V-PDB) (Ar)	$\delta^{13}C$ (‰ V-PDB) (Ar)
481.9	3.868	-3.8	-7.5
482.4	3.870	-3.8	-7.4
482.9	3.872	-3.6	-7.2
483.5	3.874	-3.5	-7.4
484.0	3.876	-3.3	-7.5
484.5	3.878	-3.5	-7.4
485.0	3.879	-3.8	-7.2
485.5	3.881	-3.8	-7.1
486.0	3.883	-3.1	-7.0
486.6	3.885	-3.3	-7.6
487.1	3.887	-3.3	-7.1
487.6	3.889	-3.1	-7.4
488.1	3.890	-3.2	-7.3
488.6	3.892	-3.7	-7.1
489.1	3.894	-3.5	-7.7
489.7	3.896	-3.5	-7.2
490.2	3.898	-3.5	-7.1
490.7	3.900	-3.3	-7.0
491.2	3.901	-3.2	-7.3
491.7	3.903	-3.4	-7.5
492.2	3.905	-3.1	-7.4
492.8	3.907	-3.6	-7.6
493.3	3.909	-3.2	-7.3
493.8	3.911	-3.2	-7.3
494.3	3.912	-3.5	-7.3
494.8	3.914	-3.1	-7.4
495.3	3.916	-3.3	-7.3
495.9	3.918	-3.4	-6.9
496.4	3.920	-3.1	-7.0
496.9	3.922	-2.9	-7.1
497.4	3.923	-3.0	-7.3
497.9	3.925	-3.1	-7.4
498.4	3.927	-3.1	-7.5
499.0	3.929	-3.3	-7.4
499.5	3.931	-2.6	-7.2
500.0	3.933	-3.0	-7.5

DBT (mm)	Model Age (cal ka BP)	$\delta^{18}O$ (‰ V-PDB) (Ar)	$\delta^{13}C$ (‰ V-PDB) (Ar)
500.5	3.934	-3.0	-7.4
501.0	3.936	-2.9	-6.9
501.5	3.938	-3.0	-6.9
502.1	3.940	-2.9	-7.2
502.6	3.942	-3.2	-7.7
503.1	3.944	-2.9	-7.1
503.6	3.945	-3.3	-7.3
504.1	3.947	-3.4	-7.2
504.7	3.949	-3.4	-7.2
505.2	3.951	-3.2	-7.1
505.7	3.953	-3.5	-7.3
506.2	3.954	-3.3	-7.5
506.7	3.956	-3.3	-7.6
507.2	3.958	-3.1	-7.3
507.8	3.960	-3.0	-7.4
508.3	3.962	-3.2	-7.5
508.8	3.964	-3.2	-7.2
509.3	3.965	-3.0	-6.6
509.8	3.967	-3.3	-7.4
510.3	3.969	-3.3	-7.5
510.9	3.971	-2.8	-7.5
511.4	3.973	-2.9	-7.3
511.9	3.975	-2.9	-7.5
512.4	3.976	-2.9	-6.9
512.9	3.978	-3.3	-7.0
513.4	3.980	-3.3	-7.3
513.9	3.981	-2.9	-7.1
514.4	3.982	-3.9	-7.3
515.0	3.983	-3.4	-7.5
515.5	3.984	-3.5	-7.4
516.0	3.986	-3.2	-7.1
516.5	3.987	-3.5	-8.0
517.0	3.988	-3.3	-7.6
517.6	3.989	-3.5	-7.7
518.1	3.990	-3.1	-7.1
518.6	3.991	-3.0	-6.8

DBT (mm)	Model Age (cal ka BP)	$\delta^{18}O$ (‰ V-PDB) (Ar)	$\delta^{13}C$ (‰ V-PDB) (Ar)
519.1	3.992	-3.3	-7.3
519.6	3.993	-3.3	-7.3
520.2	3.995	-3.6	-8.0
520.7	3.996	-3.4	-7.6
521.2	3.997	-3.4	-7.6
521.7	3.998	-3.6	-7.5
522.2	3.999	-3.5	-7.6
522.8	4.000	-3.3	-7.0
523.3	4.001	-3.4	-7.0
523.8	4.002	-3.4	-7.4
524.3	4.003	-3.2	-7.5
524.8	4.004	-3.5	-8.1
525.4	4.006	-3.2	-7.4
525.9	4.007	-3.2	-7.5
526.4	4.008	-3.4	-7.6
526.9	4.009	-3.0	-7.6
527.4	4.010	-3.2	-7.8
528.0	4.011	-2.8	-7.4
528.5	4.012	-2.9	-7.4
529.0	4.013	-3.0	-7.3
529.5	4.014	-3.3	-7.6
530.0	4.015	-3.4	-7.6
530.6	4.017	-3.1	-7.3
531.1	4.018	-3.4	-7.3
531.6	4.019	-3.4	-7.3
532.1	4.020	-3.4	-7.3
532.6	4.021	-3.2	-7.3
533.2	4.022	-3.3	-7.5
533.7	4.023	-3.1	-7.0
534.2	4.024	-3.2	-7.0
534.7	4.026	-3.3	-7.1
535.2	4.027	-3.2	-6.9
535.8	4.028	-3.1	-7.4
536.3	4.029	-3.3	-7.3
536.8	4.030	-3.3	-7.5
537.3	4.031	-3.0	-7.1

DBT (mm)	Model Age (cal ka BP)	$\delta^{18}O$ (‰ V-PDB) (Ar)	$\delta^{13}C$ (‰ V-PDB) (Ar)
537.8	4.033	-3.0	-7.6
538.3	4.034	-3.1	-7.8
538.8	4.035	-3.3	-7.6
539.3	4.037	-3.4	-7.6
539.8	4.038	-3.3	-7.6
540.3	4.039	-3.9	-8.5
540.8	4.041	-3.8	-8.4
541.3	4.042	-3.7	-7.9
541.8	4.044	-4.0	-8.5
542.3	4.045	-3.5	-7.3
542.8	4.046	-3.5	-7.8
543.3	4.048	-3.6	-8.2
543.8	4.049	-3.5	-7.6
544.3	4.050	-3.5	-7.5
544.8	4.052	-3.4	-7.5
545.3	4.053	-3.6	-7.8
545.8	4.054	-3.8	-7.6
546.3	4.056	-3.5	-7.7
546.8	4.057	-3.4	-7.5
547.3	4.058	-3.8	-8.1
547.8	4.060	-3.7	-7.6
548.3	4.061	-3.3	-6.9
548.8	4.062	-3.6	-7.1
549.3	4.064	-3.7	-7.6
549.8	4.065	-3.6	-7.3
550.3	4.066	-3.7	-7.5
550.8	4.068	-3.7	-6.9
551.3	4.069	-3.7	-6.9
551.8	4.071	-3.5	-7.2
552.3	4.072	-3.4	-7.1
552.8	4.073	-3.5	-7.2
553.3	4.075	-3.5	-7.1
553.8	4.076	-3.5	-7.2
554.3	4.077	-3.3	-6.7
554.8	4.079	-3.4	-6.9
555.3	4.080	-3.4	-6.6

DBT (mm)	Model Age (cal ka BP)	$\delta^{18}O$ (‰ V-PDB) (Ar)	$\delta^{13}C$ (‰ V-PDB) (Ar)
555.8	4.081	-3.4	-6.7
556.3	4.083	-3.4	-6.7
556.8	4.084	-3.3	-6.9
557.3	4.085	-3.3	-7.1
557.8	4.087	-3.7	-7.1
558.3	4.088	-3.4	-7.4
558.8	4.089	-3.7	-7.8
559.3	4.091	-3.7	-8.0
559.8	4.092	-3.5	-7.6
560.3	4.094	-3.7	-7.4
560.8	4.095	-3.9	-7.7
561.3	4.096	-3.7	-7.8
561.8	4.098	-3.9	-7.6
562.3	4.099	-3.6	-7.7
562.8	4.100	-3.5	-7.8
563.3	4.102	-3.8	-7.6
563.8	4.103	-4.4	-7.6
564.3	4.104	-3.6	-7.7
564.8	4.106	-3.7	-8.4
565.3	4.107	-3.6	-7.2
565.8	4.108	-3.6	-6.8
566.3	4.110	-3.4	-6.8
566.8	4.111	-4.2	-6.7
567.3	4.112	-3.4	-7.1
567.8	4.114	-3.3	-7.3
568.3	4.115	-3.4	-7.2
568.8	4.116	-3.5	-7.0
569.3	4.118	-3.1	-6.4
569.8	4.119	-3.4	-7.1
570.3	4.121	-3.0	-6.4
570.8	4.122	-3.3	-7.0
571.3	4.123	-4.4	-6.9
571.8	4.125	-3.2	-6.8
572.3	4.126	-3.0	-6.5
572.8	4.127	-4.2	-7.0
573.3	4.129	-3.1	-7.1

DBT (mm)	Model Age (cal ka BP)	$\delta^{18}O$ (‰ V-PDB) (Ar)	$\delta^{13}C$ (‰ V-PDB) (Ar)
573.8	4.130	-2.9	-7.1
574.3	4.131	-3.0	-6.9
574.8	4.133	-3.3	-7.6
575.3	4.134	-3.3	-7.3
575.8	4.135	-3.4	-7.9
576.3	4.137	-3.5	-7.3
576.8	4.138	-3.1	-6.2
577.3	4.139	-3.5	-7.4
577.8	4.141	-3.3	-6.4
578.3	4.142	-3.3	-6.6
578.8	4.144	-3.0	-6.2
579.3	4.145	-3.2	-6.8
579.8	4.146	-3.2	-6.8
580.3	4.148	-3.4	-6.8
580.8	4.149	-3.4	-6.6
581.3	4.150	-3.5	-7.0
581.8	4.152	-3.5	-7.9
582.3	4.153	-3.7	-8.0
582.8	4.154	-3.4	-7.7
583.3	4.156	-3.6	-7.7
583.8	4.157	-3.4	-7.4
584.3	4.158	-3.3	-7.3
584.8	4.160	-3.7	-6.6
585.3	4.161	-3.2	-5.9
585.8	4.162	-3.5	-6.0
586.3	4.164	-3.8	-6.8
586.8	4.165	-3.3	-6.2
587.3	4.166	-3.3	-6.8
587.8	4.168	-3.4	-7.1
588.3	4.169	-3.7	-6.9
588.8	4.171	-3.8	-7.8
589.3	4.172	-4.1	-8.1
589.8	4.173	-3.8	-7.8
590.3	4.175	-3.7	-7.5
590.8	4.176	-3.5	-7.1
591.3	4.177	-2.8	-6.5

DBT (mm)	Model Age (cal ka BP)	$\delta^{18}O$ (‰ V-PDB) (Ar)	$\delta^{13}C$ (‰ V-PDB) (Ar)
591.8	4.179	-3.1	-6.1
592.3	4.180	-3.3	-6.8
592.8	4.181	-3.3	-7.1
593.3	4.182	-3.2	-7.2
593.8	4.183	-3.2	-7.2
594.3	4.184	-3.6	-7.4
594.8	4.185	-3.2	-7.2
595.3	4.186	-3.3	-6.8
595.8	4.187	-3.0	-7.1
596.3	4.188	-3.2	-5.7
596.8	4.189	-3.1	-5.8
597.3	4.190	-3.4	-5.5
597.8	4.191	-3.8	-6.7
598.3	4.192	-3.5	-6.2
598.7	4.193	-3.3	-6.3
599.2	4.194	-3.2	-5.9
599.7	4.195	-3.3	-5.9
600.2	4.196	-3.4	-6.5
600.7	4.197	-3.3	-6.4
601.2	4.198	-3.7	-6.6
601.7	4.199	-3.5	-7.3
602.2	4.200	-3.2	-7.3
602.7	4.201	-3.4	-7.3
603.2	4.202	-3.5	-6.9
603.7	4.203	-3.2	-6.9
604.2	4.204	-3.0	-7.2
604.7	4.206	-3.7	-7.7
605.2	4.207	-3.7	-7.7
605.7	4.208	-3.6	-7.9
606.2	4.209	-3.2	-7.6
606.7	4.210	-3.3	-7.3
607.2	4.211	-3.1	-7.9
607.7	4.212	-3.4	-6.6
608.2	4.213	-3.4	-6.9
608.7	4.214	-4.1	-6.7
609.2	4.215	-3.1	-6.4

DBT (mm)	Model Age (cal ka BP)	$\delta^{18}O$ (‰ V-PDB) (Ar)	$\delta^{13}C$ (‰ V-PDB) (Ar)
609.7	4.216	-3.0	-6.6
610.2	4.217	-4.7	-9.7
610.7	4.218	-4.1	-8.9
611.1	4.219	-4.9	-9.8
611.6	4.220	-4.9	-9.9
612.1	4.221	-4.8	-9.4
612.6	4.222	-3.9	-8.3
613.1	4.223	-4.4	-8.7
613.6	4.224	-4.9	-8.2
614.1	4.225	-4.1	-8.4
614.6	4.226	-3.6	-7.9
615.1	4.227	-3.6	-7.7
615.6	4.228	-4.0	-7.6
616.1	4.229	-3.8	-8.1
616.6	4.230	-4.2	-8.6
617.1	4.236	-3.8	-8.0
617.6	4.242	-4.0	-8.4
618.1	4.248	-3.6	-7.7
618.7	4.256	-4.0	-8.2
619.2	4.262	-4.5	-9.4
619.7	4.268	-3.5	-7.9
620.2	4.274	-3.7	-7.4
620.7	4.280	-3.7	-8.0
621.2	4.286	-3.7	-7.9
621.7	4.292	-4.0	-7.7
622.2	4.298	-3.9	-7.8
622.8	4.306	-3.9	-7.8
623.3	4.312	-4.2	-7.7
623.8	4.318	-3.6	-7.6
624.3	4.324	-3.6	-8.4
624.8	4.330	-3.9	-7.9
625.7	4.335	-3.6	-8.0
626.6	4.339	-3.6	-8.1
627.5	4.344	-3.6	-7.4
628.4	4.348	-3.7	-7.9
629.2	4.353	-3.5	-7.8

DBT (mm)	Model Age (cal ka BP)	$\delta^{18}O$ (‰ V-PDB) (Ar)	$\delta^{13}C$ (‰ V-PDB) (Ar)
630.1	4.357	-3.6	-7.9
631.0	4.362	-3.5	-8.0
631.9	4.366	-3.3	-7.9
632.8	4.371	-3.8	-8.0
633.7	4.376	-3.8	-8.3
634.6	4.380	-3.4	-7.8
635.5	4.385	-3.7	-7.3
636.4	4.389	-3.7	-7.4
637.2	4.394	-3.8	-8.2
638.1	4.398	-3.5	-7.5
639.0	4.403	-3.5	-8.0
639.9	4.407	-3.6	-7.9
640.8	4.412	-3.5	-7.7
641.7	4.417	-3.7	-7.8
642.6	4.421	-3.6	-7.1
643.5	4.426	-3.5	-7.1
644.4	4.431	-3.6	-7.6
645.2	4.435	-3.5	-7.7
646.1	4.439	-3.6	-7.4
647.0	4.444	-3.6	-7.5
647.9	4.448	-3.5	-7.4
648.8	4.453	-3.6	-7.8
649.7	4.458	-4.1	-7.5
650.6	4.462	-3.7	-7.9
651.5	4.467	-3.6	-7.7
652.4	4.472	-3.4	-7.5
653.2	4.476	-3.4	-7.7
654.1	4.480	-3.4	-7.2
655.0	4.485	-3.4	-7.3
655.9	4.489	-3.4	-7.1
656.0	4.490	-3.3	-6.6
656.3	4.491	-3.2	-7.1
656.7	4.492	-3.6	-7.7
657.0	4.492	-3.7	-7.8
657.4	4.493	-3.6	-8.2
657.7	4.494	-3.4	-8.2

DBT (mm)	Model Age (cal ka BP)	$\delta^{18}O$ (‰ V-PDB) (Ar)	$\delta^{13}C$ (‰ V-PDB) (Ar)
658.0	4.495	-3.6	-8.0
658.4	4.496	-3.5	-7.8
658.7	4.496	-3.6	-7.8
659.1	4.497	-3.7	-8.0
659.4	4.498	-3.4	-7.2
659.8	4.499	-2.7	-6.7
660.1	4.499	-2.7	-6.4
660.4	4.500	-3.1	-6.5
660.8	4.501	-3.4	-7.4
661.1	4.502	-3.4	-7.3
661.5	4.503	-3.3	-6.8
661.8	4.503	-3.4	-7.7
662.1	4.504	-3.4	-7.4
662.5	4.505	-3.2	-7.6
662.8	4.506	-3.6	-7.2
663.2	4.507	-3.2	-6.7
663.5	4.507	-3.4	-7.5
663.8	4.508	-3.1	-7.1
664.2	4.509	-3.6	-8.1
664.5	4.509	-3.6	-7.7
664.9	4.510	-3.7	-8.2
665.2	4.511	-3.5	-7.9
665.5	4.512	-3.5	-8.2
665.9	4.513	-3.8	-8.1
666.2	4.513	-3.6	-8.0
666.6	4.514	-3.9	-8.5
666.9	4.515	-3.6	-7.5
667.3	4.516	-3.6	-7.4
667.6	4.517	-3.3	-6.8
667.9	4.517	-3.0	-6.7
668.3	4.518	-3.3	-6.8
668.6	4.519	-3.2	-7.6
669.0	4.520	-3.7	-8.4
669.3	4.521	-3.5	-8.1
669.6	4.521	-3.5	-8.2
670.0	4.522	-3.5	-7.8

DBT (mm)	Model Age (cal ka BP)	$\delta^{18}O$ (‰ V-PDB) (Ar)	$\delta^{13}C$ (‰ V-PDB) (Ar)
670.3	4.523	-3.7	-8.2
670.7	4.524	-3.5	-8.3
671.0	4.524	-3.5	-7.0
671.3	4.525	-2.8	-5.9
671.7	4.526	-3.0	-5.1
672.0	4.527	-3.1	-6.1
672.4	4.528	-3.5	-6.9
672.7	4.528	-3.3	-6.8
673.1	4.529	-3.6	-7.3
673.4	4.530	-3.7	-7.6
673.7	4.531	-3.9	-7.5
674.1	4.532	-3.6	-6.7
674.4	4.532	-3.4	-6.7
674.8	4.533	-4.0	-7.3
675.1	4.534	-3.8	-7.5
675.4	4.534	-3.8	-7.5
675.8	4.535	-3.7	-7.2
676.1	4.536	-3.8	-7.4
676.5	4.537	-4.0	-7.7
676.8	4.538	-4.2	-8.1
677.1	4.538	-3.9	-8.0
677.5	4.539	-3.9	-8.3
677.8	4.540	-3.9	-8.5
678.0	4.540	-4.0	-8.6
678.1	4.541	-4.1	-9.0
678.3	4.541	-4.1	-9.1
678.5	4.542	-4.7	-8.9
678.7	4.542	-4.3	-8.8
678.8	4.542	-4.5	-8.8
679.0	4.543	-4.1	-8.5
679.2	4.543	-4.0	-8.6
679.4	4.544	-4.0	-8.9
679.5	4.544	-3.8	-8.5
679.7	4.544	-4.0	-8.4
679.9	4.545	-3.7	-8.3
680.0	4.545	-3.7	-7.7

DBT (mm)	Model Age (cal ka BP)	$\delta^{18}O$ (‰ V-PDB) (Ar)	$\delta^{13}C$ (‰ V-PDB) (Ar)
680.2	4.546	-3.6	-7.9
680.4	4.546	-3.3	-7.8
680.6	4.546	-4.1	-8.0
680.7	4.547	-3.4	-7.9
680.9	4.547	-3.9	-7.7
681.1	4.548	-3.5	-6.8
681.3	4.548	-3.3	-7.3
681.4	4.548	-3.4	-6.7
681.6	4.549	-2.9	-4.6
681.8	4.549	-2.8	-3.7
682.0	4.550	-2.7	-4.9
682.1	4.550	-3.2	-5.9
682.3	4.550	-2.7	-3.3
682.5	4.551	-2.9	-3.3
682.6	4.551	-2.7	-3.5
682.8	4.551	-2.5	-3.5
683.0	4.552	-2.4	-3.7
683.2	4.552	-2.6	-3.7
683.3	4.553	-3.1	-4.1
683.5	4.553	-2.9	-4.1
683.7	4.554	-2.8	-3.8
683.9	4.554	-2.2	-3.8
684.0	4.554	-2.6	-4.0
684.2	4.555	-2.7	-4.1
684.4	4.555	-2.8	-3.9
684.5	4.555	-2.8	-4.0
684.7	4.556	-2.6	-4.5
684.9	4.834	-2.7	-4.5
685.1	4.842	-3.2	-5.1
685.4	4.854	-2.8	-4.8
685.6	4.863	-3.0	-5.1
685.8	4.871	-2.7	-4.8
686.0	4.879	-2.9	-4.4
686.2	4.887	-2.3	-4.3
686.4	4.896	-2.3	-4.2
686.7	4.908	-2.8	-4.3

DBT (mm)	Model Age (cal ka BP)	$\delta^{18}O$ (‰ V-PDB) (Ar)	$\delta^{13}C$ (‰ V-PDB) (Ar)
686.9	4.916	-2.8	-4.7
687.1	4.925	-2.8	-5.1
687.3	4.933	-3.1	-5.3
687.5	4.941	-3.0	-5.6
687.7	4.949	-3.1	-5.0
688.0	4.962	-2.7	-4.7
688.2	4.970	-2.8	-5.0
688.4	4.978	-2.8	-4.8
688.6	4.987	-3.0	-5.1
688.8	4.995	-3.2	-6.1
689.0	5.003	-3.1	-5.5
689.3	5.016	-3.4	-6.1
689.5	5.024	-3.6	-6.4
689.7	5.032	-3.1	-6.2
689.9	5.040	-3.2	-6.5
690.1	5.049	-3.1	-6.8
690.3	5.057	-3.0	-7.2
690.6	5.069	-3.1	-6.9
690.8	5.078	-3.0	-7.3
691.0	5.086	-3.4	-7.2
691.8	5.100	-3.4	-7.0
692.7	5.112	-3.6	-7.3
693.5	5.123	-3.4	-7.5
694.3	5.134	-3.3	-7.4
695.2	5.147	-3.6	-7.4
696.0	5.158	-3.5	-7.5
696.9	5.170	-3.2	-7.2
697.7	5.181	-3.3	-7.6
698.5	5.192	-3.2	-7.5
699.4	5.204	-3.3	-7.2
700.2	5.216	-3.5	-7.2
701.0	5.227	-3.6	-7.5
701.9	5.239	-3.7	-8.1
702.7	5.250	-3.5	-7.7
703.0	5.254	-3.4	-7.7
703.3	5.258	-3.5	-7.7

DBT (mm)	Model Age (cal ka BP)	$\delta^{18}O$ (‰ V-PDB) (Ar)	$\delta^{13}C$ (‰ V-PDB) (Ar)
703.6	5.262	-3.6	-7.9
703.9	5.266	-3.5	-7.9
704.2	5.270	-3.4	-7.7
704.5	5.274	-3.0	-6.8
704.8	5.278	-3.2	-7.1
705.1	5.281	-3.1	-6.6
705.4	5.285	-3.1	-6.4
705.7	5.289	-3.2	-7.0
706.0	5.293	-3.4	-7.2
706.3	5.297	-3.1	-6.9
706.7	5.302	-3.4	-6.8
707.0	5.306	-3.6	-7.6
707.3	5.310	-3.5	-7.7
707.6	5.314	-3.8	-8.2
707.9	5.318	-3.6	-8.2
708.2	5.322	-3.7	-8.3
708.5	5.326	-3.7	-8.2
708.8	5.330	-3.5	-8.0
709.1	5.334	-3.3	-8.6
709.4	5.338	-4.0	-8.3
709.7	5.342	-4.0	-8.2
710.0	5.346	-3.4	-7.9
710.3	5.350	-3.8	-7.8
710.7	5.355	-3.4	-7.0
711.0	5.359	-3.2	-6.2
711.3	5.363	-3.0	-4.6
711.7	5.368	-2.8	-5.4
712.0	5.372	-3.0	-6.0
712.3	5.376	-3.2	-6.5
712.7	5.381	-3.3	-7.1
713.0	5.385	-3.4	-7.2
713.3	5.389	-3.4	-7.0
713.7	5.394	-3.2	-6.7
714.0	5.398	-3.1	-6.9
714.3	5.402	-3.4	-7.7
714.7	5.407	-3.2	-7.5

DBT (mm)	Model Age (cal ka BP)	$\delta^{18}O$ (‰ V-PDB) (Ar)	$\delta^{13}C$ (‰ V-PDB) (Ar)
715.0	5.411	-3.7	-8.1
715.3	5.415	-3.6	-7.7
715.7	5.420	-3.4	-7.3
716.0	5.424	-3.4	-7.4
716.3	5.428	-3.5	-7.9
716.7	5.434	-3.5	-7.9
717.0	5.438	-3.5	-7.9
717.3	5.441	-3.3	-7.4
717.7	5.447	-3.3	-7.7
718.0	5.451	-3.2	-6.2
718.3	5.455	-3.3	-6.4
718.7	5.460	-3.4	-6.6
719.0	5.464	-3.5	-6.8
719.3	5.468	-3.8	-7.2
719.7	5.473	-3.7	-7.1
720.0	5.477	-3.6	-6.8
720.3	5.481	-3.6	-6.9
720.7	5.486	-3.9	-7.2
721.0	5.490	-3.1	-7.5
721.9	5.492	-3.6	-7.6
722.8	5.495	-3.9	-7.5
723.7	5.497	-4.1	-7.8
724.7	5.500	-4.1	-8.1
725.6	5.502	-3.8	-8.0
726.5	5.504	-4.0	-8.0
727.4	5.506	-3.9	-7.8
728.3	5.509	-3.8	-7.0
729.2	5.511	-3.5	-6.6
730.2	5.514	-3.5	-6.2
731.1	5.516	-3.3	-6.3
732.0	5.518	-3.3	-7.4
732.9	5.521	-2.9	-6.9
733.8	5.523	-3.6	-6.9
734.7	5.525	-3.6	-6.5
735.6	5.528	-3.4	-7.1
736.6	5.530	-3.2	-5.8

DBT (mm)	Model Age (cal ka BP)	$\delta^{18}O$ (‰ V-PDB) (Ar)	$\delta^{13}C$ (‰ V-PDB) (Ar)
737.5	5.532	-2.9	-6.2
738.4	5.535	-3.0	-6.2
739.3	5.537	-3.3	-6.4
740.2	5.539	-3.6	-7.8
741.1	5.542	-3.6	-7.3
742.0	5.544	-3.3	-7.5
743.0	5.547	-3.4	-7.1
743.9	5.549	-3.5	-7.0
744.8	5.551	-3.5	-7.0
745.7	5.554	-3.3	-6.8
746.6	5.556	-3.2	-5.9
747.5	5.558	-3.6	-6.0
748.4	5.560	-3.2	-6.0
749.4	5.563	-3.1	-6.3
750.3	5.565	-3.3	-6.6
751.2	5.568	-3.6	-6.7
752.1	5.570	-3.0	-6.2
752.6	5.581	-3.1	-6.2
753.1	5.591	-3.7	-6.3
753.6	5.602	-3.6	-7.0
754.1	5.613	-3.0	-7.7
754.6	5.623	-3.5	-7.1
755.1	5.634	-3.3	-7.0
755.7	5.647	-3.5	-7.0
756.2	5.657	-3.2	-6.4
756.7	5.668	-3.2	-6.2
757.2	5.679	-3.0	-6.4
757.7	5.689	-3.0	-7.2
758.2	5.700	-3.1	-6.6
758.7	5.711	-2.8	-7.1
759.2	5.721	-2.9	-7.0
759.7	5.732	-3.6	-7.3
760.2	5.743	-3.5	-7.2
760.7	5.753	-3.4	-7.1
761.2	5.764	-3.9	-6.8
761.8	5.777	-3.4	-6.9

DBT (mm)	Model Age (cal ka BP)	$\delta^{18}O$ (‰ V-PDB) (Ar)	$\delta^{13}C$ (‰ V-PDB) (Ar)
762.3	5.787	-3.8	-6.6
762.8	5.798	-3.3	-6.6
763.3	5.809	-3.4	-6.6
763.8	5.819	-3.7	-7.1
764.3	5.830	-3.7	-7.0
764.8	5.841	-2.9	-7.3
765.3	5.851	-3.1	-7.4
765.8	5.862	-3.8	-6.6
766.3	5.873	-3.9	-5.9
766.8	5.883	-3.3	-6.2
767.3	5.894	-2.7	-6.4
767.9	5.907	-2.9	-7.2
768.4	5.917	-4.0	-7.7
768.9	5.928	-3.7	-7.7
769.4	5.939	-3.5	-7.6
769.9	5.949	-3.4	-7.0
770.4	5.960	-3.4	-6.9
770.9	5.971	-2.7	-7.0
771.4	5.981	-3.6	-7.4
771.9	5.992	-3.5	-7.1
772.4	6.003	-3.6	-7.4